Alma Mater Studiorum - Università di Bologna

DOTTORATO DI RICERCA IN ASTRONOMIA

Ciclo XXII

Settore scientifico-disciplinare di afferenza: Area02 - Scienze Fisiche

FIS/05 Astronomia e Astrofisica

YOUNG AND OLD STAR CLUSTERS IN M31: AN HST VIEW

Presentata da: Sibilla Perina

Coordinatore Dottorato:

Relatore:

Ch.mo Prof. Lauro Moscardini

Ch.mo Prof. Francesco Ferraro

Esame finale anno 2010

Co-Relatori:

Dott. M. Bellazzini

Dott.ssa L. Federici

Prof. F. Fusi Pecci

Tesi di Dottorato discussa alla presenza della commissione costituita da:

Prof. B. Marano

Prof. R. Buonanno

Prof. A. Marconi

Prof.ssa E. Tolstoy

Prof. E. Brocato

Ad Alberto

Abstract

In this thesis I present a set of photometric studies of the stellar populations in star clusters belonging to the nearby giant spiral in Andromeda (M31), performed with instruments on board of HST.

The core project is a HST-WFPC2 survey of candidate Young Massive Clusters (YMC). Previous analyses had identified a conspicuous set of bright candidate clusters ($M_V < -6.5$) having disk kinematics and displaying blue color and strong H_β absorption lines typical of populations younger than 1 Gyr. It remained to be established (a) if that sample of candidates was dominated by real clusters or significantly contaminated by spurious sources, and (b) what it was the actual age of the clusters, an essential piece of information to establish if they are significantly more massive than Galactic Open Clusters or they are more akin to the YMCs found in the Magellanic Clouds. To answer these questions HST-WFPC2 images of 19 candidate YMC were obtained. The sample appeared to be composed almost entirely by real clusters (19/20). The reddening, age and metallicity of the surveyed clusters were robustly estimated by comparison of the observed Color Magnitude Diagrams (CMD) and completeness-corrected Luminosity Functions with proper theoretical models. The light profiles have been also derived and the structural parameters of the clusters have been obtained by fitting with models (as, for example King (1966) models). All the bona-fide candidate YMC were found to have ages in the range 25-500 Myr. The sample has been complemented with six further young clusters whose CMD was derived from archival HST-ACS images that we reduced in a fully homogenous way with respect to the main targets of the survey. The derived ages and the

integrated J,H,K magnitudes obtained from 2MASS were used to estimate stellar masses ranging from $\sim 10^4 M_\odot$ to $\sim 10^5 M_\odot$. The young target clusters turn out to be significantly brighter (and more massive) than Galactic OC in the same age range and are similar to the YMCs found in the LMC, SMC and M33. Eighty-nine low-luminosity clusters serendipitously falling into the survey images were identified and studied.

A search of HST-ACS data for M31 cluster lead to a firm reclassification for 63 objects; useful CMDs were obtained for 17 of them, and new estimates of the age and metallicity was obtained for these clusters.

Lastly, new deep HST ACS/HRC photometry revealed a previously undetected blue plume of young stars at the center of the dwarf elliptical galaxy NGC 205, a satellite of M31. With these data we have investigated the star formation history in the central $30''$ of the galaxy, estimating a star formation rate of $\sim 7 \times 10^{-4} M_\odot/yr$.

Contents

1

Introduction and summary

1.1 Star cluster species

The Milky Way (MW) has long been the main playground for studies of star clusters. The first comprehensive discussion of the properties of star clusters was given by Sir William Herschel in a series of papers published in the *Phil. Trans. R. Soc. London*. Herschel noted significant differences in the visual appearances of clusters. He used the term *globular clusters* (GC) to describe the richest and most concentrated of them (Herschel, 1814). The term *open cluster* (OC) emerged during the early 20th century (Shapley, 1916) as a common label for all non-globular clusters. Originally, this classification was purely morphological, based simply on the visual appearance of a cluster through a telescope or on a photograph. Differences in spatial distribution, with the OCs concentrated near the Galactic plane and the GCs tending to avoid it, were recognized early on Shapley (1916; and references therein). The developement of instrumentation as well as of the photographic and spectroscopic techniques allowed us to compare star clusters regarding the spectro-photometric properties of the constituent stars. However, even if the first CMDs go back to the early 1910's (Rosenberg, 1910; Shapley, 1915), it is only after Baade (1935) resolved the nucleus of the Andromeda galaxy and differentiated between stellar population I and II, that the CMD was been recognized universally as an excellent criterion to discriminate between star clusters. Therefore, the distinction between OCs and GCs as objects made of population I stars and population II stars respectively, started in the 1930's (even if we have to wait the post-war works with the large reflectors on Mount Wilson and Palomar to locate the connection of the observed GCs sequences with the main sequence well known in the OCs diagrams). From this moment the star cluster nature will be defined by the age and the chemical composition of the constituent stars, as well as the location into the galaxy and the morphology of the cluster as a whole. Today we know that OCs are, in general, metal-rich with metallicities similar to, or even exceeding, the solar value (Friel et al., 2002) and are associated with the thin disk of our Galaxy, while the Milky Way GCs are

associated with the spheroid (bulge/halo/thick disk) and have a bimodal metallicity distribution, with both peaks at subsolar values (logarithmic iron abundance, relative to solar, of [Fe/H] $\approx$ −1.5 and −0.5 dex; Zinn 1985). While the GCs are all ancient, with ages on the order of 10^{10} years and a spread of perhaps a few $\times 10^9$ years (Marín-Franch et al., 2009), the OCs are mostly younger than a few $\times 10^8$ years (Wielen, 1971), although some older OCs are also known (Friel, 1995; Bragaglia & Tosi, 2006). The lack of young GCs in the halo and bulge can be attributed to a cessation of star formation in these components long ago, but the field stars in the Galactic disk have a continuous range of ages and OCs are likely to have formed there also in the distant past. The relative deficit of old OCs, therefore, illustrates that cluster *dissolution* is important.

The globular cluster system (GCS) of the MW consists of over 150 known members (Harris, 1996). The majority of them were discovered through optical searches, biased against highly obscured objects. Since the Galaxy is estimated to have 160 ± 20 GCs (Harris, 1991), a certain number of GCs may still be hidden behind the Galactic disk. Recent all-sky near-infrared (IR) surveys (2MASS, Skrutskie et al. 1997; DENIS, Epchtein et al. 1997; GLIMPSE, Benjamin et al. 2003) made it possible to carry out a more uniform census of highly obscured Milky Way clusters (Borissova et al., 1993; Ivanov et al., 2010; Reyle & Robin, 2002; Kurtev et al., 2007, 2008).

The known Galactic OCs are over 1000, but the true total may be up to ten times higher than that. Current catalogues of OCs can only be considered reasonably complete within 1 Kpc of the Sun (Piskunov et al., 2008), in fact, extinction by interstellar dust in the Galactic plane, combined with the high stellar density along the line of sight, strongly limit our ability to detect distant OCs.

With the progress of the observational studies the distinction between OCs and GCs, that traditionally characterize the Galactic star cluster system, has become increasingly blurred. Currently in the MW we know OCs quite bright and old to be confused with the faintest GCs (e.g. Phelps & Schick 2003); on the other hand, some GCs are very faint (e.g. Koposov et al. 2007) and, at least one, Palomar 1, has an age consistent with the OCs age distribution (Sarajedini et al., 2007b)[1]. In Figure 1.1 the luminosity distribution of MW GCs and old MW OC are compared. Moreover, in even the nearest external galaxies (the Magellanic Clouds, M31 and the other Local Group galaxies), this convenient dichotomy disappears. The Clouds for example, contain small numbers of classically old, massive, metal-poor GCs as well as many analogues of open clusters, but we also find numerous examples of high-mass, young clusters that likely resemble GCs as they would have been closer to their formation time. This new category of star clusters is commonly termed *young massive clusters* (YMC).

The launch of the *Hubble Space Telescope (HST)* led to a revolution in this field. With careful modeling of the *HST* point-spread function, a typical cluster with a half-light radius of ~ 3 pc remains recognizable as an extended object out to distances of at least 40 Mpc (Harris, 2009). This leads to a formidable increase in the number of galaxies accessible to detailed study of their cluster populations also beyond the Local Group.

Large number of objects with the properties expected of young globular clusters was discovered in extragalactic starburst and merging galaxies (Holtzman et al., 1992; Whitmore et al., 1999; de Grijs et al., 2005; Smith et al., 2007) which are

---

[1]However, it has to be recalled that catalogues for OCs typically collects data of widely variyng quality. Age and especially L_T estimates may be very uncertain.
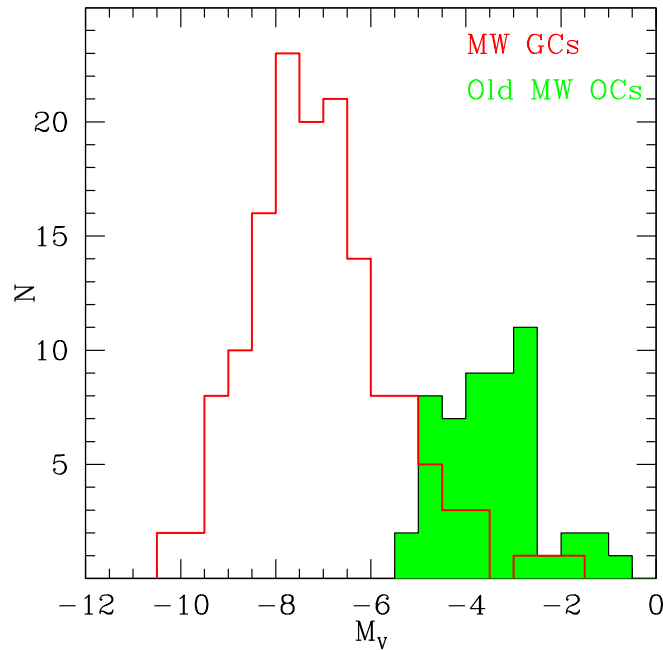
Figure 1.1: Integrated absolute V magnitude histograms of the MW GCs (red line, from the 2003 revision of Harris 1996) and of the MW OCs with a reported age $\gtrsim 1$ Gyr (shaded green, from the WEBDA database).

experiencing vigorous star formation. These data suggest that the common physical condition for the production of dense, young star clusters is a strong starburst. Where cluster masses have been derived, they are often in the range $10^4 - 10^6$ M$_\odot$ or higher, comparable to the most massive old GCs (Zhang & Fall, 1999; McCrady & Graham, 2007), with the lower end of the range usually being set by detection limits.

An increasing amount of data for normal spiral galaxies have also become available. Young clusters in the mass range $10^5 - 10^6$ M$_\odot$ have been found in some spirals (Larsen & Richtler, 2000; Larsen, 2004), showing that such objects are not unique to starbursts and interacting systems, although they may be more common there.

YMC are thought to be absent in the MW. It is only very recently that a few of these objects have been observed in the direction of the Galactic center (Clark et al., 2005; Figer, 2008; Messineo et al., 2009). Probably, their census is quite incomplete due to observational selection effects.

1.1.1 Young massive clusters

In the previous section we have established that the MW star cluster system separate out rather cleanly into the two classical subsystems: the open clusters and the globular clusters, but in the external galaxies this dichotomy disappears.

When the only well studied GCS was that of the MW, it was generally thought that this separation was because globular clusters were fundamentally different from other star clusters, perhaps because of conditions in the early universe (Peebles & Dicke, 1968; Fall & Rees, 1985). However, it is possible to produce this apparent bimodality from clusters formed in a single process, with the same cluster initial mass function. In this picture, cluster disruption mechanism, which are more effective at
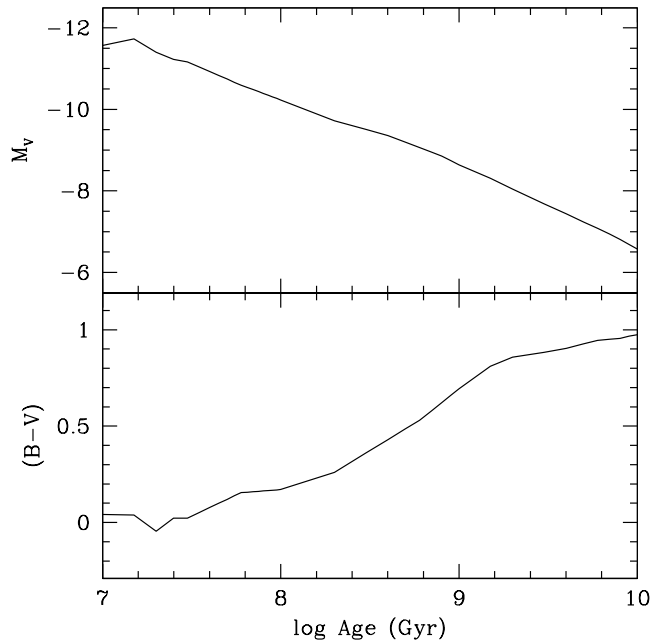
Figure 1.2: Evolution of a single-burst stellar population with a mass of $2 \times 10^5 M_\odot$. Absolute V magnitude (upper panel) and (B-V) color (lower panel) are plotted versus age in Gyr. The general trend of brighter magnitudes and bluer colors is common to all stellar population models. This figure is specifically based on Maraston (1998, 2005) models with solar metallicity, Salpeter (1955) stellar initial mass function and intermediate horizontal branch morphology.

destroying low-mass clusters in particular because of two-body relaxation (Spitzer, 1958; Spitzer & Harm, 1958), would remove almost all of the low-mass older clusters. If all clusters were born with similar cluster mass functions, than we would expect to see the occasional high-mass young cluster. In fact, we do see these in other galaxies. Rather than representing distinct entities, OCs, YMCs and GCs may represent regions within a continuous of cluster properties dependent upon local galaxy conditions (Larsen, 2003).

The lifetime of a star cluster is dependent upon its mass and environment. Most low-mass star clusters in the disk are rapidly destructed via interactions with giant molecular clouds (GMCs) (Lamers & Gieles, 2006; Gieles et al., 2007). These disrupted star clusters are thought to be the origin of much of the present field star populations Lada & Lada (2003). Surviving disk clusters may then be regarded as OCs or YMCs, depending upon their mass. Star clusters in the halo may survive longer since they are subjected to more gradual dynamical processes of two body relaxation and evaporation. The clusters which survive for an Hubble time – more likely to occur away from the disk – are termed GCs (see also Krienke & Hodge 2007). To date no known *thin* disk GCs have been identified in the MW.

Can YMCs be considered as proto-globular clusters? Predicting what GCs are expected to look like when they are young is straightforward. They should be bright, blue and compact (e.g. Ashman & Zepf 1992). The compactness is a basic characteristic of GCs, without which they would not survive within the tidal field of their host galaxy for a Hubble time. The bright luminosity and blue color comes from the fact that young stellar populations have massive stars, which are bright and blue. The luminosity and color evolution can be predicted using models of stellar

populations. As an example, Figure 1.2 shows the evolution with time of the absolute V magnitude and (B-V) color for an instantaneous burst of star formation of mass of $2 \times 10^5 M_\odot$, assuming a Salpeter (1955) stellar initial mass function and the models of Maraston (1998, 2005), for solar metallicity and intermediate horizontal branch morphology. This figure shows that young globular clusters were several order of magnitude brighter and substantially bluer in the past. Precise predictions of color and luminosity depend on the IMF and metallicity, but generally high luminosities, blue colors, and compact sizes are identifying signatures of candidate young globular clusters. It is clear that the presence of compact, young star clusters is a necessary condition for the recent formation of GCs, even thought it is not a sufficient one. The observational task is to determine if objects consistent with the properties of young globular clusters are found in various galaxies, and then to determine if these objects are likely to evolve to become GCs like those in the Milky Way or M31.

As introduced in Section 1.1, young star clusters with masses and compactness typical of GCs are observed to exist not only in starburst and merging galaxies but also in normal spiral galaxies with high star formation rates, then, the formation of GCs, which was once thought to be limited to the earliest phases of galaxy formation, appears to be continuing at the present time. Whether these YMCs will evolve to become old GCs by the time they reach an age of 13 Gyr depends to a very large extent on their environment, as we will see in the next section.

For a comprehensive and very recent review about YMCs, the reader is referred to the work of Portegies Zwart et al. (2010).

1.1.2 Cluster survival

Star clusters evolve due to a number of dissolution mechanisms. The most precarious stage in the evolution of a star cluster may be soon after it has formed, when short-term stellar evolutionary processes can lead to his disruption. This phenomenon is termed *infant mortality*, it is caused by the removal of gas left over from the cluster formation process by stellar winds and/or the first supernovae, see e.g. Lada & Lada (2003) and Bastian & Goodwin (2006). The star clusters that survive the *infant mortality* phase are still subject to long-term destructive dynamical processes. Bound star clusters in a tidal field lose mass due to internal and external effects (Spitzer, 1987). The internal effects are

1. mass loss by stellar evolution (dominant in the first $\sim 10^8$ years);

2. evaporation. Stars in clusters experience two and three body encounters, in which they can gain velocity, reach the escape velocity and leave the cluster.

The external effects are

1. galactic tides. Isolated clusters experience evaporation, but the presence of an external gravitational field (due to the host galaxy) tends to make the process more efficient (e.g. see the case of the GC Pal5 in Odenkirchen et al. 2003).

2. disk/bulge-shocking. Stars gain energy after crossing the high-density galactic disk/bulge;

3. tidal heating by encounters with giant molecular clouds.

The combination of these effects results in decreasing the cluster mass until complete destruction. The time scale of disruption depends on the initial conditions of the clusters, e.g. the stellar initial mass function and its concentration, and on the tidal forces experienced by the cluster during its galactic orbit. Low-mass clusters are particularly susceptible to evaporation and if they are formed in the disk experience also external perturbations by spiral arms and by GMCs. These perturbations are not present in the halo of a galaxy, where most of the GCs reside.

Theory predicts that the dissolution time of isolated clusters depends on their initial mass, in that massive clusters survive longer than low mass clusters (e.g. Spitzer 1958; Wielen 1985; Chernoff & Weinberg 1990; Gnedin & Ostriker 1997, and reference therein). However, for cluster in a tidal field (the real case), the mass loss rate is much higher and the lifetime shorter then for clusters in isolation since these parameters depends also by the local conditions in the host galaxy. The condition for tidal stability of a cluster is when the gravitational acceleration of its stars, that is due to the matter belonging to the cluster, is much larger then the differential acceleration felt by the stars themselves with respect to cluster center because of the galactic potential. This condition can be written in term of density as

$$\rho_{cl}(x) > \rho_{gal}(R)$$

where the densities are the mean density within a sphere of radius R (for the galaxy) and a radius x (for the cluster). The distance from the cluster center where $\rho_{cl}(x) = \rho_{gal}(R)$ is

$$r_t = R \sqrt[3]{(m_{cl}/M_{gal}(R))}$$

where m_{cl} is the cluster mass, R is the cluster distance from the galactic center and $M_{gal}(R)$ is the mass of the galaxy enclosed within a sphere of radius R. r_t is the cluster tidal radius that define the conventional limit between bound and unbound stars. As a consequence, for clusters in a tidal field t_{dis} depends also on the cluster density. As density and mass are correlated, the dependence of t_{dis} on density can be conventionally expressed as a function of mass.

The first empirical determination of the lifetime of clusters in the MW is by Oort (1958), who noticed the lack of clusters older then a few Gyr in the solar neighborhood. Later, Wielen (1971) derived a mean dissolution time of 0.2 Gyr from the age distribution of clusters. Since most of the observed clusters within about 1 Kpc from the Sun have a mass in the range of 10^2 to a few $10^3 M_\odot$, the value derived by Wielen is for clusters in that mass range. Boutloukos & Lamers (2003) assume that the disruption time of clusters, defined as $t_{dis} = (dlnM/dt)^{-1}$, depends on the mass M as

$$t_{dis} = t_4 \times (M_{cl}/10^4)^\gamma$$

where M_{cl} is the initial cluster mass (in $M_\odot$) and t_4 is the disruption time (in yrs) of a cluster with an initial mass of $M_{cl} = 10^4 M_\odot$. These authors found empirically that the constant t_4 differ greatly between regions in different galaxies, indicating that the disruption time depends strongly on the local conditions in the host galaxy. Using the results of N-body simulation (Baumgardt & Makino, 2003) Lamers et al. (2005) shown that t_4 is expected to scale with the inverse square root of the mean density in the host galaxy, that is $t_4 \propto \rho_{gal}^{-0.5}$. They assume the following expression for the
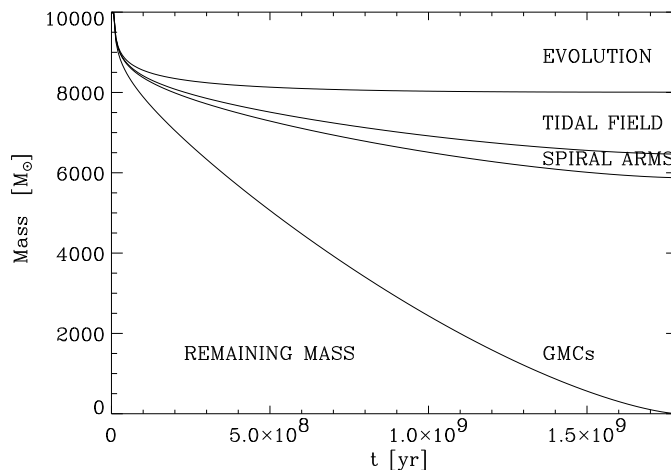
Figure 1.3: The mass evolution of a cluster with an initial mass of $10^4 M_\odot$ in the solar neighbourhood. The mass loss due to the four separate effects is indicated. Encounters with GMCs are the dominant dissolution effect in the solar neighbourhood. (From Lamers & Gieles (2006)).

disruption times of star clusters due to tidal interactions in different extragalactic environment

$$t_{dis} = C_{env}(M_{cl}/10^4 M_\odot)^{0.62}(\rho_{gal}/M_\odot pc^{-3})^{-0.5}$$

where $C_{env} \simeq 300 - 800 Myr$.

If encounters with GMCs or disk/bulge shocking becomes important, the disruption times result even more shorter. Lamers & Gieles (2006), taking into account stellar evolution, tidal stripping, shocking by spiral arms and encounters with giant molecular clouds find $t_{dis} = 1.7(M_i/10^4 M_\odot)^{0.67}$ for clusters in the solar neighborhood in the mass range of $10^2 < M_i < 10^5 M_\odot$ (see Lamers & Gieles 2006 for a detailed discussion). The evolution of a $10^4 M_{sun}$ cluster according to these formulas is shown in Figure 1.3 (Fig. 1 of Lamers & Gieles 2006). The figure shows the mass lost by each mechanism independently. Encounters with GMCs are the dominant dissolution effect in the solar neighborhood, contributing about as much as the three other effects combined. Figure 1.4 (Fig. 2 of Lamers & Gieles 2006) shows the ages of clusters when their remaining mass is 0 and 100 $M_\odot$ as a function of the initial mass. The figure also shows the dissolution times due only to the Galactic tidal field, predicted by Baumgardt & Makino (2003) from N-body simulations.

1.2 The star cluster system of M31

In this chapter the main properties of M31 star clusters are summarized, classifying them in three category in terms of brightness, age, spatial distribution and kinematics: globular clusters, open clusters and young massive clusters.

1.2.1 Globular clusters in M31

Among the Local Group galaxies, M31 is our nearest bright spiral galaxy neighbor and the most prominent member; moreover it hosts the largest population of globular clusters(GCs).
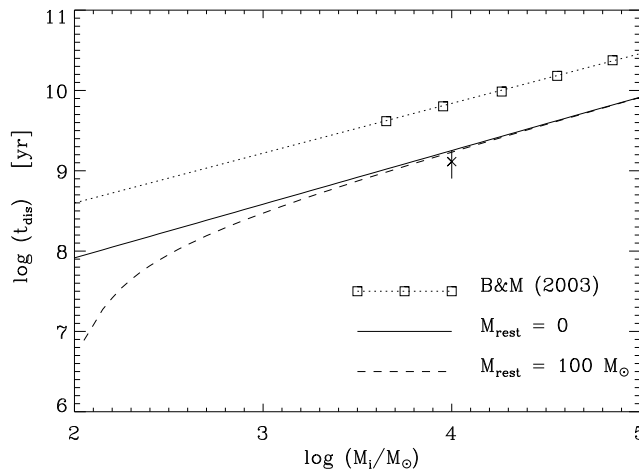
Figure 1.4: The predicted dissolution times of clusters in the solar neighbourhood due to the combined effects of stellar evolution, tidal field, spiral arm shocks and encounters with GMCs, as a function of the initial mass. Full line: total dissolution time. Dashed line: time when the remaining mass is $100 M_\odot$. Squares and dotted line: dissolution time due to stellar evolution and the Galactic tidal field only, predicted by BM03. Cross with error bar: the value of t_4 empirically derived by L05. (From Lamers & Gieles (2006).

Hubble (1932), using the 100-inch telescope at Mount Wilson, identified 140 objects near M31 that, on photographic plates, had the appearance of "nebulous stars" and proposed that they were star clusters associated with the galaxy itself. Since Hubble's pioneering observations, many studies have contributed to take inventory of the M31 GCS (see review by Hodge 1992 and reference therein) and have revealed an M31 GCS population that is more than three times the size of the MW GCS. As part of a major photographic survey of cluster candidates around M31, the Bologna Group published a compendium that included a large number of M31 GC candidates having $14 \leq V \leq 19.5$ mag within $3°$ of the M31 center. This *Bologna Catalogue* (Battistini et al., 1987, 1993) and the recently updated and expanded *Revised Bologna Catalogue*[2] (RBC, Galleti et al. 2004) have become widely used by later studies that have continued the endeavour of adding positive identifications, photometry and spectroscopy, for M31 GCs. The last RBC version (V4, 2009) contains 654 confirmed star clusters and 606 candidate clusters (see Figure 1.6.

The distance to M31 is ~ 780 kpc, it is large enough that the dispersion in distance modulus within the GC system is relatively small [50 kpc corresponds to $\delta(M - m) \sim 0.15$ mag] at thet distance. Hence the GCs can be considered as lying all at the same distance for many usefull purposes (e.g. the derivation of the $M_V(HB) vs. [Fe/H]$ relation in Rich et al. 2005). Also, their almost stellar appearance (10 pc correspond to $\sim 2''.6$) allows an easy study of their integrated properties from the ground. On the other hand, M31 is also close enough that individual stars in GCs can be resolved and measured with the Hubble Space Telescope and with very large ground-based telescopes equipped with powerful adaptive optics systems. At present, riliable optical CMDs have been published for 44 old GCs in M31. Except for one that was observed from the ground (MGC1, Martin et al. 2006), a good fraction of these have been obtained with the HST/WFPC2 reaching well below the horizontal branch (HB) (Ajhar et al., 1996; Rich et al., 1996; Fusi Pecci et al., 1996; Holland et

---

[2]www.bo.astro.it/M31

8
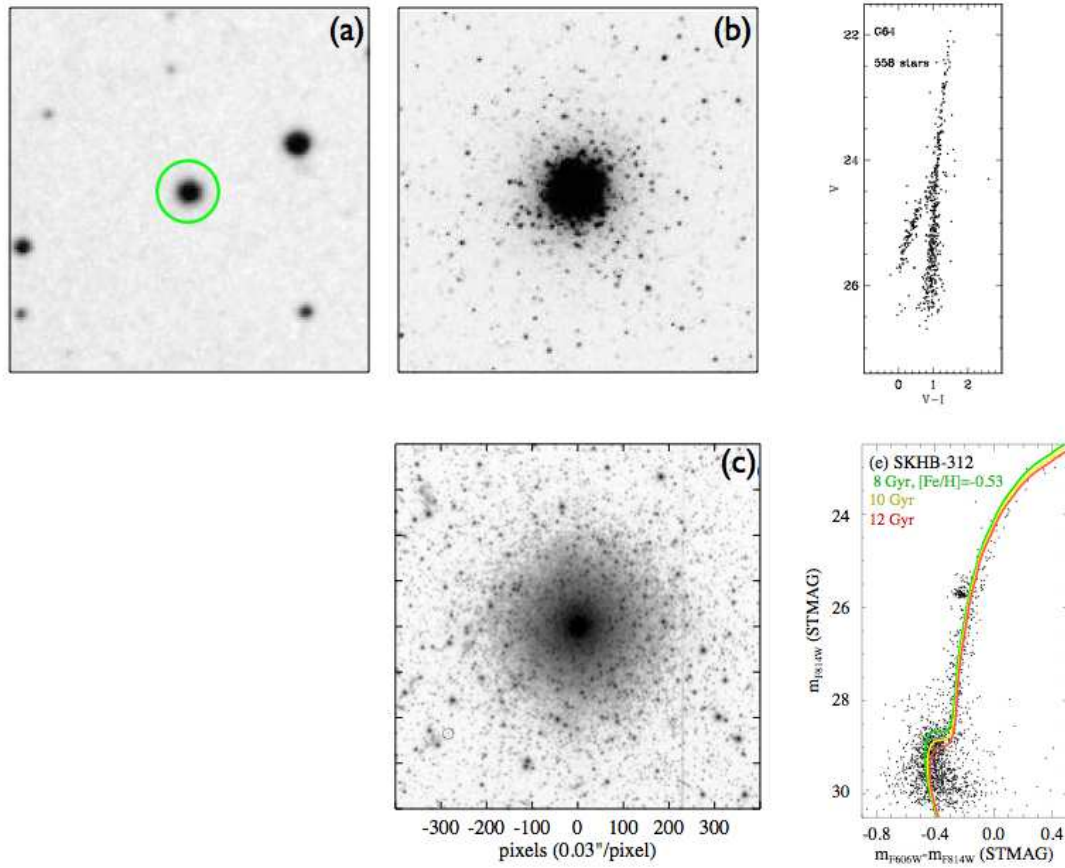
Figure 1.5: Upper panels: (a) ground-based (DSS2) image, (b) HST/WFPC2 $20'' \times 20''$ image, and CMD from WFPC2 data for the GC B012-G064 in M31 (from Rich et al. 2005). Lower pannels: (c) HST/ACS $24'' \times 24''$ image, and CMD from ACS data for the GC SKHB-312 in M31 (from Brown et al. 2004b). The green circle in the panel (a) has a radius of $10''$.
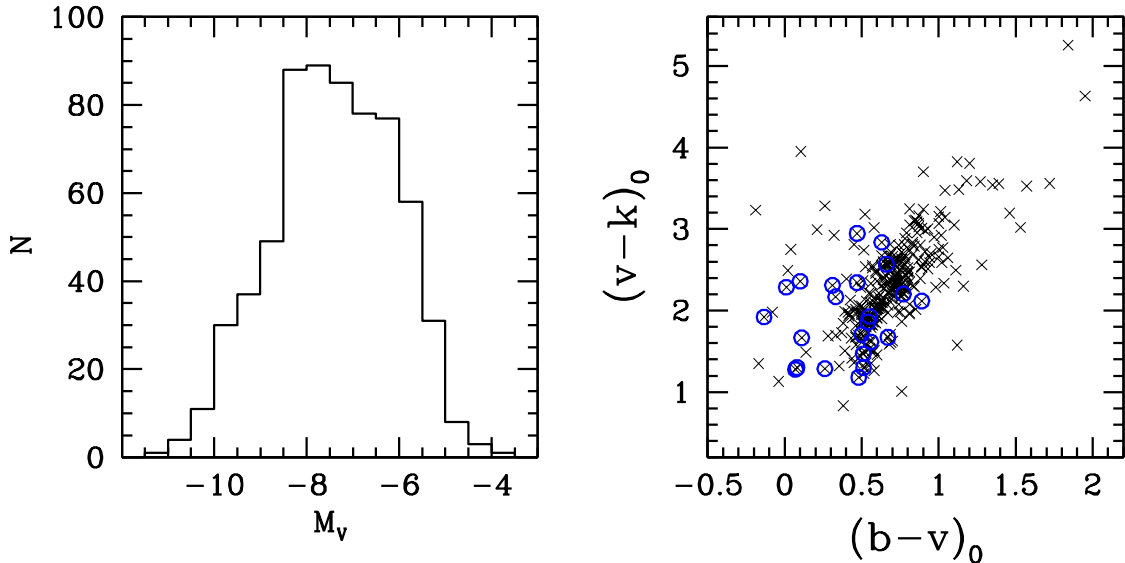
Figure 1.6: Left panel: Absolute integrated V magnitude distribution of the whole genuine star clusters in the RBC. Right panel: RBC's star clusters in the dereddened two-color diagram $(v-k)_0$ vs. $(b-v)_0$; the blue circles are genuine and candidate YMCs with $H_\beta > 3.5$ Å.

al., 1997; Jablonka et al., 2000; Meylan et al., 2001; Rich et al., 2005; Perina et al., 2009b). The better resolution and sensitivity of the ACS allowed even more accurate CMDs at fainter limiting magnitudes (Brown et al., 2004b; Huxor et al., 2004, 2005, 2008; Galleti et al., 2006b; Mackey et al., 2006, 2007). In Figure 1.5 (upper panel) a ground-based image from the Digitalized Sky Survey II (DSS2) of the M31 GC B012-G064 (a) is compared with a WFPC2 image of the same cluster (b). From the ground the cluster is unresolved, on the other hand the resolved stellar population cleary visible in the high-resolution WFPC2 image allowed to obtain the good CMD on the upper-right panel reaching the base of the red giant branch (Rich et al., 2005). In the lower pannels an ACS image of the GC SKHB-312 (c) and the CMD from very deep ACS data (lower-right panel) are shown.

In this framework, the GC system of the Andromeda galaxy (M31) plays a twofold role: as a natural reference to compare with the Milky Way (MW) GC population and as a fundamental test bed for the techniques to be applied to systems in more distant galaxies (see Barmby et al. 2000; Puzia et al. 2002; Rich 2003; Barmby 2003; Galleti et al. 2004; and references therein). Indeed, the comparison of the GC system of M31 and the MW has revealed both fundamental similarities and interesting differences, whose complete understanding may have a deep impact on our knowledge of galaxy formation and evolution (Hodge, 1992; van den Bergh, 2000; Morrison et al., 2004; Beasley et al., 2004; Burstein et al., 2004).

Similar to the Milky Way, M31 appears to have at least two GC sub-populations, a metal-rich, spatially concentrated sub-population of GCs and a more metal-poor, spatially extended GC sub-population (Barmby et al., 2000; Perrett et al., 2002; Puzia et al., 2005; Fan et al., 2008; Lee et al., 2008).

In Figure 1.7 (Galleti et al. 2009, Figure 15) the metallicity distribution (MD) of the sample of M31 GCs studied by Galleti et al. (2009) is compared with its Milky Way counterpart. These authors found that the highest peak in the M31 MD occurs at [Fe/H]~ -0.9, coinciding with the overall average of the sample $<[Fe/H]> = -0.94$,
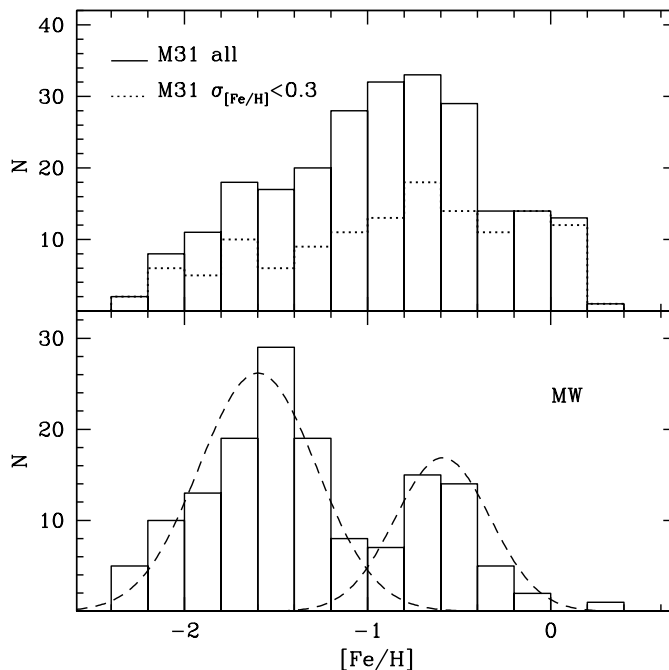
Figure 1.7: Metallicity histogram for the M31 globular cluster system (top) and the MW GC system (bottom), reported for comparison. The dashed lines in the lower plot are the gaussian curves in the best fit models as found by the KMM algorithm (Ashman et al., 1994) for two subpopulations ([Fe/H]=-1.60 and -0.59).

significantly more metal rich than in the MW case, where the maximum is at [Fe/H]$\sim$ -1.5 and the overall mean is $<[Fe/H]>= -1.30$ (Harris, 1996). The M31 system appears also to have a much larger fraction of clusters having [Fe/H]> -0.5 (23% of the total sample) with respect to the Milky Way (7%). The distribution is essentially unchanged also limiting the analysis to the subset of clusters having errors in metallicity lower than ± 0.3 dex (132 clusters; dotted histogram in the upper panel of Figure 1.7). Looking at Figure 1.7, the MD of M31 GCs do not present any obvious structure like the bimodality encountered in the GC system of the Milky Way. Nevertheless the distribution for M31 clusters does not seem to be well represented by a single Gaussian distribution. The same authors, comparing the hypothesis of a multimodal underlying distribution with a unimodal representation using parametric statistical tests, found that the distribution is likely not unimodal.

Also, again similar to the Milky Way GCs, the metal-rich GCs in M31 rotate and show "bulge-like" kinematics (Perrett et al., 2002; Galleti et al., 2009); however the rotation amplitude is larger in M31 ($\sim$ 220 $Km\ s^{-1}$ than in the MW ($\sim$ 147 $Km\ s^{-1}$) (Zinn, 1985; Armandroff, 1989). On the other hand, unlike the case in the Milky Way, the metal-poor GCs also show significant rotation (Huchra et al., 1991; Perrett et al., 2002; Lee et al., 2008; Galleti et al., 2009). Figure 1.8 (Galleti et al. 2009, Figure 17) shows the positional and kinematical properties of M31 GCs divided into three groups according to their metallicity, i.e. a metal poor (MP) group ($[Fe/H] \leq -1.0$), a metal intermediate (MI) group ($-1.0 < [Fe/H] < -0.5$), and a metal rich (MR) group ($[Fe/H] \geq -0.5$). The left panels of Figure 1.8 show the spatial distribution of the considered clusters in the canonical X,Y projected coordinate system (see Galleti et al. 2004, and references therein), with X along the major axis of the galaxy. In the right panels the radial velocity of the clusters (in the reference frame of M31) is
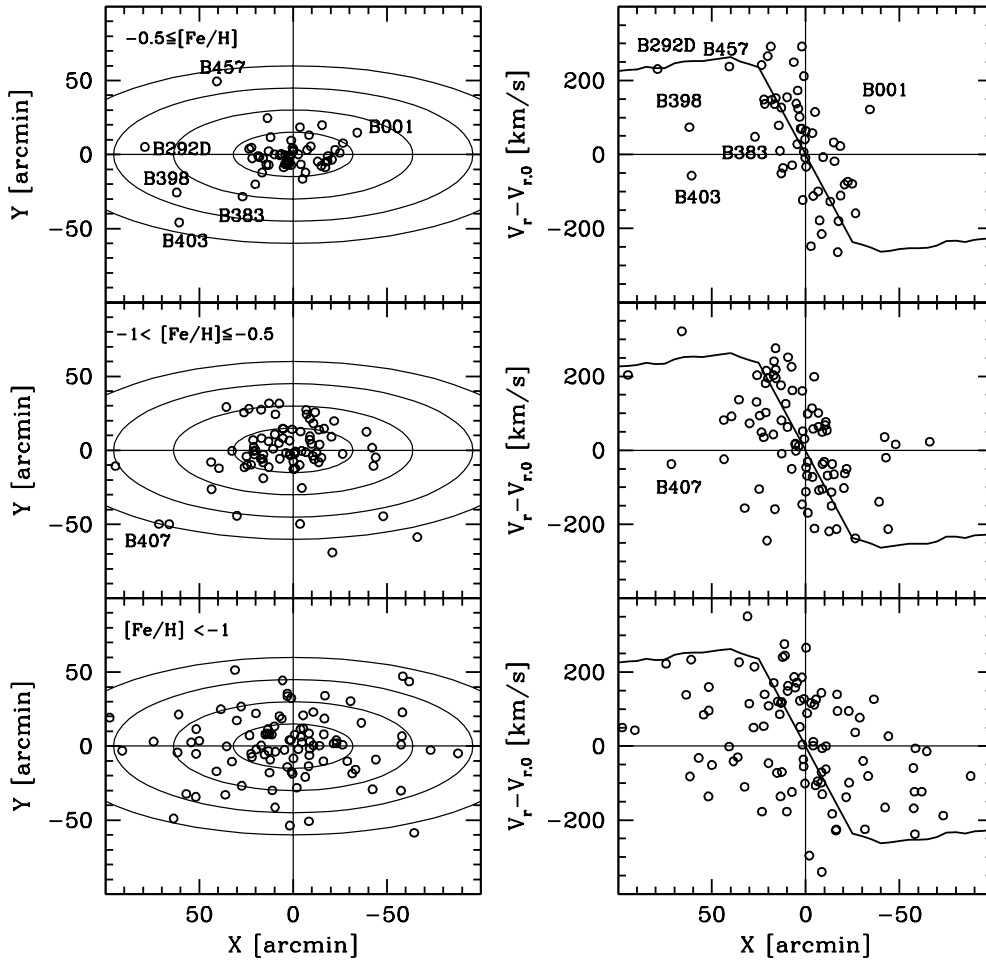
Figure 1.8: Left Panels: Spatial distribution of three metallicity groups GCs in M31. The ellipses have a semimajor axis of 15, 30, 45, 60 arcmin. Right Panels: Radial velocities vs. the projected distances along the major axis (X). The solid line shows a HI rotation curve from Carignan et al. 2006.

plotted versus the X coordinate and compared with the rotation curve of the HI disk from Carignan et al. (2006).

1.2.2   Open clusters in M31

It has been realized since long time that M31 contains a large number of open clusters roughly similar to those in our Galaxy. The first mention of an open star cluster in M31 appears in Hubble's pioneering paper (Hubble, 1929). However, a great deal more attention has been paid to globular clusters in the past. Not only the GCs are generally brighter and less restricted to the complex stellar disk, but they are also more readily usable to answer certain questions about M31, such as its distance, mass, chemical abundance and chemical history. The early observations of the open clusters were obtained in the hope or thought that the clusters in question might be globular. Hodge (1979) used the Kitt Peak National Observatory (KPNO) 4 m telescope to search for true open clusters. His was a global search, covering

all of the M31 disk as it was recognized at that time. The result was a catalog of 403 candidate open clusters, which were primarily young objects, as implied by the fact that they usually appeared resolved on the plates. Subsequently, Hubble Space Telescope (HST) images of some of them show that the sample was contaminated by small OB association and asterisms (Williams & Hodge, 2001b). Three-color CCD photometry of a selection of the cataloged clusters was carried out by Hodge et al. (1987), showing that the clusters sampled are very young objects. However, the crowding and the faint magnitudes of these clusters required the characteristics of the HST to make reliable identifications and measurements. The most important recent papers are that of Barmby et al. (2001) who identified 20 probable M31 open clusters, that of Williams & Hodge (2001b) who found 79 small young star clusters and the two of Krienke & Hodge (2007, 2008) who identified 571 new disk clusters; these two surveys, using the WFPC2 and ACS on board of HST, scanned $\sim 4.9\%$ of the area of the M31 disk, suggesting that it should contain a large number of star clusters with a wide range of observable properties (luminosity, size, color) and a wide range of implied characteristics (mass, age, dynamical history). The luminosity function of the clusters identified in these papers shows a turnover at an absolute magnitude of $M_v = -3.0$ in the magnitude range $-1 \lesssim M_V \lesssim -9$ (see Figure 1.9). The integrated color-magnitude diagram shows a wide range in color for the
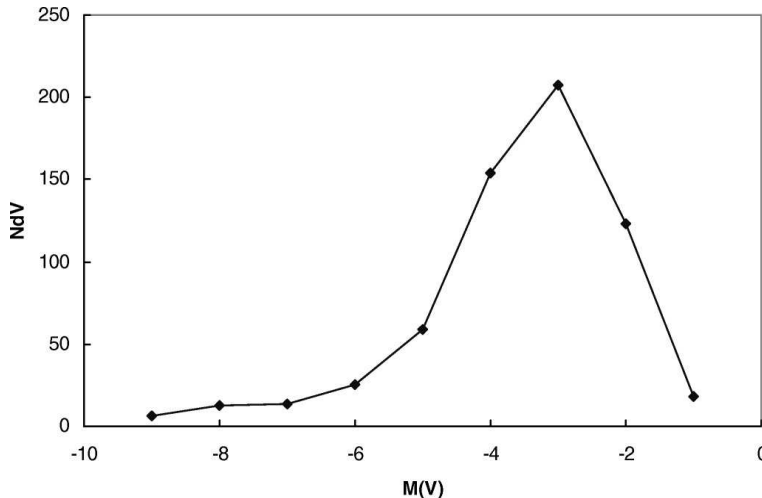
Figure 1.9: Integrated luminosity function of the M31 OCs studied in Krienke & Hodge (2007, 2008).

fainter clusters, representing a considerable range in age and reddening. The spatial distribution shows a maximum density in the range 8 to 15 Kpc and the cluster density is correlated with the distance from the nearest star-forming region. We refer the readers to these papers for a detailed discussion of these results. Chapter 6 of this thesis reports about 82 newly detected open (disk) clusters in M31, similar to those of Krienke & Hodge (2007, 2008).

1.2.3   Blue Luminous Compact Clusters: YMC in M31

Historical background. The presence in the disk of M31 of stellar systems similar to MW globulars in luminosity and shape but with integrated properties typical of young stellar populations is known since long time.

The peculiar colors of BLCCs have been previously reported by Vetesnik (1962),
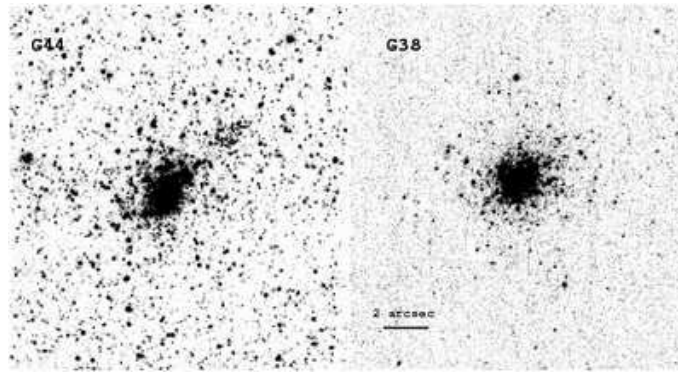
Figure 1.10: The BLCCs G38 and G44 from the HST-WFPC2 observations by Williams & Hodge (2001a).

van den Bergh (1967, 1969), Searle (1978), and this class of objects then received growing attention (Crampton et al., 1985; Cowley & Burstein, 1988; Elson & Walterbos, 1988; King & Lupton, 1991; Bohlin et al., 1993; Barmby et al., 2000; Williams & Hodge, 2001a; Beasley et al., 2004; Burstein et al., 2004), although a systematic study was still lacking.

In particular, Elson & Walterbos (1988) noted 14 such blue clusters, not included in the list of open cluster candidates by Hodge (1979), and better consistent with a GC morphology. Their absolute luminosities spanned the luminosity range $-9.5 < M_V < -6.5$, and their positions in a two-color diagram pointed to a possibly young age. For ten of these objects, King & Lupton (1991) provided supplementary UBVR photometry indicating a global luminosity around $3 \times 10^4 - 4 \times 10^5$ L$_\odot$. Based on stellar population models, their estimated age appeared to be less than a few 10^8 yrs, with a typical mass between 3×10^3 and 5×10^4 M$_\odot$. If confirmed, these values indicate that they are more massive than Galactic open clusters, but comparable to those of young, rich globulars found in the Large Magellanic Cloud (Elson & Fall, 1985; van den Bergh, 1991).

Bohlin et al. (1988, 1993), studying the UV-colors of a sample of 49 GC candidates in M31, listed 11 objects classified as blue clusters based on their location in the two-color diagram, and suggested that they are probably young. In the same line of investigation, Barmby et al. (2000) noted that their M31 catalog of GC candidates may be contaminated by several young objects with $B - V < 0.55$ and they eventually excluded 55 such objects from their analysis of old M31 clusters.

As already stressed long ago (Spinrad & Schweizer, 1972), the integrated spectrum and color of a cluster, especially in the blue, are influenced by the metal abundance and the position of the main sequence turnoff stars (MSTO) (in turn, by the cluster age), by the morphology of the horizontal branch (HB), and, to a lesser degree, by the overall luminosity function of its composing stellar population. To disentangle the different effects it is thus very important to obtain the color-magnitude distribution of the clusters. In this regard, Williams & Hodge (2001a) obtained deep HST photometry of individual stars and CMDs for four of these BLCCs leading to estimate ages in the range 60-160 Myr and metallicity from solar to 2/5 solar. This clearly supports the evidence that the exceedingly blue integrated colors of BLCCs are direct consequence of their remarkably young age.

Beasley et al. (2004) reached similar conclusions for eight BLCCs by comparing high-quality, low-resolution spectra of a sample of M31 clusters with similar data for
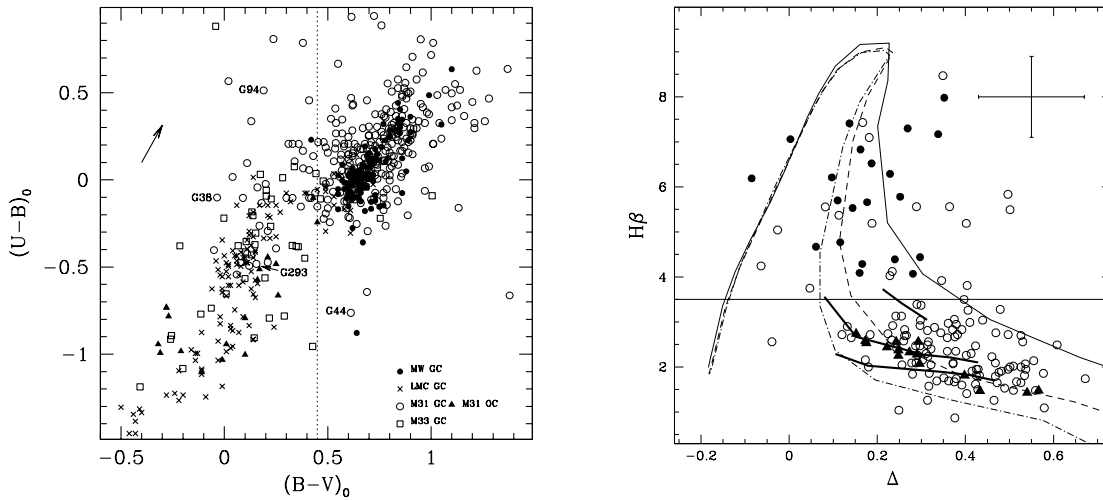
Figure 1.11: Left panel: Two-color diagram of globular clusters for Local Group galaxies. Data for M31 globulars are from the RBC (Galleti et al. 2004; open dots), those for the Milky Way are from Harris (1996; solid dots), LMC GCs are from van den Bergh (1981; crosses) and M33 data are from Chandar et al. (1999; squares). Also reported in the plot are the M31 open clusters from the Hodge (1979) catalog (solid triangles). All the data have been reddening-corrected assuming $E(B-V) = 0.11$ for M31, 0.13 for LMC and 0.07 for M33. MW globulars have been corrected according to Harris (1996). Vertical line marks the reference value $(B-V)_0 = 0.45$, adopted for BLCC selection. Labeled clusters are those observed by William & Hodge (2001) with HST. The arrow is a reddening vector for $E(B-V) = 0.1$ mag. Right panel: The M31 GC distribution in the $H\beta$ vs. Δ index plane. Reference curves for $\log g = 5$ stars of different temperature (from 5000 to 50 000 K) and metallicity ([Fe/H] from –2 to solar) are reported. Color-selected $((B-V)_o \leq 0.45)$ BLCCs are singled out (solid dots). The orizonthal line define the $H\beta = 3.5$ threshold for the BLCCs selection. For comparison, triangles show the Brodie & Hucra (1990) data for MW GCs, while thick solid lines are the locus for the Buzzoni (1989) SSP models with $t = 15$, 8 and 2 Gyr (in the sense of increasing $H\beta$), red HB morphology, and metallicity $[Fe/H] = -2.27 - +0.22$. Typical error bars for M31 data are reported top left.

MW and Magellanic Clouds globulars. Burstein et al. (2004) reported a global sample of 19 BLCCs in M31, including 13 "young" objects from the Barmby et al. (2000) list [3].

The Fusi Pecci et al. (2005) results. Fusi Pecci et al. (2005, hereafter F05) have studied the properties of a sample of 67 very blue and bright clusters in M31 extracted from the Revised Bologna Catalog, selected according to their color $[(B-V)_o \leq 0.45]$ and/or to the strength of their H_β spectral index ($H_\beta \geq 3.5$). F05 found that these clusters, that they termed *Blue Luminous Compact Clusters* (BLCCs), are fairly numerous in M31 (15% of the whole GC sample), they have positions and kinematics typical of *thin disk* objects, and, in spite of a GCs morfology (they are bright and compact objects) their colors and spectra strongly suggest that they have ages (significantly) lower than 2 Gyr (see Figures 1.10 and 1.11).

While the luminosity range spanned by BLCCs ($-6.5 \lesssim M_V \lesssim -10.0$) is comprised within that of ordinary globular clusters (see Figure 1.12), the age distribution of present-day MW globulars is obviously not consistent with the young age of BLCCs (200 Myr $\leq$ age $\leq$ 2 Gyr, as obtained from integrated colors and spectra). On the other hand, Galactic Open Clusters (OC) are comparably young but they appear

---

[3]Barmby et al. (2000) classified these clusters as possibly young because of the strong Balmer absorption lines observed in their high-resolution spectra.
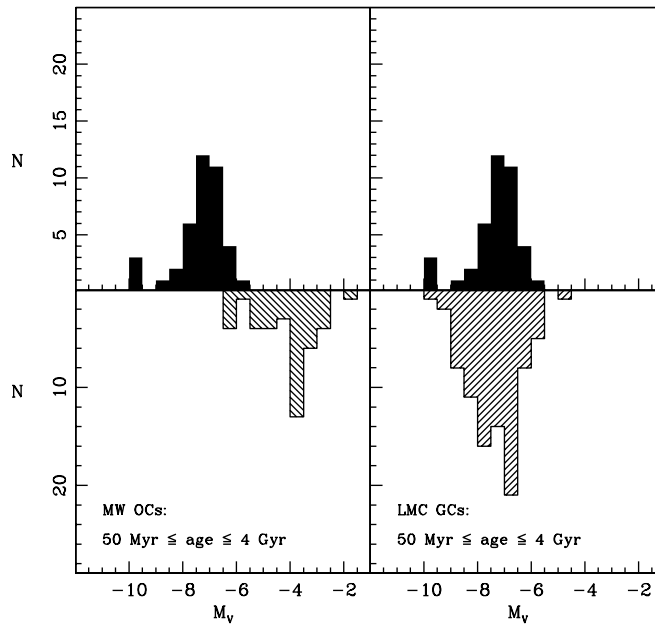
Figure 1.12: Comparison of the Luminosity Function (LF) of M31 BLCCs (filled histogram, upper panels) with: (left panel) the LF of the OC of the Milky Way in the same age range; (right panel) the LF of LMC globular clusters in the same age range.

less luminous than BLCCs (see Figure 1.12). The only Galactic OCs that reach the luminosity range covered by BLCCs are younger than 30 Myr (e.g., they are clusters whose luminosity budget is dominated by a few massive stars, much different from the BLCCs studied by Williams & Hodge (2001a) and showed in Figure 1.10). Conversely, the luminosity range spanned by M31 BLCCs is very similar to that covered by LMC YMCs (see Figure 1.12) and by the few MW YMCs recently identified in the direction of the Galactic center (see Section 1.1.1). Fusi Pecci et al. (2005, hereafter FP05) concluded that if most of the BLCCs have an age $\gtrsim 50 - 100$ Myr they are likely brighter/more massive than Galactic open clusters of similar ages, thus they should belong to a class of objects that is not present, in large numbers, in our own Galaxy. On the other hand, if BLCCs are younger than this, they should be interpreted as the counterparts of young open clusters of the Milky Way, since in this case their large brightness is essentially due to the young age and not to high masses. Unfortunately, the accuracy in the age estimates obtained from the integrated properties of the clusters is not sufficient to determine their actual nature on an individual basis, i.e., to compare their total luminosity with the luminosity distribution of OCs of similar age (see Bellazzini et al. 2008 and references therein). The color-magnitude diagram of individual stars is the only observational tool that can eventually establish the real nature of these objects on the basis of accurate age estimates.

An important question that arise from the FP05 work is how BLCCs would appear in the future, and in particular if they will look like classical globulars when they will become comparably old. FP05 made a tentative prevision using theoretical evolutionary models. If we assume BLCCs to consist of plain simple stellar populations (SSP), then one should expect their luminosity to fade with time, as far as the composing stellar population becomes older and photometrically
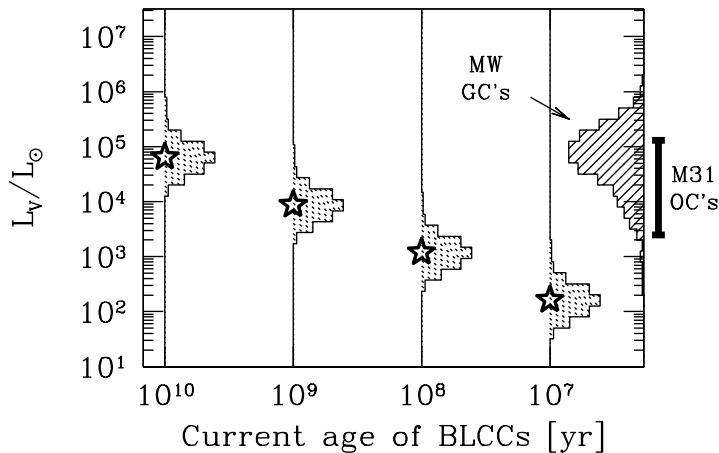
Figure 1.13: The effect of evolution on BLCC luminosity. The dotted histograms trace the expected BLCCs luminosity function as predicted at $t = 10$ Gyr, according to different values assumed for the *current* typical age of these objects (as labeled on the x axis). We assume a SSP evolution, according to Buzzoni (1989) synthesis models, for a Salpeter IMF and a (roughly) solar metallicity. For comparison, the observed luminosity distribution of MW GCs is reported on the right vertical axis, derived from Harris (1996) (shaded histogram), while the indicative luminosity range for M31 open clusters is also sketched (thick solid bar on the right) according to Hodge (1979).

dominated by low-mass stars. In particular, for a SSP of roughly solar metallicity and Salpeter IMF, evolutionary population synthesis models predict a quite tuned luminosity change such as $L_V \propto t^{-0.9}$ over a wide range of age (e.g. Tinsley & Gunn, 1976; Buzzoni, 1995a). According to the assumed age of present-day BLCCs, then one could infer the expected luminosity of these clusters at $t = 10$ Gyr and more consistently compare with the observed luminosity function of old MW GCs. The results of this illustrative exercise are summarized in Figure 1.13; it is evident from the figure that, in the more likely case of a current age in the range $10^8 - 10^9$ yrs, BLCCs would end up at 10^{10} yrs populating the low-luminosity (and low-mass) tail of current MW GC distribution. On the contrary, in the more extreme (and quite unlikely) case of a current age of only a few 10^7 yrs we would be left at 10 Gyr with extremely faint BLCCs, certainly out of the range of typical MW GCs. Finally, if nowadays BLCCs are already evolved systems (i.e. a few Gyr or older), then at $t = 10$ Gyr their expected luminosity will not change so much and their distribution would maintain them fully consistent with the bulk of both M31 open clusters and MW GCs. A fair assessment of the present-day age distribution of this kind of clusters is therefore a mandatory step to consistently locate them in the appropriate evolutionary framework.

The contamination problem. In addition to the question of the masses and ages of these BLCCs, it has been suggested that the BLCC samples in M31 may suffer from significant contamination by spurious sources. Cohen et al. (2006, hereafter C06) presented NIRC2@KeckII Laser Guide Star Adaptive Optics (LGSAO) images of six candidate BLCCs (see Figure 1.14). Their K' very-high spatial resolution images revealed that in the fields of four candidates there was no apparent cluster. This led C06 to the conclusion that some/many of the claimed BLCC may in fact be just *asterisms*, i.e. chance groupings of stars in the dense disk of M31. However, the use of the near infrared K' band (required by the LGSAO technique) may be largely

17

insensitive to very young clusters that are dominated by relatively few hot stars, which emit most of their light in the blue region of the spectrum. Hence, the imaging by C06 may be inappropriate to detect such young clusters (see, for example, the detailed discussion by Caldwell et al. (2009) and Figure 1.15). In any case, the study by C06 suggests that the true number of massive young clusters of M31 may have been overestimated.
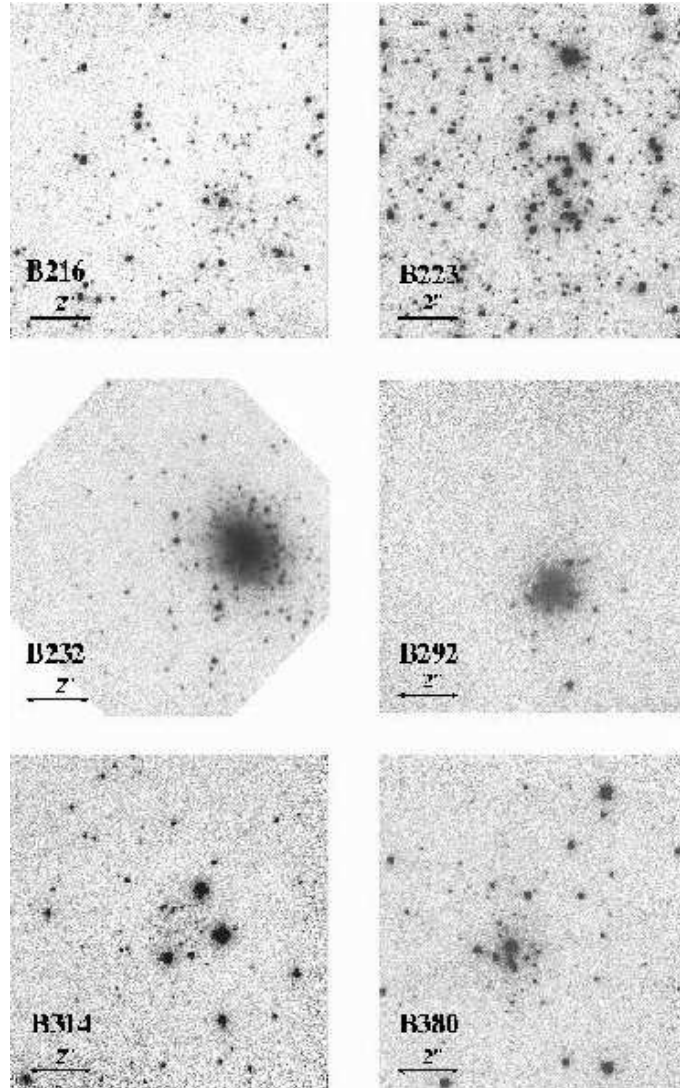
Figure 1.14: LGSAO K' images from the Keck Telescope are shown for 6 putative very young or young globular clusters in M31. The field shown for each is approximately 10 arcsec on a side with a pixel scale of 0.010 arcsec/pixel. (From Cohen et al. 2006).

Beyond FP05: an HST survey. The questions put forward by FP05 and C06 about the nature of BLCCs are the starting point of the main part of this thesis regarding the YMCs in M31.

In order to ascertain the real nature of the BLCCs studied by FP05 we have performed a survey with the Hubble Space Telescope (HST) to image 20 BLCCs in the disk of M31 (program GO-10818, P.I.: J. Cohen). The key aims of the survey are:

1. to check if the imaged targets are real clusters or asterisms, and to determine
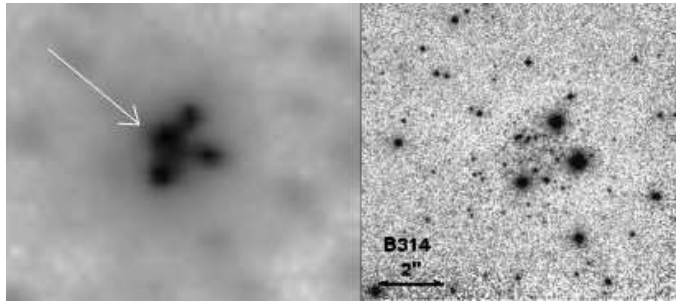
Figure 1.15: The disputed cluster B314-G037. The LGS I band image is shown on the left, next to the Cohen et al. (2005) LGSAO image, taken in the $K\prime$ band. The I band reveals the star cluster clearly (arrow). For young clusters, red supergiants would dominate the light at infrared wavelengths and the hotter mainsequence stars would appear much fainter. (From Caldwell et al. 2009).

the fraction of contamination of BLCCs by asterisms. The high resolution power of the WFPC2 allow us to clarify this point by the simple inspection of the images, in which the cluster population is resolved into stars.

2. to obtain an estimate of the age of each cluster from the color-magnitude distribution of the resolved stars in order to estimate the mass. The short exposure time of our images (400 s) is sufficient to clarify the nature of these young objects. Ultimately the survey aims to provide firm conclusions on the existence of a significant population of BLCCs (YMCs) in M31, in addition to OCs and GCs.
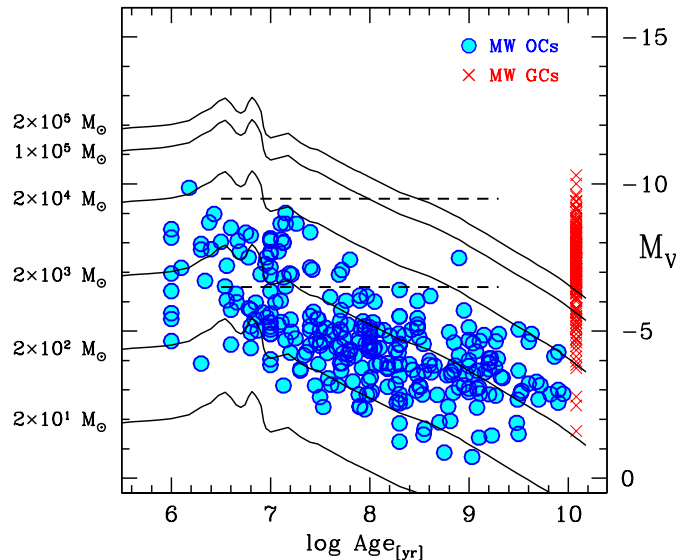
Figure 1.16: Integrated V mag and total mass as a function of age for Galactic OCs (from the WEBDA database) plotted as filled circles, and for Galactic GCs (M_V from Harris (2003); the ages have been arbitrarily assumed to be 12.0 Gyr for all the clusters) plotted as $\times$ symbols. The continuous lines are fixed-stellar-mass models from the set by Maraston (1998, 2005) for SSPs of solar metallicity, with a Salpeter's Initial Mass Function (IMF) and intermediate Horizontal Branch morphology. The two dashed lines enclose the luminosity range of BLCCs. The outlier OC at log Age≈ 9.0 is Tombaugh 1.

Figure 1.16 shows a fundamental diagnostic diagram largely used across this thesis (see Chapters 4 2, 3 and 4). In the plane M_v vs. Log Age we can compare

BLCCs with Galactic open clusters (blue circles; data taken from the WEBDA database[4]), with Galactic globular clusters (red crosses; from the latest version of Harris (1996) catalog assuming a uniform age of 12 Gyr, a reasonable approximation for our purpose), and with a grid of SSP models with solar metallicity and Salpeter's IMF from the set by Maraston[5] (continuous lines; Maraston (1998, 2005)). As a SSP ages massive stars die while the mass of the most luminous stars decreases (passive evolution). Keeping the total mass fixed, the luminosity of the population fades and, as a consequence, the stellar mass-to-light (M/L) ratio increases. The continuous lines plotted in Figure 1.16 describe the passive evolution of SSPs of various (stellar) masses: under the adopted assumptions the mass of a cluster of given age and M_V can be read from the grid of iso-mass tracks. The path of the track passing through the cluster shows what its luminosity will be in the future if the cluster did not lose stars through dynamical processes. The dotted lines enclose the BLCCs luminosity range ($-6.5 \lesssim M_V \lesssim -10.0$). With CMD-based ages we can plot the candidate BLCCs in the M_v vs. Log Age plane and estimate their mass. As claimed by FP05, if BLCCs have an age $\gtrsim 50 - 100$ Myr they are likely brighter/more massive than Galactic open clusters of similar ages, and following their passive evolutionary sequences they have the possibility, in the future, to become classical old GCs, if dynamical effects are ignored. As introduced in Section 1.1.2, the dynamical processes have a fundamental impact on the cluster evolution. The effects of these processes on the target clusters will be analysed in details in Chapters 3, 5 and 4.
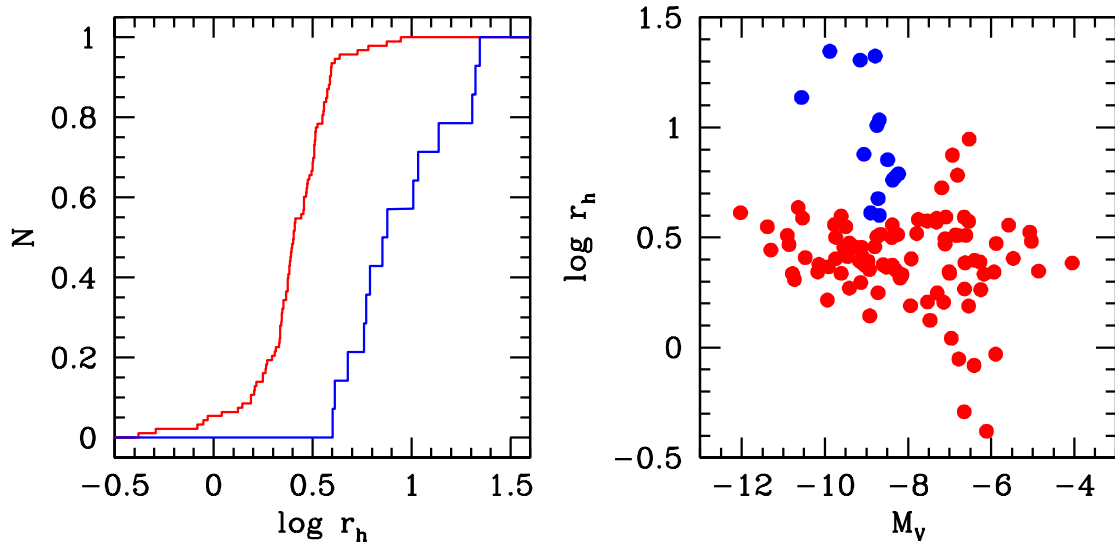
Figure 1.17: Left panel: half-light radius cumulative distributions of old globulars (red) and YMCs (blue). Right panel: Old globulars (black) and YMCs (blue) in the plane log r_h vs. M_V. Data are from Barmby et al. (2007, 2009).

1.3 Summary of contents

The various chapters of this thesis are grouped in three parts, which are summarized in Sections 1.3.1, 1.3.2 and 1.3.3.

---

[4]http://www.univie.ac.at/webda/integre.html
[5]http://www-astro.physics.ox.ac.uk/ maraston/

1.3.1 Part I: Young clusters in M31

The first part covers Chapters 2 - 6 of the thesis, and introduces an imaging survey of possible YMCs in M31 performed with the HST/WFPC2, with the main aim of estimating their age and their mass (see Section 1.2.3). In the various chapters the data will be analyzed under different aspects.

In Chapter 2 we introduce an useful diagnostic diagram: the log Age vs. integrated absolute magnitude (M_V) plane. This diagram, and its near-infrared version will be used in Chapter 3 and in Chapter 4 to estimate the mass of candidate YMCs in M31 and to compare them with Galactic OCs in the same age range.

In Chapter 3 the details of the data reduction pipeline adopted on the whole survey are presented and its application to the brightest among the targets, van den Bergh 0 (VdB0), taken as a test case, is described. The reddening, the age and the metallicity of the cluster were estimated by comparing the observed color magnitude diagram with theoretical isochrones. The stellar mass of VdB0 is also estimated by comparison with theoretical models. VdB0, with age $\simeq 25$ Myr and solar metallicity, is significantly brighter ($\gtrsim 1$ mag) than Galactic open clusters of similar age. Its present-day mass (in the range $\simeq 4 - 9 \times 10^4$ $M_\odot$), and half-light radius ($r_h = 7.4$ pc) are more typical of faint globular clusters than of open clusters. However, given its position within the disk of M31, it is expected to be destroyed by dynamical effects within the next ~ 4 Gyr.

In Chapter 4 we present the main results of the whole HST/WFPC2 survey. From the inspection of these high resolution images nineteen of the twenty surveyed candidates were confirmed to be real star clusters, while one turned out to be a bright star. Point spread function fitting photometry of individual stars was obtained for all the WFPC2 images of the targets, and the completeness of the final samples was estimated using extensive sets of artificial stars experiments. We present the color magnitude diagrams of the nineteen real clusters. The reddening, age, and metallicity of the clusters were estimated by comparing the observed CMDs and luminosity functions (LFs) with theoretical models. Stellar masses were estimated by comparison with theoretical models in the log Age *vs.* absolute integrated magnitude plane, using ages estimated from our CMDs and integrated J, H, K magnitudes from 2MASS-6X. Three of the clusters were found not to be good YMC candidates from newly available integrated spectroscopy and were in fact found to be old from their CMD. Of the remaining sixteen clusters, fourteen have ages between 25 Myr and 280 Myr, two have older ages than 500 Myr (lower limits). By including ten other YMC with HST photometry from the literature (see Section 1.3.2), we assembled a sample of twenty-five clusters younger than 1 Gyr, with mass ranging from $0.6 \times 10^4 M_\odot$ to $6 \times 10^4 M_\odot$, with an average of $\sim 3 \times 10^4 M_\odot$. In spite of the similar mass, the surveyed YMCs appear less compact than ordinary globulars (see Figure 1.17.) The clusters considered here have masses significantly higher than Galactic open clusters in the same age range. Our analysis indicates that YMCs are relatively common in all the largest star-forming galaxies of the Local Group, while the lack of known YMC older than 20 Myr in the Milky Way may stem from selection effects.

In Chapter 5 surface brightness profiles for the nineteen target clusters (plus a few other from litterature) were measured using our HST/WFPC2 images, and fit to two types of models to determine the clusters' structural properties. The target clusters have mass ($\sim 10^{4.5}$ $M_\odot$), median half-light radius 7 pc and dissolution times of a few Gyr. YMCs in M31, in the MCs and in the MW fall approximately on the

same age-size relation. The young M31 clusters are expected to dissolve within a few Gyr and will not survive to become old, globular clusters. However, they do appear to follow the same fundamental plane relations as old clusters.

In Chapter 6 we report on the properties of 89 low-mass star clusters identified in the surroundings of the main targets within the survey images. Eighty-two of the clusters are newly detected. We have determined their integrated magnitudes and colors, and raw age estimates are provided. For the clusters for which a riliable color-magnitude diagram has been obtained we have provided also ages from isochrone-fitting. The age distribution shows a steep decline of number with age, with a large decrease in number per age interval between the youngest and the oldest clusters detected.

1.3.2 Part II: Old globular clusters in M31

The second part covers Chapter 7 of the thesis.

In Chapter 7 with the aim of increasing the sample of M31 clusters for which a colour-magnitude diagram is available, we searched the HST archive for ACS images containing objects included in the Revised Bologna Catalogue of M31 globular clusters (RBC). Sixty-three such objects were found. We used the ACS images to confirm or revise their classification and we were able to obtain useful CMDs for 11 old globular clusters and 6 luminous young clusters. We obtained simultaneous estimates of the distance, reddening, and metallicity of old clusters by comparing their observed field-decontaminated CMDs with a grid of template clusters of the Milky Way. We estimated the age of the young clusters by fitting with theoretical isochrones. For the old clusters, we found metallicities in the range $-0.4 \leq$[Fe/H]$\leq$ -1.9. At least four of them display a clear blue horizontal branch, indicating ages $\gtrsim 10$ Gyr. All six candidate young clusters are found to have ages < 1 Gyr and are included in the analysis of the main survey of candidate YMCs. With the present work and with the star clusters of the main survey, the total number of M31 GCs with reliable optical CMD increases from 35 to 48 for the old clusters, and from 7 to 27 for the young ones. The old clusters show similar characteristics to those of the MW. We discuss the case of the cluster B407, with a metallicity [Fe/H]$\simeq -0.6$ and located at a large projected distance from the centre of M31 ($R_p = 19.8$ kpc) and from the major axis of the galaxy ($Y= 11.3$ kpc). Metal-rich globulars at large galactocentric distances are rare both in M31 and in the Milky Way. B407, in addition, has a velocity in stark contrast with the rotation pattern shared by the bulk of M31 clusters of similar metallicity. This, along with other empirical evidence, supports the hypothesis that the cluster (together with B403) is physically associated with a substructure in the halo of M31 that has been interpreted as the relic of a merging event.

1.3.3 Part III: NGC 205

The third part of the thesis (Chapter 8) report on the analysis of the star formation history in NGC 205, one of the brightest M31 satellites. NGC 205 is a peculiar dwarf elliptical galaxy hosting in its center a population of young blue stars. Their origin is still matter of debate, the central fresh star formation activity possibly being related to dynamical interactions between NGC 205 and M31.

In Chapter 8 the star formation history in the central $30''$ (~ 120 pc) around the NGC 205 central nucleus is investigated in order to obtain clues to the origin of the

young stellar population. New deep HST ACS/HRC photometry is compared with theoretical isochrones and luminosity functions to characterize the stellar content of the region under study and compute the recent SF rate. Our photometry reveals a previously undetected blue plume of young stars clearly distinguishable down to I 26. Our analysis suggests that $1.9 \times 10^5 M_\odot$ were produced between approximately 62 Myr and 335 Myr ago in the inner regions of NGC 205, with a latest minor episode occurring ~ 25 Myr ago. This implies a star formation rate of $\sim 7 \times 10^{-4} M_\odot/yr$ over this period. The excellent fit of the observed luminosity function of young main sequence stars obtained with a model having a constant star formation rate argues against a tidally triggered star formation activity over the last ~ 300 Myr.

1.4 Publications

1. Perina, S.; Barmby, P.; Beasley, M. A.; Bellazzini, M.; Brodie, J. P.; Burstein, D.; Cohen, J. G.; Federici, L.; Fusi Pecci, F.; Galleti, S.; Hodge, P.W.; Huchra, J.P.; Kissler-Patig, M.; Puzia, T.H.; Strader, J. 2009. A&A 494, 933-948. *An HST/WFPC2 survey of bright young cluster in M31. I. VDB0, a massive cluster seen at t ~ 25 Myr.*

2. Hodge, P. W.; Krienke, O. K.; Bellazzini, M.; Perina, S.; Barmby, P.; Cohen, J. G.; Puzia, T. H.; Strader, J. 2009; AJ 138, 770-779. *An HST/WFPC2 survey of bright young cluster in M31. II. Photometry of less luminous clusters in the fields.*

3. Barmby, P.; Perina, S.; Bellazzini, M.; Cohen, J. G.; Hodge, P. W.; Huchra, J. P.; Kissler-Patig, M.; Puzia, T. H.; Strader, J. 2002; AJ 138, 1667-1680. *An HST/WFPC2 survey of bright young cluster in M31.III. Structural Parameters.*

4. Perina, S.; Barmby, P.; Beasley, M. A.; Bellazzini, M.; Brodie, J. P.; Burstein, D.; Cohen, J. G.; Federici, L.; Fusi Pecci, F.; Galleti, S.; Hodge, P.W.; Huchra, J.P.; Kissler-Patig, M.; Puzia, T.H.; Strader, J. 2010; A&A 511, A23. *An HST/WFPC2 survey of bright young cluster in M31. IV. Ages and mass estimates.*

5. Bellazzini, M.; Perina, S.; Galleti, S.; Federici, L.; Buzzoni, A.; Fusi Pecci, F. 2008; MmSAI 79, 663. *Clusters in the log Age vs. M_V plane.*

6. Perina, S.; Federici, L.; Bellazzini, M.; Cacciari, C.; Fusi Pecci, F.; Galleti, S. 2009; A&A, 507, 1375-1392. *HST/ACS colour-magnitude diagrams of M31 globular clusters.*

7. Monaco, L.; Saviane, I.; Perina, S.; Bellazzini, M.; Buzzoni, A.; Federici, L.; Fusi Pecci, F.; Galleti, S. 2009; A&A 502, L9-L12. *Young stellar population at the center of NGC 205.*

24

2

Open Clusters in the log Age vs. M_V plane.

M. Bellazzini, S. Perina, S. Galleti, L. Federici, A. Buzzoni & F. Fusi Pecci

Abstract

In the log Age vs. integrated absolute magnitude (M_V) plane, the open clusters of the Milky Way form a well-defined band parallel to theoretical sequences decribing the passive evolution of Simple Stellar Populations and display a pretty sharp upper threshold in mass ($M \sim 2 \times 10^4 \ M_\odot$) over a 4 dex range of ages.

2.1 Introduction

The evolution of integrated spectro-photometric properties of a Simple Stellar Population (SSP, i.e. an idealized population of stars having the same chemical composition and the same age, Renzini & Fusi Pecci 1988) is one key prediction of stellar theoretical models (see, for example Buzzoni 1989; Maraston 1998 and references therein). In particular, it is well known that the total luminosity of a SSP must decrease with time as massive stars progressively exhaust their nuclear fuel and conclude their evolutionary lifetime, thus ceasing to contribute to the luminosity of the SSP.

In Fig. 2.1 we show various theoretical evolutionary sequences describing the fading with age of SPSSs (from Maraston, 1998, 2005), in the plane of the logarithm of the SSP age versus its integrated absolute V magnitude (M_V), hereafter A-M_V diagram, for brevity (see Gieles et al. 2007; Whitmore et al. 2007 and references therein, for the application of this or similar diagrams to the study of star clusters in different environments). It can be appreciated that (i) for ages $> 10^7$ yr the evolutionary sequences are essentially linear ($M_V \propto 1.8 \times \log Age_{[yr]}$, with $a \simeq 1.8$), and, (ii) the sequences depends quite weakly on the assumed metallicity and/or Initial
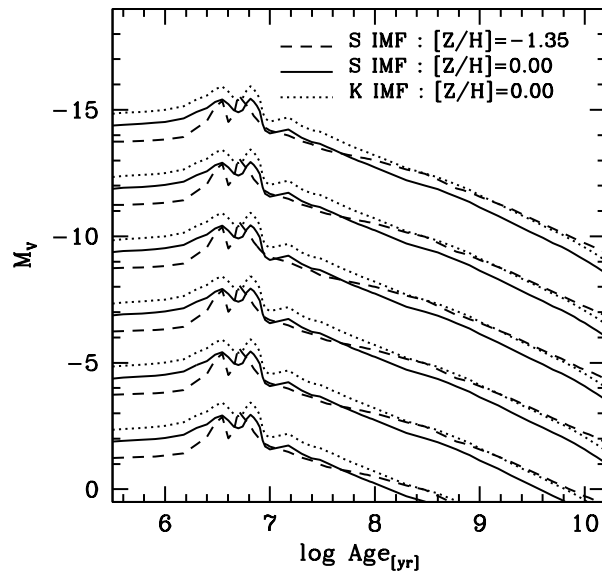
Figure 2.1: Passive evolutionary sequences for SSPs of different metallicities ([Z/H]) and IMFs (S = Salpeter; K = Kroupa, see Kroupa 2001), from Maraston (1998, 2005). Each bundle of three sequences correspond to a given total mass.

Mass Function (IMF) of the SSP. Once a metallicity and a form of the IMF are assumed, each sequence directly correspond to a total stellar mass; thus the mass of *real* SSPs can be compared in this plane independently of their respective age. Moreover, the past and future evolution of such SSPs can be directly read on this diagram. Given the weak dependence on age and IMF, in the following we will adopt a grid of solar metallicity / Salpeter-IMF sequences. These define a total-stellar-mass scale whose zero point may be uncertain up to a factor of a few, while *mass differences* should be pretty reliable and *homogeneous*. Star clusters are the best approximation of SSPs available in nature. Classical Globular Clusters (GC) are all very old and should lie in a narrow slice of the A-M_V diagram. Here, for simplicity, we adopt Age = 12 Gyr (Gratton et al., 1997) for all the Galactic GCs, for which we took M_V from Harris (1996). On the other hand, Galactic Open Clusters (OC) are known to span a large range in ages (from millions to billions years). For their sparse nature, it is quite hard to obtain reliable integrated properties of OCs; nevertheless the WEBDA database[1] collects also OC M_V from many different sources and, in general, the agreement between independent estimates is reassuringly good. We extracted, from WEBDA, ages and M_V for 293 OCs, taking the M_V estimates from Lata (2002), Battinelli et al. (1994), Spassova et al. (1985), Pandey et al. (1989), and Sagar et al. (1991), in order of preference.

In Fig. 2.2 Galactic OCs are compared to GCs and to stars cluster of the Large Magellanic Cloud (data from van den Bergh (1981), treated as in Fusi Pecci et al. (2005)), in the A-M_V diagram. It is interesting to note that OCs form a well defined band, parallel to the evolutionary sequences and approximately comprised between $M \simeq 5 \times 10^1$ $M_\odot$ and $M \simeq 2 \times 10^4$ $M_\odot$. The different distribution of LMC clusters demonstrate that the occurrence of a mass threshold is not universal, but it is likely associated with the particular environment in which clusters formed. A thorough discussion of the mechanisms that shape the distribution of cluster populations in this plane can be found in Whitmore et al. (2007), see also references therein.

Fig. 2.2 also recalls that OCs and GCs have two well separated mass distributions; while the difference in mean mass is obviously not a surprise, the bimodality of the mass distribution of Galactic star clusters as a whole (OC+GC) is far from trivial (see Fig. 2.3, and van den Bergh & Lafontaine 1984). Finally, it is interesting to note that, at the

---

[1]www.univie.ac.at/webda/
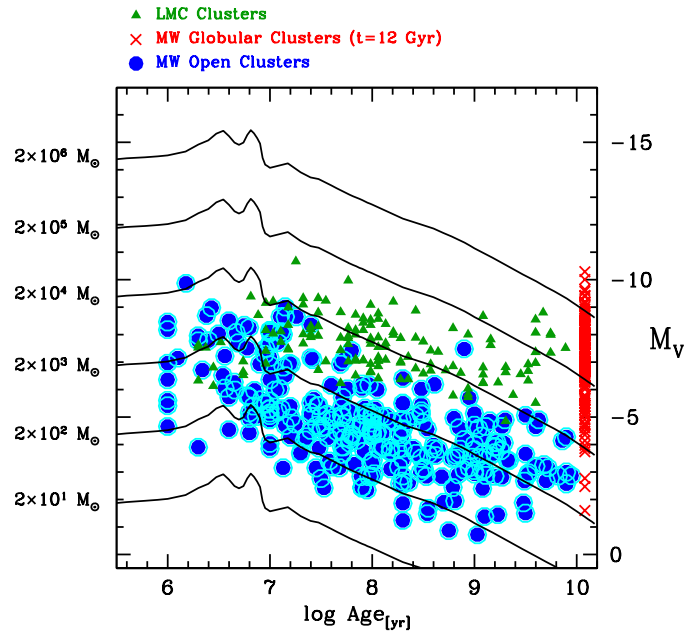
Figure 2.2: Galactic GCs and OCs and LMC clusters in the A-M_V plane. The passive-evolution sequences are for solar metallicity and Salpeter's IMF (from Maraston, 1998, 2005). The only OC clearly exceeding the 2×10^4 $M_\odot$ threshold is Tombaugh 2, around log Age ~ 9.
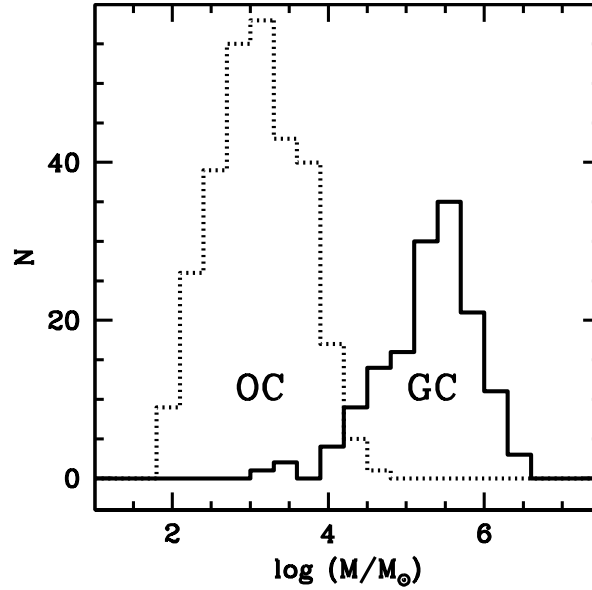
Figure 2.3: Mass distribution of Galactic OCs and GCs, from interpolation on the theoretical grid of Fig. 2.2.

dawn of the Galactic era, the progenitors of GCs had luminosities typical of dwarf galaxies ($-10 \leq M_V \leq -15$, approximately).

3

An HST/WFPC2 survey of bright young clusters in M31. I. VdB0 a massive star cluster seen at t≃ 25 Myr

S. Perina, P. Barmby, M.A. Beasley, M. Bellazzini, J.P. Brodie, D. Burstein, J.G. Cohen, L. Federici, F. Fusi Pecci, S. Galleti, P.W. Hodge, J.P. Huchra, M. Kissler-Patig, T.H. Puzia, & J. Strader

Abstract

We introduce our imaging survey of possible young massive globular clusters in M31 performed with the Wide Field and Planetary Camera 2 (WFPC2) on the Hubble Space Telescope (HST). We obtained shallow (to B~ 25) photometry of individual stars in 20 candidate clusters. We present here details of the data reduction pipeline that is being applied to all the survey data and describe its application to the brightest among our targets, van den Bergh 0 (VdB0), taken as a test case.

Point spread function fitting photometry of individual stars was obtained for all the WFPC2 images of VdB0 and the completeness of the final samples was estimated using an extensive set of artificial stars experiments. The reddening, the age and the metallicity of the cluster were estimated by comparing the observed color magnitude diagram (CMD) with theoretical isochrones. Structural parameters were obtained from model-fitting to the intensity profiles measured within circular apertures on the WFPC2 images.

Under the most conservative assumptions, the stellar mass of VdB0 is $M > 2.4 \times 10^4\ M_\odot$, but our best estimates lie in the range $\simeq 4 - 9 \times 10^4\ M_\odot$. The CMD of VdB0 is best reproduced by models having solar metallicity and age $\simeq 25$ Myr. Ages less than $\simeq 12$ Myr and greater than $\simeq 60$ Myr are clearly ruled out by the available data. The cluster has a remarkable number of red super giants ($\gtrsim 18$) and a CMD very similar to Large Magellanic Cloud clusters usually classified as young globulars such as NGC 1850, for example.

VdB0 is significantly brighter ($\gtrsim 1$ mag) than Galactic open clusters of similar age. Its present-day mass and half-light radius ($r_h = 7.4$ pc) are more typical of faint globular clusters

than of open clusters. However, given its position within the disk of M31, it is expected to be destroyed by dynamical effects, in particular by encounters with giant molecular clouds, within the next ~ 4 Gyr.

3.1 Introduction

Much of the star formation in the Milky Way is thought to have occurred within star clusters (Lada et al. 1991; Carpenter et al. 2000). Therefore, understanding the formation and evolution of star clusters is an important piece of the galaxy formation puzzle. Our understanding of the star cluster systems of spiral galaxies has largely come from studies of the Milky Way. Star clusters in our Galaxy have traditionally been separated into two varieties, open and globular clusters (OCs and GCs hereafter). OCs are conventionally regarded as young ($< 10^{10}$ yr), low-mass ($< 10^4 M_\odot$) and metal-rich systems that reside in the Galactic disk. In contrast, GCs are characterized as old, massive systems. In the Milky Way, GCs can be broadly separated into two components: a metal-rich disk/bulge subpopulation, and a spatially extended, metal-poor halo subsystem (Kinman 1959, Zinn 1985; see also Brodie & Strader 2006; Harris 2001), for general reviews of GCs).

However, the distinction between OCs and GCs has become increasingly blurred. For example, some OCs are sufficiently luminous and old to be confused with GCs (e.g., Phelps & Schick 2003). Similarly, some GCs are very low-luminosity systems (e.g., Koposov et al. 2007) and at least one has an age that is consistent with the OC age distribution (Palomar 1; Sarajedini et al. 2007a). Moreover, a third category of star cluster, "young massive clusters" (YMCs) are observed to exist in both merging (e.g., Whitmore & Schweizer 1995) and quiescent galaxies (Larsen & Richtler 1999), Indeed, YMCs have been known to exist in the Large Magellanic Cloud for over half a century (Hodge 1961). These objects are significantly more luminous than OCs ($M_V \lesssim -8$ up to $M_V \sim -15$), making them promising candidate young GCs. Once thought to be absent in the Milky Way, recent observations suggest that their census may be quite incomplete, as some prominent cases have been found recently in the Galaxy as well (Clark et al. 2005; Figer 2008).

Thus, a picture has emerged that, rather than representing distinct entities, OCs, YMCs and GCs may represent regions within a continuum of cluster properties dependent upon local galaxy conditions (Larsen 2003). The lifetime of a star cluster is dependent upon its mass and environment. Most low-mass star clusters in disks are rapidly disrupted via interactions with giant molecular clouds (Lamers & Gieles 2006; Gieles et al. 2007). These disrupted star clusters are thought to be the origin of much of the present field star populations (Lada & Lada 2003). Surviving disk clusters may then be regarded as OCs or YMCs, depending upon their mass. Star clusters in the halo may survive longer since they are subjected to the more gradual dynamical processes of two-body relaxation and evaporation. The clusters which survive for an Hubble time – more likely to occur away from the disk – are termed GCs (see also Krienke & Hodge 2007). To date, no known *thin* disk GCs have been identified in the Milky Way.

After the Milky Way, M31 is the prime target for expanding our knowledge of cluster systems in spirals. However, our present state of knowledge about the M31 cluster system is far from complete. Similar to the Milky Way, M31 appears to have at least two GC subpopulations; a metal-rich, spatially concentrated subpopulation of GCs and a more metal-poor, spatially extended GC subpopulation (Huchra et al. 1991); Barmby et al. 2000). Also, again similar to the Milky Way GCs, the metal-rich GCs in M31 rotate and show "bulge-like" kinematics (Perrett et al. 2002). However, unlike the case in the Milky Way, the metal-poor GCs also show significant rotation (Huchra et al. 1991; Perrett et al. 2002, Lee et al. 2008). Using the Perrett et al. (2002) data, Morrison et al. (2004) identified what appeared to be a *thin* disk population of GCs, constituting some 27% of the Perrett et al. (2002) sample. Subsequently, it has been shown that at least a subset of these objects are in fact young (≤ 1

Gyr), metal-rich star clusters rather than old "classical" GCs (Beasley et al. 2004; Burstein et al. 2004; Fusi Pecci et al. 2005; Puzia et al. 2005).

Fusi Pecci et al. (2005; hereafter F05) presented a comprehensive study of bright young disk clusters in M31, selected from the Revised Bologna Catalogue[1] (RBC, Galleti et al. 2004) by color [$(B-V)_0 \leq 0.45$] or by the strength of the $H\beta$ line in their spectra ($H\beta \geq 3.5$Å). While these clusters have been noted since Vetesnik (1962) and have been studied by various authors, a systematic study was lacking. F05 found that these clusters, that they termed – to add to the growing menagerie of star cluster species – "Blue Luminous Compact Clusters" (BLCCs), are fairly numerous in M31 (15% of the whole GC sample), they have positions and kinematics typical of *thin disk* objects, and their colors and spectra strongly suggest that they have ages (significantly) less than 2 Gyr.

Since they are quite bright ($-6.5 \lesssim M_V \lesssim -10.0$) and – at least in some cases – morphologically similar to old GCs (see Williams & Hodge 2001a, hereafter WH01), BLCCs could be regarded as YMCs, that is to say, candidate young globular clusters. In particular, F05 concluded that if most of the BLCCs have an age $\gtrsim 50-100$ Myr they are likely brighter than Galactic Open Clusters (OC) of similar ages, thus they should belong to a class of objects that is not present, in large numbers, in our own Galaxy. Unfortunately, the accuracy in the age estimates obtained from the integrated properties of the clusters is not sufficient to determine their actual nature on an individual basis, i.e., to compare their total luminosity with the luminosity distribution of OCs of similar age (see Bellazzini et al. 2008 and references therein).

In addition to the question of the masses and ages of these BLCCs, it has become clear that the BLCC photometric and spectroscopic samples in M31 may suffer from significant contamination. Cohen, Matthews & Cameron 2006, hereafter C06) presented NIRC2@KeckII Laser Guide Star Adaptive Optics (LGSAO) images of six candidate BLCCs. Their K' very-high spatial resolution images revealed that in the fields of four of the candidates there was no apparent cluster. This lead C06 to the conclusion that some/many of the claimed BLCC may in fact be just *asterisms*, i.e. chance groupings of stars in the dense disk of M31. While the use of the near infrared K' band (required by the LGSAO technique) may be largely insensitive to very young clusters that are dominated by relatively few hot stars, which emit most of the light in the blue region of the spectrum, the inference is that the true number of massive young clusters of M31 may have been severely overestimated.

Therefore, in order to ascertain the real nature of these BLCCs we have performed an HST survey to image 20 BLCCs in the disk of M31 (program GO-10818, P.I.: J. Cohen). The key aims of the survey are:

1. to check if the imaged targets are real clusters or asterisms, and to determine the fraction of contamination of BLCCs by asterisms;

2. to obtain an estimate of the age of each cluster in order to verify whether it is brighter than Galactic OCs of similar age. Ultimately the survey aims to provide firm conclusions on the existence of BLCCs (YMCs) in M31 as a distinct class of object with respect to OCs (see Krienke & Hodge 2007, 2008, and references therein).

In the present contribution we describe the data reduction and analysis strategies that we will apply to our cluster sample to estimate their ages and metallicities. The overall procedure is described using the brightest among the observed clusters, VdB0, as a specific case. We conclude this section with a brief presentation of the cluster VdB0, below.

The present paper is organized as follows. The observations and the data reduction procedure are described in detail in Sect. 2; the principal assumptions that will be adopted in the whole survey are also reported in this section. Sect. 3 is devoted to the analysis of the surface brightness profile and of the Color Magnitude Diagram of VdB0, including total luminosity, age and metallicity estimates. In Sect. 4 our main results are briefly summarized and discussed.

---

[1]www.bo.astro.it/M31

Table 3.1: Positional and Photometric parameters for VdB0 from the RBC[a]

NAME	alt NAME	RA$_{J2000}$	Dec$_{J2000}$	X	Y	U	B	V	R	J	H	K
VdB0	B195D[b]	00:40:29.3	+40:36:14.7	-47.2′	-4.3′	14.97	15.31	15.06	14.92	13.77	13.14	12.99

[a] X and Y are projected coordinates in the direction along (increasing Eastward) and perpendicular to the major axis of M31 (increasing Northward) respectively, in arcmin, see Galleti et al. 2004, and references therein.

[b] see Sect. 2.5.
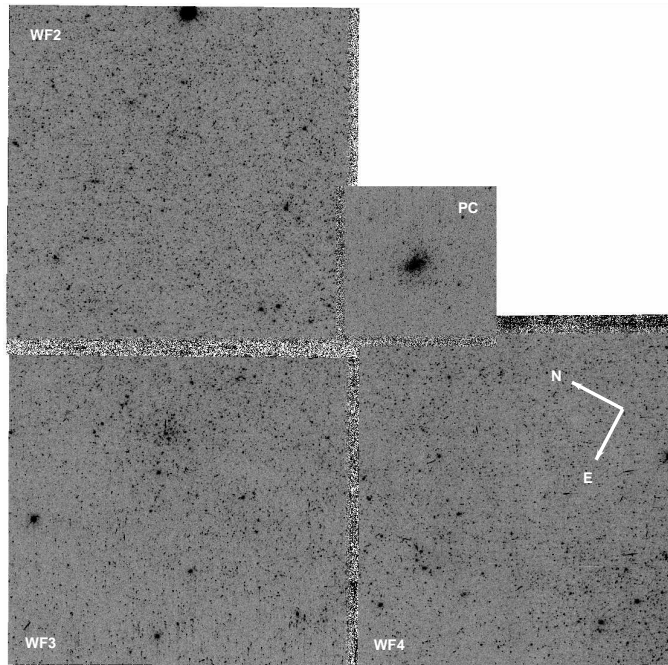
Figure 3.1: F450W mosaic of the whole field sampled by our WFPC2 observations. The cluster VdB0 is at the center of the PC camera.
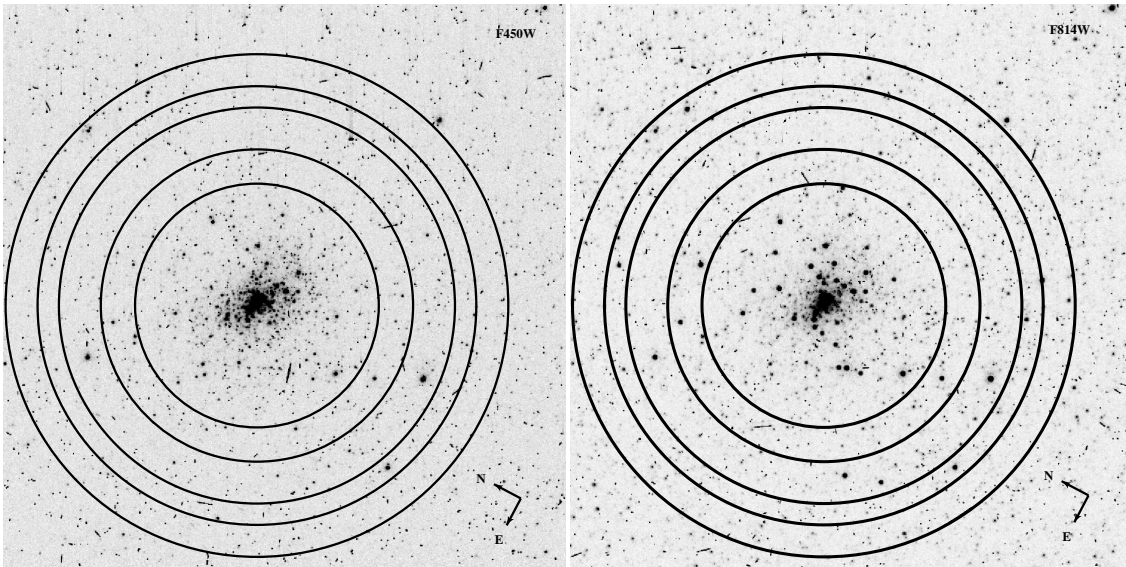
Figure 3.2: F450W (upper panel) and F814W (lower panel) images of the whole PC camera, with VdB0 at the center. The superposed circles have radius r=160, 205, 260, 288 and 330 pixels, from inside out, and mark the edges of the annuli whose CMDs are shown in Fig. 3.9, below. The light stripes associated with stars in the F450W image are due to the effect of CTE that is particularly strong in this shallow low-background image.

3.1.1 The cluster van den Bergh 0 (VdB0)

VdB0 was indicated as an open cluster by Hubble (1936) in the image on the frontispiece of his book *The Realm of the Nebulae*[2]. van den Bergh (1969) presents VdB0 as the brightest open cluster of M31, reporting an integrated spectral type A0. He also notes that the cluster contains the Cepheid variable V40 (Hubble 1929). A check of Hubble's (1929) finding charts revealed that two sources are labeled # 40 in his plate VII: one of them seems indeed associated with the cluster, while the other is $\sim 8'$ away from VdB0, near the association OB78 = NGC 206 (van den Bergh 1964; see also Hodge 1979). The cluster was re-discovered by Hodge 1979, who classified it as an open cluster (C107, see also Hodge 1981). Finally, Battistini et al. (1987) listed the cluster as their class D candidate globular cluster number 195 (B195D in the RBC). The failure to identify B195D with VdB0 was due to the fact that the coordinates provided by van den Bergh (1969) were in error by $\simeq 17''$. For this reason VdB0 and B195D survived as independent entries in M31 GC catalogues until the present day. In our survey we imaged both the clusters and the WFPC2 images revealed unequivocally that the two targets are in fact the same cluster. In particular the images intended to observe B195D have the cluster in the center of the PC camera while in the VdB0 images the cluster lie in the corner of the PC opposite to the WF cameras, such that part of the cluster is out of the image. In the following (and in the future) we will refer to the cluster as VdB0. The dataset analysed here is the one with the cluster centered on the PC images, hence the actual label in the header of the fits files is B195D.

VdB0 is located at a projected distance of $R_p = 10.8$ kpc from the center of M31 to the South-West, just $\sim 4'$ from the major axis of the galaxy (see Tab. 4.1), near the edge of one of the most prominent substructures of the M31 disk, the so called *10 kpc ring* (see Hodge 1992 and Barmby et al. 2006, and references therein) and within a the large OB association OB80 (van den Bergh 1964, A80 in Hodge (1981 atlas). Its radial velocity ($V_r = -567$ km/s, Perrett et al. 2002) is in full agreement with the rotation curve of the HI disk of M31 (Carignan et al. 2006), thus confirming the physical association with the thin disk of the parent galaxy (F05). The strong value of the H_β index supports the idea that the cluster is younger than 1 Gyr

---

[2]S. van den Bergh kindly drove our attention to this curious occurrence.

($H_\beta = 4.3$, Perrett et al. 2002[3]). The existing estimates of both V_r and H_β are nicely confirmed by recent high signal-to-noise spectra acquired at the Italian Telescopio Nazionale Galileo (S. Galleti, private communication).

With the assumed reddening and distance, the integrated V magnitude reported in the RBC (see Tab. 4.1) gives an absolute magnitude $M_V = -10.03$, much brighter than any Galactic open cluster older than 10 Myr (see Bellazzini et al. 2008, and below); it appears quite extended and irregular in shape even in ground based images. In these ways VdB0 stands out among the members of our candidate BLCC sample that are, in general, fainter and more compact than it.

3.2   Observations and Data Reduction

Our survey was originally planned for the Advanced Camera for Surveys (ACS) but it was performed with the Wide Field and Planetary Camera 2 (WFPC2) during cycle 16 because of the failure of ACS. For each target of our survey we acquired two F450W and two F814W images, all with 400 s exposure time and gain $= 7e^-/DN$. The pointings were chosen to place the main target at the center of the PC ($800 \times 800\ px^2$, with pixel scale 0.045 arcsec/px), while the three WF cameras ($800 \times 800\ px^2$, with 0.099 arcsec/px) are supposed to sample the surrounding fields. The images of VdB0 discussed here were acquired on July 2, 2007. The image of the whole WFPC2 mosaic image is shown in Fig. 1. It is clear that there are substructures and density gradients on the scale of the whole mosaic image, mainly due to the inclusion of the edges of the large stellar association embedding the cluster (A80, Hodge 1981). As the overall stellar density on the WF2 field is larger than in WF3 and WF4, we make the conservative choice to adopt the WF2 as our preferred sample of the background population that is expected to contaminate the Color Magnitude Diagram of the cluster, while we will consider the average density over all the WF fields when we will compute stellar density profiles based on star counts (Sect. 3). In the present context, when we speak of "background population" we refer to all the stars belonging to the field of M31 but unrelated to the cluster we are studying. Zoomed views of the PC field in both F450W and F814W passbands are shown in Fig. 3.2.

As the observational material and the degree of crowding are essentially the same for all the surveyed fields, we tuned our data-reduction strategy to be exactly the same in all cases, to maintain the highest degree of homogeneity in the final products of the survey. Data reduction has been performed on the pre-reduced images provided by STScI, using HSTPHOT[4] (Dolphin 2000a), a Point Spread Function -fitting package specifically devoted to the photometry of WFPC2 data. The package identifies the sources above a fixed flux threshold on a stacked image and performs photometry on individual frames, and automatically applies the correction for the Charge Transfer Efficiency (CTE, Dolphin 2000b). It then transforms instrumental magnitude to the VEGAMAG system (see Holtzman et al. (1995) and Dolphin (2000b), deals with cosmic-ray hits, and takes also into account all the information about image defects that is attached to the observational material. We fixed the threshold for the search of sources on the images at 3 σ above the background. HSTPHOT provides as output the magnitudes and positions of the detected sources, as well as a number of quality parameters for a suitable sample selection, in view of the actual scientific objective one has in mind. Here we selected all the sources having valid magnitude measurements in both passbands, global quality flag = 1 (i.e., best measured stars), *crowding* parameter < 0.3, $\chi^2 < 2.0$ and $-0.5 < sharp < 0.5$, in both passbands, (see Dolphin 2000a for details on the parameters). This selection cleans the sample from the vast majority of spurious and/or

---

[3]Note that Perret's et al. measures refers to B195D, i.e. the "alter ego" of VdB0 whose available coordinates were the most appropriate for the cluster. In this context, it is interesting to note that, adopting a calibration based on old GCs, Perrett et al. found [Fe/H]=-1.64 for VdB0, from integrated spectral indices (see F05).

[4]See http://purcell.as.arizona.edu/hstphot/
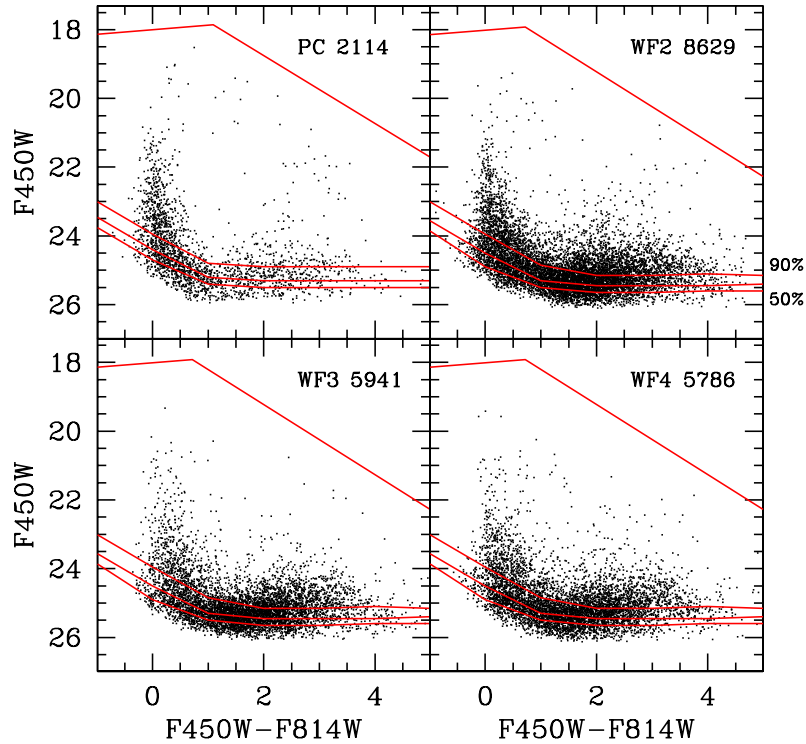
Figure 3.3: CMD of the fields sampled by the four chips of the WFPC2. The number of stars plotted is reported in the upper left corner of each panel. The upper line marks the threshold above which stars saturate the intensity scale of the images. The lower lines are CMD loci at the same level of completeness, 90%, 70% and 50% from top to bottom, respectively (see labels in the WF2 panel).

badly measured sources without significant loss of information, and it has been found to be appropriate for the whole survey.

In Fig. 3.3 the Color Magnitude Diagrams (CMD) of the fields imaged by the four chips of WFPC2 are shown. The threshold for the saturation of bright stars and the boundaries at which the completeness of the sample reaches 90%, 70% and 50% are also shown, as derived from the artificial stars experiments described below. As the CMD is quite typical of our survey, it is worthy of some general comments while a detailed analysis is deferred to Sect. 3 below. First, our photometry is relatively shallow, due the short exposure times of our images; the 50% completeness level is reached at $F450W \simeq 25.5$[5]. For the same reason our images, and particularly the F450W ones in which the background light is very low, are badly affected by CTE (see Fig. 3.2). Therefore the accuracy of the absolute and relative photometry is not particularly good (see, for example, Fig. 3.4 and Tab. 3.2, below). In spite of that, the very wide wavelength baseline provided by the F450W and F814W filters produces relatively well defined sequences in the CMD (compare, for example, with the CMD of similar fields obtained by WH01 with the same camera and longer exposure times but using F439W and F555W filters).

All the fields targeted by our survey cross the outer regions of the star-forming thin disk of M31 (see F05), and as a consequence, in most cases, the most prominent feature of the CMD

---

[5]Except for the very crowded region at the center of the cluster. For 10 px $< r \leq 50$ px, the 50% completeness level is reached at $F450W \gtrsim 23.5$.
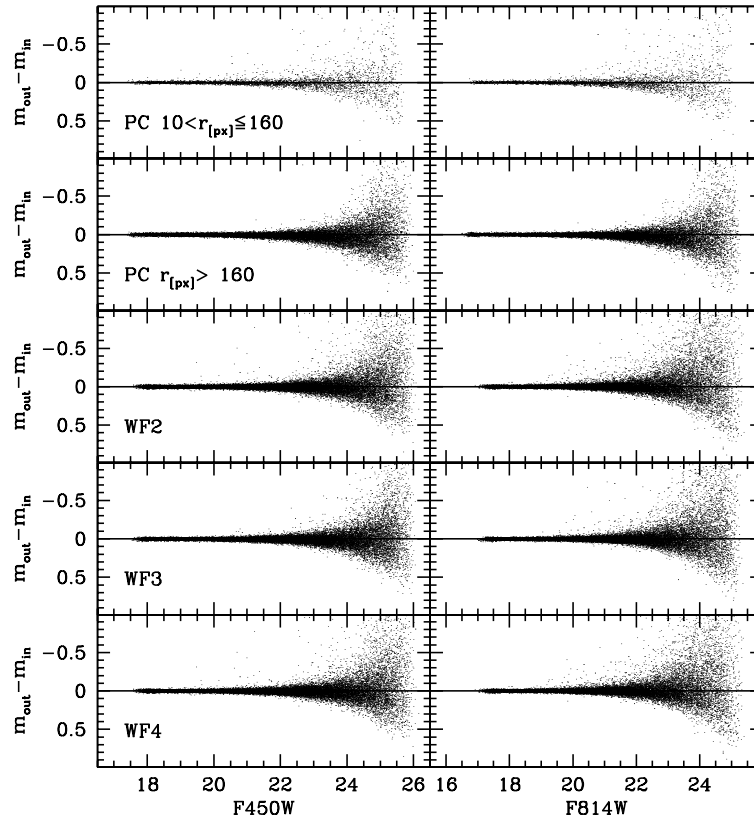
Figure 3.4: Distributions of the differences between the *output* and *input* magnitudes of artificial stars as a function of F450W (left panels) and F814W (right panels) magnitudes, for the PC and WF fields. The top panel displays the distributions for the most crowded region of the PC camera, i.e. the one containing the cluster. $r_{[px]}$ is the distance from the cluster center in PC pixel units, assuming (x,y)=(405,398) as the coordinate of the center in the reference frame of the photometric catalogue. To make the diagrams more easily readable we plot just a fraction of the whole set of artificial stars, i.e. 50000 stars per field, approximately, while more than 150000 per field are typically recovered.

is the nearly vertical plume of young Main Sequence stars that is seen in Fig. 3.3 around $F450W - F814W \simeq 0.2$. The wide blob of stars at $F450W > 24.0$ and $F450W - F814W \geq 1.5$ is consistent with being due to the brightest Red Giants near the tip of the Red Giant Branch (RGB) of the old-intermediate population that seems to be pervasive in the M31 disk (see Bellazzini et al. 2003, and references therein). Red and blue supergiants as well as other less-massive evolved stars are likely present at bright magnitudes over the whole color range covered by our CMD (see Massey 2006).

3.2.1 Artificial stars experiments

The completeness of the samples and the accuracy in the relative photometry are best estimated with extensive sets of artificial stars experiments (see Bellazzini et al. 2002a,2002b and Tosi et al. 2001 for detailed discussions and references).

HSTPHOT allows easy, fast and fully automated runs of artificial stars experiments. Fake stars in a user-selected color range, extracted at random from a Luminosity Function (LF) similar to the observed one, are added to the original frames one at a time to avoid self-crowding (Dolphin, private communication) and the photometric reduction is repeated. With the final catalogue of *input* and *output* magnitudes of artificial stars the distribution

Table 3.2: Uncertainties in the relative photometry from artificial stars experiments, for 10 px $< r \leq 160$ px, PC field.

F450W	σ^a	F814W	σ^a
18.00	0.009	18.00	0.010
18.50	0.010	18.50	0.011
19.00	0.010	19.00	0.012
19.50	0.011	19.50	0.013
20.00	0.013	20.00	0.016
20.50	0.016	20.50	0.020
21.00	0.018	21.00	0.026
21.50	0.023	21.50	0.036
22.00	0.029	22.00	0.050
22.50	0.039	22.50	0.068
23.00	0.054	23.00	0.087
23.50	0.076	23.50	0.138
24.00	0.107	24.00	0.218
24.50	0.153	24.50	0.336
25.00	0.241	25.00	0.377
25.50	0.309	25.50	0.400

[a] σ are ± 1 standard deviations after the clipping of outliers at more than 3σ from the mean.

of photometric errors and the completeness of the samples can be studied as a function of color and as a function of the distance from the center of the cluster under consideration (i.e. as a function of crowding). We simulated a total of 728398 artificial stars, roughly equally distributed on the four WFPC2 chips.

Fig. 3.4 shows the distributions of the differences between the *output* and *input* magnitudes of artificial stars as a function of F450W (left panels) and F814W (right panels) magnitudes, providing a direct estimate of the typical uncertainties of our relative photometry. The small excess of stars at negative $m_{out} - m_{in}$, increasing in number and amplitude of the difference for fainter magnitudes, is due to artificial sources that are erroneously recovered with a brighter magnitude because they are blended with real sources present on the image (see Tosi et al. 2001). Even in the most crowded region of the PC that includes the cluster (top panels of Fig. 3.4) the effects of blending are not particularly severe, at least for relatively bright stars. The probability of a star with $F450W \leq 23.5$ to have its magnitude decreased by more than 0.1(0.2) mag by the combination of blending and photometric error is 2.8%(1.4%) if its color lies in the range $-0.6 \leq F450W - F814W \leq 1.5$ and 3.5%(1.6%) for $2.0 \leq F450W - F814W \leq 4.0$. Typical photometric uncertainties as a function of magnitude are reported in Table 3.2 for the innermost region of the PC field, covering most of the cluster that is the main subject of the present study.

Finally the completeness factors (C_f) as a function of magnitude for different regions of the PC and for the WF fields are shown in Fig. 3.5, for stars in the wide color range $-0.6 \leq F450W - F814W \leq 1.5$. Outside of the innermost region of the PC including the cluster, the C_f functions are nearly indistinguishable. For $r > 50$ px the completeness is larger than 80% for $F450W \leq 24.0$ and in any case $C_f \simeq 1$ (i.e. completeness $\simeq 100\%$) for $F450W \leq 22.0$.

3.2.2 Theoretical stellar models

Most of our inferences about the physical parameters of the stellar populations (clusters or field) considered in our survey will be obtained from the comparison between the observed
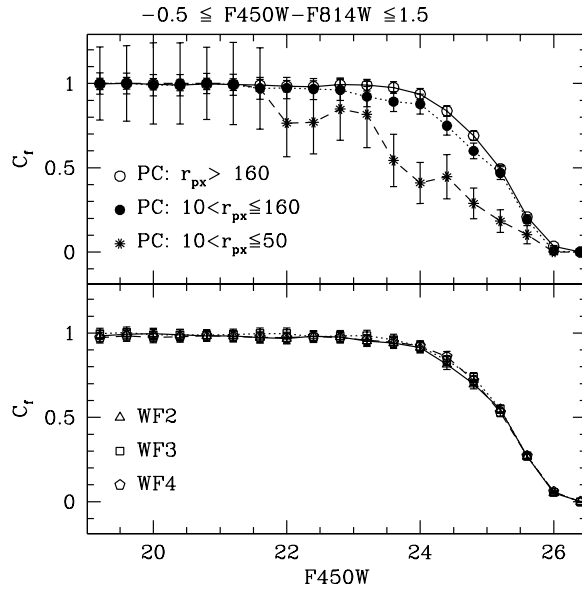
Figure 3.5: Completeness factor (C_f) as a function of F450W magnitude for the color range enclosing MS stars. Upper panel: C_f for regions of the PC field at different distances from the cluster center. Lower panel: C_f for the three WF fields. Note that the three curves are indistinguishable within the uncertainties.

CMDs and theoretical stellar models, in the form of isochrones or synthetic CMDs. The need to have models in the natural photometric system in which the observations were obtained (HST/WFPC2 VEGAMAG) and to have a set of isochrones reaching ages as young as 10 Myr led us to chose the set by Girardi et al. (2002, hereafter G02), as our reference grid of stellar models. In particular we took their HST-color version of the solar- scaled models by Salasnich et al. (2000), with overshooting and a simplified TP-AGB evolution, as this set includes 10 Myr old isochrones up to super-solar metallicities[6]. In some cases, when a particular model is needed, we use the CMD web tool[7] (Marigo et al. 2008), that allows the on-line computation of models from user specified inputs, using the G02 set.

In some cases, for comparison and/or for special applications, we use the BASTI[8] database, collecting the theoretical models by Pietrinferni et al. (2004), and updates. In particular BASTI provides a very practical Web Tool to produce synthetic CMDs of populations with ages, chemical composition, initial mass function, binary fraction (f_b) etc. selected by the user (Cordier et al. 2007), that can be used to compare models and observations in term of star counts in different color and magnitude ranges (see Fig. 3.6, for an example of application). Unfortunately, the models are not provided in the WFPC2 photometric system - so theoretical magnitudes have to be transformed - and isochrones/synthetic CMDs for ages < 30 Myr are not provided; for these reasons we didn't adopt the BASTI set as the reference for our survey. In the considered range of ages G02 and BASTI isochrones (with overshooting) provide very similar predictions of color and magnitudes, while evolving masses may differ by ~ 20% (see also Gallart, Zoccali & Aparicio 2005).

---

[6]http://pleiadi.oapd.inaf.it
[7]http://stev.oapd.inaf.it/ lgirardi/cgi-bin/cmd
[8]http://www.oa-teramo.inaf.it/BASTI/index.php
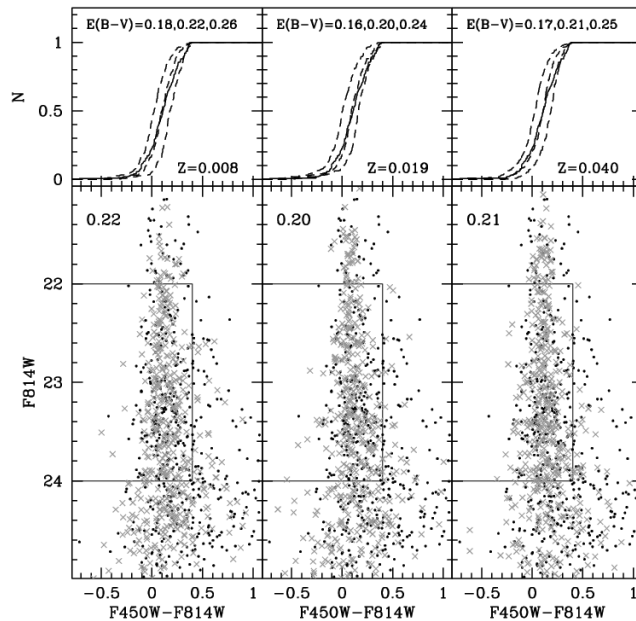
Figure 3.6: The observed CMD of VdB0 (black dots, only stars with $r \leq 160$ px) is compared with the synthetic CMD (grey $\times$ symbols) of 30 Myr old, f_b =50% populations having $Z = 0.008$ (left panel), $Z = 0.019$ (middle panel), and $Z = 0.040$, obtained from the BASTI webtool (Cordier et al. 2007), transformed to WFPC2-VEGAMAG with Dolphin (2000b) equations, and corrected for photometric errors and completeness according to the results of our artificial stars experiments. The thin lines enclose the selection box in which the cumulative color distributions shown in the upper panels have been obtained, focusing on the blue edge of the Main Sequence. In these panels the observed color distribution (continuous line) is compared to the distributions of the synthetic sample of the adopted metallicity for three different assumptions on the reddening value (dashed lines), reported in the upper label. The middle value corresponds to the distribution that best fits the observations and is also reported in the upper left corner of the CMDs. Note the very weak dependence of the reddening estimate on the metallicity of the adopted model.

3.2.3 Reddening and Distance

To correct for the effects of interstellar extinction and reddening we will always adopt the relations $A_{F450W} = 4.015 E(B-V)$ and $A_{F814} = 1.948 E(B-V)$, as reported by Schlegel, Finkbeiner & Davis (1998). As our clusters are embedded in the structured dusty disk of M31 it does not seem appropriate to assume a unique value of reddening for all of them; the typical reddening value attributed to Galactic dust toward M31 ranges from $E(B-V) = 0.06$ (Schlegel et al. 1998) to $E(B-V) \simeq 0.11$ (see Galleti 2004, and references therein), but it is likely that our clusters are more reddened than this (Barmby et al. 2000; Fan et al. 2008). To get an estimate of the reddening affecting the clusters in our survey we compare theoretical models (isochrones and synthetic CMDs) to the observed MS in the range $22.0 \lesssim F450W \lesssim 24.0$. In this range, corresponding to absolute magnitudes $-3.0 \lesssim M_{F450W} \lesssim 0.0$, the color of the MS is only weakly sensitive to metallicity and various sets of theoretical models provide very consistent predictions. An example of our analysis is presented in Fig. 3.6, where we compare the color distribution at the blue edge of the MS of the observed sample and of synthetic samples (from the BASTI webtool) of different metallicities, adopting different reddening values. The comparisons confirm that the sensitivity to metallicity of the reddening estimate is very weak, as expected. In the case of VdB0 we obtain $E(B-V) = 0.2 \pm 0.03$ with this method, and we will always adopt this value below.

In the following and for the whole survey we adopt $(m-M)_0 = 24.47 \pm 0.07$ as the distance modulus of all the considered populations, from McConnachie et al. (2005), corresponding to
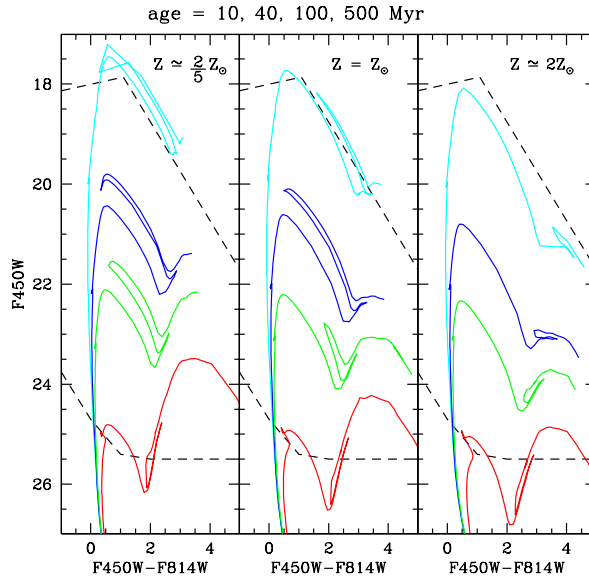
Figure 3.7: Isochrones of different ages and metal content are plotted on the "visibility window" of our CMDs, enclosed on the bright side by the saturation limits and on the faint side by the $C_f = 50\%$ line (long-dashed lines). The continuous curves are isochrones from the G02 set; ages and metallicities are indicated in the figure.

an heliocentric distance $D = 783$ kpc. At this distance $1''$ corresponds to 3.8 pc, $1''$ to 228 pc.

3.2.4   Accessible age range

As the degree of crowding of all the surveyed fields is quite similar and the observational set-up is identical in all cases, the saturation limit and the $C_f = 0.50$ limit reported in the CMDs of Fig. 3.3 can be considered representative of the typical CMD window that is accessible with the survey data. In Fig. 3.7 we compare isochrones of different ages and metallicities with this window to have an idea of the age range in which we can obtain reasonable age estimates for the considered clusters from the luminosity of their Turn Off (TO) points and/or from the distribution of their Super Giant populations.

In the metallicity range that is most likely to enclose the disk populations (we are considering $\frac{2}{5}Z_\odot \lesssim Z \lesssim 2Z_\odot$) we can detect the TO point of clusters roughly ranging from 10 to 500 Myr old. As the only BLCCs for which a direct CMD-based age estimate has been obtained are 60-160 Myr old (WH01), the age sensitivity of the survey seems rather appropriate; however clusters in the age range 0.5 - 2 Gyr may prove very difficult to age date with our data. For the oldest populations (age $\gtrsim 2$ Gyr) we can hope to detect just the tip of the RGB, as shown by the age=12 Gyr isochrones plotted as thick lines in Fig. 3.9, below.

3.3   The CMD and structure of the cluster VdB0

3.3.1   Distribution of resolved stars

To identify the stellar population of the cluster as securely as possible, it is useful to have an idea of the surface density distribution of its resolved stars. In the present context we are interested only in defining the characteristic size of the region dominated by cluster stars,
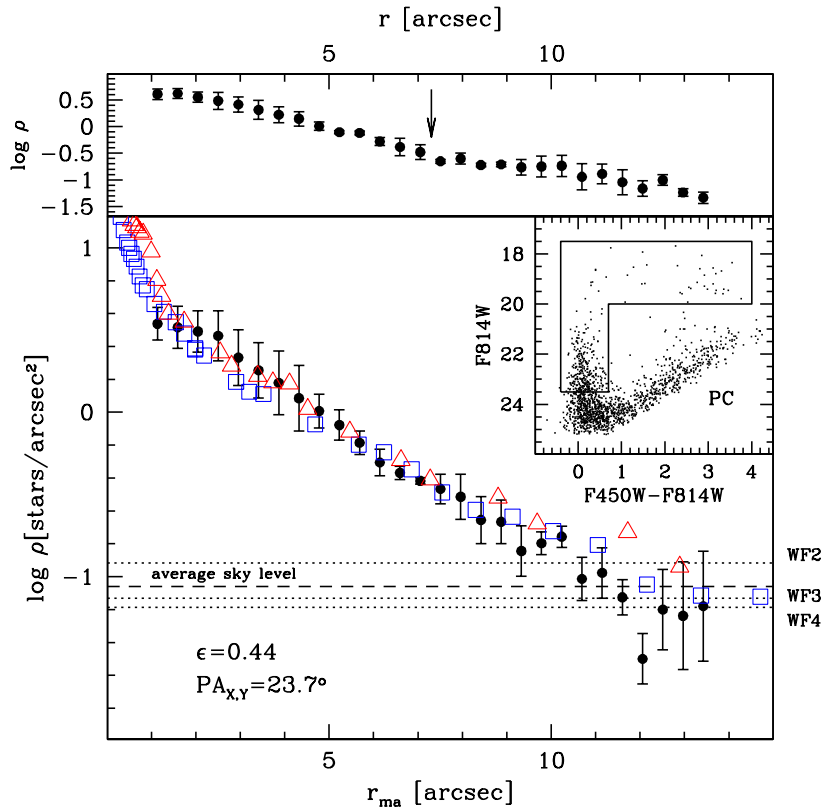
Figure 3.8: Upper panel: Background-subtracted surface density profile of VdB0 computed by counting stars on circular concentric annuli around the center of the cluster. The arrow marks the radius where a sudden change of slope in the profile appears, at $r \simeq 160$ px $= 7''.3$. Lower panel: Background-subtracted profile from star-counts (filled circles with errorbars) converted to a major-axis profile, adopting the reported values of PA and ϵ. Open symbols are the corresponding light profiles described in Sect. 3.4, squares for the F450W image and triangles for F814W, vertically shifted by an arbitrary normalization to match the star counts at $r_{ma} > 3''$. The dotted lines mark the average surface density in each of the WF cameras, the dashed line is the average of the three, which was in the end adopted as the background value to subtract to star-count profiles. Only stars within the L-shaped box plotted in the CMD in the upper right corner of the lower panel are selected for star counts, as probable cluster members.

in order to select samples of likely cluster members by radius (see Sect. 3.4 for a detailed analysis of the light profiles).

Stars were selected on the CMD from the box shown in the diagram enclosed in the lower panel of Fig. 4.5. The box is expected to pick up the best-measured MS and SG stars typical of the cluster population, while excluding populations that are clearly not associated with the cluster, such as the much older stars around the tip of the RGB. For $r \lesssim 3''$ star counts are significantly affected by radially varying incompleteness in the range of magnitudes considered. Beyond this limit the degree of completeness is fairly high and essentially constant with radius (see Fig. 3.5, above), hence the derived profile should be reliable.

In the upper panel of Fig. 4.5 we show the surface density profile obtained by counting stars on circular annuli centered on the cluster center. The observed profile displays an obvious break at $r \simeq 7.3''$, where it begins to decline with a gentler slope out to $r \sim 14''$. The break in the profile may reflect an *inner core + outer corona* structure of VdB0, which is typical of Galactic Open Clusters (see Kubiak et al. 1992, Kharchenko et al. 2005, Mackey & Gilmore 2003, Elson et al. 1985, and references therein), or it may be —at least partially– due

to the elongated distribution of the cluster stars unaccounted for by our adoption of circular annuli. To investigate this possibility we transformed the radial coordinate of each star (r) into a major-axis radius (r_{ma}) defined as

$$r_{ma} = \sqrt{X_r^2 + \left(\frac{1}{(1-\epsilon)}Y_r\right)^2} \tag{3.1}$$

where

$$X_r = (X - X_0)cos(PA_{X,Y}) + (Y - Y_0)sin(PA_{X,Y}) \tag{3.2}$$

$$Y_r = -(X - X_0)sin(PA_{X,Y}) + (Y - Y_0)cos(PA_{X,Y}) \tag{3.3}$$

and (X_0, Y_0) are the coordinate of the center of the cluster, $\epsilon = 1 - b/a$, is the ellipticity, where a and b are the semi-major and semi-minor axis, respectively, and $PA_{X,Y}$ is the position angle measured from the X axis toward the Y axis. Both ϵ and $PA_{X,Y}$ are taken (or easily derived, in the case of $PA_{X,Y}$) from the results of the analysis of the light distribution presented in Sect. 3.4, below. Eq. 3.1 has been adapted to our case from Eq. 4 by Martin et al. (2008).

The ellipticity-corrected major axis profile is plotted in the lower panel of Fig. 4.5, and it clearly shows that the change of slope in the original profile was an artifact due to the inadequacy of the assumption of circular symmetry. The result is supported by the good match between the star-counts profile and the light profiles (from Sect. 3.4) over the large radial range where they can be compared ($r > 3''$).

It is interesting to note that the cluster profile appears to extend to remarkably large distances from the center, out to $\simeq 15'' \simeq 57$ pc. As the process of profile analysis described in Sect. 3.4 includes also the fitting of King (1966, hereafter K66) models, it is interesting to note that the limiting radius of the K66 models that best fits the surface brightness profiles is also $r_t \simeq 15''$, thus supporting the conclusion that the cluster is very extended.

The elongated shape of the cluster will be taken into account in the detailed analysis of the profiles of Sect. 3.4. For present purposes it is sufficient to conclude that most of the cluster stars are enclosed within a (circular) radius of $7''.3$ (160 px) from the center. We take this as a reference radius for the following analysis of the CMD, as it allows a very simple radial selection, remembering that some cluster members are also present at larger radii.

The upper left panel of Fig. 3.9 shows the CMD of stars within $10 \leq r < 160$ px, an annulus that, as stated earlier, should be dominated by cluster stars. The innermost $r \leq 10$ px region has been excluded because of severe incompleteness. A main sequence with a TO around $F450W \sim 21.5$ is the most populated branch of the diagram, with a blue edge at $F450W - F814W \simeq 0.0$. Blue and red supergiants (BSGs, RSGs) are clearly identified, spanning a large color range ($0.0 \lesssim F450W - F814W \lesssim 3.6$ mag). A 25 Myr isochrone of solar metallicity (from the G02 set) seems to provide a satisfactory fit to the MS and to the sizable luminosity range spanned by supergiants, suggesting an extended Blue Loop phase (see Williams & Hodge 2001a). The color of the reddest supergiants is not fully reproduced (a long standing and not-so-critical problem of theoretical models, see Massey 2003). An handful of field RGB stars (at F450W$\geq$ 24.0 and F450W-F814W$\gtrsim$ 2.0) is the only population identified in this inner annulus which is clearly not associated with the cluster.

The upper right and lower left panels of Fig. 3.9 shows the CMD of outer annuli of the PC field with the same area as the 10 px $< r <$ 160 px annulus. Even if these fields still contain some cluster members, their stellar mix should be fairly representative of the surrounding field population (compare with the WF2 CMD shown in the lower right panel). The comparison of the innermost annulus with the outer two of the same area shows that the supergiant population is characteristic of the cluster and is much less frequent in the field, suggesting an older average age of the field population with respect to the cluster. The comparison between the morphologies of the MS is consistent this view. The lower right panel of the figure shows the CMD of a WF2 field whose area is 32 times that of the annuli described above. The larger sampled area provides a clearer picture of the population mix of the M31 disk in the surroundings of VdB0. While MS and evolved stars of age (mass) similar to that
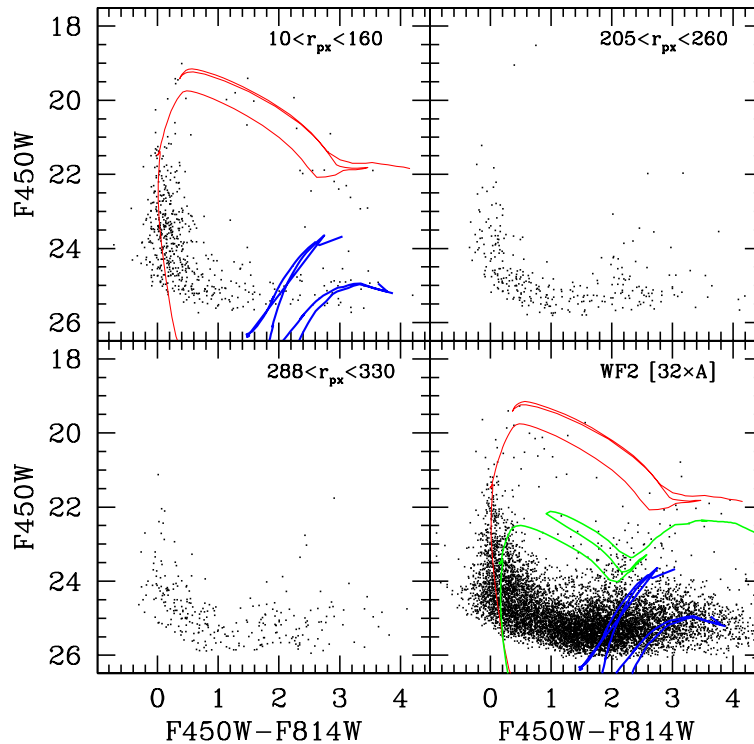
Figure 3.9: CMDs of different circular annuli around the center of VdB0 in the PC field (see Fig. 3.2, above), all having the same area, (upper panels and lower left panel) and of the whole WF2 field, whose area is 32 times that of the PC annuli (lower right panel). The thin line is a $Z = Z_\odot$ isochrone of age 25 Myr; the heavy lines at F450W ≤ 24.0 are 12 Gyr old isochrones of metallicity $Z = 6 \times 10^{-4}$ and $Z = 6 \times 10^{-3}$, from blue to red, respectively. The additional isochrone plotted in the lower right panel has $Z = 0.008$ and age 125 Myr. All the isochrones are from G02.

encountered in the cluster are present, the majority of the stars seem to have ages greater than 100 Myr. In particular the evolved stars at $F450W - F814W \gtrsim 2.0$ and $F450W \lesssim 24.0$ that are well fitted by the over-plotted 125 Myr, $Z = 0.008$ isochrone are not seen in the 10 px $< r <$ 160 px annulus.

The CMD of the cluster (innermost annulus) is very similar to that of rich Large Magellanic Cloud clusters of age $\sim$ 30-50 Myr, such as NGC 1711 (Sagar et al. 1991) and, in particular, NGC 1850 (Vallenari et al. 1994, Gilmozzi et al. 1994).

3.3.2 Supergiant Stars

The analysis illustrated in Fig. 3.10 and reported in Table 4.2 quantitatively demonstrates the presence of a significant overabundance of supergiants in the cluster with respect to the surrounding field. We counted stars in the different boxes on the CMDs shown in Fig. 3.10, sampling the upper MS (box A) and supergiants of blue (B), intermediate (C) and red (D) colors. The counts obtained in the $r \leq 160$ px and 160 px$< r <$ 330 px annuli are compared with those expected from the field population, computed by rescaling the observed counts in the WF2 field by the ratio of the sampled areas. The lower right panel shows that in the $r \leq 160$ px annulus a clear excess of stars is present in all of the boxes considered. The excess of bright MS stars is very significant and the excess of RSGs is above the 3σ level.
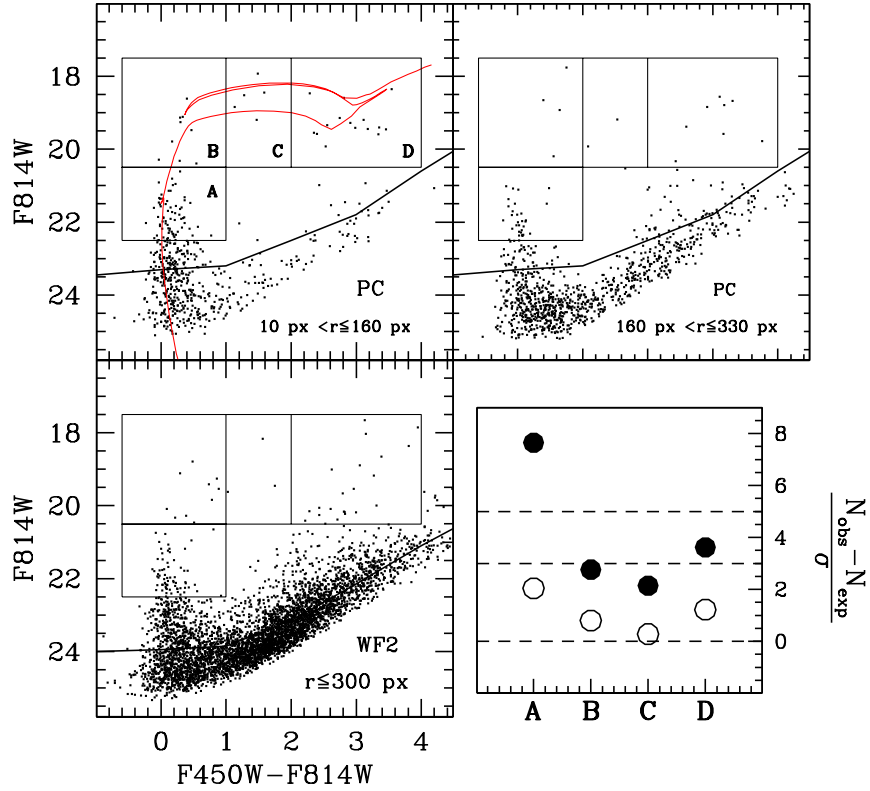
Figure 3.10: CMDs of different annuli around the center of VdB0 in the PC field (upper panels) and of a large area in the WF2 field (lower left panel), expected to sample the surrounding "field" population. An isochrone of $Z = Z_\odot$ and age 25 Myr is superposed on the upper left CMDs, as a reference. The $C_f = 0.90$ line is reported and a raster of labeled boxes is also over-plotted. The lower right panel reports the background-subtracted star counts (see Tab. 4.2) in the various boxes, in units of σ, for the inner ($r \leq 160$ px, filled circles) and outer (160 px $< r \leq 330$ px, open circles) annuli. Zero, three and five σ levels are marked by dashed horizontal lines.

Table 3.3: Star counts in the CMD boxes defined in Fig. 3.10. Box A samples the upper MS, boxes B, C, and D samples SG stars of blue, intermediate and red colors, respectively. N_{exp} is the number of stars expected in a given box from the field population, computed by rescaling the observed counts in the WF2 field by the ratio of the sampled areas. The ratio between the area of the considered field (annulus) and the area of the WF2 field (used as representative of the field population) is reported in the last column.

Field	Box **A**		Box **B**		Box **C**		Box **D**		Area$_{field}$/Area$_{WF2}$
	N_{obs}	N_{exp}	N_{obs}	N_{exp}	N_{obs}	N_{exp}	N_{obs}	N_{exp}	
PC: 10 px $< r \le$ 160 px	68	4.8 ± 0.6	9	0.7 ± 0.2	5	0.2 ± 0.1	16	1.5 ± 0.3	0.0708
PC: 160 px $< r \le$ 330 px	27	15.7 ± 1.9	4	2.3 ± 0.7	1	0.7 ± 0.4	9	5.1 ± 1.1	0.2314
WF2: $r \le$ 300 px	68	—	10	—	3	—	22	—	1.0000

Even if the low number of stars prevents the detection of significant excesses, the 160 px$< r <$ 330 px annulus shows some excess with respect to the field in all of the considered boxes, in agreement with the results of Fig. 4.5.

The total background-subtracted number of RSGs attributable to VdB0 is $\simeq 18$. The true number is likely larger than this, as some RSGs are likely to reside in the innermost $r \le 10$ px, which are not included in the present analysis as they are not well resolved in our images. According to Figer (2008) a richer harvest of RSGs is observed in only one known YMC of the Milky Way, RSGC2, with twenty-six RSG stars. RSGC1 has fourteen, while other young clusters listed by Figer have less than five. RSGC2 is reported to have an age ≤ 21 Myr, RSGC1 has age ≤ 14 Myr, and all the other clusters listed by Figer have ages ≤ 7 Myr, i.e. younger than VdB0 (see below). As noted above, some rich clusters of similar age are known in the LMC (Vallenari et al. 1994, Brocato et al. 2001), but even there RSGs are not present in large numbers.

3.3.3   Age and metallicity

Having fixed the amount of reddening and the distance modulus to the cluster, we obtain an age estimate and an indication of the metallicity by comparison with isochrones from the G02 set, following the approach used by WH01. In Fig. 3.11 we present a comparison with isochrones of various metallicities in the range $\frac{2}{5}Z_\odot \lesssim Z \lesssim 2Z_\odot$. In all the panels, the isochrone that is judged (by eye) to provide the best-fit to the observed CMD is plotted as a continuous line. Dashed lines correspond to isochrones providing strong upper and lower limits to the age estimates, which serve as conservative estimates of the associated uncertainties.

The first very basic conclusion to be drawn from the reported upper/lower limits, is that, independent of the adopted metallicity, the age of VdB0 must be within the relatively narrow range from 12 to 63 Myr.

The wide range in magnitude covered by supergiant stars strongly indicates the presence of a wide *blue loop* (Massey 2003). The super-solar isochrones clearly lack this feature, hence can likely be excluded as a possible solution. The larger range of color and magnitude covered by the $Z = Z_\odot$ isochrone in the blue loop phase seems to provide a slightly better description of the CMD, compared to the $Z = 0.008$ case. We produced a set of synthetic CMDs for populations having $Z = 0.008, 0.019, 0.04$, age 30 Myr and 50 Myr, Kroupa (2001), Salpeter (1955) and $N(m) \propto m^{-1.35}$ Initial Mass Functions[9] (IMF), using the dedicated Web Tool provided by the BASTI team. After applying the appropriate distance modulus and reddening correction and transforming to the HST VEGAMAG system using the transformations by Dolphin (2000b), we computed a Blue to Red Supergiant ratio defined as the ratio of stars having $F814W < 20.0$ and $F450W - F814W < 2.0$ (B) or $F450W - F814W > 2.0$ (R). Independent of age and IMF, all

---

[9]Salpeter's IMF has $N(m) \propto m^{-2.35}$; Kroupa's IMF has $N(m) \propto m^{-2.3}$ for $M \ge 0.5 M_\odot$, and $N(m) \propto m^{-1.3}$ for $M < 0.5 M_\odot$
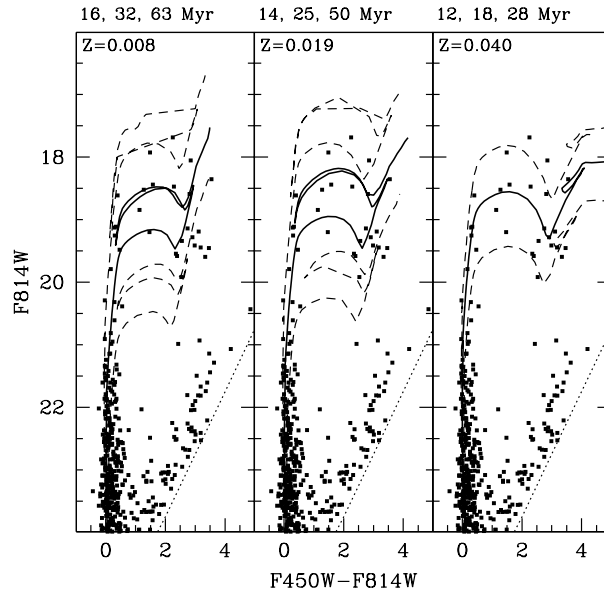
Figure 3.11: Age estimates for VdB0 for different assumptions about the total metallicity (Z). Isochrones from the G02 set are compared to the CMD of the cluster (10 px < *r* < 160 px). The best-fit isochrone is plotted as a thick continuous line while the dashed isochrones bracket the upper and lower limits on age. The ages and metallicities of the adopted isochrones are reported in each panel. The dotted lines mark the limiting magnitude as a function of color: the diagonal plume of stars just above the lines (with F450W-F814W> 1.5) is populated by likely RGB and AGB field stars, not associated with the cluster.

the $Z = 0.008$ models have $B/R \leq 0.26$ ($B/R \leq 0.02$ mag for age = 30 Myr), while the observed number is $B/R = 0.60 \pm 0.27$. The $Z = 0.04$ models have $0.15 \leq B/R \leq 0.52$, while the solar models have $0.61 \leq B/R \leq 1.17$. Therefore, the color distribution of SGs provides further quantitative support to the conclusion that the metallicity of VdB0 is nearly solar. Adopting $Z = Z_\odot$ as our best estimate for the cluster metallicity, the age may be more quantitatively constrained by the comparison of the observed MS Luminosity Function with those predicted by models of various ages. Fig. 3.12 clearly shows that an age=25 Myr model provides the best-fit to the observed drop in the star counts at $F814W \simeq 21.0$. The result is well reproduced also if a Kroupa IMF is adopted.

Our age estimate is not expected to depend critically on the set of theoretical models adopted. In their thorough comparison, Gallart, Zoccali & Aparicio (2005) showed that there is reasonably good agreement between all the theoretical isochrones they considered in this range of ages (i.e. ≤ 100 Myr), if stellar models with core overshooting are assumed. Our own (limited) set of experiments with Pietrinferni et al. (2004) models also supports this conclusion. A few tests with a set of isochrones adopting the canonical treatment of convection (from Pietrinferni et al. 2004) has shown that the adoption of such models would lead to younger age estimates, by a factor of $\sim \frac{3}{5}$, compared to models including overshooting.

Given all the above, *we adopt $Z = Z_\odot$ as our best guess for the cluster metallicity, and 25 Myr as our best estimate of its age* (see Table 4.3). The mass of the stars at the TO of the best-fit isochrone is $M_{TO} = 9.7 \ M_\odot$.

This relatively rough age estimate is sufficient for our purposes. Our final aim is to place the cluster into a log(Age) versus absolute integrated magnitude diagram such as that shown in Fig. 3.14, below (see also Bellazzini et al. 2008, hereafter B08, and references therein), to compare its stellar mass with that of Galactic open clusters of similar ages. The uncertainties reported here as the adopted upper and lower limits to the age estimates correspond to $\lesssim \pm 0.3$

46
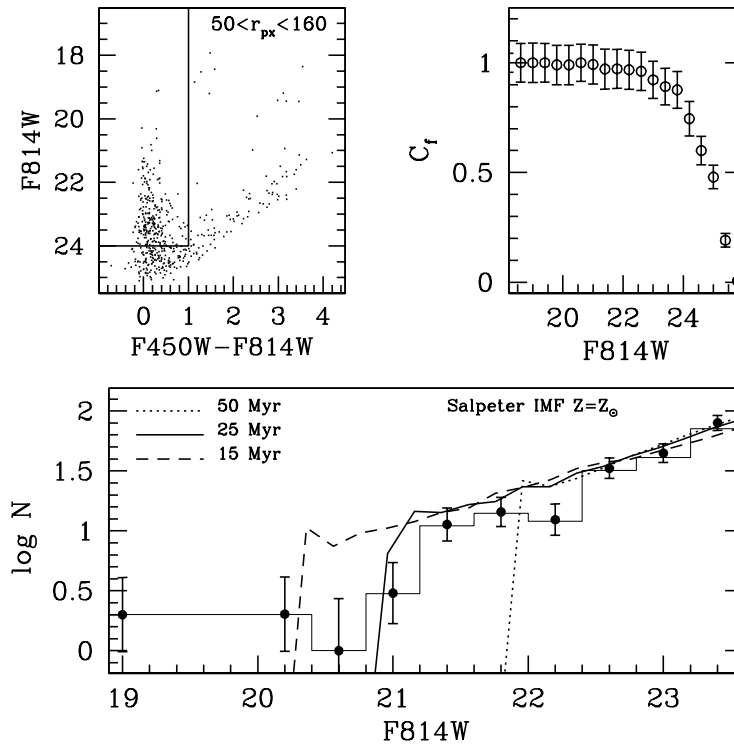
Figure 3.12: Comparison of the observed LF with theoretical models from the G02 suite. Upper left panel: CMD of VDB0 with overplotted the box adopted to select the sample of stars to be included in the LF. The considered radial range avoids the innermost region where the completeness displays significant radial variations in the range of magnitudes considered. Upper right panel: completeness as a function of magnitude for the color and radial range considered. Lower panel: the observed LF (before completeness correction = histogram; corrected for completeness = filled circles with error bars) is compared with models of different ages. Note the good fit of the drop at $F814W \simeq 21.0$ achieved by the age=25 Myr model. The theoretical LF have been arbitrarily normalized to best match the three faintest observed points .

dex in log(Age). These imply relatively small changes in the final estimate of the total stellar mass (a factor of $\lesssim 2$); the mass estimate also depends relatively weakly on the assumed IMF - see below - and very weakly on the metallicity, at least in the range considered here, see B08).

3.3.4 Integrated photometry, surface brightness profile and structural parameters

Surface-brightness profile-fitting was carried out using methods similar to those of Barmby et al. (2007). A more detailed description and the results of profile-fitting for the full cluster sample will be presented in Barmby et al. (2009, in prep.). Briefly, the two PC images in each filter were combined with the STScI Multidrizzle software. Intensity profiles were measured using the ellipse fitting routine in IRAF, on logarithmically-spaced isophotes centered on the intensity peaks of the clusters. The isophotal profiles were 'circularized' by converting the semi-major axes a of the ellipses to effective radii $R_{\rm eff} = \sqrt{a(1-\epsilon)}$, converted to electrons s^{-1} arcsec^{-2} by multiplying by $(1{\rm pixel}/0.0455'')^2 = 483.033$ and then to intensity

in $L_\odot$ pc^{-2} by multiplying by 14.276 and 6.746 for F450W and F814W, respectively[10]. The mean ellipticity and position angle obtained from the analysis of F450W and F814W images are very similar. For this reason we take their average as our best values, $\epsilon = 0.44$ and PA=45.5°, measured from North toward East. The available prescription for correcting WFPC2 photometry for CTE effects deals only with photometry of point sources, not semi-resolved objects such as extragalactic star clusters; accordingly, no CTE corrections were made to the profiles.

Cluster structural models were fit to the profile using the methods described in McLaughlin et al. (2008). Before fitting to the data, the models were convolved with a PSF profile derived from ellipse measurements of TinyTim model Point Spread Functions (PSFs) for the center of the PC camera. We considered the same three models used in Barmby et al. (2007): King (1966), Wilson (1975), and Sérsic (1968). The background level (i.e., the intensity of the largest isophotes) was allowed to vary in the fitting. Fig. 3.13 shows the profile data and the best-fit models in the two filters. Small scale bumps in the observed profile are likely due to individual bright stars (SGs). For the F450W filter the Sérsic model with index $n = 4.0$ was the best fit. This model has central intensity $I_0 = 7.9 \times 10^5 L_\odot$ pc^{-2} and scale radius $r_0 = 6.1 \times 10^{-4}$ pc. The projected half-light radius is $r_h = 9.12$ pc (2.″40) and total luminosity (corrected for extinction) $1.5 \times 10^6 L_\odot$. For the F814W image, the best-fit model was a Wilson (1975) model with $W_0 = 11.2$, central intensity $I_0 = 5.0 \times 10^5 L_\odot$ pc^{-2} and scale radius $r_0 = 0.072$ pc. The projected half-light radius is $r_h = 5.60$ pc (1.″47) and total luminosity $5.7 \times 10^5 L_\odot$. In the following analysis, we adopt the average of the two half-light radii, $r_h = 7.4 \pm 2.5$ pc (1.″94 $\pm$ 0.″66; the reported uncertainty is the standard deviation of the two values). It is also interesting to note that the half-light radius we have derived for VdB0 is larger than those for the clusters listed by Figer (see Davies et al. 2008, $r_h \simeq 0.2 - 3$pc), but smaller than NGC 1850 ($r_h \simeq 13$ pc) and very similar to NGC 1711 ($r_h \simeq 6$ pc), for example[11]. A summary of the adopted structural parameters of VdB0 is reported in Table 4.3.

The derived values of the total luminosity correspond to $M_{450W} = -10.13$ and $M_{814W} = -10.25$, respectively. Using Eq. 12 of Dolphin (2000b) these VEGAMAG magnitudes can be transformed to standard B and I using the appropriate coefficients from his Table 7. The integrated $(B-V)_0$ color required for the transformation has been taken from the RBC ($(B-V)_0 = 0.05$, Tab. 4.1, above), while we adopted $(V-I)_0 = 0.40$ from Maraston's (2005) model for a solar metallicity Simple Stellar Population (SSP[12]) with age of 25 Myr, as an observational estimate of the I magnitude of VdB0 was not available (but see below). $M_V = -9.9$ is obtained from M_{814W} and $M_V = -10.2$ from M_{450W}; we adopt the average (in flux) of the two, $M_V = -10.06$. This value is in excellent agreement with the value of $M_V = -10.03$ listed in the RBC, and coming, in turn, from the photometry by Sharov et al. (1995).

There are, however, compelling reasons to consider the estimate of M_V obtained from our HST images as significantly uncertain because of the unfortunate combination of a very extended cluster and of a very low intrinsic background level (just 1 to 2 DN in the background sky in the original raw WFPC2 images, particularly for the F450W filter). This guarantees that photometry within very large apertures will have a large uncertainty, and the resulting integrated brightness may depend on the details of how the code handles the background estimate in this photon-starved regime.

For this reason we prefer to rely on the excellent ground-based material that is publicly available to obtain a reliable estimate of the total luminosity of the cluster. Existing ground-

---

[10]This conversion assumes DN zeropoints of $Z_{450} = 21.884, Z_{814} = 21.528$, a gain of 7 electrons DN^{-1}, and $M_{\odot,\text{F450W}} = 5.31$ and $M_{\odot,\text{F814W}} = 4.14$.

[11]The surface brightness profiles of these and other LMC clusters have been studied by Mackey & Gilmore (2003) who provide the parameters of the EFF87 models that best fit the observed profiles. To derive the reported half-light radii we searched for the King (1962) model providing the best match to the EFF87 best-fit profile found by Mackey & Gilmore (2003), and adopted the corresponding r_h.

[12]A Simple Stellar Population is a population of stars all having the same age and chemical composition and having individual masses extracted from a given Initial Mass Function (IMF); this is a practical idealized model that is generally believed to be a reasonable approximation of a star cluster, see Renzini & Fusi Pecci 1988.
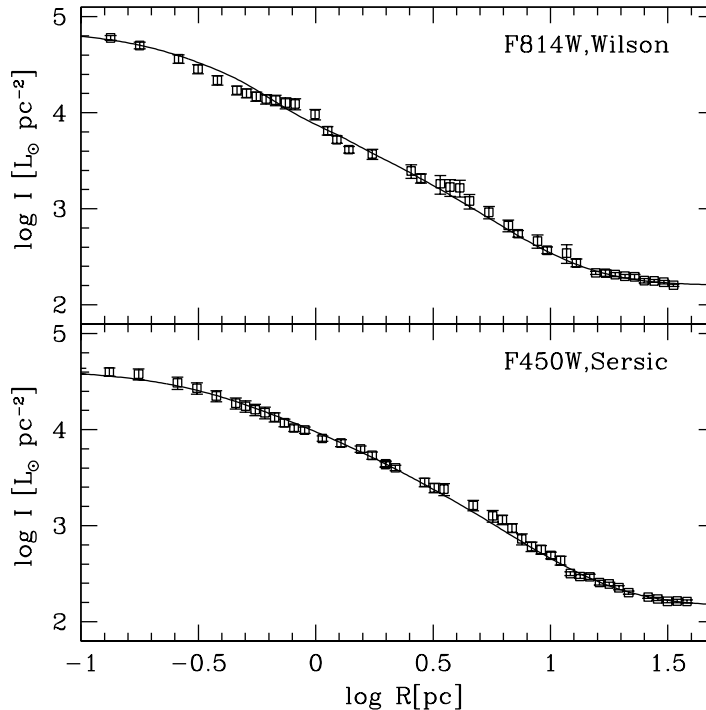
Figure 3.13: Intensity profiles from surface photometry in circular annuli from the F814W image (upper panel) and for the F450W image (lower panel). The continuous lines are the respective best-fit models, convolved with the instrumental PSF and with a constant background level added. For the parameters of the best-fit models see text.

based photometry of VdB0 taken from Sharov et al. (1995) is compiled in the RBC. However, it is possible that it was obtained adopting apertures that were not large enough to include the whole light distribution of this particularly extended cluster (see Fig. 4.5 and 3.13). We have therefore used two independent and well calibrated publicly available imaging surveys covering M31 to determine the integrated brightness of the cluster VdB0, that of Massey et al. (2006, hereafter M06) and the Sloan Digital Sky Survey (SDSS). In both cases we use an aperture with r=14.''4. From the BVRI images of the former we obtained $B = 14.94 \pm 0.09$, $V = 14.67 \pm 0.05$, $R = 14.45 \pm 0.11$ and $I = 14.01 \pm 0.11$[13]. The SDSS - Data Release 6 (DR6, Adelman-McCarthy et al. 2008) g, r, and i images yielded $B = 14.92$, $V = 14.63$, $R = 14.45$, and $I = 14.03$ using the color transformations of Lupton (2005), in excellent agreement with those inferred from the M06 images. This is $\simeq 0.4 - 0.6$ mag brighter than those reported in the RBC. In Sect. 4 we will show that the J,H,K magnitudes of VdB0 also become brighter by $\sim 0.2 - 0.5$ mag after increasing the adopted aperture from $r = 5.''0$ to $15.''0$.

Given all the above, we adopt the $r = 14.''4$ aperture photometry measured on M06 images as our preferred values, reported in Table 4.3, below. In particular $V = 14.67 \pm 0.05$ is our final best estimate of the integrated V magnitude of VdB0, corresponding to $M_V = -10.42 \pm 0.20$; these values will be adopted in the following analysis.

---

[13]We note that these values imply $(V - I)_0 = 0.41$, adopting the reddening law by Dean, Warren & Cousins (1978), in excellent agreement with the prediction, used above, of $(V - I)_0$ from Maraston's (2005) model for a solar metallicity SSP of age 25 Myr.
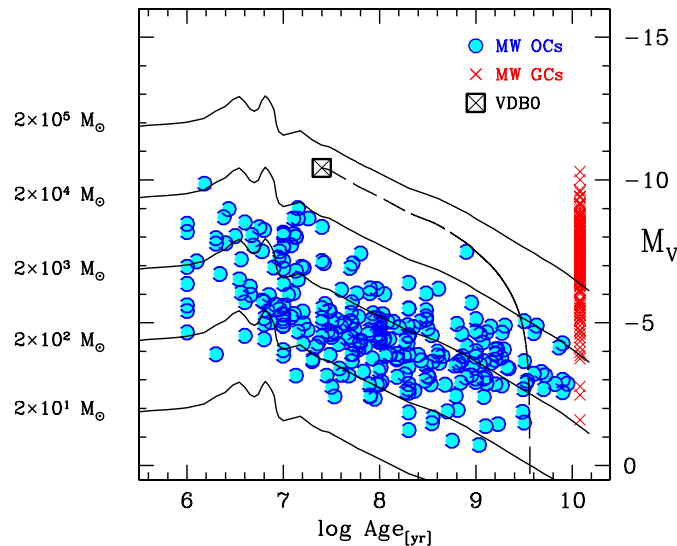
Figure 3.14: Integrated V mag and total mass as a function of age for various clusters. Galactic Open Clusters (OC, from the WEBDA database) are plotted filled circles, Galactic Globular Clusters (GC, M_V from the most recent version of the Harris (1996) catalogue, i.e. that of February 2003; the ages have been arbitrarily assumed to be 12.0 Gyr for all the clusters) are plotted as × symbols. VdB0 is represented as a crossed square at $M_V = -10.42$, from Tab. 4.3. The continuous lines are fixed-stellar-mass models from the set by Maraston (1998, 2005) for SSPs of solar metallicity, with a Salpeter's Initial Mass Function (IMF) and intermediate Horizontal Branch morphology. Note that in this plane, the dependence of the models from the assumed IMF, metallicity and HB morphology is quite small (see B08). The outlier OC at log Age≈ 9.0 is Tombaugh 1. The long dashed line is the VDB0 evolutionary track including the mass loss by dynamical effects according to the formulas by LG06. The cluster is expected to dissolve within < 4 Gyr from the present epoch.

3.4 Summary and discussion

We have outlined the data reduction and scientific analysis strategy that we adopt for our HST-WFPC2 survey of M31 candidate YMCs, whose complete results will be presented in future contributions. As an exemplary case, we have described the study of the cluster VdB0. We have found that VdB0 is a very bright and extended cluster of approximately solar metallicity and of age ∼ 25 Myr, with a rich population of blue and red supergiants.

Having clearly ascertained that VdB0 is a real cluster, it remains to be established if it is more similar to ordinary open clusters of the Milky Way than to to the Young Massive Clusters that may be considered as possible precursors of "disk globulars". The similarity with LMC objects typically classified as "Young Globular Clusters" such as NGC1850 (see Sect. 3., above) is quite remarkable and it suggests that VdB0 is not an ordinary OC (but see also point 1, below).

A more general way to compare clusters of different ages, taking into account the fading of the luminosity of SSPs as they age, it is to plot them into a diagram comparing age to some indicator of the stellar mass of the cluster (see, for example, Whitmore, Chandar & Fall 2007, Gieles, Lamers & Portegies-Zwart 2007, and de Grijs, Goodwin & Kouwenhoven 2008, for recent applications and references). Here we adopt log(Age) vs. absolute integrated magnitude as in B08.

In Fig. 3.14 VdB0 is compared with Galactic Open Clusters (data taken from the WEBDA database[14]), with Galactic Globular Clusters (from the latest version of Harris (1996) assuming a uniform age of 12 Gyr, a reasonable approximation for our purpose), and with a grid of SSP models with solar metallicity and Salpeter's IMF from the set by Maraston[15]

---

[14]http://www.univie.ac.at/webda/integre.html
[15]http://www-astro.physics.ox.ac.uk/ maraston/
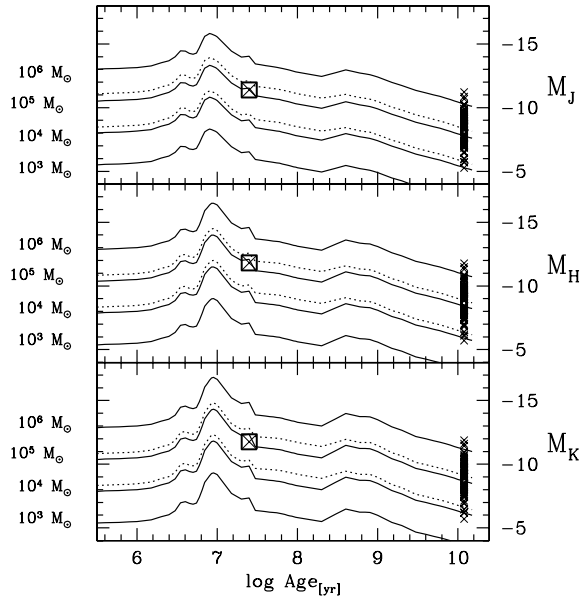
Figure 3.15: The same as Fig. 3.14 but for near infrared colors. Integrated magnitudes of GCs are taken from Cohen et al. 2007); the IR magnitudes for VdB0 are taken from Tab. 4. The dotted lines are $M = 10^4 M_\odot$ and $M = 10^5 M_\odot$ iso-mass models assuming a Kroupa 2001 IMF instead of a Salpeter (1955) IMF, plotted here to illustrate the weak effect of assumptions on IMFs.

(1998, 2005). As a SSP ages massive stars die while the mass of the most luminous stars decreases (passive evolution). Keeping the total mass fixed, the luminosity of the population fades and, as a consequence, the stellar mass-to-light (M/L) ratio increases. The continuous lines plotted in Fig. 3.14 describe the passive evolution of SSPs of various (stellar) masses: under the adopted assumptions the mass of a cluster of given age and M_V can be read from the grid of iso-mass tracks.

The path of the track passing through the cluster shows what its luminosity will be in the future if the cluster did not lose stars through dynamical processes (evaporation, tides, ecc.). The latter is clearly not the case in general, and in particular for VdB0. In addition to the relatively mild evaporation driven by two body encounters, it will suffer from the strain of the M31 tidal field and from encounters with Giant Molecular Clouds (GMC), as the cluster is embedded in the dense thin disk of M31 (Lamers & Gieles 2006, hereafter LG06, and references therein). To take these effects into account we used the analytical approach presented by LG06 to produce an evolutionary track including the cluster mass loss by stellar evolution, galactic tidal field, spiral arm shocking, and encounters with giant molecular clouds, plotted in Fig. 3.14 as a long-dashed curve. The LG06 formulas describe the evolution of a cluster located within the Milky Way (thin) disk at the Solar circle. They should provide a reasonable approximation for VdB0 which lies in the disk of M31, at a similar distance from the center of a similarly massive spiral galaxy (van den Bergh 2000). The required inputs are the cluster mass, for which we adopted the value that can be read from the SSP grid of Fig. 3.14 (see below), and the half-light radius, which we obtained in Sect. 3.3, above (see Tab. 4.3). The initial expulsion of gas not used in star formation may lead young clusters (age < 50 Myr) to lose their virial equilibrium and it may represent an additional relevant factor driving toward the destruction of clusters like VdB0 that is not included in the LG06 approach (Bastian & Goodwin 2006; Goodwin & Bastian 2006; Bastian et al. 2008).

Fig. 3.14 is worth of some detailed considerations:

51
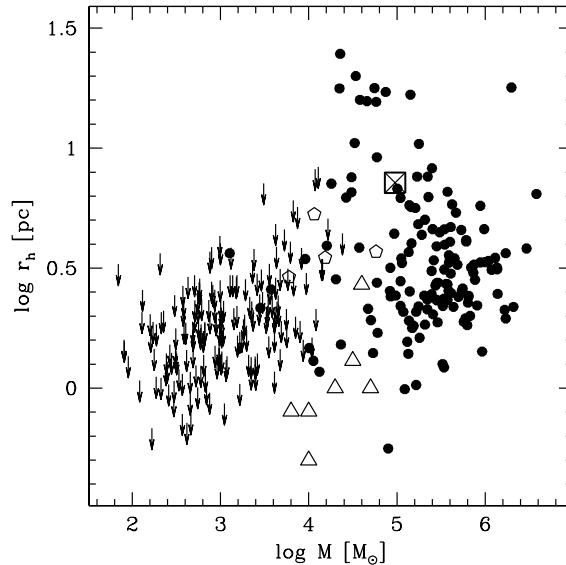
Figure 3.16: VdB0 (crossed square) is compared to other clusters in the *logarithm of the mass* vs. *logarithm of the half-light-radius* plane. Filled circles are Galactic GCs from Mackey & van den Bergh 2005). Arrows are Galactic OCs: we plot the radii where a break in the surface brightness profile occurs, taken from Kharchenko et al. (2005, their "core radii"). These should be considered as upper limits for actual r_h, which are not available for most OCs. The masses of the OCs have been computed using the grid of SSP models shown in Fig. 3.14, while for GCs we adopted age=12.0 Gyr and a grid of SSP models having $[Z/H] = -1.35$. Open pentagons are the clusters studied by WH01. Open triangles are the massive young MW clusters listed by Figer (2008); masses and radii are taken from his Table 1. Note that the radii reported by Figer for these clusters are not half-light-radii, however they should be a reasonable proxy. The good match between the two quantities has been verified in the case of RSG1, for which Figer report $r = 1.3$ pc, and Davies et al. (2008) obtain $r_h = 1.5 \pm 0.3$ pc.

1. Independently of the exact value of M_V adopted, VdB0 is significantly brighter ($\gtrsim 1$ mag) than Galactic OCs of similar ages, actually it is brighter than Galactic OCs of *any* age. The same is true also if all other known M31 OCs are considered (Hodge 1979; Krienke & Hodge 2007, 2008). However it should be noted that the population of disk clusters in M31 may be so huge (~ 80000 clusters, according to Krienke & Hodge 2007) that even the extreme tails of the luminosity distribution may be populated. (This should not be the case for the LMC, for example, as it is orders of magnitude less massive than M31). Hence it is premature to draw a conclusion from an individual cluster; when the whole sample is analyzed we will get a deeper insight on the actual nature of VdB0.

2. Assuming the RBC value for the integrated V magnitude, E(B-V)=0.0 instead of E(B-V)=0.2 and a grid of iso-mass tracks adopting a Kroupa IMF, we can obtain an extremely conservative strong *lower limit* to the stellar mass of VdB0, $M = 2.4 \times 10^4 M_\odot$. Under the same assumptions but adopting the best-fit value E(B-V)=0.2 we obtain $M = 6.5 \times 10^4 M_\odot$ with a Salpeter IMF and $M = 4.2 \times 10^4 M_\odot$ with a Kroupa IMF. These are at the threshold between the OC and GC mass distributions (see van den Bergh & Lafontaine 1984 and B08) and also at the upper end of the mass distribution of Galactic YMC (see Figer 2008 and Fig. 3.16, below). The conclusion that VdB0 is much more massive than MW clusters of similar ages seems inescapable, unless extreme IMFs are considered (i.e. IMF truncated at low masses, see Sternberg 1998).

3. If $M_V = -10.42$ is adopted, as obtained from large aperture ground-based V photometry

in Sect. 3.4, the total stellar mass is $M = 9.5 \times 10^4 M_\odot$ with a Salpeter IMF and $M = 6.0 \times 10^4 M_\odot$ with a Kroupa IMF.

4. The evolutionary tracks including the LG06 treatment of mass-loss by dynamical effects show that, independent of the actual mass (within the range outlined above), it is unlikely that the cluster VdB0 would survive for an Hubble time. Hence it is very probable that it will never have the opportunity to evolve into a classical (faint) GC. The disruption timescale is dominated by encounters with GMCs; considering this effect alone (Eq. 7 of LG06) the cluster is predicted to dissolve within $\simeq 3.6$ Gyr if its mass is $M = 9.5 \times 10^4 M_\odot$, as obtained from our best estimate of the integrated V magnitude and assuming a Salpeter's IMF.

5. In the same grid of Fig. 3.14 and under the same assumptions the masses of the BLCCs observed by WH01 - adopting their age estimates - range from $8.0 \times 10^3 M_\odot$, (G293) in the realm of OCs, to $\simeq 2 \times 10^4 M_\odot$ (G44 and G94) and $8 \times 10^4 M_\odot$ (G38), very similar to that of VdB0 and significantly larger than OCs of similar ages.

To obtain independent and more robust estimates of the present-day stellar mass of VdB0 we used the Near Infrared (NIR) version of the log Age vs. absolute integrated magnitude plane. In Fig. 3.15, J,H and K absolute magnitudes of VdB0 extracted from the Extended Sources Catalogue (XSC) of 2MASS are compared with Maraston's SSP models of solar metallicity and Salpeter's (continuous lines) or Kroupa's (dotted lines) IMFs and with Galactic GCs (from Cohen et al. 2007, ages assumed as above)[16]. NIR integrated magnitudes for significant samples of OCs are not available, at present. To account for the whole extent of the cluster we extracted $r = 15''$ aperture photometry, that is provided in the XSC, instead of the $r = 5''$ adopted in the RBC, see Tab. 4.1 and Tab. 4.3).

NIR magnitudes are more reliable mass tracers than visual magnitudes as NIR M/L ratios are smaller and have smaller variations with age, compared to optical M/L ratios. For example, according to Maraston (1998, 2005) models, a solar metallicity Salpeter-IMF SSP at Age = 10 Gyr has $(M/L)_V$=5.5, while $(M/L)_K$=1.4; the same SSP has $\frac{d(M/L)_V}{dt} \simeq 0.55$ while $\frac{d(M/L)_K}{dt} \simeq 0.13$. The independent estimates of the stellar mass from J,H, and K magnitudes are essentially identical, ranging from 6 to 9 $\times 10^4 M_\odot$, assuming a Salpeter IMF, and from 4 to 5.5 $\times 10^4 M_\odot$, assuming a Kroupa IMF. These estimates are in fair agreement with those obtained from the integrated V photometry.

Finally, in Fig. 3.16 we compare VdB0 with Galactic OCs, GCs and YMC, plus the BLCCs studied by WH01, in the log of the *stellar mass* versus log of the half-light radius plane (similar to Mackey & van den Bergh 2005 and Federici et al. 2007). The radii at which the break in the profile (core/corona transition) of Galactic OCs (from Kharchenko et al. 2005) occurs is taken as a strong upper limit for their r_h. VdB0 has a typical size that is larger than both OCs and YMCs, and is similar to that of several MW GCs of comparable mass.

In conclusion, we can say that VdB0 seems a remarkable cluster in several of its properties when compared to the other known disk clusters of the Milky Way and M31. In this paper we have presented the data reduction, data analysis and diagnostics that will be applied to the whole survey sample and that will allow us to put VdB0 and the other clusters in the more general context of the star cluster populations in the disk of spiral galaxies.

---

[16] For J,H,K colors we adopt $A_J = 0.871 E(B-V)$, $A_H = 0.540 E(B-V)$, and $A_K = 0.346 E(B-V)$, from Rieke & Lebofsky 1985. The J,H,K absolute magnitudes of the Sun are taken from Holmberg, Flynn & Portinari 2006.

Table 3.4: Newly derived coordinates, half-light radius, integrated magnitudes, reddening, age and metallicity for the cluster VdB0. The origin of each parameter is described in the last column.

par	value	note
α_{J2000}	$00^h\ 40^m\ 29.4^s$	from 2MASS-XSC
δ_{J2000}	$+40°\ 36'\ 15.2''$	from 2MASS-XSC
r_h	$1.''93 \pm 0.''66$	from intensity profile (i.p.) fit
B	14.94 ± 0.09	r=14.''4 ap. phot. on M06 images
V	14.67 ± 0.05	r=14.''4 ap. phot. on M06 images
R	14.45 ± 0.11	r=14.''4 ap. phot. on M06 images
I	14.01 ± 0.11	r=14.''4 ap. phot. on M06 images
J	13.26 ± 0.07	r=15.''0 ap. phot. from 2MASS-XSC
H	12.76 ± 0.12	r=15.''0 ap. phot. from 2MASS-XSC
K	12.77 ± 0.15	r=15.''0 ap. phot. from 2MASS-XSC
age	25 Myr	value of adopted best-fit isochrone
Z	0.019	value of adopted best-fit isochrone
E(B-V)	0.20	adopted best-fit value

4

An HST/WFPC2 survey of bright young clusters in M31. IV. Age and mass estimates[1]

S. Perina, J.G. Cohen, P. Barmby, M.A. Beasley, M. Bellazzini, J.P. Brodie, L. Federici, F. Fusi Pecci, S. Galleti, P.W. Hodge, J.P. Huchra, M. Kissler-Patig, T.H. Puzia, & J. Strader

Abstract

We present the main results of an imaging survey of possible young massive clusters (YMC) in M31 performed with the Wide Field and Planetary Camera 2 (WFPC2) on the Hubble Space Telescope (HST), with the aim of estimating their age and their mass. We obtained shallow (to B~ 25) photometry of individual stars in 19 clusters (of the 20 targets of the survey). We present the images and color magnitude diagrams (CMDs) of all of our targets.

Point spread function fitting photometry of individual stars was obtained for all the WFPC2 images of the target clusters, and the completeness of the final samples was estimated using extensive sets of artificial stars experiments. The reddening, age, and metallicity of the clusters were estimated by comparing the observed CMDs and luminosity functions (LFs) with theoretical models. Stellar masses were estimated by comparison with theoretical models in the log(Age) *vs.* absolute integrated magnitude plane, using ages estimated from our CMDs and integrated J, H, K magnitudes from 2MASS-6X.

Nineteen of the twenty surveyed candidates were confirmed to be real star clusters, while one turned out to be a bright star. Three of the clusters were found not to be good YMC candidates from newly available integrated spectroscopy and were in fact found to be old from their CMD. Of the remaining sixteen clusters, fourteen have ages between 25 Myr and

280 Myr, two have older ages than 500 Myr (lower limits). By including ten other YMC with HST photometry from the literature, we assembled a sample of 25 clusters younger than 1 Gyr, with mass ranging from $0.6 \times 10^4 M_\odot$ to $6 \times 10^4 M_\odot$, with an average of $\sim 3 \times 10^4 M_\odot$. Our estimates of ages and masses well agree with recent independent studies based on integrated spectra.

The clusters considered here are confirmed to have masses significantly higher than Galactic open clusters (OC) in the same age range. Our analysis indicates that YMCs are relatively common in all the largest star-forming galaxies of the Local Group, while the lack of known YMC older than 20 Myr in the Milky Way may stem from selection effects.

4.1 Introduction

Much of the star formation in the Milky Way is thought to have occurred within star clusters (Lada et al. (1991), Carpenter et al. (2000)); therefore, understanding the formation and evolution of star clusters is an important piece of the galaxy formation puzzle. Our understanding of the star cluster systems of spiral galaxies largely comes from studies of the Milky Way. Star clusters in our Galaxy have traditionally been separated into two varieties, open and globular clusters (OCs and GCs hereafter). OCs are conventionally regarded as young ($< 10^{10}$ yr), low-mass ($< 10^4 M_\odot$), and metal-rich systems that reside in the Galactic disk. In contrast, GCs are characterized as old, massive systems. In the Milky Way, GCs can be broadly separated into two components: a metal-rich disk/bulge subpopulation, and a spatially extended, metal-poor halo subsystem (Kinman (1959), Zinn (1985), see also Brodie & Strader (2006), Harris (2001), for general reviews of GCs).

However, the distinction between OCs and GCs has become increasingly blurred. For example, some OCs are luminous and old enought to be confused with GCs (e.g., Phelps & Schick (2003)). Similarly, some GCs are very low-luminosity systems (e.g., Koposov et al. (2007)), and, at least one, has an age that is consistent with the OC age distribution (Palomar 1, Sarajedini et al. (2007a)). Moreover, a third category of star cluster, "young massive clusters" (YMCs) are observed to exist in both merging (e.g., Whitmore & Schweizer (1995)) and quiescent galaxies (Larsen & Richtler, 1999). Indeed, YMCs have been known to exist in the Large Magellanic Cloud (LMC) for over half a century (Hodge, 1961). These objects are significantly more luminous than OCs ($M_V \lesssim -8$ up to $M_V \sim -15$), making them promising candidate young GCs. Once thought to be absent in the Milky Way, recent observations suggest that their census may be quite incomplete, as some prominent cases have been found recently in the Galaxy as well (Clark et al. (2005), Figer (2008), Messineo et al. (2009)).

Thus, a picture has emerged that, rather than being distinct groups, OCs, YMCs and GCs may represent regions within a continuum of cluster properties dependent upon local galaxy conditions (Larsen, 2003). The lifetime of a star cluster is dependent upon its mass and environment. Most low-mass star clusters in disks are rapidly disrupted via interactions with giant molecular clouds (Lamers & Gieles (2006), Gieles et al. (2007)). These disrupted star clusters are thought to be the origin of much of the present field star populations (Lada & Lada, 2003). Surviving disk clusters may then be regarded as OCs or YMCs, depending upon their mass. Star clusters in the halo may survive longer since they are subjected to the more gradual dynamical processes of two-body relaxation and evaporation. The clusters which survive for a Hubble time – more likely to occur away from the disk – are termed GCs (see also Krienke & Hodge (2007)). To date, no known *thin* disk GCs have been identified in the Milky Way.

After the Milky Way, M31 is the prime target for expanding our knowledge of cluster systems in spirals. However, our present state of knowledge about the M31 cluster system is far from complete. Similar to the Milky Way, M31 appears to have at least two GC subpopulations, a metal-rich, spatially concentrated subpopulation of GCs and a more metal-poor, spatially extended GC subpopulation (Huchra et al. (1991), Barmby et al. (2000)). Also,

again similar to the Milky Way GCs, the metal-rich GCs in M31 rotate and show "bulge-like" kinematics (Perrett et al., 2002). However, unlike the case in the Milky Way, the metal-poor GCs also show significant rotation (Huchra et al. (1991), Perrett et al. (2002), Lee et al. (2008)). Using Perrett et al. (2002) data, (Morrison et al., 2004) identified what appeared to be a *thin* disk population of GCs, constituting some 27% of the Perrett et al. (2002) sample. Subsequently, it has been shown that at least a subset of these objects are in fact young (≤ 1 Gyr), metal-rich star clusters rather than old "classical" GCs (Beasley et al. (2004), Burstein et al. (2004), Fusi Pecci et al. (2005), Puzia et al. (2005), Caldwell et al. (2009)).

Fusi Pecci et al. (2005, hereafter F05) presented a comprehensive study of bright young disk clusters in M31, selected from the Revised Bologna Catalog[2] (RBC, Galleti et al. (2004)) by color [$(B-V)_0 \leq 0.45$] or by the strength of the $H\beta$ line in their spectra ($H\beta \geq 3.5$Å). While these clusters have been noted since Vetesnik (1962) and have been studied by various authors, a systematic study was lacking. F05 found that these clusters, that they termed – to add to the growing menagerie of star cluster species – "blue luminous compact clusters" (BLCCs), are fairly numerous in M31 (15% of the whole GC sample), they have positions and kinematics typical of *thin disk* objects, and their colors and spectra strongly suggest that they have ages (significantly) less than 2 Gyr.

Since they are quite bright ($-6.5 \lesssim M_V \lesssim -10.0$) and – at least in some cases – morphologically similar to old GCs (see Williams & Hodge 2001a, hereafter WH01), BLCCs could be regarded as YMCs, that is to say, candidate young GCs (see de Grijs 2009, for a recent review). In particular, F05 concluded that if most of the BLCCs have an age $\gtrsim 50-100$ Myr they are likely brighter than Galactic open clusters (OC) of similar ages, thus they should belong to a class of objects that is not present, in large numbers, in our own Galaxy. Unfortunately, the accuracy in the age estimates obtained from the integrated properties of the clusters is not sufficient to determine their actual nature on an individual basis, i.e., to compare their total luminosity with the luminosity distribution of OCs of similar age (see Bellazzini et al. 2008, hereafter B08, and references therein).

In addition to the question of the masses and ages of these BLCCs, it has become clear that the BLCC photometric and spectroscopic samples in M31 may suffer from significant contamination. Cohen, Matthews & Cameron (2006, hereafter C06) presented NIRC2@KeckII Laser Guide Star Adaptive Optics (LGSAO) images of six candidate BLCCs. Their K' very-high spatial resolution images revealed that in the fields of four candidates there was no apparent cluster. This led C06 to the conclusion that some/many of the claimed BLCC may in fact be just *asterisms*, i.e. chance groupings of stars in the dense disk of M31. The use of the near infrared K' band (required by the LGSAO technique) may be largely insensitive to very young clusters that are dominated by relatively few hot stars, which emit most of their light in the blue region of the spectrum. Hence, the imaging by C06 may be inappropriate to detect such young clusters (see, for example, the detailed discussion by Caldwell et al. 2009). In any case, the study by C06 suggests that the true number of massive young clusters of M31 may have been overestimated.

Therefore, in order to ascertain the real nature of these BLCCs we have performed a survey with the Hubble Space Telescope (HST) to image 20 BLCCs in the disk of M31 (program GO-10818, P.I.: J. Cohen). The key aims of the survey are:

1. to check if the imaged targets are real clusters or asterisms, and to determine the fraction of contamination of BLCCs by asterisms,

2. to obtain an estimate of the age of each cluster in order to verify whether it is brighter than Galactic OCs of similar age. Ultimately the survey aims to provide firm conclusions on the existence of a significant population of BLCCs (YMCs) in M31, in addition to OCs (see Krienke & Hodge 2007, 2008, and references therein) and GCs.

In Perina et al. (2009a), hereafter Pap-I) we have described in detail the observational material coming from our survey, and the data reduction, and methods of analysis that we homogeneously adopt for the whole survey. We did that by taking the brightest of our

---

[2]www.bo.astro.it/M31
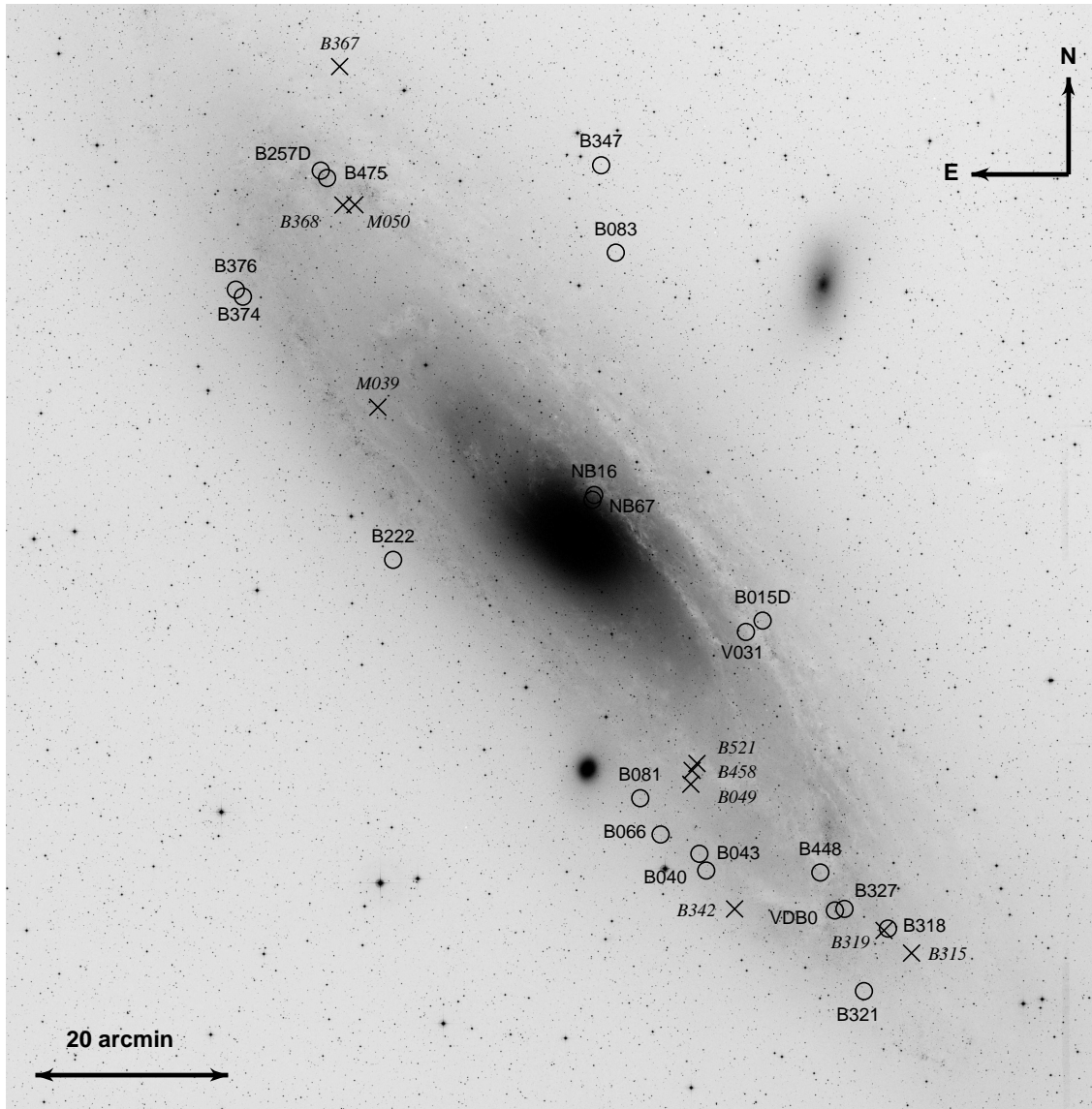
Figure 4.1: Location of the 20 targets of our survey (empty circles) projected against the body of M31. The × symbols indicate the position of the additional ten Young Clusters we included in Sect. 4.4.
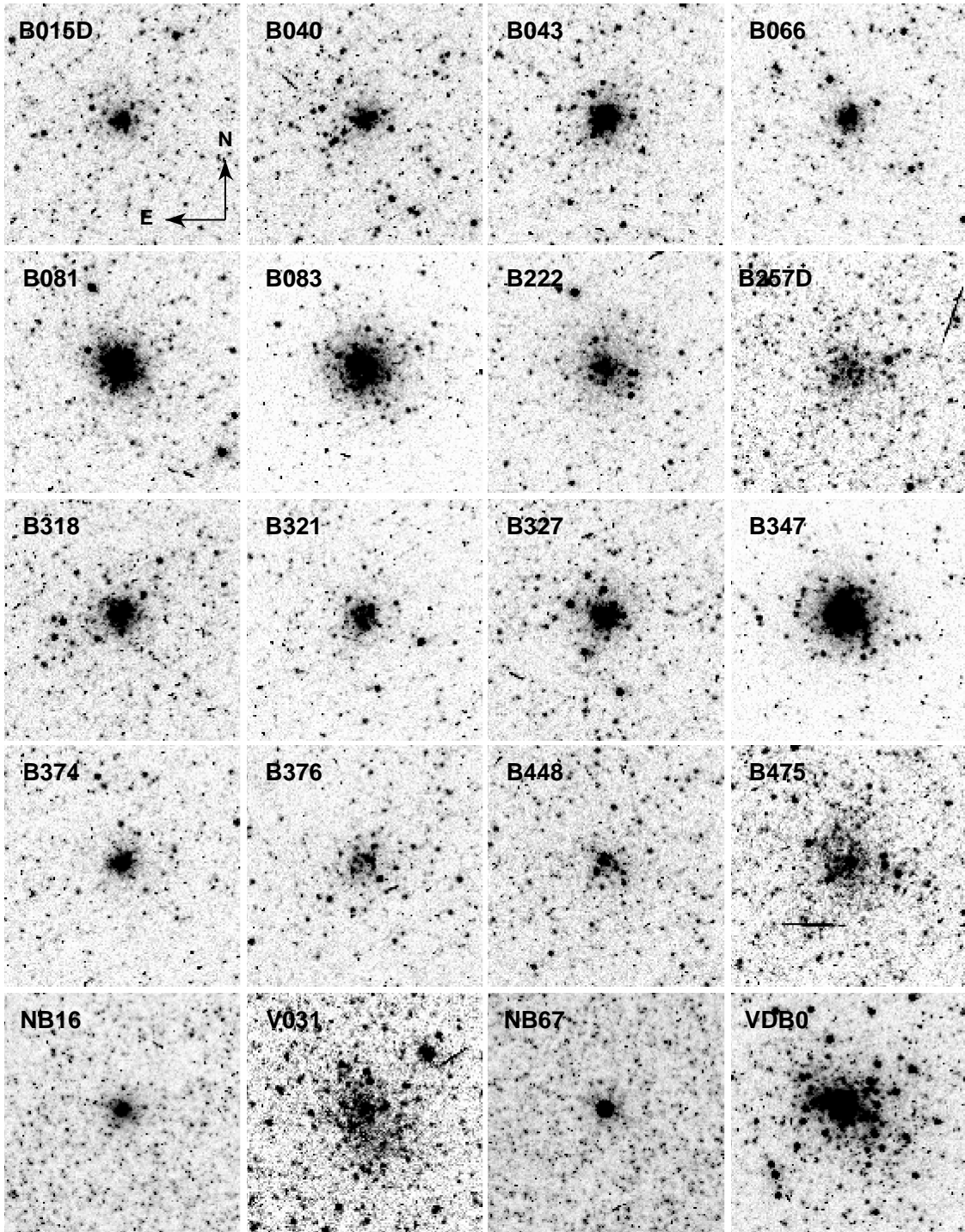
Figure 4.2: F450W images of the 20 primary targets. Each image covers the central $10'' \times 10''$ on the PC field ($10'' = 38$ pc at the assumed M31 distance modulus of 24.47). North is up and East to the left.

Table 4.1: Positional, photometric and spectroscopic parameters for the surveyed clusters.

Name	X^a (arcmin)	Y^a (arcmin)	R (arcmin)	B	V	$(B-V)_0^{F05}$	$(B-V)_0^{(t.w.)}$	H_β^{F05} ()	H_β^{G09} ()	ff^b
B015D-D041	-19.27	9.22	21.36	19.11±0.02	18.36±0.03	…	0.15	7.32	…	1
B040-G102	-35.40	-11.92	37.35	17.54±0.03	17.20±0.03	0.18	0.11	7.41	7.58± 0.30	1
B043-G106	-33.62	-11.37	35.49	17.04±0.03	16.77±0.04	0.17	0.04	5.53	5.70± 0.30	1
B066-G128	-29.55	-13.17	32.35	17.56±0.03	17.35±0.04	0.25	-0.02	4.67	4.84± 0.30	1
B081-G142	-25.26	-12.36	28.12	17.36±0.02	16.86±0.03	0.43	0.20	7.98	8.15± 0.30	1
B257D-D073	45.98	4.02	46.16	18.41±0.02	18.00±0.04	…	0.01	5.49	5.66± 0.30	1
B318-G042	-52.14	-1.32	52.16	17.02±0.03	16.82±0.03	0.06	0.03	…	5.49± 0.12	1
B321-G046	-55.50	-7.41	55.99	17.82±0.02	17.51±0.04	0.11	0.06	6.29	6.85± 0.32	1
B327-G053	-47.67	-3.45	47.79	16.75±0.03	16.58±0.03	0.21	-0.03	4.09	3.78± 0.14	1
B376-G309	42.16	-10.67	43.49	18.35±0.02	17.97±0.04	0.34	0.08	…	6.40± 0.06	1
B448-D035	-43.16	-2.97	43.26	18.01±0.03	17.46±0.04	0.50	0.20	6.70	6.87± 0.30	1
B475-V128	45.00	4.06	45.18	17.55±0.03	17.09±0.04	0.20	0.11	5.96	6.13± 0.30	1
V031	-19.03	7.17	20.34	18.16±0.03	17.62±0.04	0.57	0.19	5.84	6.01± 0.30	1
B083-G146	19.83	22.08	29.68	17.85^d	17.09^d	0.65	0.56	3.75	1.75± 0.42	1
B222-G277	10.22	-16.16	19.12	18.00±0.02	17.24±0.03	0.57	0.56	8.47	4.46± 0.31	1
B347-G154	27.74	26.74	38.53	17.23^d	16.50^d	0.62	0.67	…	2.87± 0.17	2
B374-G306	41.13	-10.55	42.46	18.69±0.03	18.23±0.04	0.33	0.16	4.07	4.24± 0.30	1
NB16	1.96	4.19	4.63	18.83±0.04	17.59±0.10	0.55	0.99	…	3.34± 0.08	2
VDB0	-47.16	-4.33	47.36	$14.94±0.09^c$	$14.67±0.05^c$	0.12	0.07	4.30	4.50± 0.07	1
NB67-AU13	1.68	3.73	4.09	16.48±0.02	15.92±0.03	0.37	0.36	…	…	1

B and V magnitudes are from new aperture photometry performed on the CCD images of Massey et al. (2006), except for B083 and B347 that are not included in the area covered by that survey.

[a] X and Y are projected coordinates in the direction along (increasing Eastward) and perpendicular to the major axis of M31, in arcmin.

[b] ff is a flag indicating if the target has been selected from Table 1 or Table 2 of F05.

[c] From Pap-I.

[d] From the RBC.

[(t.w.)] From this work: B and V from this table and E(B-V) as estimated in Sect. 3 from isochrone fitting.

[F05] From Fusi Pecci et al. (2005): $(B-V)_0$ are calculated assuming a single value of E(B-V)=0.11 for all the clusters.

[G09] From Galleti et al. (2009).

surveyed clusters (VdB0) as an example. In this contribution we apply the same process to the whole sample, obtaining metallicity, reddening and age estimates for all the targets of our survey. We incremented our final sample of candidate M31 YMC by including in the final analysis ten further clusters having age estimates available from the literature that are fully homogeneous with our own ones. In two companion papers, Hodge et al. (2009, Pap-II, hereafter) identified and studied clusters of lower mass (with respect to those studied here) that were serendipitously imaged in our survey, while Barmby et al. (2009), Pap-III, hereafter) studied the structure of the clusters that are the main targets of the survey.

The paper is organized as follows. The sample is described in detail in Sect. 2, where we also summarize the data reduction procedure. In Sect. 3 we present the individual color magnitude diagrams (CMDs) and luminosity functions (LFs), we estimate ages, metallicities and reddening of each cluster. In Sect. 4 we derive the mass estimates for the clusters of our extended sample (including data from the literature), we compare our clusters with open and globular clusters of the Milky Way, and we compare our estimates with those from the recent and extensive analysis of young M31 clusters by Caldwell et al. (2009, hereafter C09),

that are based on integrated spectra. In Sect. 5 our main results are briefly summarized and discussed. Finally, in Appendix A we report on M31 clusters or candidate clusters listed in the RBC that have been serendipitously imaged within our survey, and, in Appendix B, we report on the nature of candidate BLCC=YMC M31 clusters that have an HST image in the archive, independent of this survey.

4.2 Description of the sample

Table 4.1 lists the target clusters of our survey and reports some positional and spectro-photometric parameters that were relevant for their selection. New homogeneous large-aperture ($r_{ap} \sim 5'' - 10''$, depending on the curve of growth of each cluster) integrated B,V photometry for all the targets has been obtained from the publicly available CCD images by Massey et al. (2006), and calibrated using the published photometry from the same authors, as done in Pap-I for VdB-0 (see Pap-I for further details).

Fig. 4.1 shows that the vast majority of the targets are projected onto the so-called *10 kpc ring* (see Hodge 1992, Barmby et al. 2006, C09 and references therein), a site of ongoing star formation in the thin disk of M31. The only exceptions are B347 and B083, that are significantly farther from the center of the galaxy, and NB16 that is projected onto the outer regions of the M31 bulge. We will see below that these three clusters do not fulfill the selection criteria by F05 for *bona fide* candidate YMCs and, in fact, they are likely old (see Sect. 4.3.3).

Eighteen of the twenty targets were drawn from Tab. 1 of F05, i.e. they were confirmed clusters[3] that were classified as genuine BLCC = YMC by these authors as they had $H_\beta \geq 3.5$Å or, when lacking a measure of H_β, $(B-V)_0 \leq 0.45$. After a careful inspection of the HST archive, we excluded from the selection any cluster from Tab. 1 of F05 that had already been imaged with HST (serendipitously, in most cases, see Appendix B), and we chose the brightest 18 among the remaining ones. F05 assumed E(B-V)= 0.11 for all the considered sample, in Sect. 3 we will show that the typical reddening of these clusters is significantly higher than this, in most cases E(B-V)$\geq$ 0.20, in good agreement with the estimates by C09 (see Fig. 4.16). Hence, in general, the $(B-V)_0$ colors derived here are bluer than those adopted by F05. Galleti et al. (2009, G09 hereafter) presented new estimates of the H_β index (with respect to those reported by F05), taken either from their own observations or from the recent literature. In Table 4.1 we report both the $(B-V)_0$ and H_β values from F05 (that were used for the selection of the sample) and those derived here and in G09, when available[4]. In one case (B083) the new value of H_β is much lower than that reported by F05 (1.75Å instead of 3.75Å) and than the selection limit. Moreover, even with the new E(B-V) estimate derived here, $(B-V)_0 = 0.551$, significantly redder that the limit adopted for the selection. For these reasons B083 can no longer be considered as a candidate YMC, as it does not fulfill the selection criteria when the newly available data are considered. The analysis of the CMD (in Sect. 3) will confirm that the cluster is in fact much older than genuine YMC, and possibly as old as classical GCs.

The remaining two targets (NB16 and B347) were selected form Tab. 2 of F05, including clusters not fulfilling their selection criteria for YMC but classified as young (or possibly young) by some author in the past. In both cases H_β were lacking at the time, and the new values reported by G09 are significantly below the selection threshold for a YMC. B347 is also much redder than $(B-V)_0 = 0.45$. On the other hand, we find $(B-V)_0 = 0.399$ for NB16. In this case the criterion based on H_β must prevail over that based on de-reddened color as the former is reddening-independent, while relatively low photometric and/or reddening errors can shift the color of this cluster above or below the selection threshold. In conclusion, the newly available data indicates that both NB16 and B347 are not good YMC candidates, as will be confirmed by their CMDs (see Fig. 4.11). Hence, just re-considering the original

---

[3]RBC class f=1, meaning that they have been classified as bona-fide M31 clusters by some author, based on their spectra and/or high resolution images.

[4]Note that the scales of the H_β index adopted by F05 and G09 are slightly different. The $H_\beta \geq 3.5$Å threshold by F05 translated into $H_\beta \geq 3.7$Å in the scale by G09 (see the latter paper for discussion and details).
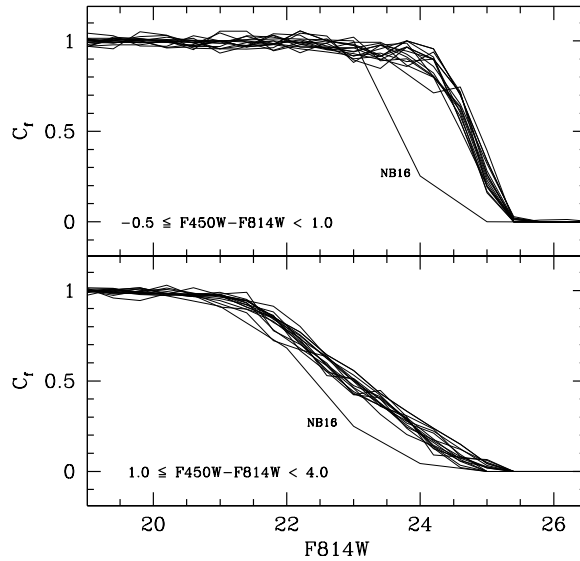
Figure 4.3: Completeness (C_f) of the samples as a function of F814W magnitude, obtained from artificial stars experiments, for all the clusters of our survey (listed in Tab. table:1) and for two different color ranges. The upper panel is for a color range enclosing the MS of young clusters, the lower panel is for a color range enclosing the red giant stars. The $C_f(F814W)$ function of each cluster (for each color range) is computed considering only artificial stars enclosed in the radial range that is used to select the sample dominated by cluster stars that will be studied in the following (typically $r \leq 5''$, see Sect. 4.2.2 and Sect. 4.3). Note that all the $C_f(F814W)$ functions are very similar, except for the case of the exceedingly compact (and crowded) cluster NB16, labeled in both panels.

selection in the light of new estimates of integrated properties, our sample of *bona fide* YMC candidates is reduced to 17 objects, including VdB0 which was studied in detail in Pap I.

Postage stamp images of all the targets, from our HST data, are presented in Fig. 4.2 (see Sect. 4.2.1). Inspection of the images reveal that all our targets are actually *genuine* clusters, with the only exception of NB67 that is a bright star projected into a dense background of M31 (disc) stars (see also Pap-III, for the light profiles of the clusters). For obvious reasons NB67 will be not considered further in the following analysis. A first conclusion that can be drawn just from this preliminary analysis is that the incidence of spurious objects in our sample is of $1/17 \simeq 6\%$, much lower than hypothesized by C06. If we consider the set of 36 objects listed by F05 in their Tab. 1 for which HST images were available in the archive we obtain the same result (see Appendix 4.B, for discussion and further details). Moreover, none of the considered clusters is in fact an *asterism* (including those considered in Appendix 4.B)[5]. Finally, if we extend our analysis to all the objects classified as YMC by F05 that have been ever imaged with HST we find the same very low degree of contamination (see Appendix 4.B). Hence we are dealing with a significant class of real stellar systems. A second conclusion is that while some of the considered cluster appear quite extended and sparse (like, for example, B257D, B475, and V031), there are also rather compact globular-like clusters (like, B043, B081, and B327, as noted earlier B347 is likely old).

---

[5]Bright stars are well-known classical contaminants in lists of candidate M31 clusters of any kind, see Galleti et al. 2006a.

4.2.1   Observations, data reduction and assumptions.

The characteristics of the survey data and the whole process of data reduction and data analysis that has been applied in this study is described in detail in Pap-I. In these section we briefly summarize the key characteristics of the dataset and of the process, for the convenience of the reader.

Two $t_{exp} = 400$ s images per filter (F450W and F814W) were acquired for each cluster with the Wide Field and Planetary Camera (WFPC2) on board of HST, keeping the target at the center of the PC field. Unlike the case of VdB0, treated in Pap-I, the clusters studied here have limiting radii significantly smaller than the size of the PC camera ($\simeq 39'' \times 39''$, see Pap-III), therefore both the cluster population and the surrounding field can be studied using the PC images alone (see Sect. 4.2.2) without relying on the WF cameras. The analysis of the field population in the portions of the M31 disk sampled by our WF images will be the subject of another contribution (Perina et al., in preparation).

Photometry of the individual stars has been obtained with HSTPHOT (Dolphin 2000a), a Point Spread Function fitting package specifically developed for WFPC2 data. The reduction process includes cleaning of cosmic-ray hits and bad pixels, correction for Charge Transfer Efficiency (CTE, Dolphin 2000b), and absolute photometric calibration in the VEGAMAG system (Holtzman et al. 1995, Dolphin 2000b). The images were searched for sources having peak intensities at 3σ above the background. The output catalogs were cleaned of spurious and/or badly measured sources by selecting stars with HSTPHOT global quality flag=1, *crowding* parameter < 0.3, $\chi^2 < 2.0$ and $|sharp| < 0.5$. The final catalogs containing position and F450W, F814W photometry of the PC fields will be made publicly available through a dedicated WEB page[6].

We estimated the completeness of our samples as a function of magnitude, color and position on the field by means of extensive artificial stars experiments (more than 10^5 artificial stars were simulated, per field of view, i.e. more than 4×10^5 per cluster), as described in detail in Pap-I. Fig. 4.3 show the completeness factor (C_f) as a function of magnitude for all the clusters, for two different color ranges (one covering the clusters' main sequence (MS) and one covering the Red (Super) Giant branches). The reported C_f curves refers to the circles enclosing most of the cluster population that are defined in Sect. 4.2.2, hence they are fully relevant for the following analysis. Note that the completeness conditions are very similar for all the clusters (including VdB0, presented in Pap-I), except NB16. This cluster is so compact that the considered region is much more crowded than all the other cases, thus the completeness is significantly worse. The typical photometric uncertainties as derived from the artificial stars experiments are $\lesssim \pm 0.02$ for $F450W \simeq F814W \leq 21$, $\lesssim \pm 0.05$ for $F450W \simeq F814W \leq 22.5$, and $\lesssim \pm 0.2$ for $F450W \simeq F814W \leq 24.0$ (see Pap-I, for details).

In the following we will always assume $(m - M)_0 = 24.47$, from McConnachie et al. 2005, corresponding to $D = 783$ kpc. At this distance $1''$ corresponds to 3.8 pc, $1'$ to 228 pc. We adopt $A_{F450W} = 4.015E(B - V)$ and $A_{F814W} = 1.948E(B - V)$, from Schlegel et al. 1998. We will use theoretical isochrones and LFs in the HST/WFPC2 VEGAMAG system from the set by Girardi et al. (2002, hereafter G02), considering only models in the range of metallicity $\frac{2}{5}Z_\odot \lesssim Z \lesssim 2Z_\odot$, that seem appropriate for young disk clusters. Details and discussion regarding the choices outlined above can be found in Pap-I.

4.2.2   Radial selection and first classification

Before proceeding with the analysis of the CMDs of the clusters, we need to select - for each cluster - a sub-sample of the PC field that is as representative as possible of the cluster population, possibly minimizing the contamination by the surrounding M31 field. Following Pap-I we adopt a radial selection, retaining in the final *cluster sample* the stars lying within a certain distance from the cluster center. To determine the selection radius to be adopted for each individual cluster we proceeded as follows:

---

[6]www.bo.astro.it/M31/YMC
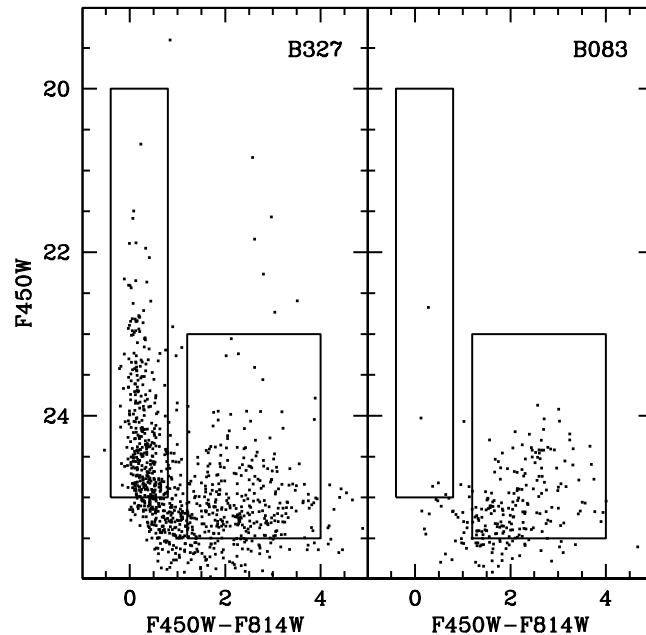
Figure 4.4: Selection boxes used for the stellar surface density profiles shown in Fig. 4.5, are superimposed on the CMD of two of the surveyed clusters taken as examples: a young cluster with a prominent MS (left panel) and an older cluster displaying just the tip of the RGB (right panel). The blue box at $F450W - F814W \sim 0.5$ selects bright MS stars (young population), the faint redder box ($F450W - F814W > 1.0$) selects red giant stars (old population). In a few cases, the boxes have been slightly shifted in color to best match the MS and RGB features of a cluster with higher reddening.

- We defined two broad selection boxes on the CMD, one enclosing the bright MS typical of young clusters (Blue Box) and one enclosing a redder region that should be dominated by old stars at the tip of the red giant branch (RGB) but can enclose also intermediate-age asymptotic giant branch (AGB) and some red super giant (RSG) stars, as illustrated in Fig. 4.4 (Red Box).

- We derived surface-density radial profiles by counting stars selected in the two boxes on concentric annuli. To obtain smoother profiles with the relatively low number of stars available we adopted overlapping annuli of width $1.8''$, with a radial step of $0.9''$ between subsequent annuli. The profiles from main sequence (MS) stars and from red stars (shown in Fig 4.5) are normalized to the minimum surface-density encountered in the raster of radial annuli, that should be considered as roughly representative of the surrounding field. For example, the profiles of B066, in the middle left panel of Fig 4.5 (upper figure), shows that at the center of this cluster the surface density of bright MS stars is $\gtrsim 20$ times higher than in the surrounding field, while there is no overdensity of red stars correlated to the cluster.

- Based on the scale of the detected overdensity we fixed the selection radius of each cluster (marked in the plots as a vertical dashed line), with the aim of isolating a circle that should be dominated by cluster stars. The typical selection radius is $r \sim 5''$.

In the following we will analyze only the CMDs of the radially selected samples, as the best representation of the population of each cluster. The CMDs of the surrounding fields are shown in Fig. 4.6, for comparison with those of the respective clusters that are studied in detail in Sect. 4.3.

Fig 4.5 deserve some further comment. First of all, it has to be noted that all the clusters (at their centers) show an overdensity of a factor of $\gtrsim 10$ with respect to the surrounding field,
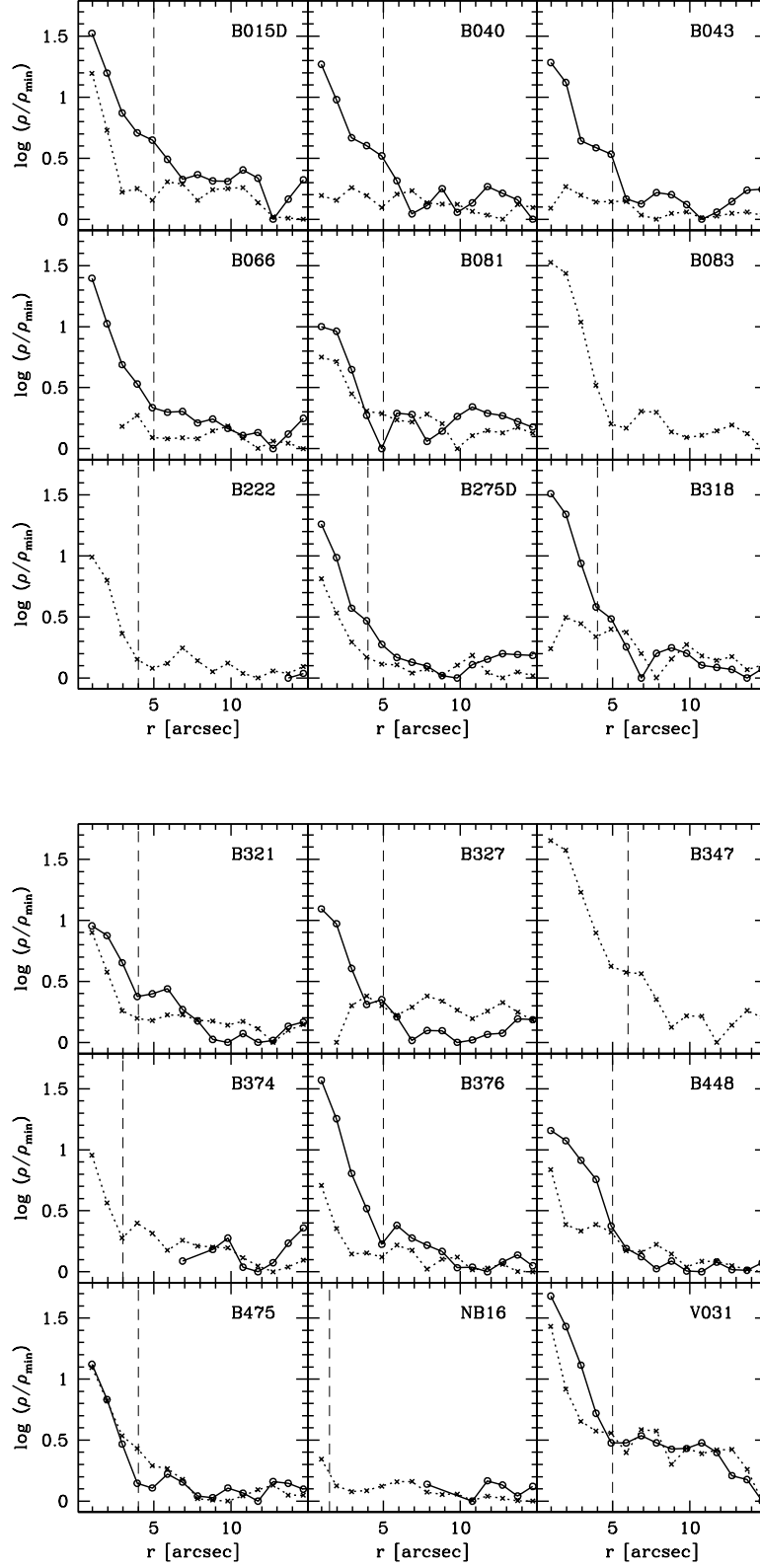
Figure 4.5: Stellar surface density profiles of the young (open circles connected by a continuous line) and old (crosses connected by a dashed line) populations (as defined by the selection boxes illustrated in Fig. 4.4) for the surveyed clusters.
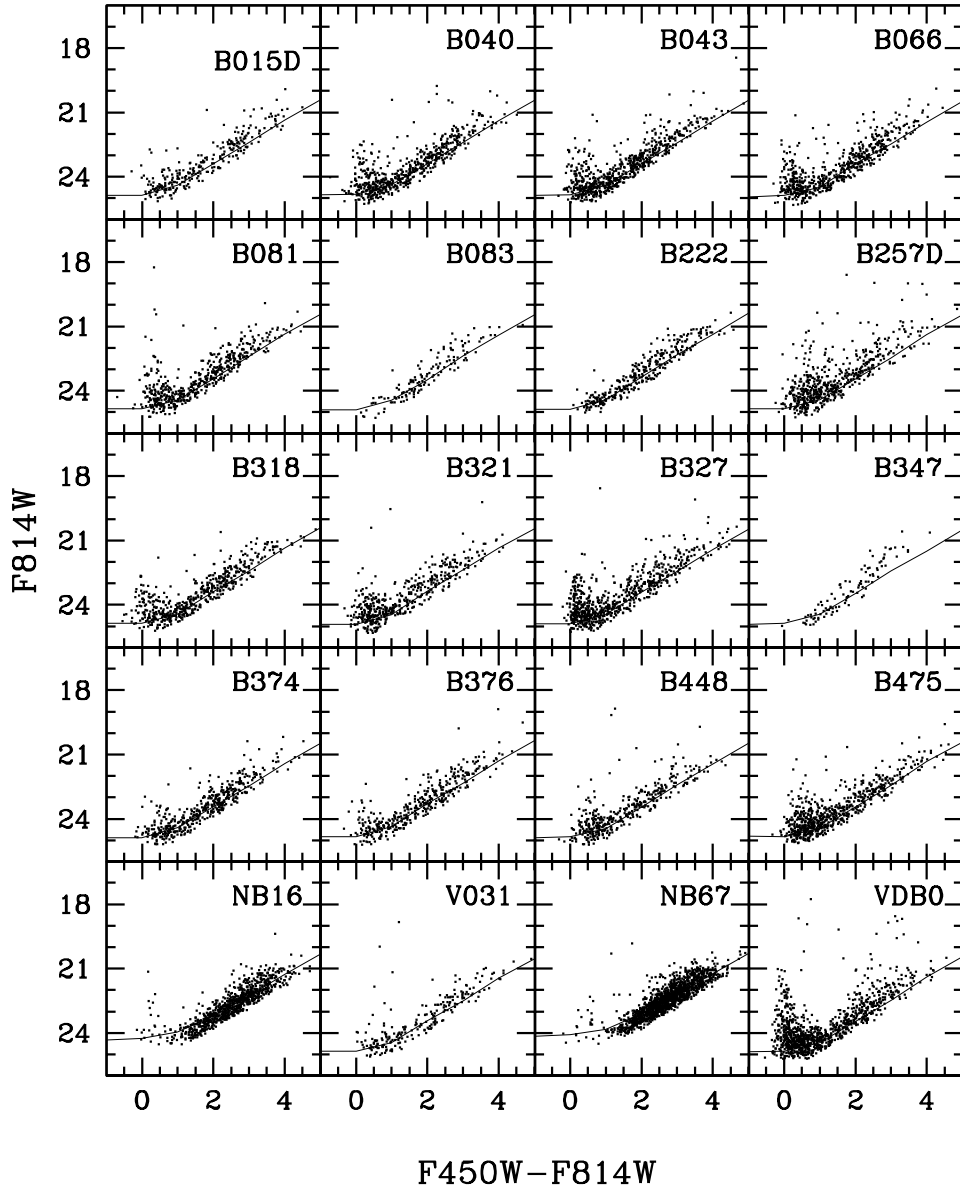
Figure 4.6: CMDs of the fields surrounding the target clusters. Only stars lying in the radial range $5'' r \leq 16.5''$ on the PC chips are plotted. The thin lines are the loci where the completeness reaches 50%.

at least in one of the two profiles. The only exception is NB16 that is so compact that only a tiny corona is resolved into stars, resulting in a low ($\sim 2\times$) overdensity of red stars (but see the light profile obtained in Pap-III). Note that in many cases, the very central region of the cluster is not fully resolved, thus the reported central overdensities are just lower limits to the true ones. Second, there are five clusters that show no sign of overdensity in the Blue Box. B083, B347, and NB16 have been discussed above; they cannot be considered as YMC candidates anymore. B222 and B374 on the other hand have both $H_\beta > 3.5$Å. In four cases the cluster show no sign of overdensity in the Red Box, in particular, B040, B043, B066, B327. In all the other cases, the overdensity is detected in both the Blue and Red boxes populations, even if not necessarily in similar degree. In general the overdensity from MS stars is larger than in RGB/AGB/RSG, as expected from evolutionary considerations (Renzini & Fusi Pecci

1988).

4.3 Age and metallicity

Once established that our targets are real clusters, the main purpose of our survey is to obtain a reliable age estimate for all of them from their CMDs. This will be done by comparison with theoretical isochrones from the set by Girardi et al. (2002, G02 hereafter, the models are in the same photometric system as the data; see Pap-I for a discussion about the choice of the set of theoretical models), following the approach described in detail in Pap-I. The procedure provides a simultaneous estimate of the age, the reddening and the metallicity of each cluster under consideration, by eye-aided isochrone fitting. In Pap-I we have shown that the data from our survey can be used to reliably estimate ages in the range from ~ 10 Myr to < 500 Myr (also depending on the total mass of the considered clusters, i.e. on the number of stars populating the MS), from the luminosity and color of the Turn Off (TO) point. The distribution of RSG may help to constrain the metallicity of the population, while the color of the blue edge of the MS is the best indicator of the degree of interstellar extinction (see Pap-I).

In our sample, there are eleven clusters that have a significant number of MS stars brighter than $F814W = 24.0$. As the completeness of the sample is $C_f \gtrsim 80\%$ above this limit, (in the color range enclosing the MS, see Fig. 4.3), reliable completeness-corrected LFs of the MS population can be obtained, and used to further constrain the age of these clusters, as one in Pap-I. All of these eleven clusters have ages lower than $\simeq 200$ Myr. They are homogeneously analyzed in Sect. 4.3.1. Also VdB0 belongs to this class but it is not considered here as it has been already treated in Pap-I.

Two clusters (B475 and V031) show a clear MS population only for $F814W > 24.0$. As their observed MS lie in a range where the completeness factor drops from $C_f \sim 80\%$ to $C_f \sim 0$ in ~ 2 magnitudes their LF would be strongly affected by large completeness corrections. For these reason we limit our analysis to isochrone fitting for these clusters (Sect. 4.3.2).

Finally, there are five clusters that do not display any obvious MS population in the range of magnitudes accessible with our data. For these clusters we can provide only a strong lower limit to their age, that must be older than 300-500 Myr. These clusters are discussed in Sect. 4.3.3. The final results of the analysis of the CMD presented below are reported in Tab. 4.2.

4.3.1 Clusters with bright MS (age< 200 Myr)

Fig. 4.7, 4.8 and 4.9 show the observed CMDs and LFs of the eleven clusters having a significant MS population brighter than $F814W = 24.0$. The boxes overplotted on the CMDs have been used to select the stars that were used to derive the LFs.

For each cluster we explored the space of parameters to find the isochrone and the reddening providing the best overall fit to the observed CMDs. As differential reddening may move stars toward the red and the presence of binary systems also has the effect of broadening the MS toward the red side, we searched for solutions where the theoretical MS fits the blue side of the MS. As noted above, the distribution of RSGs was used as a guide to fix the metallicity of the best-fit model (see Pap-I). Following the approach of Pap-I, we adopt Z=0.019 as the starting guess for the metallicity of the cluster, trying other metallicity only if this was required to better fit some feature of the CMD. A correct interpretation of the cluster CMD was aided by a comparison with the CMD of the surrounding field, to establish, for example, if a population of a few RSG can be considered as characteristic of the cluster or compatible with belonging to the field. The typical uncertainty on the reddening estimate is ±0.04 mag (see Pap-I).

The theoretical LF of the isochrone that best-fits the observed CMD morphology (thick continuous line in the right panels) is compared to the observed LF (filled dots with error bars) to check the compatibility of the solution with the star counts (Salpeter's 1955 Initial
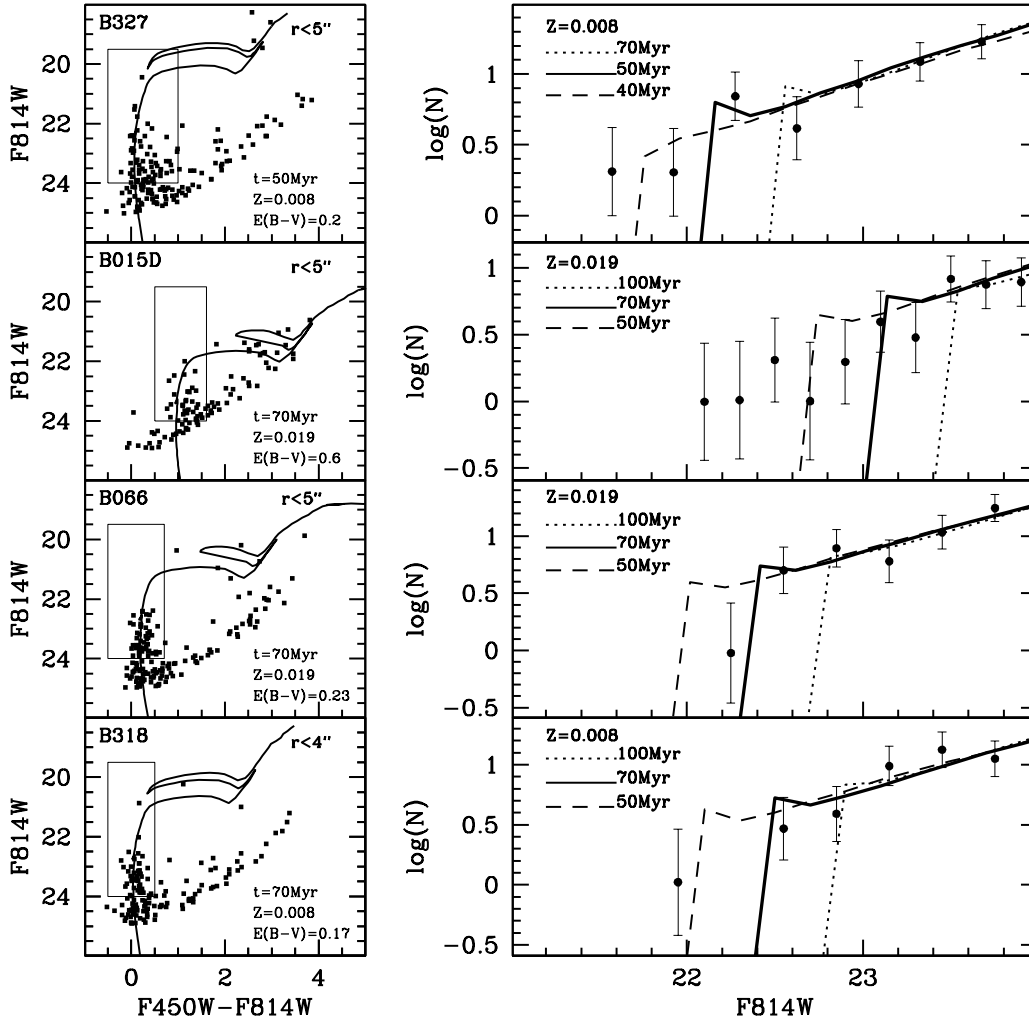
Figure 4.7: Left panels: CMDs of the clusters B327, B015D, B066, and B318, displaying only stars within the radial selection reported in the upper right corner of each panel. The adopted best-fit value of the reddening and the age and metallicity of the best-fit isochrone (thick continuous line) are reported in the lower right corner of each panel. The rectangular boxes adopted to select the stars used to obtain the LFs shown in the right panels are also plotted. Right panels: the observed completeness-corrected LFs of the cluster MS (filled circles with error bars) are compared with theoretical models of different ages. The thick continuous line corresponds to the best-fit model shown in the CDMs. In all cases, it provides a reasonable fit to the observed LF and, in particular, to the sudden drop of star counts at the upper limit of the MS. The dotted and dashed lines are theoretical LFs corresponding to strong upper and lower limits to the age, respectively, as they are the nearest models that can be clearly excluded by the data. The theoretical LFs have been arbitrarily normalized to best match the three faintest observed points.
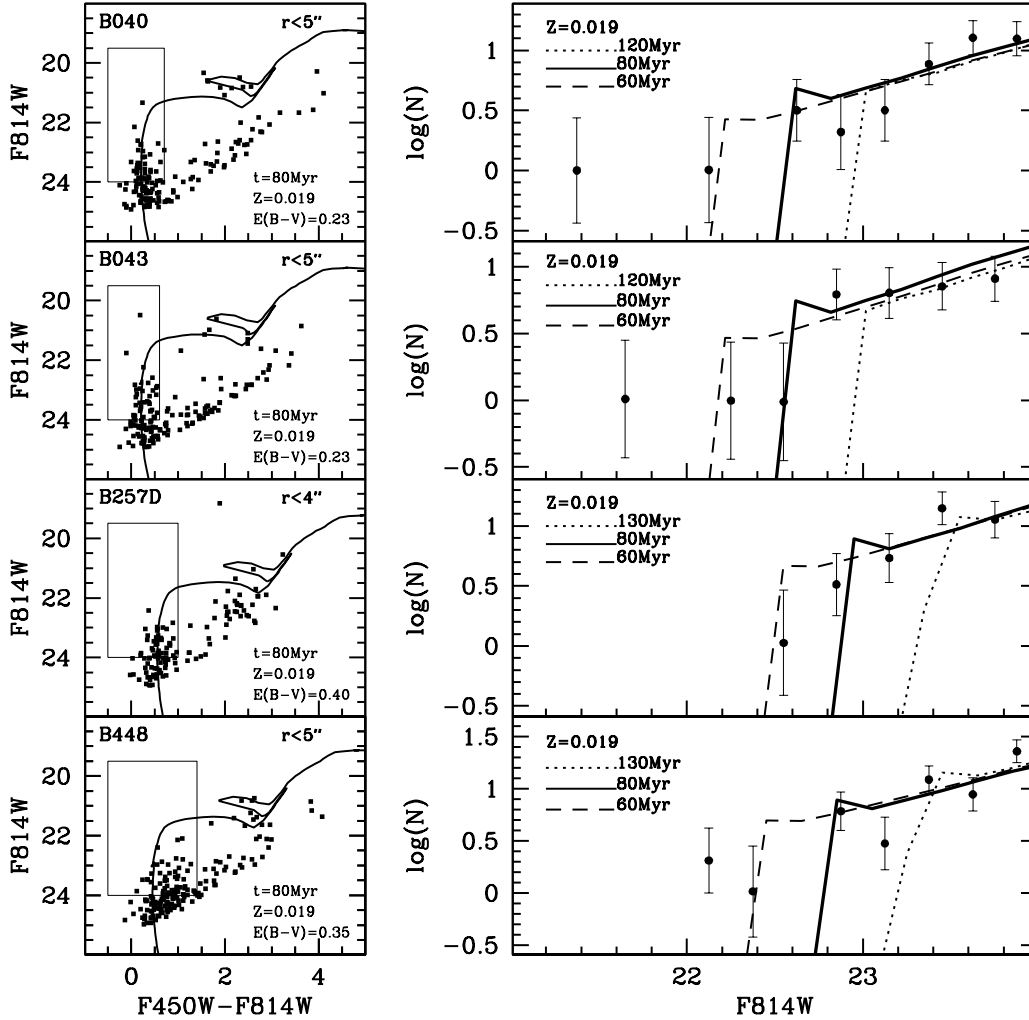
Figure 4.8: Same as Fig. 4.7 but for the clusters B040, B043, B257D, and B448.

Mass Function is adopted). In all the cases considered the adopted theoretical LF is in good agreement with the observations and, in particular, it reproduces the sudden drop in star counts corresponding to the upper luminosity limit of the MS, a feature that is mainly sensitive to age (see Pap-I and references therein). Two theoretical LFs of the same metallicity as the main solution but different ages are used to show the maximum and minimum age that are not compatible with the observed LF. The difference between these values and the age of the best-fit solution are taken as the uncertainty associated with our age estimate. Nine of the eleven clusters considered in this section have ages between 50 Myr and 100 Myr. All of them show a recognizable (and in same case sizable, see B040, for example) population of RSG stars, in addition to an obvious MS. The other two clusters, B081 and B321 have ages of 140 and 170 Myr, respectively.

4.3.2 Clusters with faint MS (200 Myr≤age≤ 500 Myr)

Fig. 4.10 shows the CMDs of the two clusters whose MS is fainter than *F814W* = 24.0. The F450W magnitude is plotted here instead of F814W (adopted in Fig. 4.7, 4.8 and 4.9)
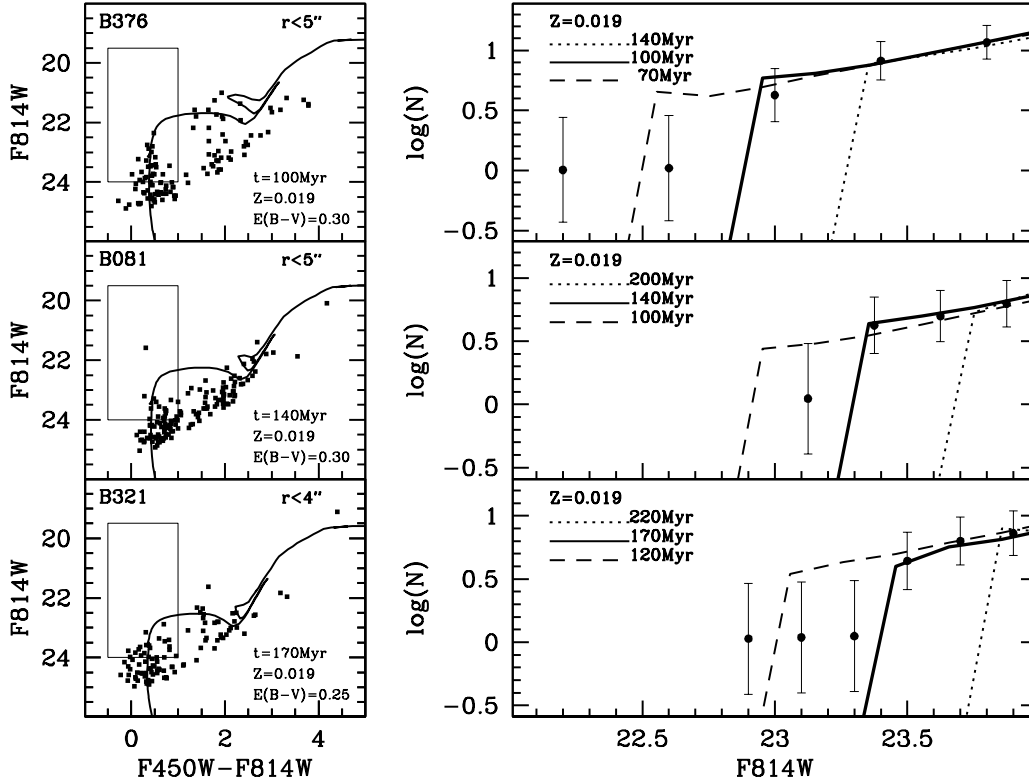
Figure 4.9: Same as Fig. 4.7 but for the clusters B376, B081, and B321.

as this makes the faint MS of these clusters more clearly visible. The best fit isochrones are plotted as thick lines. The thin lines are isochrones having ages that bracket the age solutions that can be considered still compatible with the data. The difference in age between these solutions and the assumed best-fit are adopted as the uncertainty associated with our age estimates for this cases (see Pap-I). The two clusters have ages of ≃200 Myr (B475) and ≃280 Myr (V031).

4.3.3   Clusters whose MS is not detected (age> 500 Myr)

Fig. 4.11 shows the CMDs of the clusters that do not display a clear MS in the considered range of magnitudes. In each panel we plot (a) the "youngest" isochrone that is compatible with the observed CMD morphology, to provide a firm lower limit to the age of these clusters (thick continuous line), and, (b) a 12 Gyr old isochrone (thick dashed line), showing that the observed CMD is also compatible with very old ages. In all the cases we adopt the metallicity value that provided a satisfactory match of the color of the (putative) RGB.

Three of the five clusters considered here (B083, NB16 and B347) have integrated properties that are compatible with old ages (see Sect. 4.2). B083 and B347 display a steep and well populated red sequence, much bluer than the limits imposed by the run of the completeness as a function of color (thin dotted lines), typical of the RGB of classical old (and metal deficient) GCs. The handful of stars resolved in NB16 are also compatible with being near the tip of an old RGB, but their scarcity poses strong caveats on any interpretation.

B347 and B222 are more interesting cases: both have two independent concordant estimates of H_β indicating $H_\beta > 4.0$Å, and both have some stars just above the detection limits in the blue, that may be compatible with the bright end of a fainter MS. The observational scenario is fully consistent with the hypothesis that these two clusters might be intermediate-
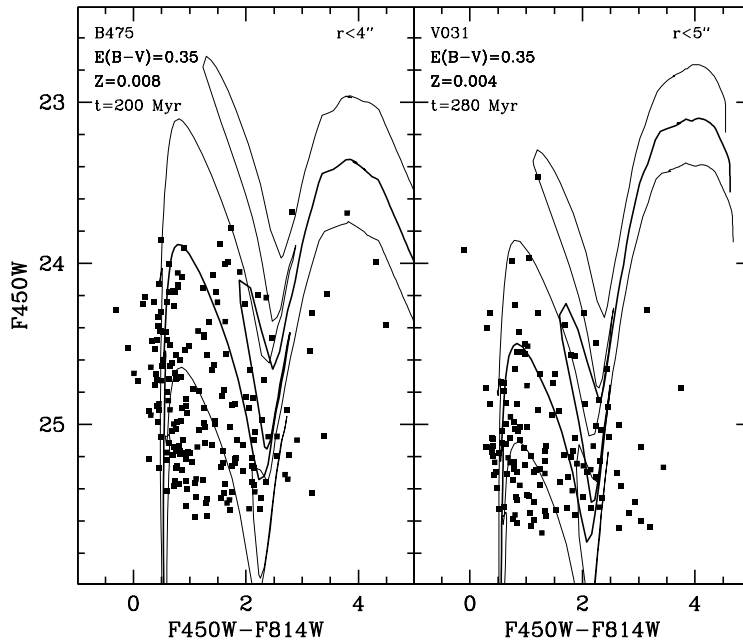
Figure 4.10: Observed CMDs of the clusters B475 (left panel) and V031 (right panel) in the plane F450W vs. F450W-F814W where the MS population of these older clusters is more clearly visible. Only stars with the radial selection reported in each panel are plotted. The best-fit isochrone is plotted as thick line (age, metallicity and reddening values are reported in each panel). The thin isochrones bracket the upper and lower limits on the age, and correspond to age $\simeq$ 125 Myr and 315 Myr for B475, and age 200 Myr and 400 Myr for V031.

age (age~ $0.5 - 2$ Gyr). A deeper photometry follow-up is clearly required to settle the issue of the age of these clusters. It is worth noting that a convincing case for an M31 cluster in the age range 1-8 Gyr with age estimated from a CMD has never been provided.

4.4 Masses from ages and J,H,K integrated photometry

In Table 4.2 we report the age, metallicity and reddening estimates obtained from the analysis of the CMDs presented above. To increase the sample of YMC to be considered in the following we added a total of 10 further clusters whose ages have been derived from CMDs obtained from HST data in a way fully homogeneous with that adopted here. In particular we add six clusters from Perina et al. (2009b, P09b hereafter) and four clusters from Williams & Hodge (2001, WH01 hereafter; see Pap-I). All of them lie in the range of V luminosities typical of YMC ($M_V \lesssim -6.5$, according to F05), with the only (possible) exceptions of M050 and M039 that appear somewhat fainter than this, and of B521 that lacks an estimate of its V magnitude (but it is found to have a mass similar to other YMC, based on its Near Infrared Magnitudes, see below). We decided to keep these clusters within our sample, being well aware that the threshold between the brightest of the clusters studied in Pap-II and Krienke & Hodge (2007, 2008) and the faintest clusters considered here is somewhat blurred, both by lack of a clear-cut definition and by observational uncertainties. In particular, Fig. 4.19, will show that some of the clusters studied in Pap-II appear to have masses typical of YMC. Still we preferred not to include these massive Pap-II clusters as main objects of the present analysis as most of them have their ages estimated from integrated colors, i.e. with significantly greater uncertainties than those obtained here from CMDs (see, e.g., Fig. 8 of
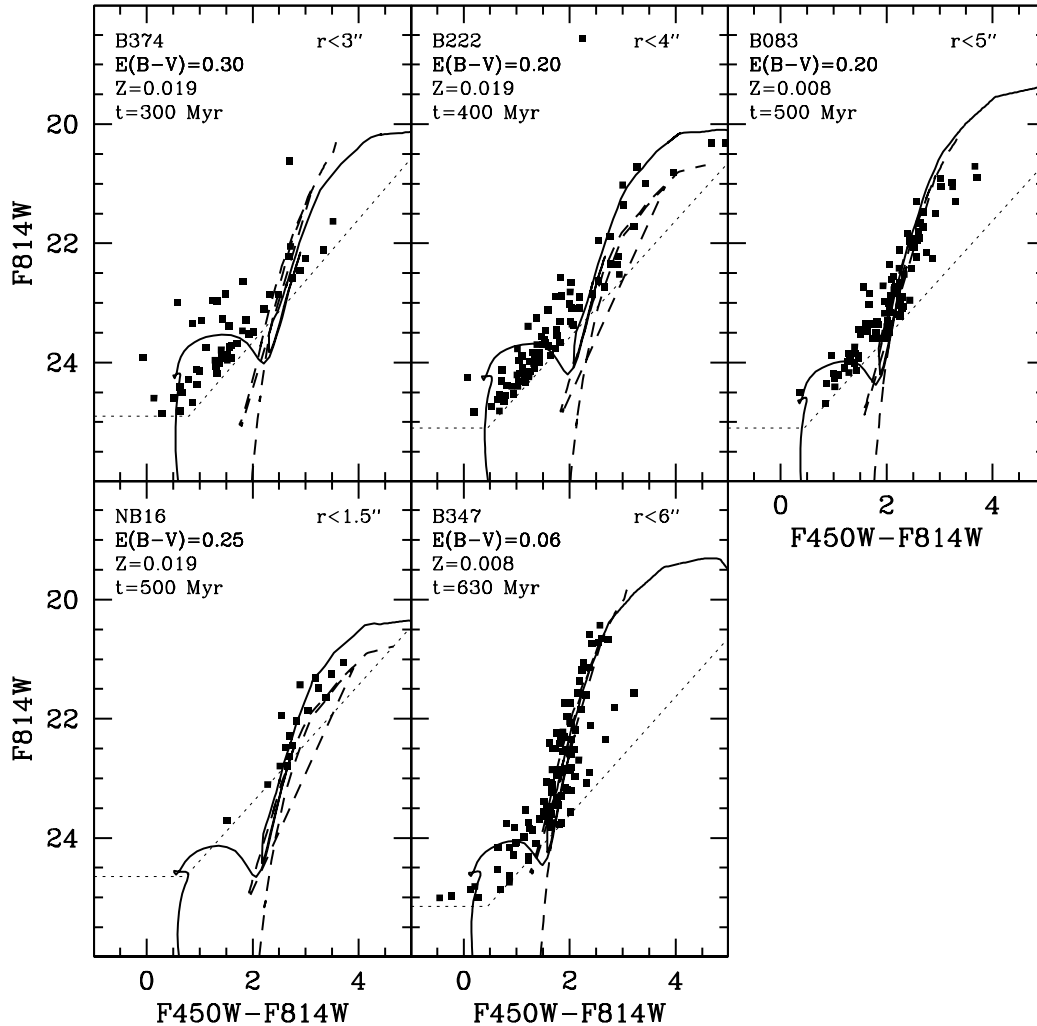
Figure 4.11: CMDs of the clusters B374, B222, B083, NB16, and B347. Only stars within the radial selection reported in each panel are plotted. The thin dashed lines marks the locus where the completeness of the sample reaches ≃ 0% (see Pap 1), to illustrate the selection effects on the CMD morphology imposed by the run of limiting magnitude as a function of color. In each panel, the continuous line is the youngest age isochrone that is compatible with the observed CMD, providing a strong lower limit to the age of each cluster. The adopted age, metallicity and reddening values are reported in the upper left corner. The dashed line is a 12 Gyr old isochrone matching the color of the observed RGB. The metallicity of these old-age isochrones is $Z = 0.001, 0.004, 0.001, 0.004,$ and 0.001 for B374, B222, B083, NB16, and B347, respectively.

Pap-II)[7].

Five of the newly included clusters are projected onto the 10 kpc ring, as most of our original targets, four lie slightly nearer to the center of the galaxy, and one is in the outskirts of the visible disk (see Fig. 4.1). B049, B367, B458, B315 and B317 have two independent estimates of H_β, all of them higher than 4.5Å (F05, G09). B342 has just one estimate

_____

[7]There are only two clusters from Pap-II having $M_V \lesssim -6.5$ and ages estimated from their CMD, but also in these cases the associated age uncertainties are relatively large, i.e. 0.5-0.6 dex in log(Age) vs. a typical uncertainty of 0.2 dex for our main sample, see Tab. 4.2.

($H_\beta = 7.06$Å, FP05), while the other four clusters lack any measure of this index. B368 lacks H_β but has $(B-V)_0 = 0.06$. For M039, M050 and B521 there is no $(B-V)_0$ estimate available. In any case all the six clusters from P09b and the four from WH01 have age < 1 Gyr, as derived from their CMD.

To derive the most reliable estimate of the total stellar mass of the clusters in our sample we couple our age estimates with integrated Near Infra Red (NIR) photometry, as stellar mass-to-light ratios in NIR bands have a much shallower dependence on age than their optical counterparts (see Pap-I for discussion). As the best estimate of the integrated J,H,K magnitudes we took the values of the $r = 10''$ aperture magnitudes from the 2MASS-6X-PSC catalog (see Nantais et al. 2006), that is obtained from deeper observations (with respect to the normal 2MASS data, Skrutskie et al. 2006) over a limited region of the sky that, luckily, includes M31. The adopted NIR photometry as well as the accurate positions reported in 2MASS-6X-PSC are listed in Table 4.3. Only two clusters have no valid measures in 2MASS-6X-PSC, i.e. B367 and M039. To preserve the homogeneity of the analysis we do not include these clusters in any of the following analyses that make use of mass estimates, however, for completeness, in Tab. 4.3 we provide a tentative mass estimate derived from the log(age) *vs.* M_V diagram presented in Fig. 4.13. The apparent magnitudes are transformed into absolute ones adopting the reddening estimates derived here (Tab. 4.2), the distance modulus (from McConnachie et al. 2005) and the reddening laws (from Rieke & Lebofsky 1985) adopted in Pap-I.

In Fig. 4.12 we compare the position of our clusters in the integrated (J,H,K) magnitude vs. log(age) plane with a grid of models of Simple Stellar Population (SSP) of solar metallicity and various total mass, from the set by Maraston (2001, 2002, see Pap-I). In B08 and in Pap-I we have shown that the mass that can be deduced from these plots depends only weakly on the assumed metallicity and IMF. Here we get an independent estimate of the mass from each (J,H,K) plot and we take the weighted average of the three values as our final estimate. The uncertainties were obtained on each individual estimate from J, H, K by finding the maximum interval in mass that was compatible with the errors in age and in integrated magnitudes. Then the three values (per cluster) were combined into the final *weighted* error that is reported in Table 4.3 together with the final mass estimates.

It is very reassuring to note that the three plots provide very similar age estimates: all the clusters considered appear to have masses between $\sim 10^4 M_\odot$ and $\sim 10^5 M_\odot$. The estimates from the three different NIR magnitudes typically agree within a factor of 2. The adoption of a Kroupa 2001) IMF instead of that of Salpeter would change the mass estimates by less than a factor of 2 (Pap-I). The adoption of different sets of models would lead to a maximum difference of the same amount in the final mass estimates (we have compared the M/L predictions adopted here with those from the sets by Pietrinferni et al. 2004 and Bruzual & Charlot 2003, in the age range that is relevant for our clusters). Finally, if models with age-dependent M/L are adopted (i.e. including the effects of differential mass loss, Kruijissen & Lamers 2008), the mass estimates for our clusters change by a mere $\lesssim 20\%$ (see also Pap-III). Taking all of these factors into account it turns out that our mass estimates should be accurate within a factor of $\lesssim 3$, as confirmed also by the comparison with the independent estimates from Pap-III and C09.

There is only one case of significant disagreement in the position of a cluster in the different NIR passbands, i.e. B347 whose reported H magnitude implies a (lower limit) mass estimate nearly one order of magnitude lower than J and K. We attribute this occurrence to an error of the integrated H magnitude reported in 2MASS-6X as this value is at odds with that of all the other clusters while B347 is normal in all other respects. For instance it has a J-K color well within the range of the other clusters of the sample while its H-K color is more than one magnitude redder than any other. Finally we note that the independent lower limit mass obtained from the log(age) vs. M_V diagram (see Fig. 4.13), are in good agreement with that estimated from J and K magnitude for B347. Finally, as we have obtained just a lower limit to the age of B347 we do not provide an age estimate for this cluster. B347 as well as all the other clusters for which we can provide only a lower limit to the age are not included in the analysis of Sect. 4.5 that is limited to the young clusters that constitute the main subject

Table 4.2: Newly derived ages, metallicity and reddening for the target clusters and other clusters included in the analysis[a].

Name	log(t)	Δlog(t)	Z	E(B-V)	M_v[b]
This survey					
B015D-D041	7.85	±0.15	0.019	0.60	-8.53
B040-G102	7.90	$^{+0.20}_{-0.15}$	0.019	0.23	-7.80
B043-G106	7.90	$^{+0.20}_{-0.15}$	0.019	0.23	-8.22
B066-G128	7.85	±0.15	0.019	0.23	-7.76
B081-G142	8.15	±0.15	0.019	0.30	-8.60
B257D-D073	7.90	$^{+0.20}_{-0.15}$	0.019	0.40	-8.31
B318-G042	7.85	±0.15	0.008	0.17	-7.98
B321-G046	8.23	$^{+0.10}_{-0.15}$	0.019	0.25	-7.57
B327-G053	7.70	$^{+0.15}_{-0.10}$	0.008	0.20	-8.51
B376-G309	8.00	±0.15	0.019	0.30	-7.34
B448-D035	7.90	$^{+0.20}_{-0.15}$	0.019	0.35	-8.07
B475-V128	8.30	±0.20	0.008	0.35	-8.00
V031	8.45	±0.15	0.004	0.35	-8.12
VDB0	7.40	±0.30	0.019	0.20	-10.03
B083-G146	>8.70	…	0.008	0.20	-8.00
B222-G277	>8.60	…	0.019	0.20	-7.66
B347-G154	>8.80	…	0.008	0.06	-8.16
B374-G306	>8.50	…	0.019	0.30	-7.09
NB16	>8.70	…	0.019	0.25	-7.69
P09b					
B049-G112	8.45	±0.20	0.019	0.30	-7.84
B367-G292	8.30	±0.20	0.019	0.25	-6.79
B458-D049	8.50	±0.20	0.019	0.25	-7.40
B521	8.60	±0.30	0.019	0.55	…
M039	8.50	±0.20	0.019	0.10	-5.84
M050	8.75	±0.30	0.019	0.15	-6.22
WH01					
B315-G038	8.00	$^{+0.15}_{-0.20}$	0.008	0.31	-8.96
B319-G044	8.00	$^{+0.15}_{-0.20}$	0.008	0.23	-7.57
B342-G094	8.20	$^{+0.15}_{-0.20}$	0.008	0.20	-7.36
B368-G293	7.80	±0.10	0.019	0.20	-7.17

For five surveyed clusters only a lower limit to the age can be obtained from our CMDs.

[a] The additional clusters are six clusters studied in Perina et al (2009a), from HST archive data, and the four clusters studied by Williams & Hodge (2001).

[b] Integrated V magnitudes from the RBC.
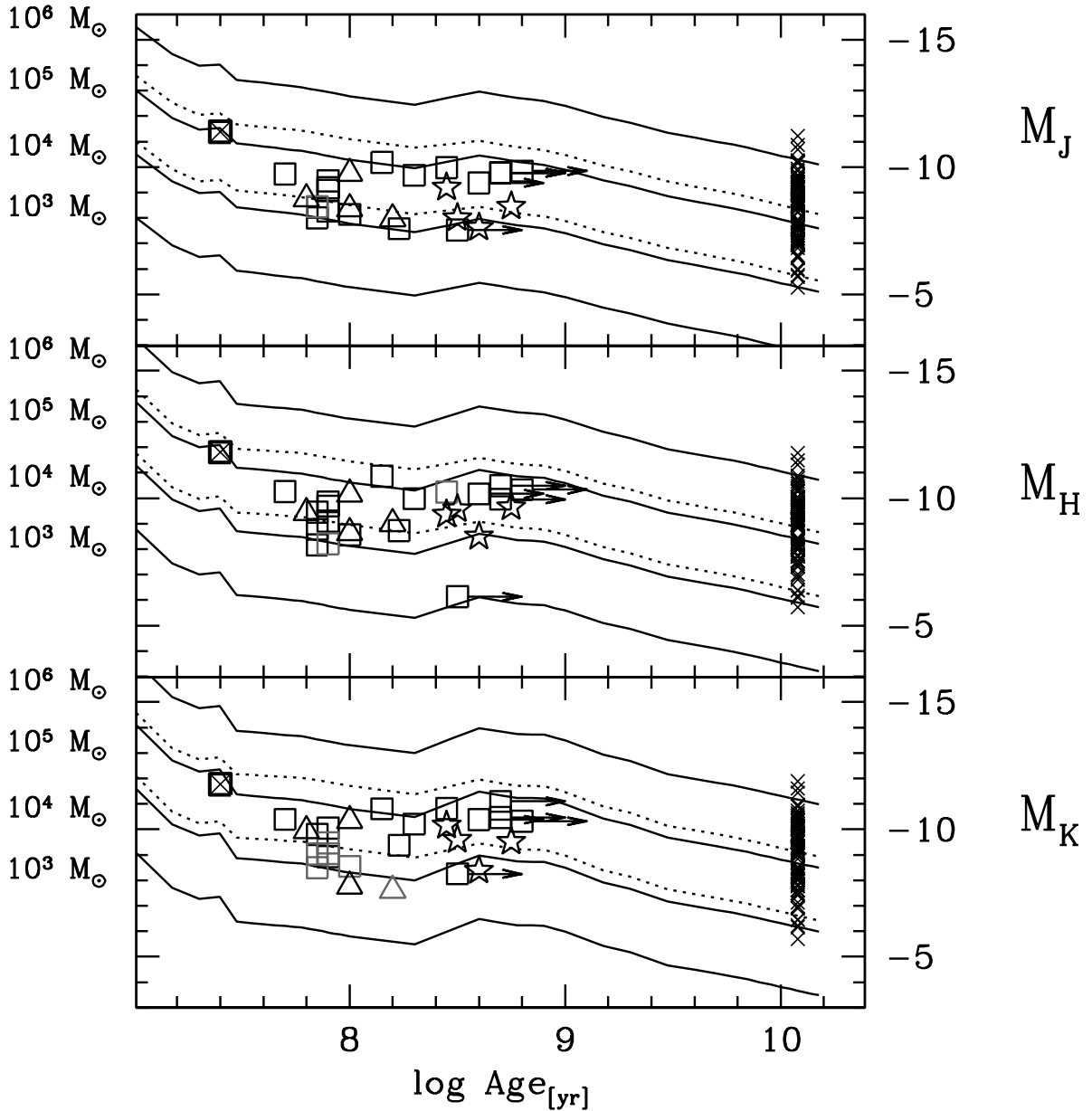
Figure 4.12: Log(age) vs. integrated magnitude plane for near infrared colors. The target clusters are represented as open squares (VDB0 as a crossed square), the clusters from P09b as open stars, and the clusters from WH01 clusters as open triangles, IR magnitudes are taken from Tab. 4.3. Note that B367 and M039 are not plotted because they lack NIR photometry in the 2MASS-6X-PSC catalog. The gray symbols show the clusters that have "null" error on IR magnitudes in the 2MASS-6X-PSC catalog. Integrated magnitudes of Galactic GCs ($\times$ symbols) are taken from Cohen et al. (2007). The continuous lines are fixed-stellar-mass models from the set by Maraston (1998, 2005) for SSPs of solar metallicity, with a Salpeter's Initial Mass Function (IMF) and intermediate Horizontal Branch morphology. Note that in this plane, the dependence of the models from the assumed IMF, metallicity and HB morphology is quite small (see B08). The dotted lines are $M = 10^4 M_\odot$ and $M = 10^5 M_\odot$ iso-mass models assuming a Kroupa (2001) IMF instead of a Salpeter (1955) IMF, plotted here to illustrate the weak effect of assumptions on IMFs.
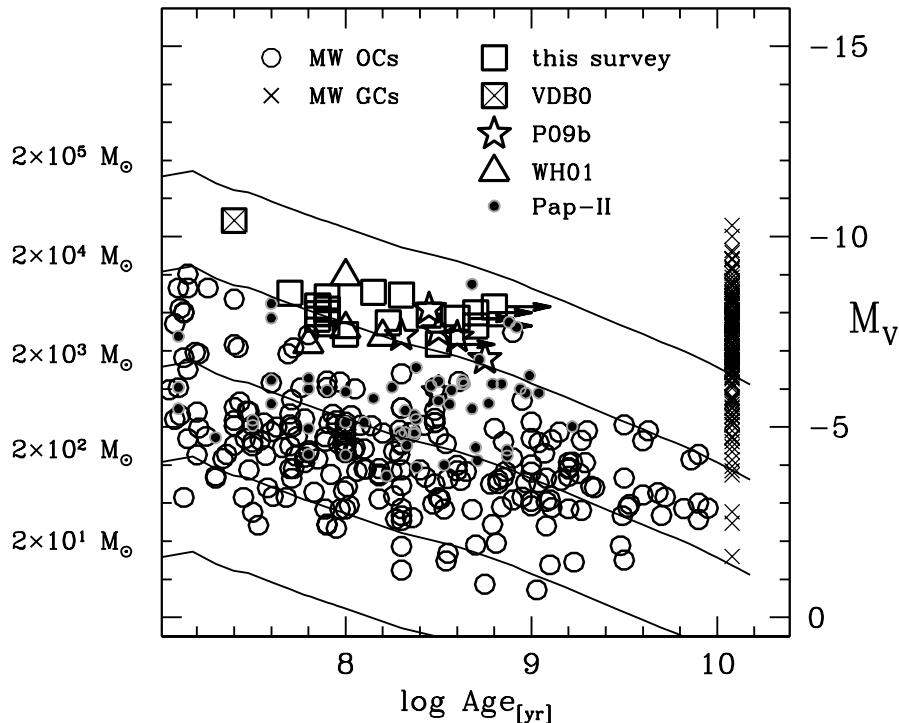
Figure 4.13: Integrated V mag and total mass as a function of age for various samples of clusters. Galactic open clusters (OC, from the WEBDA database) are plotted as filled circles, Galactic globular clusters (GC, M_V from the most recent version of the Harris (1996) catalog, i.e. that of February 2003, the ages have been arbitrarily assumed to be 12.0 Gyr for all the clusters) are plotted as × symbols. The target clusters are represented as open squares (VDB0 as a crossed square), the clusters from P09b as open stars, and the clusters from WH01 clusters as open triangles. M_V magnitudes of the target clusters and of the P09b clusters are from the new aperture photometry performed on the CCD images by Massey et al. (2006), except for B083 and B347 whose magnitudes are from RBC (see Tab. 4.1. M_V magnitudes of the WH01's clusters are from RBC. Log Age is from Tab. 4.2. Points with arrows have only lower limits to the age. Filled circles are M31 OCs from Pap-II. The continuous lines are fixed-stellar-mass models from the set by Maraston (1998, 2005) for SSPs of solar metallicity, with a Salpeter's Initial Mass Function (IMF) and intermediate Horizontal Branch morphology. Note that in this plane, the dependence of the models from the assumed IMF, metallicity and HB morphology is quite small (see B08). The outlier OC at log Age≃ 9.0 is Tombaugh 1.

of our study.

4.4.1 Comparison with Galactic open clusters

In Fig. 4.13 we show the log(age) vs. absolute magnitude plot analogous to Fig. 4.12 but using M_V instead of M_J, M_H, M_K. While NIR magnitudes are preferred to get reliable estimates of the stellar mass of our clusters (see Sect. 4.4 and Pap-I), the use of M_V allows us a direct comparison with different kinds of clusters for which integrated magnitudes in NIR passbands are lacking, Galactic OCs in particular (B08, Pap-I).

Inspection of Fig. 4.13 confirms the tentative conclusions of Pap-I (and F05). The distribution of our target clusters marginally overlaps with the high-mass tail of the Galactic OC distributions, but *the bulk of the sample of candidate YMC considered here is significantly more massive than Galactic OCs in the same age range*. In this sense, the brightest, most massive and youngest cluster of our sample, VdB0 having age=25 Myr and $M \simeq 6 \times 10^4 \, M_\odot$, may appear similar to the handful of massive young clusters recently identified in the Milky Way (see Figer 2008 and Messineo et al. 2009, hereafter M09, for recent reviews), that have masses between $0.7 \times 10^4 \, M_\odot$ and $4.0 \times 10^4 \, M_\odot$ and ages between 0.3 Myr and 18 Myr, according
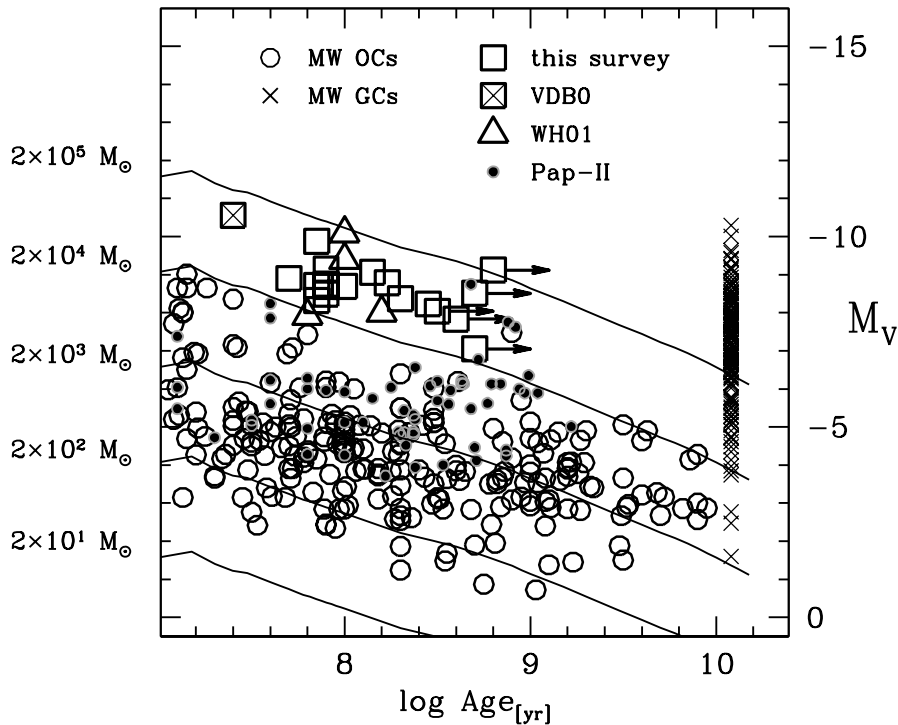
Figure 4.14: Same as Fig. 4.13 but with M_V magnitudes of the target clusters and of the WH01's clusters obtained from fitting King (1966) models to our HST data, from Pap-III. The clusters from P09b are not included in the plot as they have not been considered in Pap-III.

to M09. The other clusters of our sample have similar (or slightly greater) masses than the Galactic YMC but they are all significantly older (by a factor of $> 2\times$, see Sect. 4.5 for further discussion). It is worth to note that the masses estimated from Fig. 4.13 are in agreement with those from Fig. 4.12, typically, within a factor of 2.

In Pap-I we showed that in the case of VdB0, an exceptionally extended cluster, the integrated magnitudes reported in the RBC were significantly underestimated. However our shallow HST exposures were not ideal to perform integrated photometry on such large areas (VdB0 cover the whole extent of the PC field). For these reasons we recurred to the new homogeneous CCD survey by Massey et al. 2006; see Pap-I for discussion) to obtain a reliable estimate of the total luminosity of that cluster; as said, the integrated B,V magnitudes for the clusters considered here have been obtained from the same source and with the same method (Tab 4.1). These cases are less problematic, as the clusters are more compact than VdB0. However, it seems wise to check how the comparisons shown in Fig. 4.13 may depend on the actual way in which M_V is estimated. To do that we present in Fig. 4.14, a new version of Fig. 4.13 in which the M_V values derived from Tab. 4.1 are replaced with M_V estimates obtained in Pap-III from profile fitting (with King 1966 models) performed on our HST images (with the same assumptions on distance and reddening adopted here). Again, it is very reassuring to note that the conclusions drawn above from Fig. 4.13 are fully confirmed also by the new set of M_V from Pap-III. In fact, the differences between the YMC of our sample and Galactic OCs are even more pronounced in the new plot, as the total V luminosities estimated in Pap-III are larger than the values adopted here by a factor of $\simeq 1.6$, in average. For the reasons discussed in Pap-I and for homogeneity with that analysis we retain our ground-based M_V estimates as our reference.

It is interesting to note that the clusters identified by Krienke & Hodge (2007, 2008), and, by analogy, those found in Pap-II[8], have an observed LF peaking around $M_V = -3$ and

---

[8]It should be recalled that clusters listed in the RBC were excluded from the analysis performed in
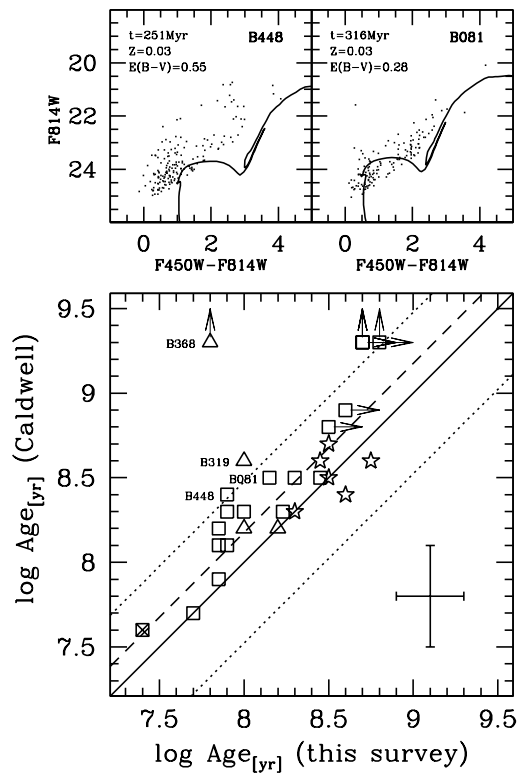
Figure 4.15: Bottom panel: comparison of the CMD-based ages from Tab. 2 with the ages obtained by C09 from integrated spectra. The symbols are the same as in Fig. 4.13. B257D is not plotted because it is not included in the C09 sample. The error bars show the average errors. The vertical arrows indicate clusters defined as "older" than 2 Gyr by Caldwell et al. (2009). The two clusters from our own survey for which the two independent estimates show the greatest difference are labeled (B448 and B081). Top panels: Comparison of the observed CMD for B448 and B081 with the isochrone corresponding to the age, metallicity and reddening estimates provided by C09 for these clusters (values reported in the upper left corner of each panel). Note that in the case of B448 the reddening estimated by C09 is obviously too large, while in the case of B081, the metallicity assumed by C09 (Z=0.03 for all the clusters) seems the principal responsible for the mismatch.

virtually dropping to zero at $M_V \gtrsim -6$, very similar to Galactic OCs (see Fig. 4.18), hence they appear as the natural counterpart of the OCs observed in the Milky Way.

In Pap-III the problem of the survival of our target clusters was discussed in some detail and dissolution times including the effects of internal and external evolution (Lamers & Gieles 2006), were computed. These values are reported also here, in Tab. 4.3, for convenience of the reader. The dissolution times of young clusters are all shorter than a Hubble time, hence it is likely that none of them will survive long enough to become old (age$\gtrsim$ 10 Gyr), and some of them are probably in the latest phase of their dissolution (B321, B342; Pap-III). However, a few clusters have dissolution times longer than 1 Gyr, and it is not inconceivable that some of them may reach an age of several Gyr before dissolving into the M31 disk (see Pap-III).

4.4.2 Comparisons with Caldwell et al. (2009)

A comparison of the results obtained here from the analysis of our HST-WFPC2 CMDs with those of the extensive and the independent analysis by C09, based on high-quality integrated spectra is clearly worthwhile, in this context.

Pap-II.

Table 4.3: Newly derived masses and dissolution times for the studied clusters.

Name	α_{J2000}	δ_{J2000}	J	H	K	log Mass ($M_\odot$)	εlog Mass ($M_\odot$)	$t_{diss}^{Pap-III}$ (Myr)
B015D-D041	$00^h\,41^m\,02.74^s$	$+41°\,06'\,36.63''$	17.03 ± 0.42	15.37 ± 0.27	14.89 ± 0.25	4.2	0.09	112
B040-G102	$00^h\,41^m\,38.90^s$	$+40°\,40'\,54.15''$	15.48 ± 0.08	14.90 ± 0.19	14.50 ± 0.15	4.6	0.07	631
B043-G106	$00^h\,41^m\,42.31^s$	$+40°\,42'\,39.86''$	15.58 ± 0.07	15.50 ± 0.31	15.08 ± 1.00	4.4	0.10	3467
B066-G128	$00^h\,42^m\,03.14^s$	$+40°\,44'\,48.55''$	16.25 ± 0.19	15.81 ± 0.47	16.06 ± 1.00	4.2	0.08	891
B081-G142	$00^h\,42^m\,13.59^s$	$+40°\,48'\,38.96''$	14.55 ± 0.05	13.77 ± 0.07	13.76 ± 0.06	5.1	0.04	955
B257D-D073	$00^h\,44^m\,59.35^s$	$+41°\,54'\,47.47''$	15.28 ± 0.10	14.77 ± 0.20	15.53 ± 1.00	4.6	0.09	302
B318-G042	$00^h\,40^m\,00.80^s$	$+40°\,34'\,09.06''$	16.17 ± 1.00	16.39 ± 0.66	15.49 ± 1.00	3.8	0.29	1905
B321-G046	$00^h\,40^m\,15.33^s$	$+40°\,27'\,45.98''$	17.11 ± 0.45	15.88 ± 0.57	15.18 ± 0.29	4.2	0.13	200
B327-G053	$00^h\,40^m\,24.12^s$	$+40°\,36'\,22.38''$	14.91 ± 0.07	14.32 ± 0.10	14.14 ± 0.15	4.5	0.06	2754
B376-G309	$00^h\,45^m\,48.38^s$	$+41°\,42'\,39.87''$	16.59 ± 0.18	16.07 ± 0.80	16.02 ± 1.00	4.1	0.09	295
B448-D035	$00^h\,40^m\,36.52^s$	$+40°\,40'\,14.94''$	16.51 ± 0.34	16.45 ± 1.00	15.66 ± 1.22	4.1	0.16	115
B475-V128	$00^h\,44^m\,55.92^s$	$+41°\,54'\,00.33''$	15.10 ± 0.08	14.68 ± 0.12	14.38 ± 0.17	4.7	0.07	1445
V031	$00^h\,41^m\,12.17^s$	$+41°\,05'\,30.21''$	14.80 ± 0.06	14.42 ± 1.00	13.77 ± 0.11	4.8	0.10	1230
B083-G146	$00^h\,42^m\,16.46^s$	$+41°\,45'\,20.53''$	14.88 ± 0.05	14.62 ± 0.12	14.07 ± 0.13	>4.7	…	…
B222-G277	$00^h\,44^m\,25.29^s$	$+41°\,14'\,11.62''$	15.27 ± 0.13	14.41 ± 0.09	14.16 ± 0.08	>4.6	…	…
B347-G154	$00^h\,42^m\,22.89^s$	$+41°\,54'\,27.40''$	14.68 ± 0.05	14.17 ± 0.04	14.17 ± 0.18	>4.7	…	…
B374-G306	$00^h\,45^m\,44.53^s$	$+41°\,41'\,55.10''$	17.21 ± 0.50	18.50 ± 0.82	16.32 ± 0.84	>3.9	…	…
NB16	$00^h\,42^m\,33.11^s$	$+41°\,20'\,16.48''$	14.91 ± 0.09	14.11 ± 0.07	13.46 ± 0.11	>4.8	…	…
P09b								
B049-G112	$00^h\,41^m\,45.59^s$	$+40°\,49'\,54.53''$	15.53 ± 0.13	15.27 ± 0.23	14.42 ± 0.06	4.5	0.09	…
B367-G292	…	…	…	…	…	$[4.3]^a$	[0.11]	…
B458-D049	$00^h\,41^m\,44.60^s$	$+40°\,51'\,20.40''$	16.69 ± 0.35	15.04 ± 0.15	14.96 ± 0.15	4.1	0.15	…
B521	$00^h\,41^m\,41.80^s$	$+40°\,52'\,02.41''$	17.32 ± 0.51	16.27 ± 0.43	16.28 ± 0.60	3.9	0.16	…
M039	…	…	…	…	…	$[3.8]^a$	[0.16]	…
M050	$00^h\,44^m\,40.83^s$	$+41°\,30'\,09.68''$	16.14 ± 0.14	14.90 ± 0.19	15.01 ± 0.31	4.3	0.13	…
WH01								
B315-G038	$00^h\,39^m\,48.51^s$	$+40°\,31'\,30.33''$	14.99 ± 0.09	14.49 ± 0.10	14.24 ± 0.09	4.6	0.05	4074
B319-G044	$00^h\,40^m\,03.03^s$	$+40°\,33'\,58.25''$	16.30 ± 0.12	15.94 ± 0.47	16.78 ± 0.52	3.9	0.10	182
B342-G094	$00^h\,41^m\,24.15^s$	$+40°\,36'\,48.55''$	16.67 ± 0.48	15.57 ± 0.38	16.94 ± 1.00	4.0	0.17	214
B368-G293	$00^h\,44^m\,47.50^s$	$+41°\,51'\,09.39''$	15.89 ± 0.27	15.14 ± 0.35	14.60 ± 0.21	4.4	0.08	251

In a few cases the data allowed us to obtain only a lower limit to the mass. α_{J2000} and δ_{J2000} are from 2MASS-6X-PSC catalog, J, H, K are from r=10$\rlap{.}''$0 ap. phot. in the 2MASS-6X-PSC catalog. Note that err_{JHK}=1.00 corresponds to err_{JHK}=null in the 2MASS-6X-PSC catalog.

[a] Estimated from Fig. 4.13, as these clusters lack NIR photometry. These mass estimates will not be used in the following to preserve the homogeneity of the sample.

In the lower panel of Fig. 4.15, the age estimates from Table. 4.2 are compared with those by C09. The two set of ages do agree within the uncertainties, but there is a clear systematic offset as C09 ages are larger than those listed in Tab. 4.2 by a factor of $\simeq 1.5$, in average, and up to a factor of $\gtrsim 3$ in the worst case (we are considering only clusters having age estimates in both sets, not lower limits). We note that this systematic offset occurs also if one restricts the sample by WH01, and also to the three clusters for which C09 provides CMD-based age estimates of their own (see their Tab. 7), hence it is a characteristic feature of their spectroscopic age estimates.

A difference that may produce a systematic offset between our ages and those by C09 is that they adopt super-solar metallicity models ($Z = 0.04$) for all the clusters, while we leave metallicity as a free parameter of our fit and, in fact, we adopt solar or less-than-solar metallicity models in all cases (see Tab. 4.2). If both sets of ages were derived from isochrones fitting the effect should be the opposite, i.e. a younger isochrone is required to fit a given CMD with a model of higher metallicity. However it is not clear if this general behavior is shared also by models of integrated spectra.

In the upper panels of Fig. 4.15 we show the two cases (among those included in our own survey) that display the widest difference between the two age estimates. We superposed on the observed CMDs the isochrones corresponding to the best-fit estimates by C09, corrected by the reddening provided by these authors. The case of B448 shows very clearly that the solution provided by C09 significantly overestimates the reddening, and it is not compatible with the observed CMD. In the case of B081, the comparison suggests that the choice of super-solar metallicity models by C09 may be particularly unsuitable for this cluster, leading to a larger-than-average error in the age estimate.

Two cases of especially remarkable differences occur also with the set by WH01 (open triangles in Fig. 4.15). B319=G44 is considered also in Tab. 7 of C09, where a spectroscopic age of 0.28 Gyr is reported, to be compared to the CMD-based age estimated of 0.10 Gyr by WH01. Moreover the reported spectroscopic value is most probably a typo, as in Table 2 of C09 (their primary source of cluster ages) they report log(age)=8.6 for B319=G44, corresponding to 0.398 Gyr (the value that is plotted in Fig. 4.15). In any case, the spectrum appears to be reasonably fitted by a Z=0.04, age=500 Myr model (N. Caldwell, private communication), while the CMD shown by WH01 is clearly not compatible with such an old age. The a-priori assumption of super-solar metallicity models by C09 may also be the origin of this mismatch. The case of B368=G293 (not included in Tab. 7 of C09), that is classified by C09 as "older than 2 Gyr" while the CMD by WH01 indicates age $\lesssim 80$ Myr, has to be ascribed to a typographical error by C09; in fact the cluster was not observed by that authors (N. Caldwell, private communication).

Fig. 4.16 shows the comparison between our estimates of E(B-V) and those by C09. In this case as well there is reasonable overall agreement, most of the differences being within the uncertainties. The most discrepant case is B448, already discussed above (see Fig. 4.15). Finally, in Fig. 4.17 the mass estimates are compared. Also in these cases the two set of estimates agree within the uncertainties (1 σ is a factor of 2.4), the strongest discrepancy is to be attributed to the overestimate of the age for B319=G44 by C09 discussed above.

In conclusion, while we are unable to identify the reason of the (modest) systematic overestimate of the ages by C09, it has to be concluded that the agreement between the two independent sets of age, reddening, and mass estimates is quite satisfactory, if the observational uncertainties are taken into the due account.

4.5   Summary and Discussion

We presented the main results of a survey aimed at the determination of the nature of a sample of 20 candidate YMC in the thin disk of M31 (one of which, VdB0, was studied in Pap-I). One of the targets surveyed turned out to be a bright star projected onto the dense disk of M31, and thus erroneously classified as a possible cluster. All the other targets were revealed to be genuine star clusters and we were able to obtain reliable CMDs for all of them.
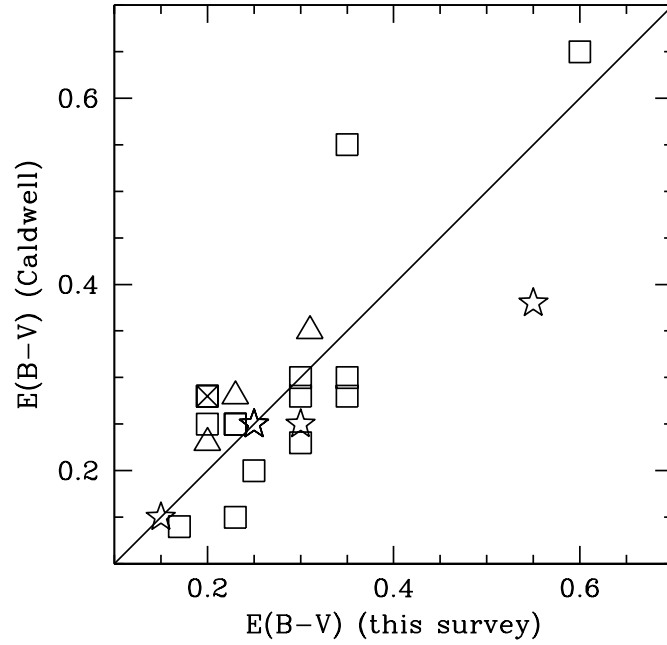
Figure 4.16: Comparison of the E(B-V) estimates from Tab. 3 with those by C09. The symbols are the same as in Fig. 4.13.
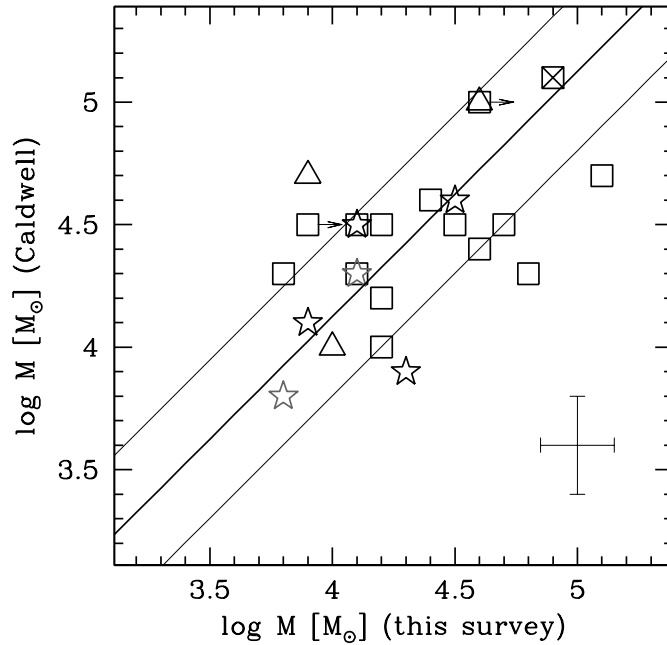
Figure 4.17: Comparison of the masses estimates from Tab. 3 with those by C09. The symbols are the same as in Fig. 4.13. The grey symbols show the clusters that have "null" error on IR magnitudes in the 2MASS-6X-PSC catalog. The thick line is the $M_{t.s.} = M_{C09}$ locus, the thin lines bracket the $\pm 1\sigma$ range about this locus. The error bars show the average errors.

The main results from our own survey can be summarized as follows:

1. New integrated-light spectroscopy became available for many of our targets since the original selection was performed. Three of them (B083, NB16 and B347) were revealed by the new data to be not good YMC candidates as defined by F05. The CMDs obtained in this study confirms that they are likely old clusters.

2. Among the remaining 17 targets, 16 are genuine clusters and one is in fact a star (NB67), as said above. Thus the fraction of spurious objects in our well-defined sample of BLCC=YMC is just 1/16 = 6.2%. Even excluding the two clusters considered at point 3., below, the incidence remains below 10%. The extended sample considered in Appendix 4.B fully confirms these results. We must conclude that M31 YMC are not especially plagued by contamination from spurious sources and most of the clusters considered in the original analysis by F05 should be real[9]. In particular, *asterisms*, suggested as a possible major contaminant of the sample by C06, are in fact found to be not a particular reason of concern, in this context (see also the discussion by C09).

3. Two of the sixteen genuine clusters (B374 and B222) have integrated properties compatible with being YMCs but they do not show a detectable MS in the range of magnitudes sampled by our CMDs. We can provide only an upper limit to the age of these clusters ($\gtrsim 300$ Myr), but the available data suggest that they are good candidate intermediate-age clusters that indeed would merit follow-up with deeper HST photometry.

4. The fourteen confirmed young clusters (including VdB0, studied in Pap-I) show a clear MS in the range of magnitudes sampled by our CMDs, hence we were able to obtain reliable estimates of their ages, reddenings and (an educated guess of) metallicities by comparison of the observed CMD and LF with theoretical models. Ten of them have ages in the range 25-100 Myr, the other four range between 140 Myr and 280 Myr. The adopted metallicities include $Z = 0.004$ (one case), $Z = 0.008$ (three cases), and $Z = 0.019$ (solar metallicity, ten cases). The estimated reddenings range from E(B-V)=0.06 to E(B-V)=0.60, with E(B-V)=0.20-0.30 as most typical values.

To increment our final sample of YMC we included ten further clusters for which the age was estimated from their CMDs (obtained from HST imaging) with methods strictly homogeneous with those adopted here, from WH01 and P09b. In this way we assembled a final sample of 24 confirmed young clusters. For 22 of these we were able to obtain reliable estimates of the total stellar mass by coupling our age estimates with the integrated J,H,K magnitudes taken from the 2MASS-6X catalog. These clusters have masses ranging from $0.6 \times 10^4 M_\odot$ to $6 \times 10^4 M_\odot$, with an average of $\sim 3 \times 10^4 M_\odot$[10]. Our estimates of ages and masses are in good agreement with recent independent studies based on integrated light spectra (see also Pap-III for the comparison with the results by Pfalzner 2009).

4.5.1 The nature of M31 YMC

In the upper panel of Fig. 4.18 the mass distribution of our extended sample of M31 YMCs is compared with the distributions of Galactic OCs and GCs (masses from B08). The clusters considered here appear to lie in the middle of the two distributions, overlapping with the high-mass end of the OCs and with the low-mass end of GCs. This comparison provide a further confirmation that the YMCs (=BLCCs) of M31 are indeed more similar to the YMCs of the LMC than to classical OCs of the Milky Way, i.e. the original hypothesis advanced in F05. This is in full agreement with the main conclusions by C09, obtained with a completely independent method (less sensitive to age than ours) on a wider sample.

---

[9]It may be useful to stress again that the clusters of our survey were selected among the class f=1 RBC entries, see Sect. 4.2 and Galleti et al. 2006a.

[10]The remaining two clusters, that lack NIR photometry, also have masses lying in the same range, according to the estimates obtained using the integrated V magnitude instead of J,H,K ones.
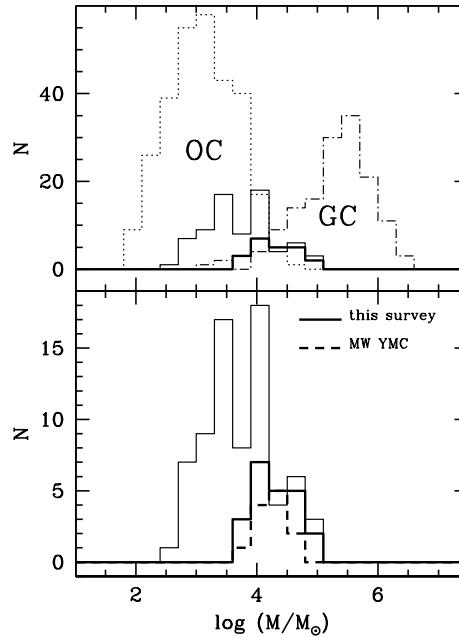
Figure 4.18: Upper panel: The mass distribution of YMC studied here (from Tab. 4.3, thick continuous line) is compared with the mass distribution of Galactic OCs (dotted line) and Galactic globular clusters (dashed line). Masses of Galactic clusters are from B08. Lower panel: zoomed view of the distribution of M31 YMC compared with the distribution of the YMC of the Milky Way (dashed line; data from M09). The thin line shows the distribution of the M31 YMC sample merged with the sample of OC presented in Pap-II.

The lower panel of Fig. 4.18 compares our clusters with the YMCs seen toward the center of the Milky Way as listed by M09. The two samples have very similar mass distributions, suggesting that they are also similar in nature. An obvious difference between the two sets of clusters was already suggested in Pap-I and is confirmed here: the M31 YMCs of our sample are significantly older that the YMC discovered until now in the Galaxy ($\gtrsim 50$ Myr vs. $\lesssim 20$ Myr; see below for possible explanations). We confirm that the M31 YMCs studied here have larger sizes (half-light-radii) with respect to their MW counterparts (see Pap-I and Pap-III); this seems in agreement with the age-size relations proposed by Pfalzner 2009; see Pap-III for discussion).

A more thorough comparison between various samples of YMCs is presented in Fig. 4.19, where Galactic OCs and YMCs, YMCs from M33 (San Roman et al. 2009; for further discussion on M33's star clusters see Sarajedini & Mancone 2007b, Zloczewski et al. 1985, Park et al. 2009), the LMC, the Small Magellanic Cloud (McLaughlin & van der Marel 2006), and M31 are plotted together in a log(age) *vs.* log Mass diagram. Fig. 4.19 is affected by a number of selection effects that deserve to be described in some detail.

1. The minimum mass threshold appears to increase with age (at least for age $\gtrsim 10$ Myr, see the Galactic OCs if Fig. 4.19): this is due to the fact that the lower the mass of a cluster, the shorter is its dissolution time, as the cluster is less resilient to all the internal and external effects that may lead to its disruption (Gieles et al. 2007, Pap-III, and references therein). The minimum mass threshold for samples in external galaxies is obviously due to the inherent magnitude limits.

2. Also the maximum mass threshold increases with age in log Age vs. log Mass plots (Hunter et al. 2003; Gieles 2009); the effect is clearly evident in Fig. 4.19 if one looks at the MW OCs, that cover the widest range in ages). This general behavior can be easily explained as a simple consequence of varying the sample size as a function of the
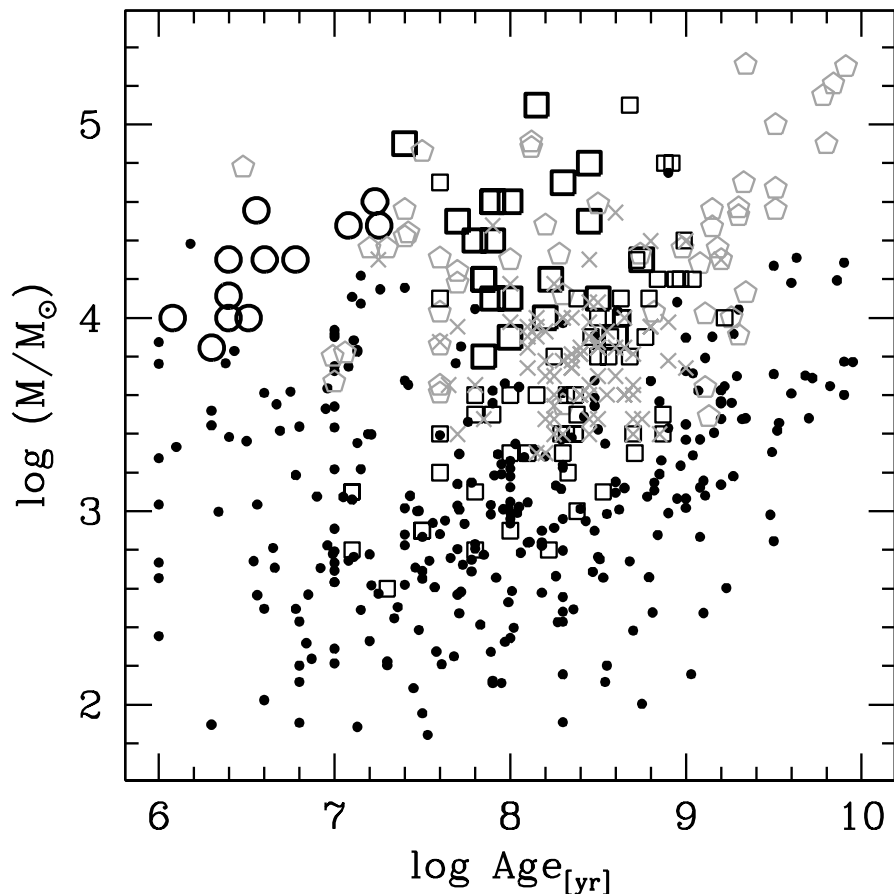
Figure 4.19: Comparison between Galactic OCs (small filled circles), M31 YMC from the present study (big open squares), MW YMC from M09 (big open circles), M31's clusters from pap-II (small open squares), Magellanic Clouds clusters (grey open pentagons), and M33's clusters (grey crosses) in the log(age) *vs.* log Mass plane. Masses of Galactic OCs are from B08, masses of Magellanic Clouds clusters are from McLaughlin & van der Marel (2006) and masses of M33 clusters are from San Roman et al. (2009). For M33 and the Magellanic Clouds only clusters younger then 10 Gyr are shown.

age bin in the logarithmic scale. Assuming a power-law mass function and a constant Cluster Formation Rate (CFR) the number of cluster per logarithmic age bin increases with age. For an exponent of the power law mass function ($N(M) \propto M^{-\alpha}$) $\alpha = 2$, that is a reasonable approximation for most of the observed cluster systems, $\log M_{max} \propto \log$ Age (see Gieles 2009), for detailed discussion and references).

3. While the lack of massive ($M \gtrsim 10^4 M_\odot$) clusters older than 400 Myr in the Milky Way is probably real, the typical limiting magnitude ($V \sim 27$, Rich et al. 2005) of available CMDs of M31 clusters prevent us from drawing firm general conclusions about objects in that age range in M31. The cases of B222 and B374, treated here, are excellent examples of clusters that may populate that region of the diagram but lack a reliable age estimate because the available photometry is too shallow (see Puzia et al. 2005).

4. The lack of massive ($\log (M/M_\odot) > 3.6$) M31 clusters younger than 25-50 Myr may be due to the contribution of several biases. First, such young clusters may be hard to select from the RBC as there are no objects bluer than $(B - V)_0 \simeq 0.0$ in the list of confirmed clusters (see F05). This is not surprising as the RBC was intended to be a catalog of globular clusters. Second, for ages $\lesssim 8$ Myr the H_β index is expected to fall below the threshold adopted to select YMC candidates (see, for example, Fig. 7 of F05), thus (possibly) preventing the selection of these objects for our survey. Third, very

young objects should have their luminosity dominated by a few massive stars near their centers, thus leading to objects that may appear more like blended stars than like a star cluster at the distance of M31, even in HST images, thus preventing their inclusions in lists of candidate YMCs. Fourth, it can be hypothesized a positive correlation between the age of the clusters and their height above the disk plane, such that the youngest clusters are more deeply embedded in the thin dust layer of the M31 disc, out of our reach even from our privileged point of view, while most/some of the older clusters would be visible just because they lie above the densest part of that layer. There are indications that this kind of correlation actually holds in our own Galaxy (V.D. Ivanov, private communication).

5. The lack of massive ($\log (M/M_\odot) > 3.6$) MW clusters *older* than 25-50 Myr may also be associated with an observational bias. Galactic YMC have been identified as clumps of bright stars in the near and mid IR and the youngest clusters, having the brightest RSG, are easier to detect in this way. Moreover the sample of Open/YM Galactic clusters is limited (essentially by the effect of interstellar extinction in the Galactic disc) to a volume of a few kpc around the Sun, while M31 (or M33) YMCs can be selected over the whole disk of their parent galaxy, thus introducing a bias that favors the detection of rarer cluster species (massive clusters) in the latter galaxies with respect to the MW.

6. There seems to be a significantly under-dense region in Fig. 4.19, for masses $\gtrsim 10^3$ $M_\odot$ and ages between ~ 15 Myr and ~ 50 Myr ($7.2 \lesssim \log$ Age $\lesssim 7.7$). The same feature was noted by Whitmore et al. (2007) in their study of the cluster system of the Antennae and it was attributed by a degeneracy in age dating from broad band colors occurring in that age range due to the prompt onset of the RSG phase (see Whitmore et al. 2007, for details, discussion and further references). Virtually all the clusters plotted in Fig. 4.19 had their ages estimated from the CMD of their stars (instead of broad-band colors, see also Pap-II), hence our sample should not be affected by this bias, at least in principle. However the coincidence of the feature with that noted by Whitmore et al. (2007) suggests that the same kind of bias against ages in that interval may be at work also in Fig. 4.19.

7. The samples of clusters from all the galaxies involved in Fig. 4.19 have been selected according to different criteria, by color, magnitude, etc.

Given all the above considerations, it does not seem possible to draw any firm conclusion from the comparison shown in Fig. 4.19. The only straightforward conclusion is that *YMCs in the age range 50-500 Myr are relatively common in all the most massive star-forming galaxies of the Local Group* (M31, M33, LMC and SMC). The only exception (the Milky Way) may be ascribable to observational biases, but it cannot be excluded that it is instead (at least partly) associated with intrinsic properties of the Milky Way, that appears peculiar under several aspects with respect to the typical spiral galaxies (and to M31, in particular see Hammer et al. 1996, and Yin et al. 2009). As the samples of M33 and M31 should be subject to the same kind of biases (as the distances are similar and the data have been collected with HST in both cases), the difference in the maximum mass limit between the two samples is likely real, and it can probably be ascribed to the difference in total mass between the disks of the two galaxies: larger disks should host more numerous populations of clusters, thus enhancing the probability of producing clusters with higher (maximum) masses (see Gieles 2009, and references therein).

4.5.2 Radial trends

Given the wealth of data collected for our target clusters, it may be useful to look for correlations between their physical parameters, including their position within the M31 disc. Limiting the analysis to the young clusters (age < 1 Gyr), that constitute a more homogeneous sample of bona-fide thin disk objects, it turns out that our sample is still too sparse for a thorough analysis of these correlations. In particular the covered ranges of age, mass and
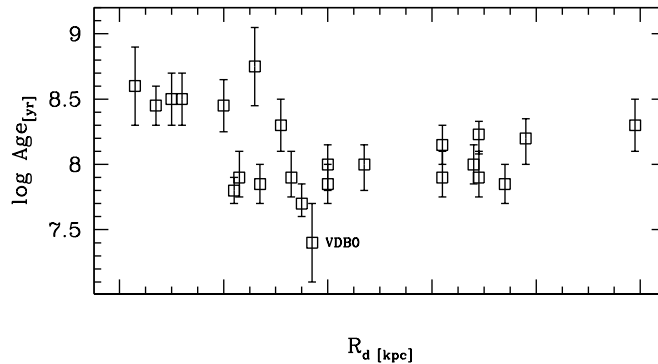
Figure 4.20: Age as a function of the deprojected galactocentric distance for the young clusters (open squares with error bars). The cluster VdB0 has been labeled as it is by far, the youngest of the whole sample.

position are quite limited, thus not allowing us to reveal large scale trends, in most cases. Moreover, the adopted approach of CMD analysis provides just an educated guess of the metallicity of the clusters, aimed at obtaining the most reliable estimate of the clusters age, which was the main objective of our analysis. These limitations prevent the possibility of a meaningful study of the radial metallicity gradient with our data. It should also be recalled that the correlations bewteen the structural parameters of the clusters (mass, radius, density etc.) have already been discussed in Pap-III, hence here we consider only age, mass, deprojected galactocentric distance (R_d; assuming and inclination of $i = 12.5°$ of the disk with respect to the plane of the sky, see Simien et al. 1978 and Pritchet & van den Bergh 1994), X, Y, and reddening.

Having checked all the combination of parameters, the only correlation that appeared remarkable to us is presented in Fig. 4.20. It is a trend of decreasing age with galactocentric distance, that seems statistically significant if one consider the associated errors. Given the relatively limited range of galactocentric distance covered, in our view the observed distribution can be interpreted in two ways:

- as a part of a larger trend resulting from a inside-out wave of cluster formation. In this case the trend toward older mean ages should continue at lower radii and Fig. 4.20 shows the transition between a regime of decreasing age with galactocentric distance and an asymptotic regime of constant age in the outermost fringes of the disc;

- more likely, as a sharp transition in the epoch of the highest rate of star/cluster formation occurring at the onset of the $R_d \sim 10$ kpc "ring of fire". This would be consistent with the well known burst of recent star formation that characterize this prominent structure of the M31 disc.

While not especially conclusive or insightful, the result shown in Fig. 4.20 gives a clear idea of how useful YMCs can be as tracers of the structure and evolution of the disk itself, in particular if large and reliable samples can be assembled.

4.5.3 Final remarks

This research has demonstrated that the conspicuous population of bright disk objects studied by F05 consists of genuine YMC, similar to those found in the LMC, SMC and M33 galaxies. These clusters may open a new window to the study of the recent star formation history in the disk of M31. A systematic analysis over the whole extent of the M31 disk may provide the opportunity to study a rich system of young clusters using a sample much less affected by selection biases than in our own Galaxy, and to better constrain the models of dynamical evolution of clusters within the disks of spiral galaxies. M31 YMCs like

those studied here provide also an excellent tracer of the disk kinematics in that galaxy, independent of (and in addition to) the HI gas. Recent wide-field surveys (Vansevicius et al. 2009; see also Pap-II) suggest that a rich harvest of genuine YMCs await to be discovered in the disk of our next neighbor giant galaxy in Andromeda.

4.A   RBC clusters serendipitously imaged in our survey

To ascertain the real nature of candidate M31 clusters proposed by various authors is a daunting but necessary task to keep cluster catalogs as complete and clean as possible from spurious sources. There are several criteria that may be used to check candidates (see Galleti et al. 2006a for references and discussion), but resolving them into stars by means of high spatial resolution imaging is by far the safest method of all. In addition to the clusters that were the main target of our survey, and to the low-luminosity clusters identified by Hodge et al. 2009, our WFPC2 images serendipitously included several clusters and candidate clusters listed in the RBC. Inspection of our images allowed us to place their classification on firmer footing. The results of this analysis are summarized in Table 4.4. Their classification in the RBC has been modified accordingly. In Table 4.4 we report the name of the object (column 1, name), the classification flag originally reported in the RBC (col. 2, f), the name of the cluster that was the original target of the images (col. 3, field), a flag indicating if the object was imaged with the PC or with one of the WF cameras (col. 4, chip), and, finally, a comment on its classification as derived from the inspection of the new images. In some case the classification remains uncertain (comments with "?"). In some cases the image reveals that the object is extended but do not clarify its nature (cluster/galaxy/HII region etc.), in these cases we report the comment "not a star". An estimate of the radial velocity will suffice to definitely establish if these objects are M31 clusters or background galaxies (see Galleti et al. 2006a). In some cases, some clusters that were among the main targets of our survey were serendipitously re-imaged in the WF field surrounding other targets. For obvious reasons these cases are not reported in Table 4.4. On the other hand some clusters have been serendipitously imaged in two different pointings: in these cases we report the classification derived from both sets of images. Some of the clusters of Table 4.4 were independently re-identified in Pap-II (B061D, B319, B014D, B256D, DAO84), for two of them a meaningful CMD was also obtained there (B061D and B319); this lends additional support to the reliability of their classification. Finally, we reported in the table also some clusters whose nature was already confirmed by previous HST imaging, for completeness (see the case of B319=G044, observed by WH01).

It may be interesting to note that among the 19 RBC class f=2 (candidate clusters) objects listed in Tab. 4.4, 3 turn out to be real clusters (or likely clusters), 5 are extended objects that lack the v_r measure needed to ultimately establish their membership to M31, while 11 are non-clusters (or likely non-clusters), most of them being stars. According to this limited sample it can be concluded that the fraction of genuine M31 clusters among class f=2 entries of the RBC ranges from $\frac{3}{19}$=16%± 14% to $\frac{8}{19}$=42%± 12%. These numbers should be considered as somewhat pessimistic as they are computed on a sample of clusters projected on the densest regions of the M31 disc, where the probability of contamination from bright stars of M31 is at its maximum. To give a rough idea of the number of genuine clusters that are still hidden among the candidates listed in the RBC one can take the 16% of the number of class=2 RBC entries, i.e. $0.16 \times 1049 \simeq 168$. A significant fraction of these may be YMCs ($\gtrsim$ 15%, according to F05).

Considering the objects listed in Tab. 4.1 and Tab. 4.4, the survey images allowed us to verify the nature of 25 objects classified as genuine clusters (class f=1) in the RBC. We confirm that 23 of them are real clusters while 2 are (one or two) stars. From this number one can estimate the fraction of spurious sources among class f=1 RBC entries as $\frac{2}{25}$=8%±8%, that is remarkably low and is in excellent agreement with the estimate by G09 that finds $\lesssim$4% from a sample of 252 objects.

Considering the fraction of real clusters among class f=1 entries as 92% and that among f=2 entries as 16%, the expected number of genuine M31 clusters in the RBC (GC+YMC) is

estimated as ~ 630, while the number of old clusters (GCs) should be ~ 530, in reasonable agreement with the results by Barmby et al. 2000 and F05. Note that, at present, the number of confirmed (likely) old clusters (f=1 and y=0) in the RBC is 418; correcting this for contamination leads to 384 bona-fide GCs, more than double than the number of GCs encountered in the Milky Way galaxy ($\simeq$ 150, Harris 1996).

4.B Other candidate M31 YMCs with archival HST imaging

Before selecting the actual targets for our survey we searched the HST archive for YMC candidates, as listed in Tab. 1 (or Tab. 2) of F05, that had already been (serendipitously) imaged from HST. As the nature of these objects (cluster / asterism / star) can be determined from existing images they were not included in our final list of targets. In Tab. B.1. (referring to objectively selected candidates from Tab. 1 of F05) and Tab. B.2. (referring to candidates suggested from various authors adopting different criteria, from Tab. 2 of F05) we list the results of that research. In these tables we report (1) the cluster name(s), (2) the HST program number(s) of the retrieved images, (3) the instrument(s) and (4) the filter(s) used to obtain the inspected images, (5) the classification of the object based on the inspection of the HST images, following the approach adopted in Tab. 4.4, above, and, finally, (6) the classification provided by C09 based on their spectra and/or on ground-based imaging (S indicates that the objects was classified by from its spectrum, I indicates that the object was classified with imaging, SI means that both imaging and spectrum were considered for the classification, according to C09). At the epoch when the table was compiled (September 2009), 36 out of the 66 objects listed in Tab. 1 of F05 (including those studied in this paper) had one (or more) images in the HST archive: 34 of them are recognized as *real* star clusters from the inspection of the available HST images, while 2 are stars. This leads to a fraction of spurious objects in the sample of 5.5% ± 4.0%, in full agreement with the fraction we obtained from our original sample (Sect. 4.2). Analogously, 14 out of 21 objects listed in Tab. 2 of F05 (including those studied in this paper) had one (or more) image(s) in the HST archive: 13 of them are recognized as *real* star clusters from the inspection of the available HST images, while 1 is a star. This leads to a fraction of spurious objects in the sample of 7.1% ± 7.4%, again in full agreement with the fraction we obtained from our original sample (Sect. 4.2) and with the above results. Note that (a) all the classifications we obtained from HST imaging confirm those independently obtained by C09 for the same objects, and (b) all the objects listed in Tab. B.2. were classified as clusters by some other author before (see F05).

Of the 37 objects in Tab. B.1. and Tab. B.2. lacking HST-based classification, 31 are classified as *clusters* by C09; the remaining 6 have uncertain classification. Coupling the results from HST and C09 it turns out that 60 of the 66 objects from Tab. 1 of F05 are real clusters, two are stars, and four have uncertain classification; 18 of the 21 objects from Tab. 2 of F05 are real clusters, one is a star, and two have uncertain classification. We thus conclude that the large majority ($\gtrsim$90%) of the objects identified (or proposed) by F05 as (possibly) young clusters are indeed genuine star clusters. Finally, three clusters listed in the RBC but not comprised in the study by F05 where found in Pap-II to have age < 1 Gyr (B014D, B061D, B256D).

Table 4.4: RBC clusters serendipitously imaged in our survey.

Name	f[1]	Field	Chip	Comment
B014D	2	B015D	PC	cluster
B061D	2	NB16	WF	cluster
B256D	2	B257D	WF	cluster[2]
B256D	2	B475	WF	cluster[2]
SK067B	2	B015D	WF	not a star
SK071C	2	B475	WF	not a star
SK185B	2	B475	WF	not a star
B068D	2	NB16	WF	not a star
B068D	2	NB67	WF	not a star
B019D	2	V031	WF	not a star
NB64	2	NB16	WF	star?
NB64	2	NB67	WF	star?
SK091B	2	B066	WF	star
B048D	2	B081	PC	star
SK091C	2	B374	WF	star
SK188B	2	B475	WF	star
NB47	2	NB16	WF	star
SK083B	2	B043	WF	2 stars + nebula?
B057D	2	NB16	WF	2 stars
NB43	2	NB67	WF	2 stars
B192D	2	B327	WF	galaxy
SK194C	2	B376	WF	galaxy
B376	1	B374	WF	cluster
B257D	1	B475	WF	cluster
B319	1	B318	WF	cluster
DAO84	1	B374	WF	not a star[3]
DAO84	1	B376	WF	not a star[3]
SK047A	1	B081	WF	two stars
NB68	6	NB16	WF	star?
NB68	6	NB67	WF	star?
B113	6	NB16	WF	star?
SK069D	6	B083	WF	star
B185D	6	B318	PC	star
SK046D	6	B327	WF	star
B065D	6	NB67	WF	star
SK041D	6	B321	WF	two stars
B121	3	NB16	WF	star?
B121	3	NB67	WF	star

[1] f is the original RBC classification flag (1 globular cluster, 2 candidate globular cluster, 3 controversial object, 6 star/s).

[2] While the visual inspection of the images does not permit a clear cut classification, the objective analysis performed in Pap-II recognizes B256D as a star cluster.

[3] DAO84 has a radial velocity estimate that clearly identifies it as a member of M31 (see the RBC).

Table 4.5: Classification of candidate young clusters listed in Tab. 1 of F05.

Name	Obs-ID	Camera	Filters	Class HST	Class C09
B008-G060	10407	ACS/WFC	F606W F435W	cluster	cluster(SI)
B028-G088					cluster(SI)
B040-G102	10818	WFPC2	F450W F814W	cluster	cluster(SI)
B043-G106	10818	WFPC2	F450W F814W	cluster	cluster(SI)
B047-G111					cluster(S)
B049-G112	10407(10631)	ACS/WFC	F435W F606W	cluster	cluster(SI)
B057-G118	10407(10631)	ACS/WFC	F435W F606W	cluster	cluster(SI)
B066-G128				cluster	cluster(SI)
B069-G132	10273	ACS/WFC	F555W F814W	cluster	cluster(SI)
B074-G135					cluster(S)
B081-G142	10818	WFPC2	F450W F814W	cluster	cluster(SI)
B083-G146	10818	WFPC2	F450W F814W	cluster	cluster(S)
B091-G151	10273	ACS/WFC	F555W F814W	cluster	cluster(SI)
B114-G175	5907	WFPC2	F555W F814W	cluster	cluster(SI)
B160-G214	9480(10273,7426)	ACS/WFC, WFPC2	F775W F555W F814W F606W	cluster	cluster(SI)
B170-G221					cluster(SI)
B210-M11	9709	WFPC2	F606W	cluster	cluster(SI)
B216-G267					cluster(SI)
B222-G277	10818	WFPC2	F450W F814W	cluster	cluster(SI)
B223-G278					cluster(SI)
B237-G299					cluster(SI)
B281-G288					cluster(SI)
B295-G014					cluster(S)
B303-G026					cluster(SI)
B307-G030					cluster(SI)
B314-G037					cluster(SI)
B315-G038	8296	WFPC2	F336W F439W F555W	cluster	cluster(SI)
B318-G042	8296(10818)	WFPC2	F336W F439W F450W F555W F814W	cluster	cluster(SI)
B319-G044	8296	WFPC2	F336W F439W F450W F555W F814W	cluster	cluster(SI)
B321-G046	10818	WFPC2	F450W F814W	cluster	cluster(SI)
B322-G049					cluster(SI)
B327-G053	10818	WFPC2	F450W F814W	cluster	cluster(SI)
B331-G057	6699	WFPC2	F555W F814W	cluster	cluster(SI)
B342-G094	8296	WFPC2	F336W F439W F555W	cluster	cluster(SI)
B354-G186					cluster(S)
B355					possible star(S)
B358-G219					candidate
B367-G292	10407	ACS/WFC	F435W F606W	cluster	cluster(SI)
B368-G293	8296	WFPC2	F336W F439W F555W	cluster	cluster(I)
B374-G306	10818	WFPC2	F450W F814W	cluster	cluster(SI)

Table 4.5: continued.

Name	Obs-ID	Camera	Filters	Class HST	Class C09
B376-G309	10818	WFPC2	F450W F814W	cluster	cluster(SI)
B380-G313					cluster(SI)
B431-G027					cluster(SI)
B443-D034					cluster(SI)
B448-D035	10818	WFPC2	F450W F814W	cluster	cluster(SI)
B451					possible star(I)
B453-D042					cluster(SI)
B458-D049	10407	ACS/WFC	F435W F606W	cluster	cluster(SI)
B475-V128	10818	WFPC2	F450W F814W	cluster	cluster(SI)
B480-V127					cluster(SI)
B483-D085					cluster(SI)
B484-G310					cluster(SI)
B486-G316					cluster(S)
B189D-G047					cluster(SI)
VDB0-B195D	10818	WFPC2	F450W F814W	cluster	cluster(SI)
NB21-AU5	10006	ACS/WFC	F435W	cluster	cluster(SI)
NB67	10818	WFPC2	F450W F814W	star	star(SI)
NB83	5907	WFPC2	F555W F814W	star	star(SI)
B006D-D036					cluster(SI)
B012D-D039					cluster(SI)
B015D-D041	10818	WFPC2	F450W F814W	cluster	cluster(SI)
B111D-D065	9794	WFPC2	F336W F439W F555W F675W F814W	cluster	cluster(SI)
B206D-D048					cluster(SI)
B257D-D073	10818	WFPC2	F450W F814W	cluster	cluster(I)
DAO47					cluster(SI)
V031	10818(9709)	WFPC2	F450W F606W F814W	cluster	cluster(SI)

Table 4.6: Classification of candidate young clusters listed in Tab. 2 of F05.

Name	Obs-ID	Camera	Filters	Class HST	Class C09
B015-V204					cluster(SI)
B030-G091	6671	WFPC2	F555W F814W	cluster	cluster(SI)
B090	10260	ACS/WFC	F606W F814W	cluster	cluster(SI)
B101-G164					cluster(SI)
B102	10260	ACS/WFC	F606W	star	star(SI)
B117-G176	9087	WFPC2	F336W	cluster	cluster(SI)
B146	10118(5435)	ACS/WFC, WFPC2	F160BW F255W F300W F814W	cluster	SLH
B154-G208	9087	ACS/WFC	F435W	cluster	cluster(SI)
B164-V253					cluster(SI)
B197-G247					cluster(SI)
B214-G265					cluster(SI)
B232-G286	8059	WFPC2	F300W F450W F606W F814W	cluster	cluster(SI)
B292-G010	10631	ACS/WFC	F435W F606W	cluster	candidate
B311-G033	6671(11081)	WFPC2	F555W F606W F814W	cluster	cluster(SI)
B324-G051	6699	WFPC2	F555W F814W	cluster	cluster(SI)

B328-G054	6699	WFPC2	F555W F814W	cluster	cluster(SI)
B347-G154	10818	WFPC2	F450W F814W	cluster	cluster(S)
B423	idate				candidate
B468	5112	WFPC2	F555W F814W	cluster	cluster(I)
NB16	10818	WFPC2	F450W F814W	cluster	cluster(SI)
B150D					candidate

5

An HST/WFPC2 Survey of Bright Young Clusters in M31 III. Structural Parameters[1]

P. Barmby, S. Perina, M. Bellazzini, J.G. Cohen, P.W. Hodge, J.P. Huchra, M. Kissler-Patig, T.H. Puzia, & J. Strader

Abstract

Surface brightness profiles for 23 M31 star clusters were measured using images from the Wide Field Planetary Camera 2 on the *Hubble Space Telescope*, and fit to two types of models to determine the clusters' structural properties. The clusters are primarily young ($\sim 10^8$ yr) and massive ($\sim 10^{4.5}$ $M_\odot$), with median half-light radius 7 pc and dissolution times of a few Gyr. The properties of the M31 clusters are comparable to those of clusters of similar age in the Magellanic Clouds. Simulated star clusters are used to derive a conversion from statistical measures of cluster size to half-light radius so that the extragalactic clusters can be compared to young massive clusters in the Milky Way. All three sets of star clusters fall approximately on the same age-size relation. The young M31 clusters are expected to dissolve within a few Gyr and will not survive to become old, globular clusters. However, they do appear to follow the same fundamental plane relations as old clusters; if confirmed with velocity dispersion measurements, this would be a strong indication that the star cluster fundamental plane reflects universal cluster formation conditions.

5.1 Introduction

The spatial distribution of stars within a star cluster is an important indicator of the cluster's dynamical state, and the structural parameters (e.g. core, half-light, and tidal radii; central surface brightness, and concentration) indicate on what timescales the cluster is 'bound' to dissolve. The work of Spitzer (1987) showed that core collapse is an inevitable part of cluster dynamical evolution. Djorgovski & King (1986) were among the first to determine the fraction of core-collapsed Milky Way globular clusters (GCs), while Djorgovski & Meylan (1994) examined a large sample of Milky Way clusters and defined the 'fundamental plane', showing that surface brightness profiles of Galactic GCs were well-described by only a few parameters. Meylan & Djorgovski (1987) surveyed GCs in the LMC and SMC for core collapse and found that only a handful of clusters were core-collapse candidates; they suggested that environmental or age effects were responsible for the difference with Milky Way globulars.

A few spatially-resolved studies of GCs beyond the Magellanic Clouds were done with ground-based data. Racine (1991) and Racine & Harris (1992) used high-resolution imaging to distinguish M31 GC candidates from background galaxies, and Cohen & Freeman (1991) determined the tidal radii of 30 M31 halo GCs, finding them to be similar to Milky Way GCs. However, detailed studies of the structures of M31 GCs awaited the angular resolution of the *Hubble Space Telescope*. The first work on M31 GCs by Bendinelli et al. (1993) and Fusi Pecci et al. (1994) was followed by numerous others including Rich et al. (1996), Grillmair et al. (1996), Holland et al. (1997), and Barmby et al. (2002, 2007). Clusters in Local Group galaxies are near the limit for resolution into individual stars by the *Hubble Space Telescope* (HST), although some structural information such as half-light radii can be recovered for clusters in more distant galaxies (e.g., Haşegan et al., 2005). Conclusions of the studies of extragalactic globulars include the dependence of cluster size on galactocentric radius, first pointed out for the Milky Way by Djorgovski & Meylan (1994) and van den Bergh (1994); a possible difference between sizes of clusters in different metallicity groups (for a detailed discussion see Jordán, 2004); and a recognition that globular clusters in a variety of environments appear to lie on the same fundamental plane (Barmby et al., 2007).

Structural studies of younger star clusters present more difficulties. Open clusters (OCs) in the Milky Way are generally much less massive than globular clusters. As viewed from our location in the Milky Way, they are embedded within the disk, so that the cluster is easily lost against the much more numerous field stars, and determining stellar membership in these less-concentrated objects is not straightforward. Comprehensive studies of Milky Way open clusters are relatively recent: Kharchenko et al. (2005) and follow-up work (Schilbach et al., 2006; Piskunov et al., 2007, 2008) measured a variety of radii (core, corona, tidal) for several hundred clusters and found their masses to be in the range 50–1000 $M_\odot$. Bonatto & Bica (2005) analyzed in more detail a much smaller number of Milky Way open clusters, finding that the cluster size increased with both age and Galactocentric distance. These authors also found that their sample of clusters showed evidence for an 'open cluster fundamental plane.'

Milky Way open clusters are not the only known population of young star clusters, and possibly not even the best one to study. The Galactic OCs cover a limited range in age and mass and their census is suspected to be far from complete because of extinction in the Galactic plane. The Magellanic Clouds (MCs) have many young star clusters, recently cataloged by Bica et al. (2008). The brighter MC clusters were studied in a pioneering work by Elson et al. (1987). These authors analyzed the radial profiles of 10 clusters and found them to be better-fit by 'power-law' profiles of the form $I(R) \propto [1 + (R/r_0)^2]^{-(\gamma-1)/2}$ than by the King (1966) models conventionally used to fit globular cluster profiles. McLaughlin & van der Marel (2005) re-analyzed a large set of MC cluster data and found the situation to be somewhat more complex. Those authors argued that the extended envelopes characteristic of the power-law profiles are a generic feature of many young *and old* star clusters and that "the development of a physically motivated model accounting for this ... could lend substantial new insight into questions of cluster formation and evolution."

Outside the Milky Way, many galaxies are found to have 'young massive clusters' (YMCs; Holtzman et al. 1992; Whitmore & Schweizer 1995). These clusters have ages up to a few

Gyr (Brodie et al., 1998) and masses comparable to globular clusters (Larsen & Richtler, 1999). Studies of YMC structures show correlations of power-law slope γ with age (Larsen, 2004), core radius with age (Mackey & Gilmore, 2003), and mass of the brightest cluster with galaxy star formation rate (Weidner et al., 2004). As of yet there is no comprehensive study of star cluster structures over the full age and mass ranges seen in nearby galaxies. M31 is now recognized to also have a large population of young star clusters (Fusi Pecci et al., 2005; Caldwell et al., 2009), although their relationship to both the YMCs and globular clusters is not well-understood. The purpose of this paper is to carry out an initial study of the structural properties of some young M31 clusters. We analyze a sample of 23 clusters using data from the Wide Field Planetary Camera 2 (WFPC2) onboard the *Hubble Space Telescope*; extensive analysis of 'artificial clusters' (see Appendix) informs our analysis procedures. Throughout this work we assume a distance to M31 of 783 kpc (Stanek & Garnavich, 1998), for which $1''$ corresponds to 3.797 pc. All magnitudes are in the Vega system, and cluster names use the convention of the Revised Bologna Catalog (Galleti et al., 2004);[2] see that work for cluster coordinates and other properties.

5.2 Data and analysis methods

5.2.1 Cluster sample

The study of star clusters in M31 has a long history dating back to at least Hubble (1932), so any attempt to assemble a sample of young massive clusters necessarily draws on many previous works. While a number of studies of the *globular* cluster system have noted the presence of possible young clusters in M31 (Barmby et al., 2000; Williams & Hodge, 2001a), the first comprehensive list of such objects was assembled by Fusi Pecci et al. (2005), who called them 'blue luminous compact clusters', or BLCCs. Krienke & Hodge (2007, 2008) and Hodge et al. (2009) searched for M31 'disk clusters' in archival HST imaging data, and Caldwell et al. (2009) presented a comprehensive list of nearly 150 young cluster candidates from a spectroscopic survey. Caldwell et al. (2009) noted that the handful of their young clusters with measured structural properties (from Barmby et al. 2007) covered a wide range in parameter space. The HST resolved-star study of four 'massive and compact young star clusters' by Williams & Hodge (2001a) (program GO-8296) did not include an analysis of the objects' structural properties.

The main sample of clusters studied here is described in detail by the companion papers by Perina et al. (2009a, 2010). The present project began with an interest in confirming the results of Cohen et al. (2005) who used adaptive optics imaging to show that some of the clusters proposed as young were in fact asterisms (but see the contrary view of Caldwell et al. 2009 and the discussion in Perina et al. 2009a). HST program GO-10818 was aimed at imaging all of the 'class A' clusters proposed by (Fusi Pecci et al., 2005) which did not already have HST imaging, a total of 21 objects. In the course of the program we found that two clusters in the candidate list were in fact the same object (Perina et al., 2009a), and the object NB67 was a star, so the program contains 19 objects. Perina et al. (2010) showed that 16 of the clusters are young, with ages < 1 Gyr, and five (B083, B222, B347, B374, and NB16) are in fact intermediate-aged or old (see also Caldwell et al. 2009). We retain these five clusters in our sample but show them with different symbols in the analysis. We augmented the GO-10818 data with archival data on the four clusters studied by Williams & Hodge (2001a) to bring the total number of clusters to 23. HST archival data exists for additional clusters but in the interests of dealing with a mostly-homogeneous dataset we restricted the sample to only the GO-10818 and GO-8296 clusters. Three of the clusters in the latter dataset had structural parameters reported in Barmby et al. (2002); here we re-analyze them in a manner consistent with the other clusters. Except for B083 and B347, all of the clusters are projected against the M31 disk (see Fig. 1 of Perina et al. 2010).

---

[2]Online version at `www.bo.astro.it/M31`

Table 5.1: Data for M31 young clusters

NAME[a]	Dataset 1	Dataset 2	Filter 1	Exposure 1 [s]	Filter 2	Exposure [2] s	$E(B-V)$	log age [yr]
B015D	u9pi140[12]	u9pi140[34]	F450W	800	F814W	800	0.65	7.85
B040	u9pi050[12]	u9pi050[34]	F450W	800	F814W	800	0.23	7.90
B043	u9pi022[12]	u9pi022[34]	F450W	800	F814W	800	0.23	7.90
B066	u9pi240[12]	u9pi240[34]	F450W	800	F814W	800	0.23	7.85
B081	u9pi170[12]	u9pi170[34]	F450W	800	F814W	800	0.30	8.15
B083	u9pi250[12]	u9pi250[34]	F450W	800	F814W	800	0.20	10.11
B222	u9pi180[12]	u9pi180[34]	F450W	800	F814W	800	0.20	8.90
B257D	u9pi100[12]	u9pi100[34]	F450W	800	F814W	800	0.30	7.90
B315	u5bj010[12]	u5bj010[78]	F439W	1600	F555W	1200	0.31	8.00
B318	u9pi020[12]	u9pi020[34]	F450W	800	F814W	800	0.17	7.85
B319	u5bj020[12]	u5bj020[78]	F439W	1600	F555W	1200	0.23	8.00
B321	u9pi150[12]	u9pi150[34]	F450W	800	F814W	800	0.25	8.23
B327	u9pi030[12]	u9pi030[34]	F450W	800	F814W	800	0.20	7.70
B342	u5bj030[12]	u5bj030[78]	F439W	1600	F555W	1200	0.20	8.20
B347	u9pi230[12]	u9pi230[34]	F450W	800	F814W	800	0.06	10.11
B368	u5bj040[12]	u5bj040[78]	F439W	1600	F555W	1200	0.20	7.80
B374	u9pi070[12]	u9pi070[34]	F450W	800	F814W	800	0.30	8.80
B376	u9pi080[12]	u9pi080[34]	F450W	800	F814W	800	0.30	8.00
B448	u9pi200[12]	u9pi200[34]	F450W	800	F814W	800	0.35	7.90
B475	u9pi090[12]	u9pi090[34]	F450W	800	F814W	800	0.35	8.30
NB16	u9pi120[12]	u9pi012[34]	F450W	800	F814W	800	0.25	10.11
V031	u9pi130[12]	u9pi130[34]	F450W	800	F814W	800	0.35	8.45
VDB0	u9pi010[12]	u9pi010[34]	F450W	800	F814W	800	0.20	7.60

[a] Naming convention of the Revised Bologna Catalog (Galleti et al., 2004) is used. See that work for coordinates.

5.2.2 Data reduction and surface brightness profiles

The GO-10818 program was originally intended to be carried out with the Advanced Camera for Surveys (ACS), but because that instrument failed, the images were obtained instead with the Wide-Field Planetary Camera 2 (WFPC2). All objects were observed with two 400-s dithered images in each of 2 filters: F450W and F814W (for further detail, and an example of the CMD analysis, see Perina et al. 2009a). The GO-8296 program was also carried out with WFPC2 and involved two 800-s images in F439W and two 600-s images in F555W (as well as longer images in F336W which are not used here). The target clusters were on the PC chip in all cases, and only data from that chip is used in the present analysis. Table 5.1 summarizes the datasets together with other pertinent information about the clusters.

The multiple images were combined with the STScI Multidrizzle software, using the 'recipes' provided on the drizzle webpage. The pixel scale of the resulting images was 0.0455″, or 0.172 pc at the M31 distance. While correcting for Charge Transfer Efficiency losses would be desirable, there is currently no prescription available for correcting surface photometry of extended objects so no correction has been made in the present analysis. Although M31 star clusters are relatively large (a few arcsec) compared to the HST optical point-spread function (PSF), convolving model profiles with the PSF prior to comparison with the data should improve the accuracy of measurements of the cluster cores. Model PSFs were generated for the relevant filters at the camera center using TinyTim. The clusters are small compared to the camera field-of-view, and PSF variation over the cluster extent is negligible.

Transforming instrumental magnitudes to calibrated surface brightness was done following the prescription in Barmby et al. (2007). Image counts were first multiplied by the inverse square of the pixel scale to give counts C in units of s^{-1} arcsec^{-2}. These can be transformed to magnitudes arcsec^{-2} through $\mu = Z - 2.5\log(C)$, where Z is the instrument

Table 5.2. Calibration data for WFPC2 imaging

filter	zeropoint	$M_\odot$	Conversion factor[a]
F439W	22.987	5.55	45.138
F450W	23.996	5.31	14.274
F555W	24.621	4.83	5.163
F814W	23.641	4.14	6.744

[a]Multiplicative conversion between surface brightness in counts s^{-1} arcsecc^{-2} and intensity in $L_\odot$ pc^{-2}.

zeropoint. They can also be transformed to intensity I in $L_\odot$ pc^{-2} through $I = 10^{0.4(Z'-Z)}C$. (Independent of the instrument used, $Z' = (m-M)_{M31} + M_\odot + 5\log(\beta) = 21.5715 + M_\odot$ where β is the number of arcsec corresponding to 1 pc; $\beta = 0.2644$ at the assumed distance of M31.) The zeropoints used come from the respective instrument handbooks; the solar magnitudes are from calculations by C. Willmer[3]. All are listed in Table 5.2 for reference.

Studies of surface brightness profiles of Local Group star clusters are in a somewhat different regime from either Galactic clusters or clusters in more distant galaxies. Local Group star clusters are resolved into stars in their outer regions but not in their cores. They differ from galaxies with comparable angular sizes ($\lesssim 10$ arcsec for M31 and M33 clusters) in that the galaxies are composed of many more stars and have much smoother light distributions. To better understand the limitations of our analysis, we simulated artificial star clusters, measured their surface brightness profiles, and fit those profiles to models: these simulations are described in Appendix 5.A.

Surface brightness profiles for the M31 clusters were measured by combining integrated photometry with star number counts (the 'hybrid' procedure described in Appendix 5.A). In the inner regions of the clusters, surface brightness profiles were derived using the IRAF ELLIPSE package to fit circular isophotes to the image data. The isophote centers were fixed at a single value for each cluster, with centers determined as the intensity-weighted centroid in a 75 by 75 pixel box. Star counts were derived only from stars within specified regions of the CMD, with the designated region varying by cluster depending on the age. The details of the star counts for the GO-10818 clusters are given by Perina et al. (2010); for the GO-8296 clusters, star counts were computed from background-subtracted CMDs (Fig. 6 of Williams & Hodge 2001a) with positional data kindly provided by B. Williams. The star counts were used for radii > 7 pc (40 pixels) from the cluster centers, and scaled to linear intensity units ($L_\odot$ pc^{-2}) by matching the counts and photometry over the overlap region 5–10 pc. The same star counts were matched to integrated photometry profiles in both red and blue filters, but with different scaling factors; star count uncertainties were matched to the photometry uncertainties by scaling as for the intensity. No background subtraction was performed on the star counts.

5.2.3 Profile-fitting methods

There are a number of possible choices for star cluster density profiles, including King (1966), hereafter King, Wilson (1975), hereafter Wilson, King (1962), Elson et al. (1987, also known as 'power-law' or 'EFF'), and Sérsic (1968). Unlike the other three types of model profile, the King and Wilson models have no analytic expressions for density or surface brightness as a function of projected radius; profiles are obtained by integrating phase-space distribution functions over all velocities and then along the line of sight, assuming spherical symmetry (for a review, see McLaughlin, 2003). The King model is the most commonly-used

---

[3]www.ucolick.org/ cnaw/sun.html

in studies of star clusters; however, McLaughlin & van der Marel (2005) showed that, with data that extends to sufficiently large projected radii, many Local Group clusters are better-fit by the more-extended Wilson models. Globulars in NGC 5128 are also better-fit by Wilson models (McLaughlin et al., 2008), although an analysis using nearly identical techniques (Barmby et al., 2007) found that massive M31 globulars were better-fit by King models. Taken together, these recent analyses showed that fitting the King (1962), Elson et al. (1987), and Sérsic (1968) models did not add significant information beyond that provided by the King and Wilson models, so we consider only these two models in our analysis.

The King and Wilson models are single-stellar-mass, isotropic models defined by phase-space distribution functions of stellar energy E:

$$f(E) \propto \begin{cases} \exp[-E/\sigma_0^2] - 1 & , E < 0 \quad \text{(King)} \\ \exp[-E/\sigma_0^2] - 1 + E/\sigma_0^2 & , E < 0 \quad \text{(Wilson)} \\ 0 & , E \geq 0 \quad \text{(both)} \end{cases} \tag{5.1}$$

where σ_0 is the central velocity dispersion. The effect of the extra term in the Wilson model $f(E)$ is to make clusters more spatially extended. Both sets of models are characterized by three parameters: a dimensionless central potential W_0, which measures the degree of central concentration; a scale radius r_0, which sets the physical scale; and a central intensity I_0, which sets the overall normalization. For the King models, W_0 has a one-to-one correspondence with the more-familiar concentration $c = \log(r_t/r_0)$, where r_t is the tidal radius at which the density $\rho(r_t) = 0$. Possibly contrary to intuitive expectations, for two profiles with the same scale radius, the profile with a larger value of c or W_0 declines more slowly.

Deriving the structural properties of the simulated clusters involved fitting their projected surface density profiles to models using the GRIDFIT program described by McLaughlin & van der Marel (2005, see also McLaughlin et al. 2008). The program uses a grid of model density profiles, pre-computed for a range of values of W_0, then finds the scale radius r_0 and central surface brightess I_0 to minimize the weighted χ^2 for each W_0; the best-fitting model is the one with the global χ^2 minimum. The model profiles are convolved with the instrumental PSF before comparison to the data. Since no background subtraction was performed on the star counts, the background level was determined as one of the parameters of the model fitting. For a few clusters the fitting algorithm converged to unreasonably large or small values, and a fixed background corresponding to the lowest level reached by the star counts was subtracted before re-fitting; in general this procedure improved the reduced χ^2 of the fits.

5.2.4 Profile-fitting: results

Figure 5.1 shows the cluster surface brightness profiles together with the best-fitting models. The parameters of the models are given in Table 5.3, corrected for extinction using the values of $E(B-V)$ given by Perina et al. (2010) or Williams & Hodge (2001a).

Conversion of filter-specific measurements to the V-band is done using the transformations described in the appropriate HST Instrument Handbooks; briefly, we compute the extinction-corrected color $(V-x)_0$, where x is the observed-band magnitude, as a function of color in standard bands (e.g., $(V-I)_0$). Ground-based integrated colors from Galleti et al. (2007) are used for the standard-band colors, to avoid iteration; uncertainties of 0.1 mag in $(V-x)_0$ are assumed and propagated through the parameter estimates. As previously shown by McLaughlin & van der Marel (2005), differences between Wilson and King model profiles occur primarily in the outer parts of cluster profiles, where our signal-to-noise is low. The similarity between model profiles also means that, in general, the best-fit models of the two families have very similar χ^2, with no strong systematic preference for one model or the other. Typical χ^2 values are 85–90; with ~ 20 datapoints and 3 or 4 model degrees of freedom, the resulting reduced values are $\chi_\nu^2 \sim 6$. This indicates that the uncertainties produced by integrated photometry are likely underestimates, and one reason may be that these uncertainties do not account for the uncertainty in the background level. Rather than modify the uncertainties to achieve $\chi_\nu^2 \sim 1$, we modified our use of χ^2 in computing parameter
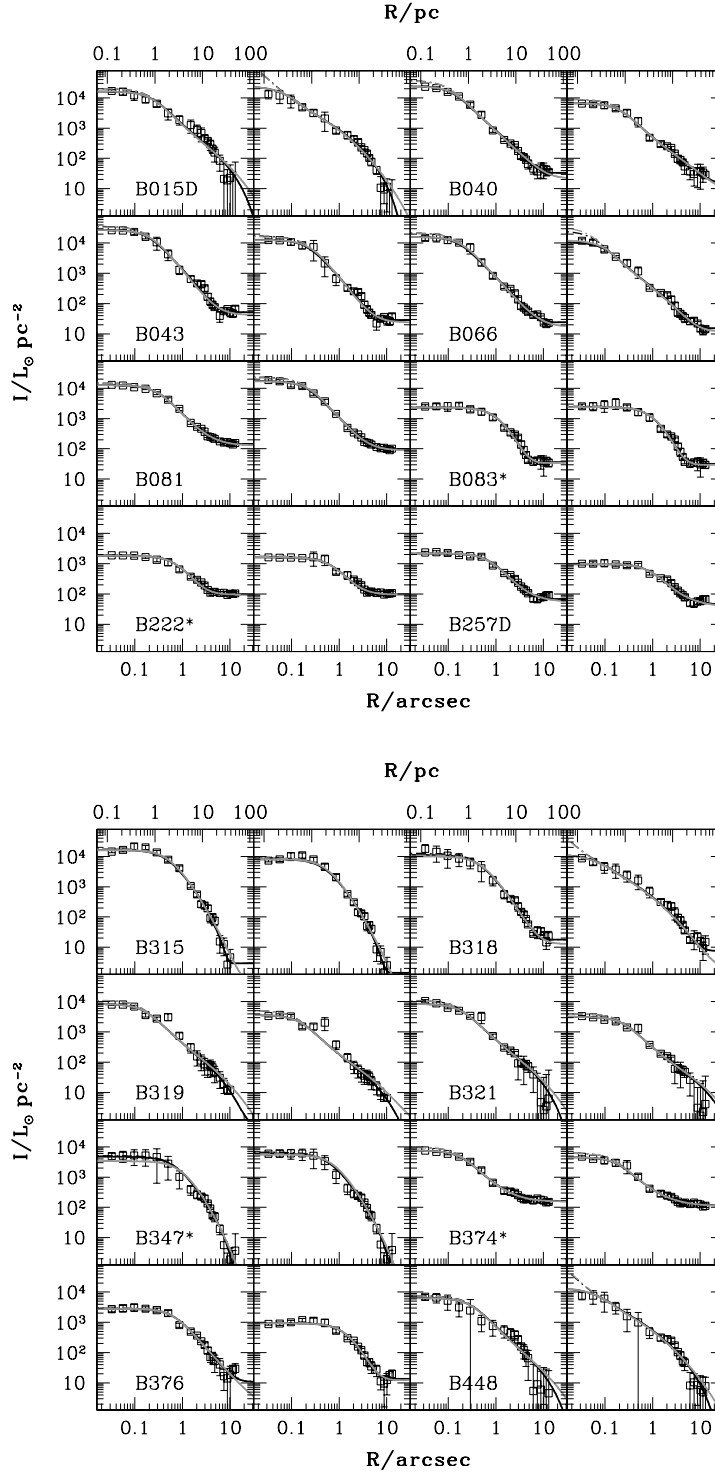
Figure 5.1: M31 cluster surface brightness profiles together with the best-fitting models. Each cluster is shown in two sub-panels, with the bluer filter (F439W or F450W) on the left and the redder filter (F555W or F814W) on the right. Clusters with an asterisk after their names are likely to be old. Black lines are best-fitting King (1966) models; grey lines (most are directly over the black lines) are best-fitting Wilson (1975) models. Solid lines are model profiles after convolution with the PSF; dash-dot lines are profiles before convolution.

99
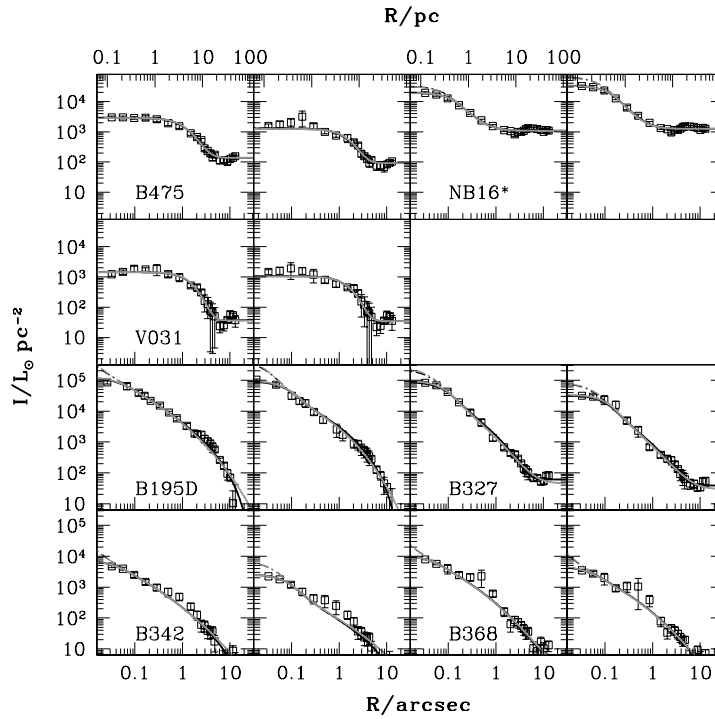
Figure 5.1: Continued. Note that the last four clusters are plotted with a different vertical scale.

Table 5.3: Basic Parameters of Fits to Profiles of M31 Young Clusters

Name	Filter	$N_{\rm pts}$	Model	$\chi^2_{\rm min}$	$I_{\rm bkg}$ $(L_\odot\,{\rm pc}^{-2})$	W_0	c	μ_0 (mag arcsec^{-2})	$\log r_0$ (arcsec)	$\log r_0$ (pc)
B015D	F450W	21	K66	323.12	7.5	$10.20^{+0.90}_{-0.80}$	$2.39^{+0.18}_{-0.17}$	$16.12^{+0.15}_{-0.15}$	$-0.640^{+0.108}_{-0.112}$	$-0.061^{+0.108}_{-0.112}$
			W	386.35	7.5	$10.80^{+1.10}_{-1.00}$	$3.38^{+0.13}_{-0.05}$	$16.11^{+0.16}_{-0.14}$	$-0.650^{+0.121}_{-0.111}$	$-0.071^{+0.121}_{-0.111}$
B015D	F814W	21	K66	231.70	12.8	$14.40^{+1.40}_{-1.00}$	$3.23^{+0.31}_{-0.21}$	$12.61^{+0.48}_{-0.69}$	$-1.758^{+0.196}_{-0.279}$	$-1.179^{+0.196}_{-0.279}$
			W	377.92	12.8	$14.90^{+1.50}_{-1.20}$	$4.15^{+0.39}_{-0.30}$	$12.47^{+0.51}_{-0.70}$	$-1.804^{+0.215}_{-0.287}$	$-1.225^{+0.215}_{-0.287}$
B040	F450W	21	K66	44.18	33.18 ± 3.56	$9.60^{+0.40}_{-0.30}$	$2.26^{+0.09}_{-0.07}$	$15.44^{+0.08}_{-0.11}$	$-0.967^{+0.048}_{-0.067}$	$-0.387^{+0.048}_{-0.067}$
			W	50.75	21.84 ± 5.10	$9.80^{+0.50}_{-0.40}$	$3.32^{+0.02}_{-0.00}$	$15.48^{+0.08}_{-0.10}$	$-0.931^{+0.054}_{-0.069}$	$-0.352^{+0.054}_{-0.069}$

Note. Table 5.3 is available in its entirety in the electronic edition of the Journal. A short extract from it is shown here, for guidance regarding its form and content. Column descriptions: $\chi^2_{\rm min}$: unreduced χ^2 of best-fitting model; $I_{\rm bkg}$: model-fit background intensity (values without uncertainties indicate clusters for which the background was fixed manually); W_0: model-fit central potential; $c = \log(r_t/r_0)$: model-fit concentration (r_t is tidal radius, given in Table 5.4); μ_0: model-fit central surface brightness; $\log r_0$: model-fit scale radius. Uncertainties are 68% confidence intervals, computed as described in the text.
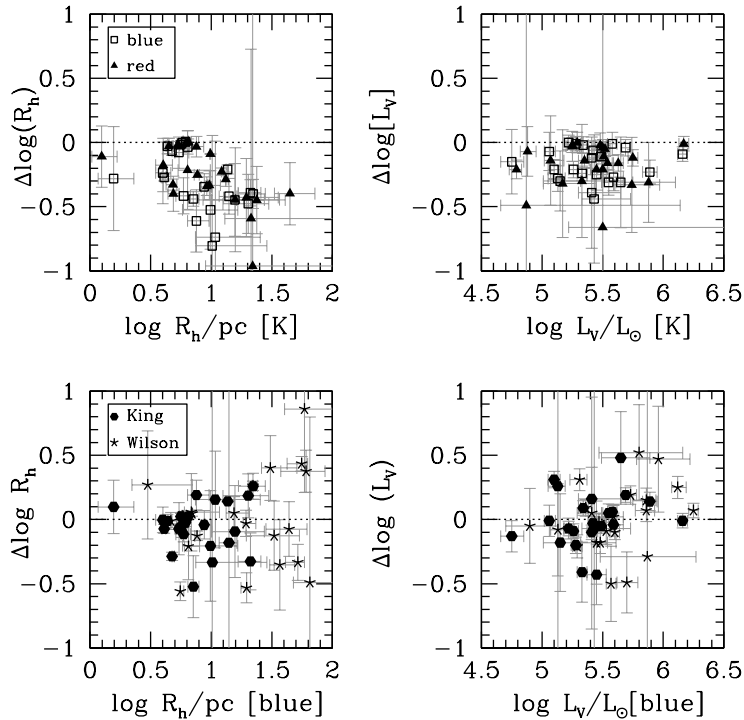
Figure 5.2: Comparison of half-light radii and total luminosity (converted to the *V* band) for Wilson and King models fit to surface brightness profiles of M31 young clusers. Bottom: comparison between observations of the same cluster in different filters (hexagons: King models, stars: Wilson models). Top: Comparison of Wilson and King model fits to the same cluster (squares: red filter, triangles: blue filter).

uncertainties (see also McLaughlin et al. 2008). We scaled the reduced χ^2 values such that the best-fit model had $\chi^2_\nu \equiv 1$. The 68% confidence limits on the parameters are then the minimum and maximum values found in the set of models with $\chi^2_\nu \leq 2$. This rescaling gives more realistic estimates of the parameter uncertainties than would otherwise be the case.

How robust are the physical parameters derived from our model fits? One way to estimate this is to compare various fits to the same cluster. Although W_0 and r_0 have slightly different meanings in King and Wilson models and cannot be directly compared, some derived quantities such as the half-light radius and total luminosity are directly comparable. For all clusters we have profile data in two different bandpasses, although the outer parts of the profile, derived from number counts, are the same in both. There are physical reasons why profiles might change with wavelength (e.g., mass segregation, differential reddening), but comparison of model fits in different filters is a useful sanity check. Figure 5.2 shows this comparison: the scatter between filters is 0.2–0.3 dex. A similar comparison between fits for M31 globular clusters by Barmby et al. (2007) found a much smaller scatter, probably because that work analyzed bright clusters, using much deeper data. Figure 5.2 also compares R_h and L_V between Wilson and King models. The scatter is again rather large, 0.15–0.25 dex, with the Wilson models offset to larger values. To some extent this is to be expected, since Wilson models have larger halos; however some of the Wilson model values (e.g., $R_h > 50$ pc for B015D, B257D, B321, B376, and B448) are physically implausible, because the model-fitting resulted in a very large values of the central potential W_0. We do not completely understand the reason for this but speculate that it may be related to the combination of the additional power in the haloes of Wilson models and the low signal-to-noise of the profiles in the same region. These results indicate the limitations of our relatively shallow data, and the limited precision of the model measurements will need to be kept in mind during the following analysis.

For the analysis in the remainder of this paper, we use only a single set of model parameters per cluster. Because the King models have fewer implausible values, and also somewhat less scatter between filters, we use on the King model parameters for the present cluster sample. Our results in Appendix 5.A indicate that King model fits may be more robust than Wilson model fits in the case where background levels are uncertain, even where the underlying cluster profile is actually a Wilson model. Using King models also allows us to compare the present sample to the combined sample of M31 globulars analysed in Barmby et al. (2002, 2007): all of that sample has King fits while only about one third has Wilson-model fits. Because the focus of this paper is the young M31 clusters, dominated by blue stars, we use the F439W or F450W-band measurements in preference to those from the redder filters.

The left panel of Figure 5.3 shows the properties of the present sample of clusters as a function of luminosity. Four clusters (vdB0, B327, B342, B368) stand out as having very high central surface brightnesses; all except B327 also have correspondingly high concentrations. Figure 5.1 shows that the cores of these clusters do not appear to be resolved in our data. This could be due to the short exposure times: if the central cluster light is dominated by a few bright stars, the true integrated profile could be very difficult to recover. Structural parameters for these clusters are uncertain. Figure 5.1 also shows that the three M31 young clusters with the largest inferred half-light radii (B015D, B321, B448) have relatively low contrast against the resolved stellar background of M31, so it is possible that the number counts include some field stars and the resulting R_h values are overestimates. The old cluster NB16 has a much smaller R_h and total luminosity than the other members of the sample: this cluster is projected on the M31 bulge and its outer stars may be lost against the bright background. These issues highlight the limitations of our dataset for the kind of structural analysis we are attempting, but the generally good match of model profiles with the observational ones gives us confidence that the cluster parameters we measure are reasonable.

Analyzing the physical properties of M31 young clusters requires converting the observed flux-based measurements to luminosities and mass-linked quantities. Conversion from luminosity to mass is done using V-band mass-to-light ratios from the population synthesis models of Bruzual & Charlot (2003), assuming a Chabrier (2003) IMF and solar metallicity for all but the oldest clusters. Table 5.1 lists the assumed ages for all clusters: those given by Perina et al. (2010) for the young clusters from GO-10818, by Williams & Hodge (2001a) for the clusters from GO-8296, and assumed ages of 13 Gyr for the clusters B083, B222 and B347, B374 and NB16. We assume uncertainties of 10% in M/L_V and propagate these through the parameter estimates. While using M/L_V ratios determined directly from measured velocity dispersions would avoid the reliance on models, velocity dispersions are not available for most of the M31 clusters considered here. The use of a single set of population synthesis models also facilitates comparison of clusters in different galaxies; the comparison data for other galaxies, (McLaughlin & van der Marel, 2005; Barmby et al., 2007; McLaughlin et al., 2008) also used the same model mass-to-light ratios. Tables 5.4 and 5.5 give various derived parameters for the best-fitting models for each cluster (the details of their calculation are given by McLaughlin et al. 2008). Recently, Kruijssen & Lamers (2008) have discussed of star cluster mass-to-light ratios due to preferential loss of low-mass stars with cluster age. This effect is expected to be most important for old clusters, and we have used the Kruijssen & Lamers models to confirm that the change in M/L for young clusters is minimal ($\lesssim 20\%$). Since our focus in this paper is the young M31 clusters, we therefore do not correct for this effect.

5.3 Discussion: young and old clusters in M31 and other galaxies

Using star clusters as markers of the history of galaxies is aided by knowing how the clusters' structural properties change with age and environment. Although absolute ages of star clusters are notoriously difficult to determine, relative ages are more straightforward,
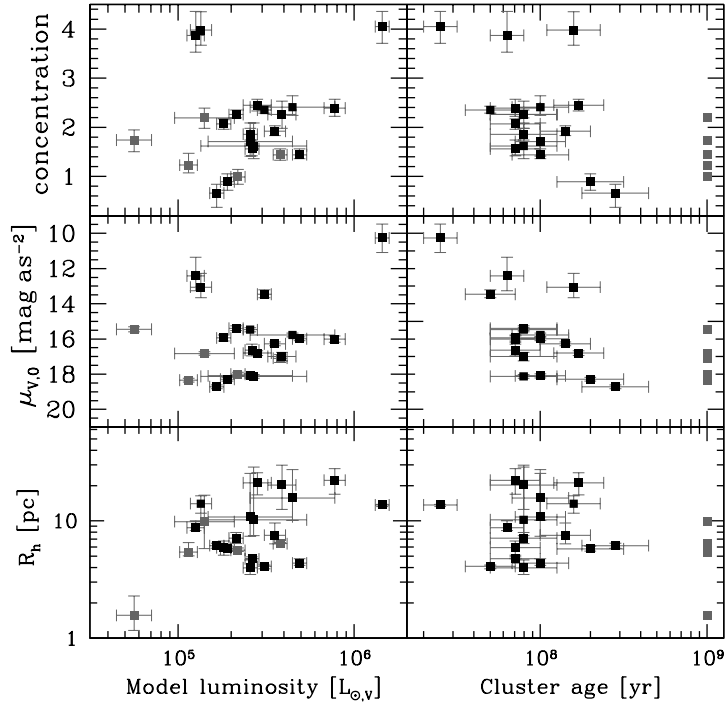
Figure 5.3: Concentration index, central surface brightness, and half-light radius for M31 young clusters as functions of total model luminosity (left) and estimated age (right). The old clusters are shown with gray symbols; although their ages are estimated at $> 10^{10}$ yr, they are plotted at 10^9 yr in the right panel to condense the horizontal axis scale.

and all of the clusters in our sample have ages estimated by CMD fitting (Williams & Hodge, 2001a; Perina et al., 2010). Can we see evidence for changes in cluster properties with age? In the right panel of Figure 5.3, structural properties for the M31 young clusters are shown as a function of estimated age. None of the properties plotted depends on mass-to-light ratio, which is strongly dependent on age. Although our sample is small and covers a limited range in age, there is an interesting hint that central surface brightness becomes fainter and concentration decreases as age increases. This is consistent with the increase in core radius with age for MC clusters noted by Mackey & Gilmore (2003). Figure 5.4 explores this further by plotting μ_0, c, R_c, and central mass density ρ_0 for both the M31 young clusters and young clusters in the Magellanic Clouds. While the MC clusters also show a trend for central surface brightness to fade with age, it is much weaker than the trend implied by the M31 clusters alone, and the high-surface-brightness M31 clusters appear to be outliers (possibly artifacts due to the limited spatial resolution). Since the central mass density shows very little trend with age, the central surface brightness trend is likely due to fading of stellar population and the (weak) increase of core radius with age. The dashed line in the central surface brightness panel shows the effects of mass-to-light ratio change predicted by the Bruzual & Charlot (2003) models with a Chabrier (2003) IMF and solar metallicity; the slope shows a reasonable match to the cluster trend.

Figure 5.4 shows that, with a few exceptions, the young M31 clusters have similar spatial structure to young clusters in the Magellanic Clouds. A number of young massive clusters have recently been identified in the Milky Way; Pfalzner (2009) compiled size and mass measurements of these clusters (Figer, 2008; Wolff et al., 2007) to argue that cluster evolution occurs along two well-defined tracks in the density-radius plane. Using the conversion between Milky Way cluster size measurements and half-light radii described in Appendix 5.A, we have compared cluster half-light radii and ages for the young Milky Way clusters together
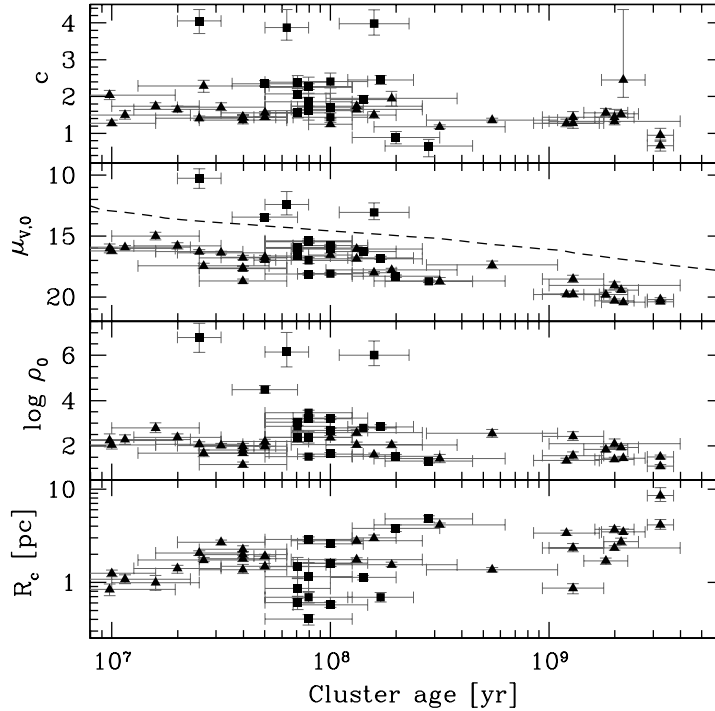
Figure 5.4: Concentration index, central surface brightness, and central mass density for M31 (squares) and Magellanic Cloud (triangles) young clusters as functions of estimated age. The dashed line in the central surface brightness panel shows the expected change in surface brightness due to changes in mass-to-light ratio with age (vertical normalization is arbitrary).

with the M31 and MC clusters in Figure 5.5. The M31 and MC clusters have similar sizes to the 'leaky' Milky Way clusters but lie on the extrapolation of the age-R_h trend of the 'starburst' MW clusters. This suggests that the starburst clusters (which tend to be more massive) are perhaps closer to being analogs of the young massive clusters in other galaxies. We speculate that the two evolutionary paths of Pfalzner (2009) may be simply due to extinction effects, with the 'starburst' clusters having left their host cocoon and the 'leaky' clusters still affected by excessive extinction in their outer regions (projection effects may also be important). This would imply that starburst clusters are more easily identified in external galaxies, explaining the reasonable match between extragalactic young clusters and Milky Way starburst clusters.

An important question in the study of young massive clusters is whether they will eventually become old massive clusters resembling the globular clusters we see today in the Galaxy. Once formed, star clusters have no easy way to gain mass, but they do have a number of ways to lose mass or even be completely disrupted (Spitzer, 1987; Vesperini, 1998; Lamers & Gieles, 2006). We have computed dissolution times for our cluster sample considering the effects of both the stellar and dynamical evolution of star clusters through time. These calculations explicitly account for age, metallicity, and half-light radius of all sample star clusters, and treat the effects of evaporation of low-mass stars, mass loss due to stellar evolution, encounters with spiral arms and giant molecular clouds following in part the prescriptions of Lamers et al. (2005) and Lamers & Gieles (2006) The results are shown in Figure 5.6. All clusters have dissolution time greater than their ages; however, for 2 young clusters (B321, B342) and the old cluster B374 these quantities are nearly equal, suggesting that they are in the process of dissolving. On average, the young clusters' dissolution times are too short to expect them to become old ($> 10^{10}$ yr) clusters. However, a few have $t_d > 1$ Gyr and, if they avoid collisions with giant molecular clouds, might survive to become sparse old
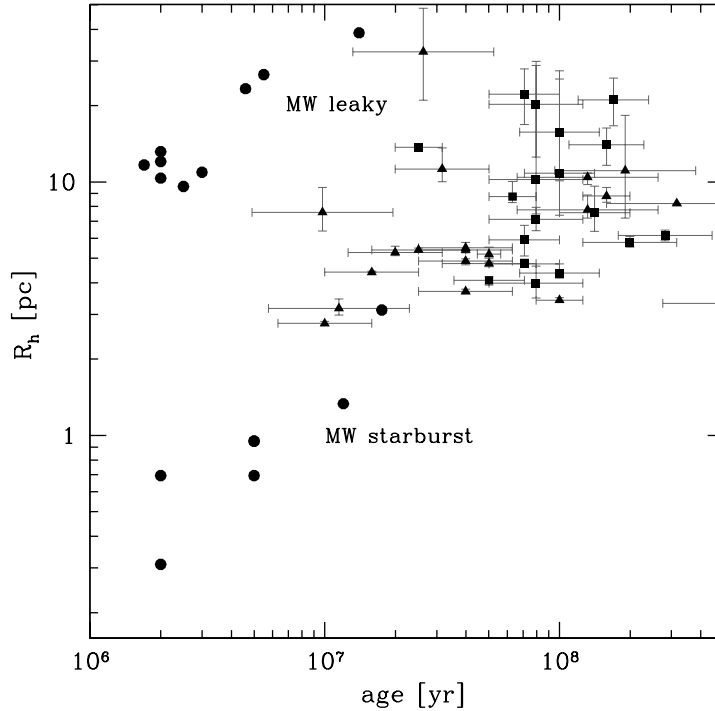
Figure 5.5: Young star cluster ages and sizes. Squares: M31 clusters from the present sample; triangles: young Magellanic Cloud clusters; circles: young massive Milky Way clusters from Figer (2008) and Wolff et al. (2007). The two groups of Milky Way clusters identified by Pfalzner (2009) are labeled.

globulars. In general, the dissolution times confirm the importance of cluster dissolution to the evolution of the star cluster mass function (see also, e.g., Gnedin & Ostriker 1997; Gieles 2009. Lower-mass and/or more-diffuse clusters in M31, such as those discovered by Krienke & Hodge (2007, 2008) and Hodge et al. (2009), would be even more likely to dissolve.

Work to date suggests that the structural parameters of old star clusters in several nearby galaxies show only a weak dependence on environment (Barmby et al., 2007), and the comparisons above indicate that young clusters in different galaxies are also similar. How do young and old clusters compare? Figure 5.7 shows cluster properties as a function of mass for M31 young clusters, Magellanic Cloud young clusters and Milky Way globulars (McLaughlin & van der Marel, 2005), M31 globulars (Barmby et al., 2002, 2007), and recently-discovered extended M31 halo clusters (Huxor et al., 2005).[4] The joint mass-age distribution of the clusters differs by galaxy: some of this is due to complex selection effects (e.g., the M31 globular sample is incomplete and biased toward more luminous clusters, and the sample of Milky Way YMCs is also incomplete), but there are hints of real differences between galaxies; see Perina et al. (2010) for a more detailed discussion. The properties of the five old clusters in our sample are similar to those of M31 and Milky Way globulars, while the properties of M31 young clusters overlap with those of both the young Magellanic Cloud clusters and the low-mass Milky Way globular clusters. Thus the M31 young clusters do not appear to be fundamentally different types of object from those already known. On average, the younger clusters have larger sizes and higher concentrations (where larger c implies a larger tidal radius for the same scale radius) than old clusters of the same mass. The young clusters therefore have larger tidal radii, which makes them more susceptible to dynamical

---

[4]Mass measurements for all clusters are derived using mass-to-light ratios. As discussed in §5.2.4, these ratios are affected by cluster dynamical evolution. Correcting for this effect is non-trivial and beyond the scope of this paper; however the results of Kruijssen (2008) imply that doing so would increase the spread of the old clusters' mass distribution and shift it to lower masses.
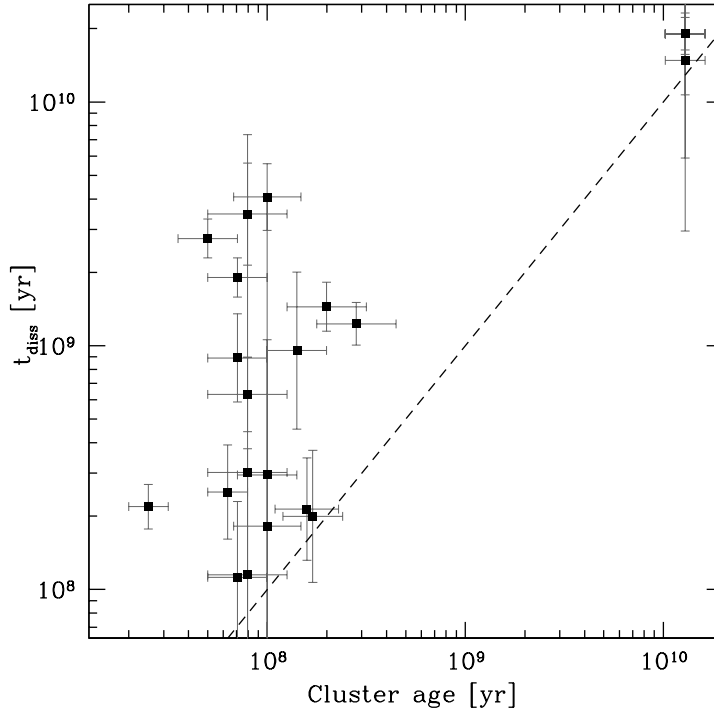
Figure 5.6: Dissolution times for M31 star clusters, compared to cluster ages. Four of the five old clusters are plotted at the same position, with dissolution times 20 Gyr and assumed ages 13 Gyr.

destruction: small-r_t clusters are more likely to survive to old age. The larger spread in properties of low-mass clusters compared to higher-mass clusters may indicate lower data quality for these fainter objects, rather than an intrinsic difference in properties.

By now it is well-known that old star clusters in the Milky Way and other galaxies describe a 'fundamental plane' (FP) in structural properties (Djorgovski, 1995; Djorgovski et al., 1997), although the separation of clusters from other types of objects has become less well-defined in recent years. The results of Bastian et al. (2006) and Kissler-Patig et al. (2006) indicate that young massive clusters fall on similar fundamental planes to those of old clusters. Those results make use of cluster velocity dispersions, while in this work, we must use mass-to-light ratios from population synthesis models applied to the photometry instead of independent mass estimates. The upper-right panel of Figure 5.7 shows one view of the FP, as defined by McLaughlin (2000). The old clusters in our sample fall nicely on this relation, as do most of the younger clusters. The observed correlation between mass and binding energy E_b is expected, since by definition $E_b = f(c)M^2/R_h$ where $f(c)$ is a weak function of cluster concentration c. However, the tightness of the correlation shows that there is very little relation between young cluster mass and R_h (see also lower-right panel), and no offsets in the basic properties of the cluster shapes between old and young clusters.

Figure 5.8 shows a different view of the fundamental plane, more akin to the parameters usually shown for elliptical galaxies (see also McLaughlin, 2003; Strader et al., 2009). The left two panels show the surface-brightness-based fundamental plane relations, with a large offset between the young M31 and MC clusters (light grey symbols) and the old clusters. This is to be expected because of the young clusters' lower mass-to-light ratios. When we instead plot quantities related to the mass density (right panels), the young clusters fall on the same relations as the old clusters. The tightness of the relations primarily reflects the use of mass-to-light ratios to compute both central velocity dispersion σ_0 and mass density Σ. Again, however, the lack of offset and similar scatter between the young and old clusters confirms their similar overall structures. Recent measurements of M31 globular clusters'

106
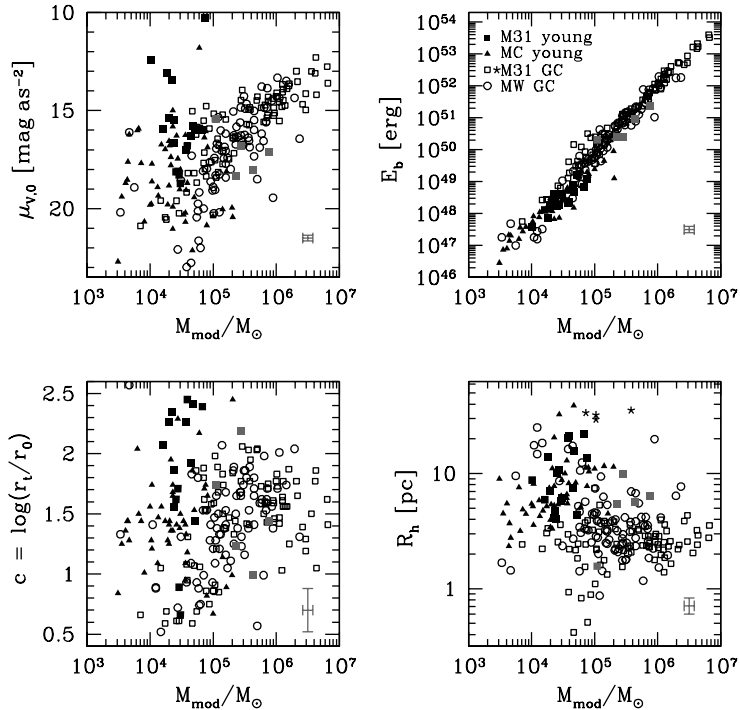
Figure 5.7: Structural properties of young and old star clusters in M31, young clusters in the Magellanic Clouds, and globular clusters in the Milky Way, shown as a function of cluster mass. Top left: central surface brightness; top right: binding energy; lower left: concentration; lower right: half-light radius. Filled squares: M31 clusters from the present sample (black: young clusters, grey: old clusters); open squares: old M31 clusters from Barmby et al. (2007, 2002); stars: 'extended luminous clusters' in M31 from Huxor et al. (2005); filled triangles: young Magellanic Cloud clusters. Error bars show median uncertainties for the young M31 clusters.

mass-to-light ratios (Strader et al., 2009) have shown that these clusters do follow the FP relations as expected from model mass-to-light ratios. Similar measurements for young clusters should show whether young clusters do the same. If so, this would indicate that the FP reflects conditions of cluster formation and is not merely the end product of cluster dynamical evolution.

Bonatto & Bica (2005) argue that Milky Way open clusters fall on a plane in the three-dimensional space of total mass, core radius, and projected core mass density. We can compare this space to the FP using with an approximate relation between mass and central velocity dispersion. The least-squares fit for the young MC clusters (the most populous sample of young clusters available) gives $\log \sigma_0 = 0.34 \log M - 1.38$; combined with the Bonatto & Bica (2005) cluster parameters, we find that the Milky Way open clusters fall approximately on the other young clusters with $\Sigma_0 \sim 10^2$ $M_\odot$ pc^{-2} in the top right panel of Figure 5.8. This suggests that the Milky Way open cluster plane indicated by Bonatto & Bica (2005) may in fact be the same FP defined by other star clusters, which have projected mass densities higher by up to four orders of magnitude. As Bonatto & Bica (2005) discuss, this result remains to be confirmed with large samples, but it is certainly intriguing in its implications for a 'universal' star cluster fundamental plane.

5.4 Summary and Directions for Future Work

This series of papers has established that a sample of candidate young star clusters in M31 are indeed young, massive clusters, with properties similar to those of other young
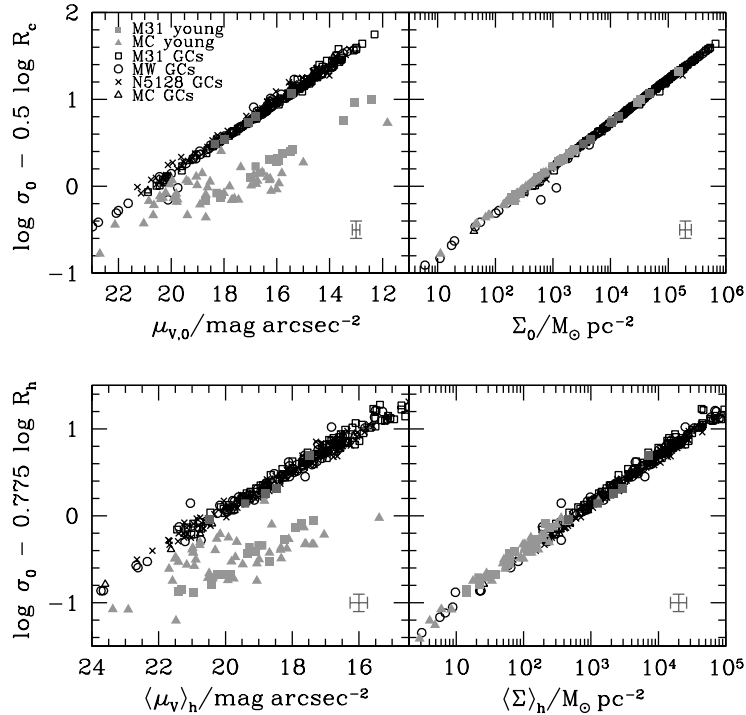
Figure 5.8: Views of the star cluster fundamental plane, with core parameter relations in the bottom panels and half-light parameter relations in the top panels. σ_0 is predicted central velocity dispersion and Σ represents surface mass density either in the cluster core or at the half-light radius. Left panels show surface brightness while right panels show mass surface density. Filled squares: M31 clusters from the present sample (light grey: young clusters, dark grey: old clusters); open triangles: old Magellanic Cloud and Fornax clusters; open circles: Milky Way globulars; crosses: NGC 5128 globulars. Other symbols as in Figure 5.7. Error bars show median uncertainties for the young M31 clusters.

clusters in Local Group galaxies. Our current data does not allow us to detect the extended haloes characterized by Wilson models and seen in other young clusters; the more compact King models provide adequate fits to the data. The structural parameters measured in this paper show the M31 clusters to be typical young clusters, with masses of 10^{4-5} M$_\odot$, half-light radii of 3–20 pc, and dissolution times of < 5 Gyr. While the basic similarity between young clusters in different Local Group galaxies, and between young and old clusters, seem well-established, many questions remain. What is the precise form of the age-size relation? Do cluster mass-to-light ratios evolve with age as predicted by dynamical and stellar evolution models? What fraction of the stellar disk in galaxies is comprised of dissolving clusters? Is there a relation between the cluster formation and local star formation rate, or other galaxy properties? Large cluster samples with high-quality data will be needed to address these and other questions about the relationship and history of star clusters and their parent galaxies.

5.A Artificial cluster tests

Deriving surface brightness profiles of star clusters in Local Group galaxies requires careful analysis. The clusters are only partially resolved into individual stars, and they are observed together with a galactic background which may also be resolved into stars. The purpose of this section is to investigate the best methods for extracting structural parameters of 'semi-resolved' clusters, particularly from relatively shallow images, and to quantify the uncertainties of those parameters. This can best be done by analyzing profiles derived from images of artificial clusters whose structural parameters are known. A related study by Noyola & Gebhardt (2006) simulated integrated photometry from HST observations of Galactic GCs; however the focus of that study was on recovering the structure of cluster cores rather than overall structure. Bonatto & Bica (2008) also carried out a similar study, but considering only King (1962) models for Galactic clusters.

The first step in analyzing simulated star cluster profiles is to determine the type of model profile and range of parameter space to be covered. The analysis of McLaughlin & van der Marel (2005) showed that Wilson models were adequate to describe both Milky Way and Magellanic Cloud cluster profiles, so we chose this set of models for our artificial clusters. Since we are interested in differences between young and old clusters we examined the distribution of scale radius r_0 and central potential W_0 for both young and old Magellanic Cloud clusters as given by McLaughlin & van der Marel (2005): W_0 ranged from 1 to 10 with a typical value $W_0 \approx 5$ while r_0 ranged from 0.2 to 20 pc with a typical value $r_0 \approx 2$ pc. The range of implied half-light radii is 1–35 pc.

Our artificial clusters were generated from Wilson profiles with 8 values of r_0 between 0.5 and 11 pc, and 9 values of W_0 between 2 and 10. For each (W_0, r_0) pair we generated clusters with four different population sizes: $N_* = 100, 300, 1000, 3000$. The stars' projected spatial positions were generated by selecting the projected radial coordinate from the probability distribution associated with the Wilson profile

$$p(R) = \frac{R \Sigma_{W_0, r_0}(R)}{\int_0^{R_{\max}} \Sigma(R') R' dR'} \tag{5.2}$$

and generating the angular coordinate θ at random. The stars' luminosities were generated by selecting from an observed 'young cluster' luminosity distribution, uncorrected for completeness. The distribution was generated by combining the observed magnitudes of stars in the four most populous clusters in the GO-10818 program (VdB0, B257D, B475, B327). Separate luminosity distributions were used in each of the two observational bands.

The specific observations being modeled are the same as those in the GO-10818 program. We generated images of the simulated clusters by inserting artificial stars modeled with the appropriate PSF near the center of a WFPC2/PC image of a field in M31. The background images used were the observations of 'B195D' from the GO-10818 program; the PC chip was essentially empty in this observation because of an error in the input coordinates (for details, see Perina et al. 2009a). This field is located in the south-west disk of M31. Figure 5.9 shows a sample of the simulated cluster images, together with some sample M31 clusters for comparison. The simulated clusters cover a wider range of properties than the real clusters: some of the simulated clusters were in fact not visually apparent in the images. These 'clusters' had few stars ($N_* = 100$ or $N_* = 300$) and very large half-light radii, more akin to dwarf galaxies than to objects recognizable as star clusters. They are not considered further in this analysis.

Surface density profiles for the simulated clusters were derived in several different ways. The first method ('number counts'), derived the surface density as simply the number of stars per unit area in annular bins. Since the locations of all stars are known precisely for the simulated clusters, this method represents the best possible data for surface density profiles. Deriving structural parameters from such data tests the fitting routine itself and also the extent to which density profiles can be derived from a limited number of stars. Stars were counted in overlapping annular bins of width 3 pixels (0.5 pc) inside a radius of 20 pixels (3.4 pc) and width 10 pixels (1.7 pc) outside this radius.
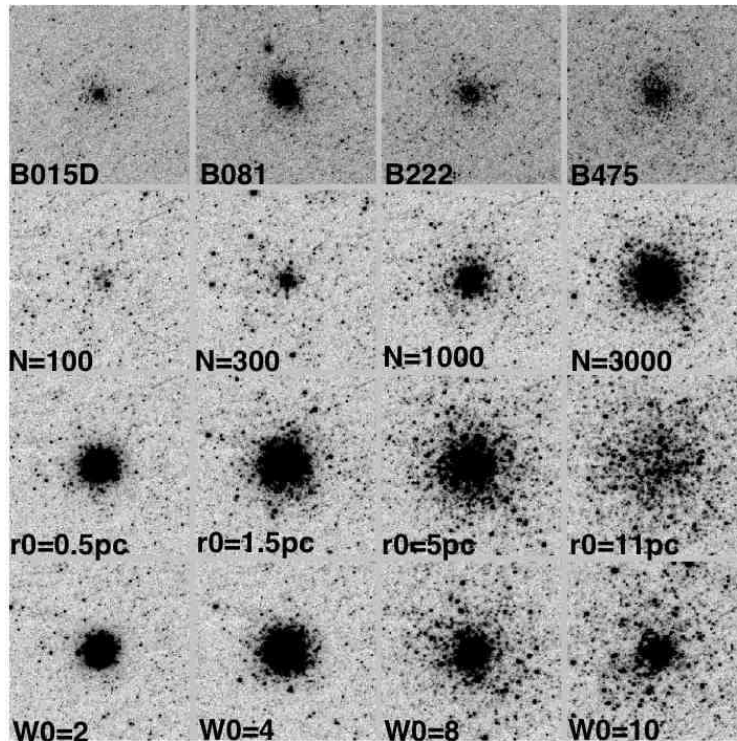
Figure 5.9: Top row: four M31 star clusters observed as part of program GO-10818 with HST. Left to right: B015D, B081, B222, B475. Second row: simulated clusters with central potential $W_0 = 6$ and scale radius $r_0 = 2$ pc, with (left to right) $N_* = 100, 300, 1000, 3000$. Third row: simulated clusters with $N_* = 3000$, central potential $W_0 = 6$ and scale radius (left to right) $r_0 = 0.5, 1.5, 5, 11$ pc. Fourth row: simulated clusters with $N_* = 3000$, scale radius $r_0 = 2$ pc, and (left to right) $W_0 = 2, 4, 8, 10$. All images are 800 s exposures in the F450W filter on the WFPC2/PC chip; each sub-image is 13.7×13.7 arcsec (51.7×51.7 pc at the distance of M31).

For real star clusters, crowding limits the ability to resolve individual stars and hence derive surface density profiles through number counts. We also derived surface density profiles of clusters using isophotal photometry with the IRAF ELLIPSE package, similar to the method described in Barmby et al. (2007). We refer to this as the 'integrated photometry' method. We also combined the number count and integrated photometry methods in a 'hybrid' method similar to that used by Federici et al. (2007). This involves matching the intensity scales of the two profiles by fitting both profiles to smooth curves in the region $r = 5 - 10$ pc. The switch-over from integrated photometry to number counts was made at a radius of 7 pc (40.6 pixels), where in general both types of profile had good signal to noise.

Wilson models were fit to the artificial cluster data using the GRIDFIT program described in §5.2.3. As for the real clusters, instrumental PSF profiles were convolved with the model profiles before comparison to the data. Unlike the real clusters, however, the background level for the artificial clusters was fixed at zero. For clusters of all sizes, the number count input returned fitted parameters in good agreement with the input parameters. The offsets between input and output parameters are (mean ± standard error) $\Delta W_0 = (W_{0,\text{in}} - W_{0,\text{out}})/W_{0,\text{in}} = 0.06 \pm 0.02$ and $\Delta r_0 = (r_{0,\text{in}} - r_{0,\text{out}})/r_{0,\text{in}} = -0.13 \pm 0.03$ pc. As expected, the larger-N_* clusters return more accurate values, with scatter 2–3 times lower for $N_* = 3000$ than for $N_* = 300$ clusters. Figure 5.10 compares the best-fit and input structural parameters of the simulated clusters for the integrated photometry and hybrid methods. Particularly for clusters with larger input r_0, integrated photometry alone tends to result in overly-large values of W_0 and overly-small values of r_0. For these clusters, the distinction between profiles of different W_0 occurs at a point in the radial profile where the density of stars is too low for the ELLIPSE algorithm to converge. The addition of number count data beyond this point improves the fit, as the figure
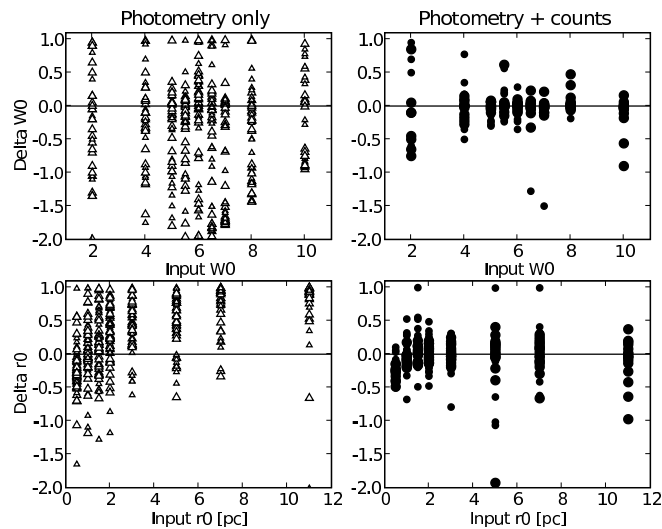
Figure 5.10: Comparison of input and output structural parameters for simulated star clusters. The ouput parameters are derived from fitting Wilson models to surface density profiles derived from simulated HST/WFPC2 images of the clusters. Left: profiles measured with integrated photometry only; right: profiles measured with integrated photometry and number counts; top: difference in central potential $\Delta W_0 = (W_{0,\text{in}} - W_{0,\text{out}})/W_{0,\text{in}}$; bottom: difference in scale radius $\Delta r_0 = (r_{0,\text{in}} - r_{0,\text{out}})/r_{0,\text{in}}$;

shows. For integrated photometry alone, $\Delta W_0 = -0.56 \pm 0.07$ and $\Delta r_0 = 0.24 \pm 0.04$ pc; for the hybrid method, $\Delta W_0 = -0.02 \pm 0.02$ and $\Delta r_0 = -0.05 \pm 0.03$ pc.

When fitting model profiles to cluster data, the correct model family is not not known *a priori*. What happens if artificial 'Wilson' clusters are fit with King models instead? We tried this experiment with our artificial clusters and were surprised to find that, except for a handful of objects, the two model families returned nearly identical χ^2 values: the median fractional difference $(\chi^2_K - \chi^2_W)/\chi^2_W = 0.01$. While the meaning of model parameters such as the scale radius r_0 differs between model families, some derived quantities such as the core and half-light radii (R_c, R_h: see Table 5.4 for description) are directly comparable. Figure 5.11 shows this comparison. There is very good agreement between the two model families in measurements of core radii, and reasonable agreement in measurements of half-light radii. The agreement in R_h is poorer for the largest clusters ($R_h \gtrsim 20$ pc, a larger size than usually seen in real clusters), where the King models return smaller sizes than the Wilson models. This is consistent with the results of McLaughlin & van der Marel (2005) who found that the two model families gave generally consistent results for Milky Way and Magellanic Cloud clusters as long as the radius of the last data point $R_{\text{last}} \gtrsim 5R_h$.

The situation of observational profiles with a limited radial range bears further investigation. The analysis of simulated clusters to this point has not considered the effects of background level fluctuations. The GRIDFIT code is able to fit a constant background level added to the intensity profile, and we verified through simple experiments that input values were correctly recovered. However, the limitations of short exposures and small-number statistics suggest that determining the correct background level—and thus being able to correctly trace cluster profiles out to large projected radii—will be much more difficult for the real cluster data. We therefore experimented with removing points in the profile data beyond $R_{\text{last}} = 1, 2$, and $5R_h$ (where R_h was computed from the input model profile) and fitting both King and Wilson models to the remaining points. As expected, recovery of the input cluster parameters was better for the more extensive profiles, for both model families. For $R_{\text{last}} = 1$, both model families returned R_h values that were, on average, larger than the input. Some model fits were 'catastrophic failures', with $R_h(\text{out}) > 2R_h(\text{in})$; this situation usually occurred for clusters where the number of profile data points was < 10. Interestingly, for all three
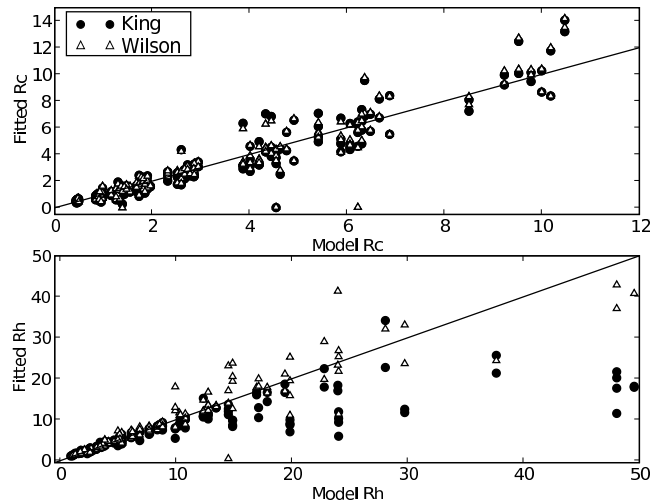
Figure 5.11: Comparison of cluster size measurements for fits of model density profiles to artificial cluster profiles. Top: core radius R_c; bottom: half-light radius R_h; circles: King (1966) model fits; triangles: Wilson (1975) model fits.

values of R_{last}, King model fits had fewer catastrophic failures than Wilson models, and also slightly smaller scatter in the difference between fit and true parameters. Since the primary difference between King and Wilson model profiles is the more extended halo of the latter, this suggests that King models may be a better choice for fitting noisy cluster profiles.

Finally, we considered the issue of comparison between different measurements of star cluster size. While Milky Way globulars and extragalactic clusters are most often characterized with half light or core radii, recent complilations of data for massive young Milky Way clusters (Figer, 2008; Wolff et al., 2007) measure cluster size as the mean or median distance ($\langle R \rangle$ or $\tilde{R}$) of the cluster stars from the geometric centroid. Since these young Milky Way clusters may well not be dynamically relaxed (Goodwin & Bastian, 2006), it may not make sense to fit the same types of dynamical models to them as to old clusters, but it is still desirable to find a way to compare sizes between groups of clusters. Since we know the positions of all stars in our artificial clusters, we can easily compute the statistical measurements of size for our model clusters, and compare them to (model values of) R_c and R_h. $\langle R \rangle$ and $\tilde{R}$ are very well-correlated for all of our model clusters, with a best-fit linear relation $\tilde{R} = 0.67\langle R \rangle - 0.36$. The correlation between $\langle R \rangle$ and R_c is rather poor (unsurprising as R_c depends critically on the exact shape of the cluster profile), but there is a good match between $\langle R \rangle$ and R_h for models which are not too extended ($W_0 \lesssim 6$). Figure 5.12 shows the data and least-squares fits: $\langle R \rangle = 0.77R_h + 0.23$, and $\tilde{R} = 0.53R_h + 0.10$. We conclude that, with some scaling, the mean or median projected separation of stars from a cluster center are reasonable proxies for the half-light radius.
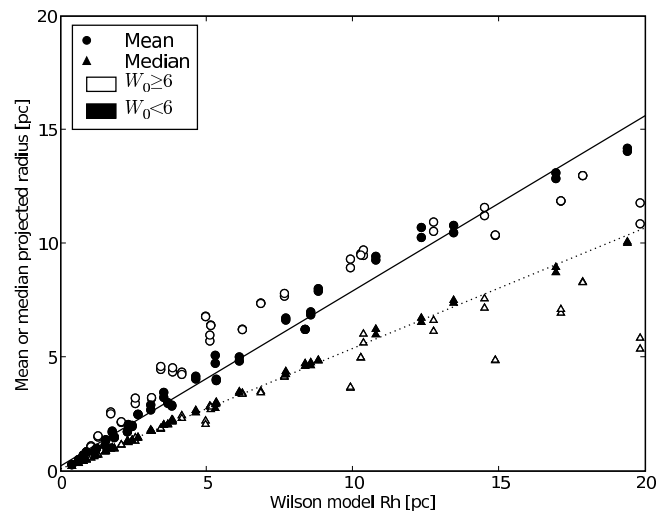
Figure 5.12: Comparison of model half-light radius R_h to mean and median projected radius for artificial clusters. Circles: mean; triangles: median; filled symbols: models with $W_0 < 6$; open symbols: models with $W_0 \geq 6$. Solid line: least-squares fit to filled circles; dotted line: least-squares fit to filled triangles.

Table 5.4. Derived Structural and Photometric Parameters for M31 Young Clusters

Name	Filter	V color [mag]	Model	$\log r_{\rm tid}$ [pc]	$\log R_c$ [pc]	$\log R_h$ [pc]	$\log(R_h/R_c)$	$\log I_0$ [$L_{\odot,V}\,{\rm pc}^{-2}$]	$\log j_0$ [$L_{\odot,V}\,{\rm pc}^{-3}$]	$\log L_V$ [$L_{\odot,V}$]	$V_{\rm tot}$ [mag]	$\log I_h$ [$L_{\odot,V}\,{\rm pc}^{-2}$]
B015D	F450W	-0.114 ± 0.1	K66	$2.33^{+0.06}_{-0.07}$	$-0.065^{+0.106}_{-0.110}$	$1.346^{+0.100}_{-0.120}$	$1.411^{+0.210}_{-0.226}$	$4.16^{+0.07}_{-0.07}$	$3.92^{+0.17}_{-0.17}$	$5.89^{+0.06}_{-0.06}$	$14.59^{+0.15}_{-0.16}$	$2.39^{+0.20}_{-0.16}$
			W	$3.30^{+0.07}_{-0.00}$	$-0.076^{+0.118}_{-0.108}$	$1.746^{+0.061}_{-0.051}$	$1.821^{+0.170}_{-0.169}$	$4.16^{+0.07}_{-0.08}$	$3.93^{+0.17}_{-0.27}$	$6.12^{+0.07}_{-0.05}$	$13.99^{+0.14}_{-0.17}$	$1.83^{+0.08}_{-0.08}$
B015D	F814W	0.457 ± 0.1	K66	$2.05^{+0.03}_{-0.01}$	$-1.178^{+0.196}_{-0.279}$	$1.086^{+0.014}_{-0.001}$	$2.264^{+0.288}_{-0.194}$	$5.33^{+0.28}_{-0.20}$	$6.21^{+0.56}_{-0.39}$	$5.75^{+0.04}_{-0.04}$	$14.93^{+0.10}_{-0.11}$	$2.78^{+0.04}_{-0.04}$
			W	$2.93^{+0.10}_{-0.08}$	$-1.224^{+0.215}_{-0.286}$	$1.312^{+0.053}_{-0.025}$	$2.537^{+0.340}_{-0.240}$	$5.39^{+0.28}_{-0.21}$	$6.31^{+0.57}_{-0.42}$	$5.87^{+0.05}_{-0.05}$	$14.61^{+0.12}_{-0.13}$	$2.45^{+0.05}_{-0.09}$
B040	F450W	-0.029 ± 0.1	K66	$1.88^{+0.02}_{-0.02}$	$-0.393^{+0.047}_{-0.066}$	$0.853^{+0.047}_{-0.045}$	$1.245^{+0.113}_{-0.092}$	$4.40^{+0.06}_{-0.05}$	$4.49^{+0.12}_{-0.09}$	$5.33^{+0.04}_{-0.04}$	$15.98^{+0.10}_{-0.10}$	$2.82^{+0.09}_{-0.09}$
			W	$2.97^{+0.05}_{-0.05}$	$-0.361^{+0.052}_{-0.067}$	$1.292^{+0.022}_{-0.032}$	$1.652^{+0.089}_{-0.084}$	$4.39^{+0.06}_{-0.05}$	$4.54^{+0.04}_{-0.17}$	$5.57^{+0.04}_{-0.04}$	$15.37^{+0.11}_{-0.10}$	$2.19^{+0.06}_{-0.05}$

Note. — Table 5.4 is available in its entirety in the electronic edition of the Journal. A short extract from it is shown here, for guidance regarding its form and content. Column descriptions: r_t: model tidal radius ($\rho(r_t) = 0$); R_c: model projected core radius, at which intensity is half the central value; R_h: model projected half-light, or effective, radius (contains half the total luminosity in projection); R_h/R_c: measure of cluster concentration; I_0: model central luminosity surface density in the V band; j_0: logarithmic central luminosity volume density in the V band; L_V: total integrated model luminosity in the V band; $V_{\rm tot} = 4.83 - 2.5\log(L_V/L_{\odot}) + 5\log(D/10\,{\rm pc})$: total, *extinction-corrected* apparent V-band magnitude; $I_h \equiv L_V/2\pi R_h^2$: V-band luminosity surface density averaged over the half-light radius. Uncertainties are 68% confidence intervals, computed as described in the text.

Table 5.5. Derived Dynamical Parameters for M31 Young Clusters

Name	Filter	Υ_V^{pop} [$M_\odot L_{\odot,V}^{-1}$]	Model	log M_{tot} [$M_\odot$]	log E_b [erg]	log Σ_0 [$M_\odot$ pc^{-2}]	log ρ_0 [$M_\odot$ pc^{-3}]	log Σ_h [$M_\odot$ pc^{-2}]	log $\sigma_{p,0}$ [km s^{-1}]	log $v_{esc,0}$ [km s^{-1}]	log t_{rh} [yr]	log f_0 [$M_\odot$ (pc km s^{-1})$^{-3}$]
B015D	F450W	$0.088^{+0.01}_{-0.01}$	K66	$4.83^{+0.08}_{-0.08}$	$48.82^{+0.09}_{-0.09}$	$3.10^{+0.09}_{-0.09}$	$2.86^{+0.18}_{-0.18}$	$1.34^{+0.21}_{-0.16}$	$0.256^{+0.039}_{-0.042}$	$0.914^{+0.032}_{-0.034}$	$9.91^{+0.17}_{-0.20}$	$0.891^{+0.251}_{-0.242}$
			W	$5.07^{+0.08}_{-0.08}$	$48.91^{+4.13}_{-3.46}$	$3.11^{+0.08}_{-0.09}$	$2.88^{+0.18}_{-0.27}$	$0.78^{+0.09}_{-0.09}$	$0.251^{+0.076}_{-0.043}$	$0.924^{+0.548}_{-0.034}$	$10.61^{+0.12}_{-0.10}$	$0.915^{+0.250}_{-0.351}$
B015D	F814W	$0.088^{+0.01}_{-0.01}$	K66	$4.69^{+0.06}_{-0.07}$	$48.76^{+0.09}_{-0.09}$	$4.28^{+0.28}_{-0.20}$	$5.15^{+0.56}_{-0.39}$	$1.72^{+0.06}_{-0.07}$	$0.286^{+0.031}_{-0.033}$	$1.017^{+0.036}_{-0.036}$	$9.47^{+0.04}_{-0.03}$	$3.096^{+0.561}_{-0.395}$
			W	$4.82^{+0.07}_{-0.07}$	$48.80^{+0.09}_{-0.10}$	$4.33^{+0.29}_{-0.22}$	$5.25^{+0.57}_{-0.43}$	$1.40^{+0.07}_{-0.10}$	$0.290^{+0.031}_{-0.033}$	$1.028^{+0.035}_{-0.036}$	$9.87^{+0.10}_{-0.06}$	$3.184^{+0.578}_{-0.437}$
B040	F450W	$0.094^{+0.01}_{-0.01}$	K66	$4.30^{+0.06}_{-0.06}$	$48.25^{+0.09}_{-0.09}$	$3.38^{+0.07}_{-0.07}$	$3.46^{+0.12}_{-0.10}$	$1.80^{+0.10}_{-0.11}$	$0.229^{+0.031}_{-0.034}$	$0.875^{+0.030}_{-0.032}$	$8.94^{+0.08}_{-0.08}$	$1.570^{+0.148}_{-0.109}$
			W	$4.54^{+0.06}_{-0.06}$	$44.89^{+7.58}_{-0.09}$	$3.36^{+0.07}_{-0.07}$	$3.51^{+0.06}_{-0.18}$	$1.16^{+0.08}_{-0.07}$	$0.198^{+0.087}_{-0.032}$	$0.940^{+0.530}_{-0.062}$	$9.70^{+0.05}_{-0.06}$	$1.604^{+0.050}_{-0.183}$

Note. — Table 5.5 is available in its entirety in the electronic edition of the Journal. A short extract from it is shown here, for guidance regarding its form and content. Column descriptions: $\Upsilon_V^{pop} L_V$: assumed mass-to-light ratio in the V band; $M_{tot} = \Upsilon_V^{pop} L_V$: integrated model mass; $E_b \equiv -(1/2) \int_0^{r_t} 4\pi r^2 \rho \phi \, dr$: integrated binding energy; Σ_0: central surface mass density; ρ_0: central volume density; Σ_h: surface mass density averaged over the half-light radius; $\sigma_{p,0}$: predicted line-of-sight velocity dispersion at cluster center; $v_{esc,0}$: predicted central "escape" velocity; log t_{rh}: two-body relaxation time at model projected half-mass radius; log $f_0 \equiv \log\left[\rho_0/(2\pi\sigma_c^2)^{3/2}\right]$: a measure of the model's central phase-space density or relaxation time. For f_0 in these units, and t_{rc} in years, $\log t_{rc} \simeq 8.28 - \log f_0$ (McLaughlin & van der Marel, 2005). Uncertainties are 68% confidence intervals, computed as described in the text.

6

An HST/WFPC2 survey of bright young clusters in M31. II. Photometry of less luminous clusters in the fields

P. W. Hodge, O. K. Krienke, M. Bellazzini, S. Perina, P. Barmby, J. G. Cohen, T. H. Puzia, & J. Strader

Abstract

We report on the properties of 89 low-mass star clusters located in the vicinity of luminous young clusters ("blue globulars") in the disk of M31. Eighty-two of the clusters are newly detected. We have determined their integrated magnitudes and colors, based on a series of Hubble Space Telescope (HST)/Wide Field Planetary Camera 2 exposures in blue and red (HST filters F450W and F814W). The integrated apparent magnitudes range from F450W = 17.5 to 22.5, and the colors indicate a wide range of ages. Stellar color-magnitude diagrams for all clusters were obtained and those with bright enough stars were fit to theoretical isochrones to provide age estimates. The ages range from 12 Myr to ¿500 Myr. Reddenings, which average E(F450-F814) = 0.59 with a dispersion of 0.21 mag, were derived from the main-sequence fitting for those clusters. Comparison of these ages and integrated colors with single population theoretical models with solar abundances suggests a color offset of 0.085 mag at the ages tested. Estimated ages for the remaining clusters are based on their measured colors. The age-frequency diagram shows a steep decline of number with age, with a large decrease in number per age interval between the youngest and the oldest clusters detected.

6.1 Introduction

This paper reports on the study of open (disk) star clusters in M31 (NGC224) detected on images from the Hubble Space Telescope (HST), obtained as part of a program designed to

determine the nature of 19 luminous star clusters that were originally classified as globular clusters, but which have blue measured colors. The first paper of a series that reports on the results of that program concerns the highly luminous young cluster VdB0 (Perina et al., 2009a). This paper is a survey of less luminous ("open") clusters in M31, similar to those of Krienke & Hodge (2007, hereafter KHI), who reported results from archival images obtained with the Wide Field Planetary Camera 2 (WFPC2), and Krienke & Hodge (2008, hereafter KHII), who reported results from archival images from the Advanced Camera for Surveys (ACS). "Open" or "disk clusters" in M31 have been recognized since Hubble's pioneering work. He identified the cluster subsequently known as VdB0 as an open cluster, as shown in the frontispiece of his book "The Realm of the Nebulae" (Hubble, 1936). Most subsequent studies of such clusters have dealt with the more luminous examples, especially those mistaken for globulars; see an excellent history of the subject of M31's luminous blue clusters in Caldwell et al. (2009). As in Paper I, we adopt a distance modulus for M31 of $(m - M)_0 = 24.47 \pm 0.07$.

6.2 Observations

6.2.1 The Images

The observations, obtained with WFPC2 of the HST, were described in detail in Perina et al. (2009a). The images were obtained with blue (HST F450W) and red (HST F814W) filters, approximately in the traditional B and I bands. Exposures were relatively short (2×400 seconds per filter). The scale of the WF fields is 0.099 arcsec pixel^{-1} and for the PC fields it is 0.045 arcsec pixel^{-1}. While the main program dealt with the bright globular-like clusters on the PC images, we searched both the PC and the WF images, identifying star clusters, measuring their integrated properties, and carrying out stellar photometry of their member stars. Figure 6.1, in a color version produced by one of us (T.P.), reproduces a sample WF field showing several open clusters. The total area covered by the survey is 48.1 $arcmin^2$.

6.2.2 Cluster Identification

The clusters included in the survey range from large, very luminous clusters to small objects that are barely resolved in our rather short exposures. The brightest disk clusters in this sample have absolute magnitudes of $M(F450)_0 = -8$, while we were able to identify a few clusters as faint as $M(F450)_0 = -2.5$. Thus our brightest clusters are equivalent to the mean absolute magnitudes of M31's globular clusters (though bluer and less massive), while our faintest are fainter than the faint limit of most cluster catalogs for nearby galaxies. The disk of M31 presents a dense star field, in which low-density star clusters are difficult to detect even with special statistical techniques. For that reason we chose to select only conspicuous objects for which there would be little or no question of their being physical clusters (see examples in Figure 6.2). Our cluster identification criteria included (1) a conspicuous spatial concentration, (2) a centrally peaked radial distribution, (3) detectability in both colors, (4) recognition of more than four well-resolved stars above an unresolved background, (5) a normal luminosity distribution (number increasing with magnitude), and (6) a color-magnitude diagram that shows a distribution different from that of the background.

Two of the authors (P.H. and O.K.K.) searched the frames independently in both colors, varying brightness and contrast. We categorized objects as definitely clusters or as candidates, and for borderline cases, we met, discussed images, and reached agreement.

As a final test, we asked each other whether we could defend an object against being classed as an asterism, background galaxy, or other type of noncluster. Figure 6.2 provides F450 images of 12 of the clusters.

Figure 6.1: A sample WF image, containing several recognizable star clusters. This figure demonstrates how clusters are distinguished by their resolution, high stellar density, and blue color, compared to the background of the M31 disk stars.
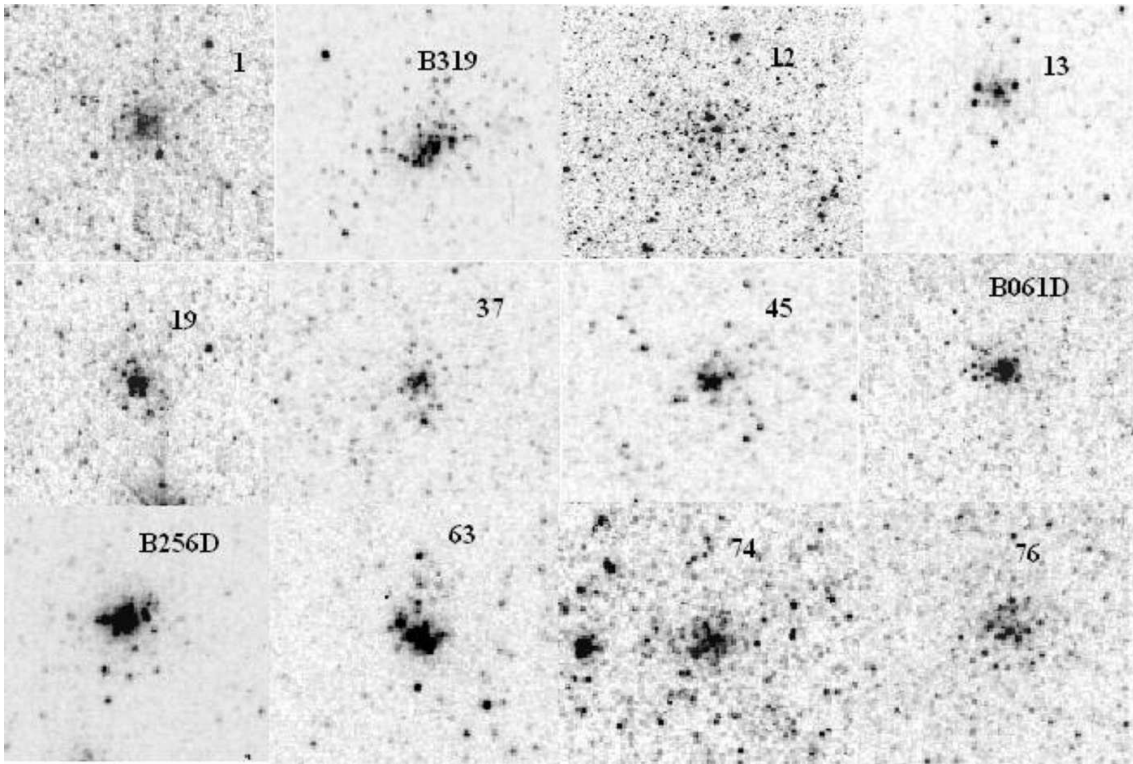
Figure 6.2: Images of 12 of the brightest clusters in the sample. Each small field is 7 arcsec on a side, except for cluster 12, for which the sides are 14 arcsec. The images are from the F450W filter and the WF camera.

6.3 Data Reduction

6.3.1 Integrated Photometry

We determined integrated magnitudes and colors of the clusters using a photometric program written by Krienke in IDL and described in detail in KHI. Magnitudes in the HST photometric system were calibrated according to the results of Holtzman et al. (1995). The program determines the cluster properties within a contour chosen to include most of the light, but omitting any bright foreground stars. The critical feature of the photometry is determining the background surface brightness (the "sky"). Because many of the clusters have both a low surface brightness and a significant size, the M31 background is often a significant fraction of the measured signal. Our program measures a probable background level and determines the uncertainty of it by sampling several (10-24) similarly dimensioned fields on the image. These data are refined by Chauvenet criteria, rejecting samples with less than 0.02 probability of belonging to the set. The average of the remaining values of the background is then flux subtracted from the total flux within the cluster contour. The correction to the magnitudes due to the background subtraction was usually several tenths of a magnitude, but in some cases, where the cluster surface brightness was especially faint compared to the background, it reached values as large as 2 mag (see Figure 6.3). Clearly, the background correction is an important element in this photometry and it is essential that it and its uncertainty be evaluated carefully. The photometric uncertainties provided in Figure 6.4 and Table 1 include that of the background, which, in some cases, dominates the uncertainty.

120
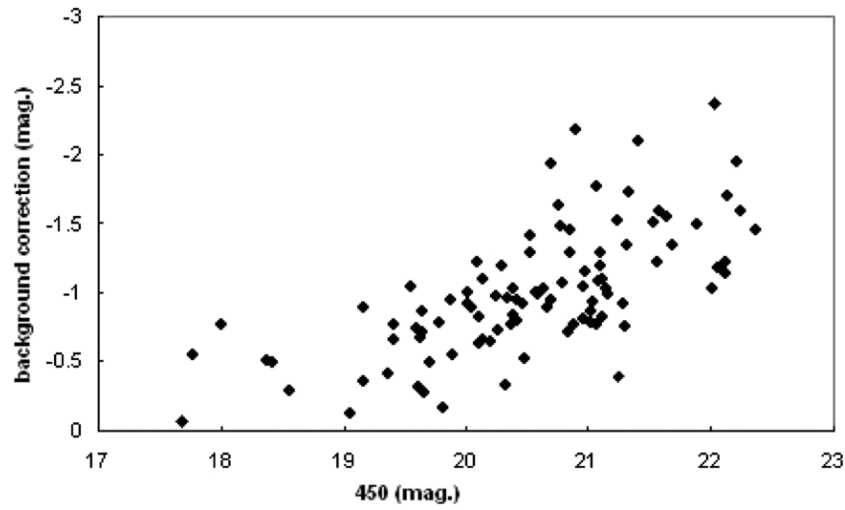
Figure 6.3: Background corrections plotted against the corrected integrated F450 magnitudes of the clusters. Magnitudes are not reddening-adjusted.
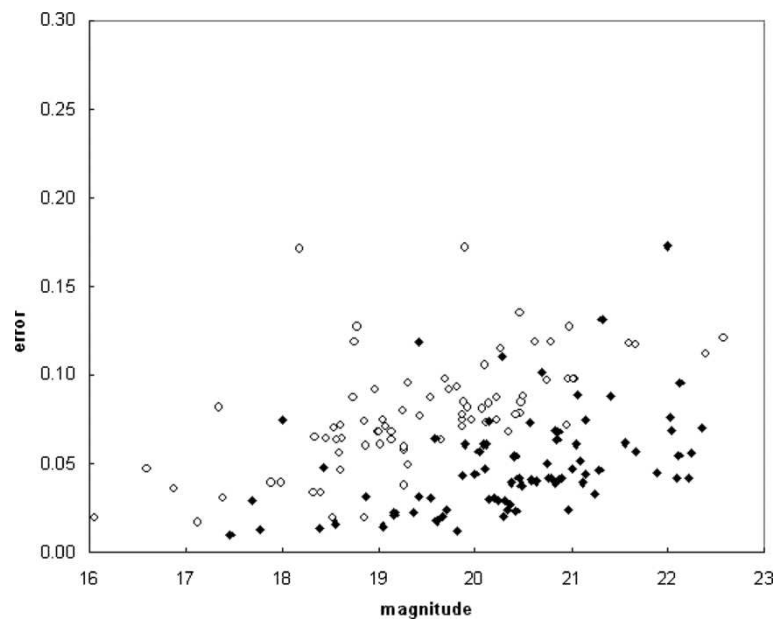
Figure 6.4: Photometric errors derived from the measurements of the integrated magnitudes, uncorrected for reddening. Filled symbols are for the F450 data and open symbols are for the F814 data.

Table 6.1: Star Clusters of the Survey

Name	R.A. (J2000)	Decl. (J2000)	F450	Err	F450-F814	Err	Notes
KHM31-22	9.99416	40.59044	20.36	0.03	1.38	0.07	
1	10.00226	40.59630	20.00	0.04	1.48	0.05	
B319	10.01277	40.56638	17.77	0.01	0.89	0.04	
WH	10.03147	40.58568	20.75	0.05	0.64	0.09	
2	10.05996	40.47970	21.10	0.05	0.11	0.12	*y
3	10.06724	40.46574	20.87	0.07	0.72	0.11	y
4	10.07673	40.46278	20.23	0.03	0.93	0.06	y
5	10.08475	40.47733	21.29	0.05	0.81	0.10	y
6	10.09359	40.46366	22.10	0.04	0.50	0.13	y
7	10.10565	40.61191	21.23	0.13	-1.01	0.18	*y
8	10.12093	40.60816	20.31	0.03	0.67	0.07	y
9	10.12172	40.62505	20.68	0.08	0.30	0.13	*y
10	10.12880	40.62470	20.26	0.04	0.01	0.11	*y
11	10.13828	40.61543	21.08	0.10	1.06	0.15	
12	10.14448	40.61308	18.00	0.08	1.42	0.09	y
13	10.15506	40.65390	19.36	0.02	1.47	0.05	y
14	10.15727	40.66958	20.83	0.04	1.71	0.06	y
15	10.17087	40.65345	20.96	0.06	0.74	0.11	*
B014D	10.25410	41.10937	19.60	0.02	1.63	0.04	
16	10.25739	41.12103	21.01	0.05	1.14	0.09	y
17	10.26360	41.11692	21.11	0.04	1.15	0.08	
18	10.27091	41.11649	20.42	0.02	1.16	0.04	y
19	10.27805	41.12904	19.41	0.12	1.23	0.21	y
20	10.31100	41.11747	22.03	0.08	1.23	0.14	y
21	10.32247	41.11345	20.69	0.10	1.95	0.16	y
22	10.32486	41.10686	21.40	0.09	1.18	0.12	y
23	10.32638	41.09547	21.88	0.05	1.60	0.10	
24	10.40369	40.72710	21.31	0.04	-0.36	0.12	*y
25	10.40514	40.68031	20.56	0.07	1.42	0.10	y
26	10.41120	40.73322	18.55	0.02	0.21	0.07	*y
27	10.41445	40.67577	19.81	0.01	1.11	0.03	y
28	10.41904	40.72756	21.63	0.03	-0.95	0.12	*y
29	10.42279	40.66916	20.19	0.03	0.92	0.07	y
30	10.42782	40.71453	19.66	0.02	0.69	0.07	y
31	10.43303	40.71460	21.08	0.04	0.12	0.11	*
32	10.43314	40.71762	21.09	0.05	1.22	0.09	y
33	10.43358	40.71122	20.89	0.04	2.04	0.09	
34	10.43870	40.72325	20.38	0.04	1.33	0.08	y
35	10.44996	40.71653	20.79	0.04	0.70	0.11	y
36	10.45031	40.69453	21.05	0.06	0.59	0.10	y
37	10.45168	40.69946	19.16	0.02	0.38	0.07	y
38	10.45521	40.72142	20.66	0.04	0.27	0.10	*y
39	10.45635	40.73367	21.08	0.26			y
40	10.46038	40.70244	20.58	0.04	0.69	0.09	y
41	10.51435	40.76969	20.14	0.03	1.53	0.08	
42	10.51689	40.74818	21.25	0.03	0.82	0.09	y
43	10.52399	40.77104	21.15	0.04	1.22	0.09	y
44	10.52901	40.76606	20.84	0.07	1.58	0.09	y
45	10.52987	40.76940	19.17	0.02	0.71	0.07	y
46	10.53052	40.77541	20.95	0.04	0.37	0.10	*y

Table 6.1: continued.

Name	R.A. (J2000)	Decl. (J2000)	F450	Err	F450-F814	Err	Notes
47	10.53562	40.77516	19.70	0.02	0.71	0.07	y
48	10.55479	40.82819	20.63	0.04	1.20	0.09	
49	10.57024	40.81240	20.76	0.04	1.22	0.10	y
50	10.57764	40.81500	22.11	0.06	1.08	0.11	
51	10.57851	40.81922	19.89	0.06	1.35	0.09	
B061D	10.63578	41.36173	19.41	0.03	0.67	0.09	*
52	11.10224	41.25305	20.34	0.02	1.73	0.05	
53	11.11621	41.23792	20.96	0.02	2.11	0.03	
54	11.12238	41.23356	22.21	0.04	1.86	0.08	
55	11.22630	41.88489	21.28	0.04	0.19	0.10	*
56	11.23180	41.91120	20.29	0.02	0.92	0.04	
57	11.23438	41.89684	22.04	0.07	2.31	0.12	
58	11.23474	41.89572	20.11	0.06	1.15	0.11	y
59	11.23536	41.88171	20.45	0.04	2.06	0.05	
60	11.23619	41.91635	20.41	0.05	1.80	0.08	
61	11.24062	41.89716	22.12	0.10	1.38	0.14	y
B256D	11.24448	41.91018	17.57	0.02	1.58	0.03	
62	11.24560	41.89819	20.09	0.06	0.84	0.10	y
63	11.24637	41.91047	19.05	0.02	1.93	0.02	
64	11.24650	41.91050	18.87	0.03	1.88	0.05	
65	11.24744	41.89167	21.55	0.07	-0.84	0.13	*y
66	11.24854	41.90391	20.21	0.09	1.43	0.12	y
67	11.24969	41.93580	20.85	0.06	0.78	0.10	y
68	11.24973	41.90117	21.32	0.13	1.06	0.17	y
69	11.25109	41.90682	21.06	0.09	1.17	0.19	y
70	11.25216	41.88646	20.48	0.04	1.17	0.10	y
71	11.25366	41.88541	19.87	0.04	0.85	0.08	y
72	11.25606	41.89460	21.76	0.13	0.76	0.17	
73	11.25914	41.91537	19.97	0.04	1.31	0.07	
74	11.26204	41.89759	20.52	0.09	0.67	0.12	y*
75	11.26219	41.90101	20.38	0.08	-0.08	0.16	*y
76	11.26942	41.89441	20.02	0.06	1.03	0.11	
77	11.28053	41.90742	21.67	0.06	0.83	0.11	y
78	11.28957	41.91235	21.56	0.06	0.61	0.10	y
79	11.29089	41.91942	20.10	0.05	1.50	0.07	y
80	11.43302	41.72510	19.63	0.03	0.55	0.08	y
81	11.45692	41.71174	22.35	0.07	1.85	0.11	
82	11.45853	41.70832	22.23	0.06	1.61	0.13	
DA084	11.46799	41.71365	19.59	0.06	0.81	0.14	

Notes. Objects with asterisks have uncertain colors because of a low ratio of signal to galaxy background in the F814W image. Objects with "y" have CMDs indicating young ages, less than $\sim 5 \times 10^8$ years.

6.3.2 Stellar Photometry

We carried out two independent programs of stellar photometry of the clusters. In one case, all of the WFPC2 images of each field were measured at Bologna as part of the luminous young clusters program. The details of that photometry are given in Paper I (Perina et al., 2009a). For this paper we have extracted from the Bologna database the magnitudes and colors of stars within our outline of a cluster's boundary. Following the practice of Perina et al. (2009a), we provide HST Vega magnitudes as measured in the two filters, which we refer to in the following as "F450" and "F814." A second photometric program was carried out in Seattle using a program developed by one of us (O.K.K.), based on DAOPHOT (Stetson,

1987) and written within IDL. It was adjusted to allow us to measure stars in the more crowded central areas of clusters, where there are often bright stars, frequently including the brightest main-sequence stars in the cluster. Without at least approximate photometry of these stars, we would be missing important information about the ages of the clusters. Zero points were adopted from Holtzman et al. (1995). PSFs were derived from several bright, well-separated stars in the field. A comparison of the magnitudes and colors of the two sets of photometry showed good agreement. We identified stars in common by using both magnitudes and positions, finding that most bright stars were easily identified, while for the faintest stars there was sometimes an ambiguity. For stars with F450 magnitudes brighter than 23.0 the mean differences (Bologna-Seattle) were -0.12±0.05 mag in F450 and -0.13±0.11 mag in F814. At fainter magnitudes, where the photometry is strongly affected by crowding and by the short exposures of the images, the dispersion is larger. We have adjusted the Seattle photometry to the Bologna system by using the above offsets.

6.4 Properties of the clusters

6.4.1 The Cluster Catalog

Table 1 provides the positions, integrated magnitudes, and integrated colors of the clusters. Five of the clusters were found to have been identified previously according to the Revised Bologna Catalog of M31 Globular Clusters (Galleti et al. 2004, hereafter RBC). One of them, DAO84, was identified as a possible galaxy by Caldwell et al. (2009), but our images show a clearly defined star cluster. Additionally, one coincides with an open cluster identified in KHI and one to a cluster discovered by Williams & Hodge (2001a). Only two of the previously identified clusters, B319 and KH22, had published magnitudes in B and only B319 had previously published magnitudes in both B and I. We transformed our magnitudes to Johnson-Cousins B and I for comparison. The average difference (previous - this paper) in B was found to be 0.16 mag. and the difference in I is 0.18 mag. As a ground-based check on the HST photometry, one of us (J.S.) determined the integrated magnitudes and colors of 16 of the brighter clusters from the SDSS database. Measures were obtained in the SDSS system (u, g, r, i, z) and transformed to B and I in the J-C system. All measures used a circular aperture with a radius of 4 arcsec. The measures produced data that agreed fairly well with mean differences (CfA-Seattle) of ΔB = -0.24±0.39 and $\Delta(B-I)$ = 0.23±0.14. Experiments with HST photometry using a 4 arcsec aperture indicated that the differences are probably caused at least partly by nearby bright stars that were avoided by the original HST photometry, which used smaller apertures.

6.4.2 The Integrated Cluster Color-Magnitude Diagram

Figure 6.5 shows the color-magnitude diagram (hereafter CMD) of the present sample (we include in this diagram and in Figure 6.6 two clusters from the main target program, which were found serendipitously on the WF frames). It closely resembles the two diagrams published for similar samples of M31 clusters by KHI and KHII, though with different filter pairs. The mean absolute magnitude for the cluster sample plotted is $M(F450)_0$ = -4.59 and the mean unreddened color is $(F450 - F814)_0$ = 0.67.

The clusters are nearly uniformly distributed over the diagram, but with a mild concentration at about F450 = 21 and F450 - F814 = 1. For reference, a cluster with observed values of F450 = 21.0 and F450 - F814 = 1.0 will have an age of about 70 Myr and a mass of 450 solar masses, assuming a Salpeter stellar luminosity function and Girardi (2006) population models. But note that the age-color diagram is multivalued at these colors (see Section 5.2).

The mean size of the isophotal radii of all clusters was 1.61 arcsec (6.12 pc).
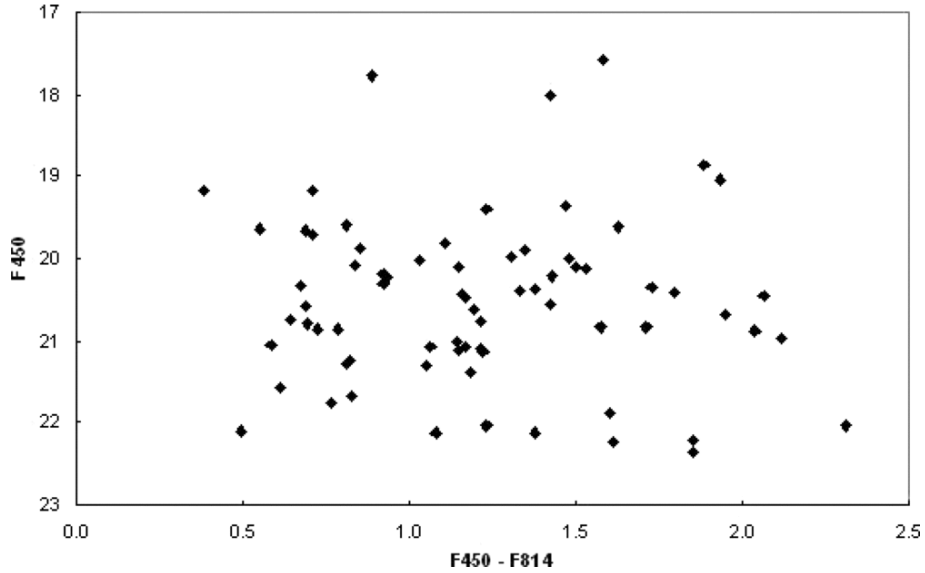
Figure 6.5: CMD for the integrated colors and magnitudes of clusters in this survey. The plot shows observed values, before corrections for reddening.
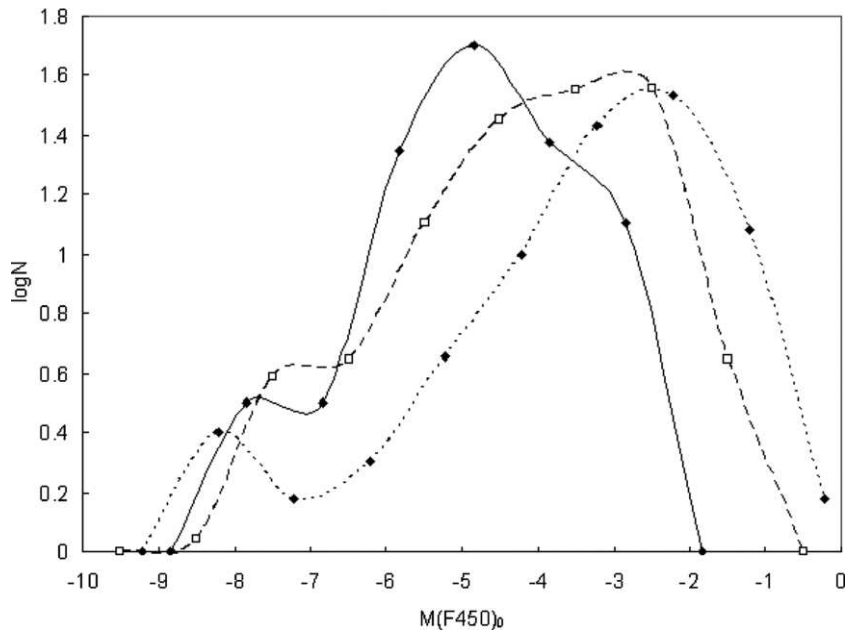
Figure 6.6: Luminosity function for the clusters of this survey (solid line) compared to that of KHI (dotted line) and KHII (dashed line). The latter two are normalized to the total number of clusters in the present survey.

Table 6.2: Characteristics of Cluster CMDs with Well Defined Main Sequences.

Cluster no.	log age (yrs)	Uncertainty	E(F450-F814)	Uncertainty
KH22	7.6	0.35	0.4	0.15
B319	7.6	0.5	0.5	0.25
3	7.5	0.45	0.8	0.2
5	8.0	0.6	0.5	0.3
8	7.5	0.35	0.55	0.2
11	7.3	0.6	0.5	0.2
12	7.6	0.6	0.55	0.25
13	7.1	0.5	0.85	0.8
18	7.1	0.35	0.5	0.2
34	8	0.45	0.65	0.25
37	7.9	0.35	0.5	0.25
45	7.8	0.3	0.5	0.15
B061D	7.8	0.6	0.5	0.15
58	7.6	0.2	0.8	0.15
62	8.0	0.2	0.25	0.15
68	7.8	0.3	0.82	0.15
74	8.1	0.3	0.65	0.15
75	7.8	0.5	0.5	0.25
80	7.1	0.45	0.75	0.15

6.4.3 The Integrated Cluster Luminosity Function

The luminosity function of the clusters is shown in Figure 6.6, where the magnitudes are corrected for extinction, assuming a mean reddening of F450-F814 of 0.51 (see Section 6). The shape of the luminosity function is approximately Gaussian, with a maximum at M(F450)(0) = -4.2. All three samples show an enhanced frequency at the bright end, compared to a symmetrical curve. Artificial cluster tests on the WFPC2 HST images in KHI indicated that much of the turn-down at faint magnitudes results from detection limits. It is not yet clear what the shape of the true luminosity function is at such faint limits. While KHI suggested that the luminosity function may continue to rise, at least to M(F450) = -1, similar HST searches for faint clusters in the SMC have produced contrary results (Rafelski&Zaritsky, 2005). In any case, the luminosity function at the faint end is a complicated product of selection effects, evolutionary fading rates and dynamical disruption (Hunter et al., 2003).

6.4.4 Individual Cluster CMDs

As described in Section 3.2, we measured stellar CMDs for all clusters. Most diagrams looked reasonable, but not all of the clusters were well enough resolved to allow meaningful interpretation. Especially for the faintest clusters, the number of stars on the F814 frame was often quite small, on the order of 5-10.

Figures 6.7 and 6.8 show the CMDs for 10 clusters for which the CMDs show a well defined main sequence. These clusters show a main sequence with F450-F814 near 0.5 and with the tip of the main sequence in the range with F450 magnitudes = 20 to 24. The CMDs in Figures 6.7 and 6.8 have been adjusted for reddening (see Section 5.1).

Table 2 lists the clusters for which it was possible to determine age and reddening by comparison with the Girardi models. The quoted uncertainties indicate the extreme limits of acceptable fits judged by eye.
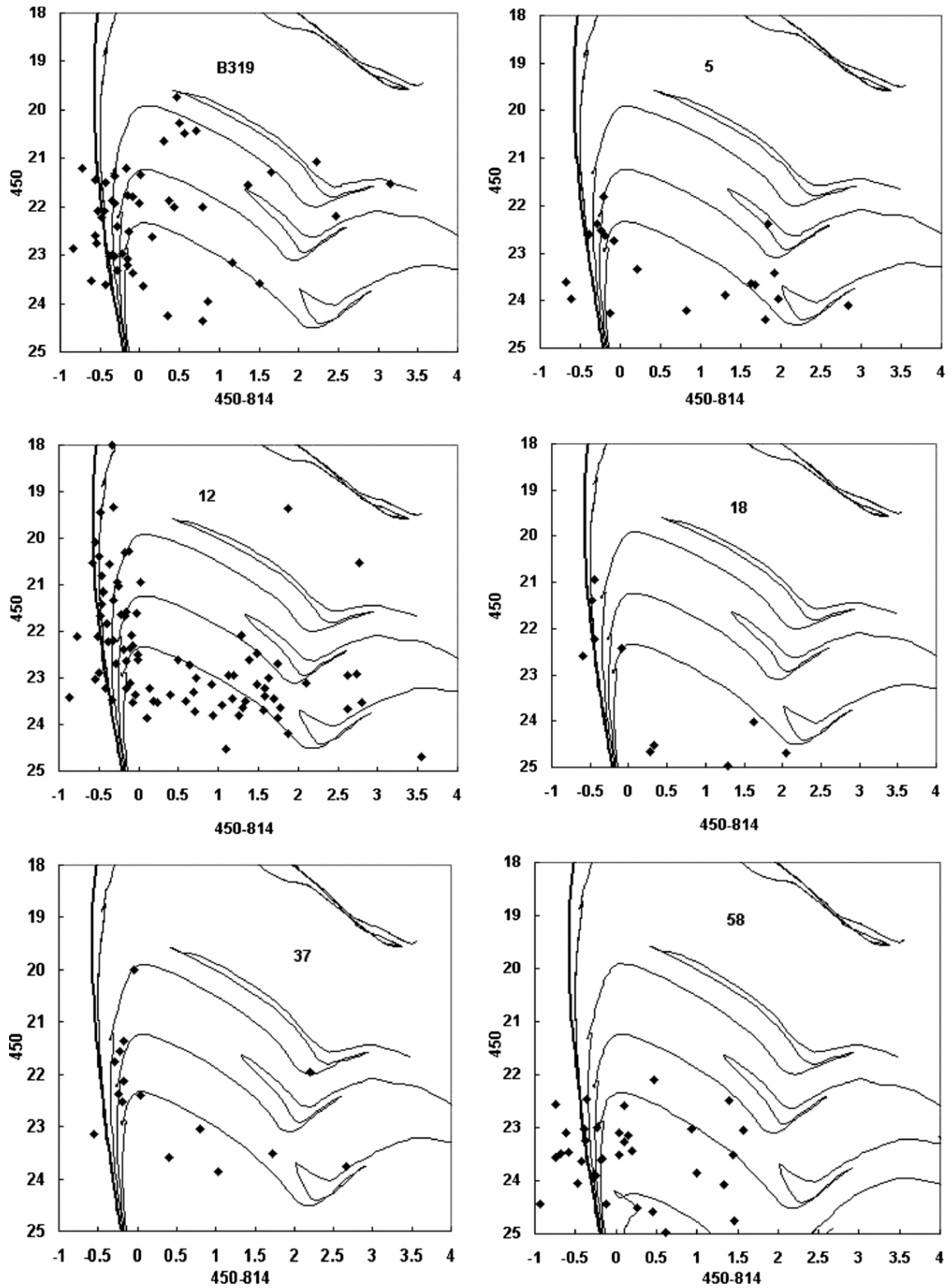
Figure 6.7: CMDs for 6 young clusters with well defined main sequences, fitted by eye to Girardi (2006) isochrones for solar abundance and ages with log(age) of 7.0, 7.6, 8.0, 8.25, and 8.7 years.
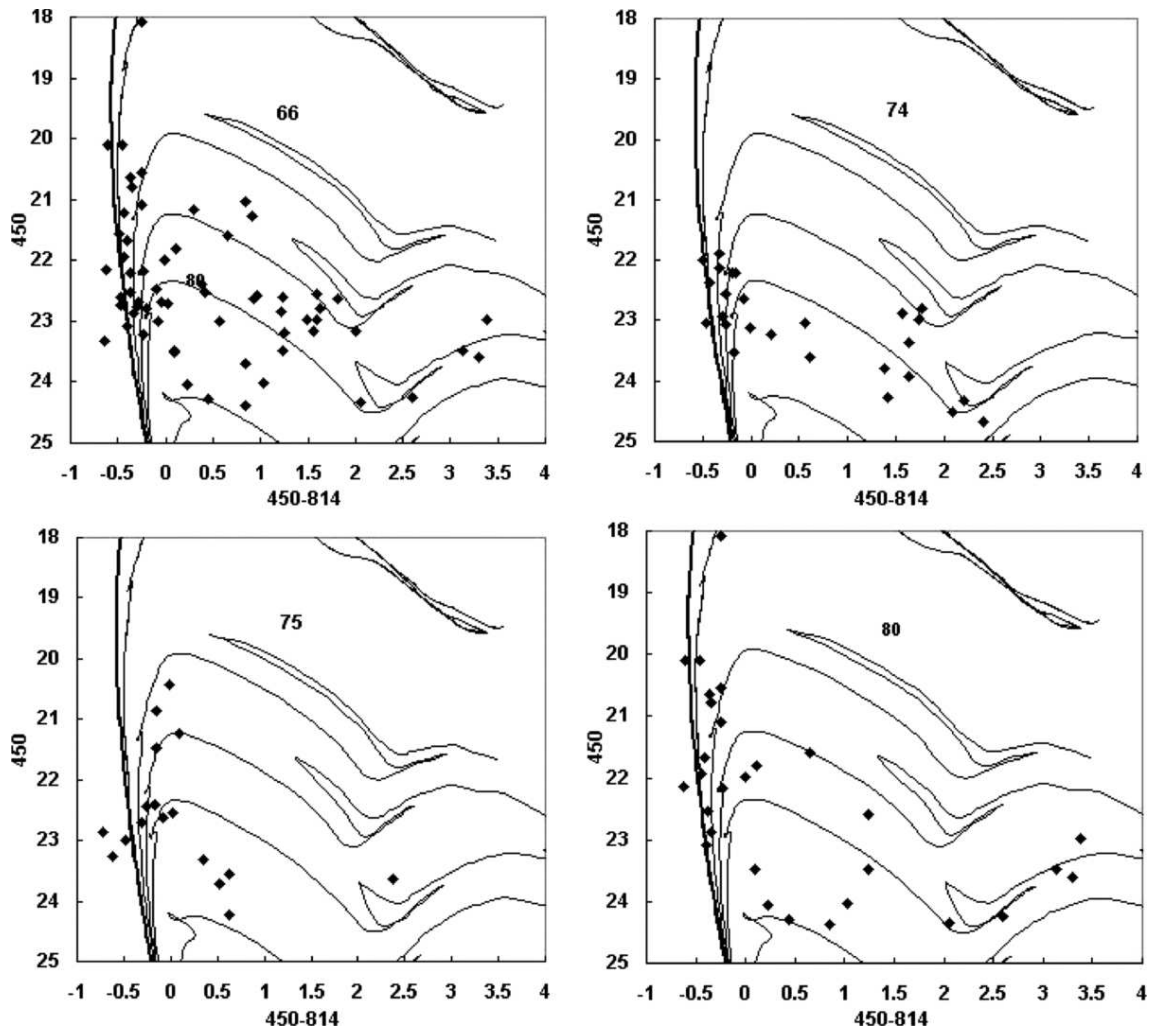
Figure 6.8: CMDs for other 4 young clusters with well defined main sequences, fitted by eye to Girardi (2006) isochrones for solar abundance and ages with log(age) of 7.0, 7.6, 8.0, 8.25, and 8.7 years.

One of the clusters, B319 (also known as G44) has been studied previously using other HST images (Williams & Hodge, 2001a). The present CMD is shallower and it covers only the central region of B319, but the two CMDs are morphologically similar. We cannot usefully make detailed comparisons because the Williams & Hodge data were taken with different filters (F 336W, F439W, and F555W).

A careful inspection of the CMDs of the clusters and their surrounding fields shows that the degree of contamination of the cluster MS by field stars is negligibly low and does not affect our estimates of age and reddening.

6.5 Ages and reddenimgs

6.5.1 From the CMDs

For clusters with a sufficiently well-defined sequences of stars, especially young clusters with narrow main sequences, it was possible to determine approximate reddenings and ages. Based on the case for VdB0 (Perina et al., 2009a), we assumed that these young clusters are characterized by solar abundances. We compared the observations with evolutionary model isochrones made available from the Padua Web page (Girardi, 2006) and determined the offset by eye, providing approximate values of age and reddening (Table 3). Because of the faintness of the magnitudes, the crowding and the sparseness of the CMDs, these values have fairly large uncertainties, as quoted in the table. Within the accuracy of the fitting and if our assumption of solar abundances is correct, the fits provide individual reddenings for the selected clusters, which range from E(F450-F814) = 0.25 to 0.85, with a mean uncertainty of 0.23. The average reddening for this sample is 0.59 with a standard deviation of 0.21 mag. Selection effects, of course, severely limit our sample of clusters with bright main sequences to the youngest clusters in the sample; most are younger than 200 million years.

For the remaining clusters in the sample, the CMDs are difficult to interpret in terms of ages and reddenings except in approximate terms. Table 1 notes those clusters that have significant numbers of stars in the blue section of their CMDs to indicate that they are younger than a few times 10^8 years. Most of the remaining clusters are older, as is also indicated by their integrated colors.

6.5.2 From the Integrated Cluster Photometry

Integrated colors of open clusters can be used to estimate cluster ages by comparison with theoretical models. There are a number of problems with this procedure in our case:

1. The colors are intrinsically uncertain because of the spatially variable brightness and color of the M31 background, which is the major source of the photometric uncertainty.

2. The theoretical models show a dependence on the elemental abundances, which are unknown.

3. For young small-mass clusters, the colors depend on small number statistics in the presence or absence of the most luminous blue stars or a few red giants (see Frogel et al. 1983 and Cervino&Luridiana 2004 for quantitative treatments of this problem).

4. Different theoretical models, even for the same abundances, give different relationships for the age-color diagram.

5. For the colors used in this program (F450 and F814), the change with color for young clusters ($< 2 \times 10^8$ yr) is multivalued for some regimes and is generally smaller than the measurement uncertainties (Figure 6.9).

In spite of these difficulties, it is possible to estimate approximate ages from the colors and, for the younger clusters, the average reddening. Figure 6.9 shows the colors of the clusters with well defined main sequences compared to the theoretical colors for single-age populations with solar abundances (Girardi, 2006). The colors plotted are the measured

Table 6.3: Ages for Older Clusters Based on Integrated Colors.

Name	log age (yrs)
1	8.63
14	8.77
B014D	8.72
16	8.29
17	8.30
19	8.38
20	8.38
21	8.94
22	8.33
23	8.70
25	8.56
27	8.25
32	8.37
33	8.97
34	8.50
41	8.64
43	8.37
44	8.68
48	8.37
49	8.38
50	8.22
51	8.50
52	8.79
53	9.04
54	8.87
57	9.22
59	8.99
60	8.84
61	8.53
B256D	8.68
63	8.92
64	8.88
66	8.57
69	8.32
70	8.32
73	8.46
76	8.15
79	8.63
81	8.87
82	8.71
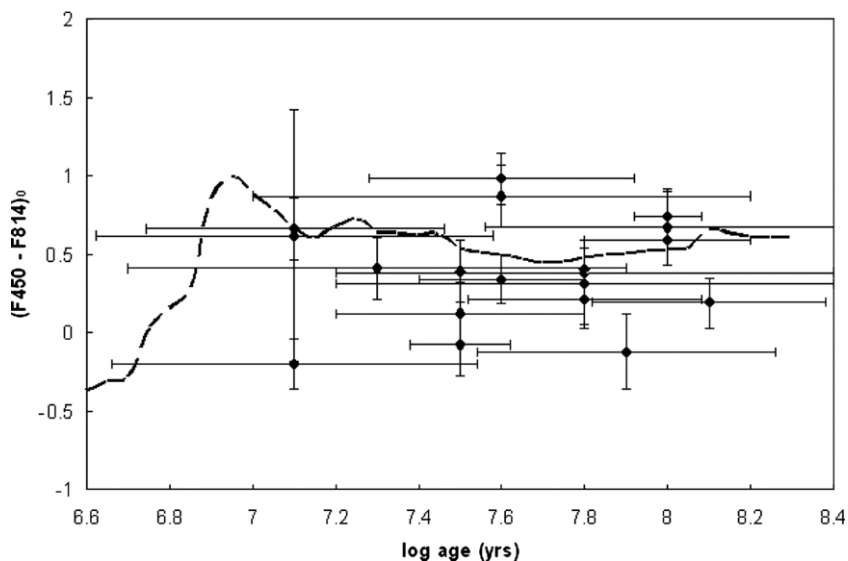
Figure 6.9: Ages and reddening-corrected colors determined from MS fitting compared to the theoretical age-color relationship for young clusters (Girardi, 2006).

colors corrected for reddening and the reddening and ages are those determined from main-sequence fitting. The colors cluster close to the theoretical distribution but are clearly offset to the blue. This may be due to abundances that are different from our assumption of solar abundance ratios. Alternatively, if we assume the offset to be due to overestimation of reddening, then the best fit to the models is for a mean reddening 0.085 mag smaller than derived from the MS fitting, and gives a mean reddening of E(F450-F814) = 0.50 (this corresponds to E(B-V)~ 0.25). For our complete sample we adopt this value for the mean reddening.

For ages of clusters older than ~ 300 million years the theoretical curve is single-valued and fairly sensitive to the measured colors. Because of our shallow exposures, it is not possible to derive ages from CMDs for these clusters, but we can estimate ages from colors, if we assume a mean reddening and a particular model set and abundance. Table 3 provides approximate ages for the clusters with colors redder than (F450-F814) = 1.0. These data are calculated with a mean reddening of E(F450-F814) = 0.50 and use the models provided by Girardi (2006). Formal errors of the colors correspond to approximately an uncertainty of 0.10 in log age, but the true uncertainties of the ages are considered to be much larger, for the reasons outlined at the beginning of this section. The reddest clusters in the sample have reddening-corrected colors of F450-F814 = ~ 1.8, which corresponds to an age of approximately 1.5×10^9 years.

6.5.3 The Age Distribution

We have suggested above that the CMD of integrated magnitudes (Figure 6.5) indicates that the clusters are not distributed uniformly in age. To examine the age distribution we have combined the age data for the young clusters based on main-sequence fitting with that for older clusters based on colors. Figure 6.10 shows the distribution for our sample of 82 clusters. The number falls off rapidly with age, approximately exponentially. A least-squares linear fit gives

$$\log(N) = -1.625 \log(t) + 11.676.$$

Also shown in Figure 6.10 is a similar curve for the clusters in KHI, where the number has been normalized to adjust for that survey's larger sampling area. The two agree within their errors, though there is a suggestion of a small difference in slope, which is possibly caused by
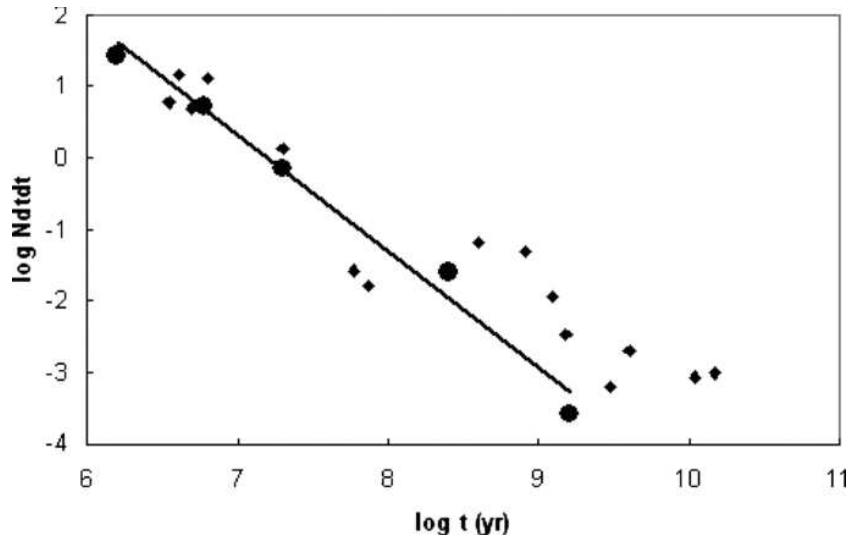
Figure 6.10: Age distribution for the clusters in this survey (large circles) compared to that reported in KHI (diamonds). The line is a least-squares linear fit to this paper's data.

the shallower exposure times of the present survey, which probably missed a larger fraction of older clusters.

As discussed briefly in KHI and in a large and diverse recent literature, these kinds of data are useful for determining the survival rate of clusters in a galaxy's gravitational field (e.g., Kruijssen&Lamers 2008; Gieles et al. 2006; Chandar et al. 2006; Lamers & Gieles 2006 and many others). Before such use can be made of the data, however, it is necessary to know both the rate of evolutionary fading of the clusters and the detection efficiency of the survey. We note that the fading rate is dependent on the abundances, which are unknown, and the detection efficiency is dependent on the exposure times, on the structural properties of the clusters and on the background surface brightness and its variability. To determine the detection efficiency for a collection of such faint and varied clusters would require a much larger sample, as each of the determining factors would need to be explored. In view of these difficulties, we believe that the current survey is not appropriate for deriving a tidal destruction rate for M31 clusters.

6.6 Summary

This paper supplements the HST/WFPC2 Survey of Luminous Young Clusters in M31, which examines the nature of 19 globular-like objects that are anomalously blue. Our search for other, less luminous clusters on the images has produced a catalog of 89 clusters, 82 of which are newly identified.

We have obtained integrated magnitudes and colors of the clusters and have measured CMDs for their resolved stars. The absolute magnitudes of the clusters range from M(F450) = -8 to -2.5 and their colors indicate a large range of ages, from a few million to a few times 10^9 years. The richest young clusters have well-defined main sequences that have been fitted to theoretical isochrones, providing ages ranging from approximately 12 million to 100 million years. The CMDs of these clusters indicate reddenings averaging E(F450-F814) = 0.59, with a dispersion of 0.21 mag, while a comparison of integrated colors of a larger sample of the young clusters with theoretical population models indicates a somewhat smaller average reddening of 0.50 mag. We derive a cluster luminosity function that shows a peak value of $M(F450)^0$ of -4.2 and which extends from values of -9 to -2. The least luminous clusters are among the faintest measured for clusters in LG galaxies. There is a suggestion of a small number of anomalously luminous clusters at the bright end of the luminosity function. The distribution

of the number of detected clusters with age shows a very steep gradient.

HST/ACS colour-magnitude diagrams of M31 globular clusters[1]

S. Perina, L. Federici, M. Bellazzini, C. Cacciari, F. Fusi Pecci, & S. Galleti

Abstract

With the aim of increasing the sample of M31 clusters for which a colour-magnitude diagram is available, we searched the HST archive for ACS images containing objects included in the Revised Bologna Catalogue of M31 globular clusters [2].

Sixty-three such objects were found. We used the ACS images to confirm or revise their classification and were able to obtain useful CMDs for 11 old globular clusters and 6 luminous young clusters. We obtained simultaneous estimates of the distance, reddening, and metallicity of old clusters by comparing their observed field-decontaminated CMDs with a grid of template clusters of the Milky Way. We estimated the age of the young clusters by fitting with theoretical isochrones.

For the old clusters, we found metallicities in the range $-0.4 \leq$[Fe/H]≤ -1.9. The individual estimates generally agree with existing spectroscopic estimates. At least four of them display a clear blue horizontal branch, indicating ages $\gtrsim 10$ Gyr. All six candidate young clusters are found to have ages < 1 Gyr. The photometry of the clusters is made publicly available through a dedicated web page.

With the present work the total number of M31 GCs with reliable optical CMD increases from 35 to 44 for the old clusters, and from 7 to 11 for the young ones. The old clusters show similar characteristics to those of the MW. We discuss the case of the cluster B407, with a metallicity [Fe/H]$\simeq -0.6$ and located at a large projected distance from the centre of M31 (R_p = 19.8 kpc) and from the major axis of the galaxy (Y= 11.3 kpc). Metal-rich globulars at large galactocentric distances are rare both in M31 and in the Milky Way. B407, in addition, has a velocity in stark contrast with the rotation pattern shared by the bulk of M31 clusters

---

[1]Based on observations made with the NASA/ESA *Hubble Space Telescope*, obtained from the data archive at the Space Telescope Science Institute. STScI is operated by the Association of Universities for Research in Astronomy, Inc., under NASA contract NAS 5-26555.

of similar metallicity. This, along with other empirical evidence, supports the hypothesis that the cluster (together with B403) is physically associated with a substructure in the halo of M31 that has been interpreted as the relic of a merging event.

7.1 Introduction

Over the past ~20 years, the globular cluster (GC) system of M31 has been the subject of intensive study both from the ground and from space-borne observatories (see Rich et al. 2005; Galleti et al. 2004 - hereafter G04, 2006a, 2007; Huxor et al. 2008; Lee et al. 2008 and Caldwell et al. 2009 - hereafter C09, for recent reviews and references). One of the main aims of these studies was to collect as much as possible information on the GCs in M31 and compare it with our knowledge of the GCs in the Galaxy, so as to derive better insight into the formation and (chemical and dynamical) evolution of these two spiral galaxies and possibly of galaxies in general. The advent of the Hubble Space Telescope provided the unprecedented opportunity to obtain colour-magnitude diagrams (CMD) of M31 clusters, thus adding a completely new perspective to this research.

Substantial contributions in this field have been made by many investigators. At present, sufficiently accurate visual CMDs for a meaningful comparison with their Galactic counterparts have been published for 35 GCs in M31. Except for one that was observed from the ground (MGC1, Martin et al. 2006), a good fraction of these have been obtained with the HST-WFPC2 (Ajhar et al. 1996, Rich et al. 1996, Fusi Pecci et al. 1996, Holland et al. 1997, Jablonka et al. 2000, Meylan et al. 2001, Rich et al. 2005) until the better resolution and sensitivity of the ACS allowed even more accurate CMDs at fainter limiting magnitudes (Brown et al. 2004; Huxor et al. 2004, 2005, 2008; Galleti et al. 2006b; Mackey et al. 2006, 2007).

In addition to photometric quality, which is essential for the analysis of individual objects, a good statistical coverage is also important for a better understanding of the GC system. To increase the sample of M31 GCs with a CMD of individual member stars, we searched the HST archive for ACS images of objects that are listed in the Revised Bologna Catalogue of M31 clusters (RBC, see G04). We found useful ACS images containing 69 such objects (see Fig. 7.1). The retrieved material allowed us to confirm or revise the classification of all of them and to obtain CMD of individual stars for 17, 11 likely old globulars, and 6 young luminous clusters (like those discussed in Williams & Hodge 2001; Fusi Pecci et al 2005 and Perina et al. 2009a). This paper is devoted to the analysis of these data.

In Sect. 2 we present the target list, and in Sect. 3 we describe the adopted reduction procedures that yielded the CMDs. Section 4 is devoted to describe the method we have used to estimate the metallicity, reddening, and distance from each individual CMD for which a sufficiently reliable decontamination from the non-member field components was feasible. In Sect. 5 specific notes and comments on the results are presented for each of the 11 GCs (the primary targets) and for the other objects for which a sufficiently meaningful photometry was carried out. In Sect. 6 we discuss a possible connection between a few clusters and a large substructure recently found in M31. Finally, Sect. 7 contains some general considerations and conclusions.

7.2 The targets

A search by coordinates allowed us to find ACS images [3] for 69 entries of the RBC V3.5, independently of their original classification (see G04, and Galleti et al. 2006a). In two cases the images revealed that there were two catalogue entries referring to the same object (i.e.

---

[3]released until June 2007 from the HST Archive.
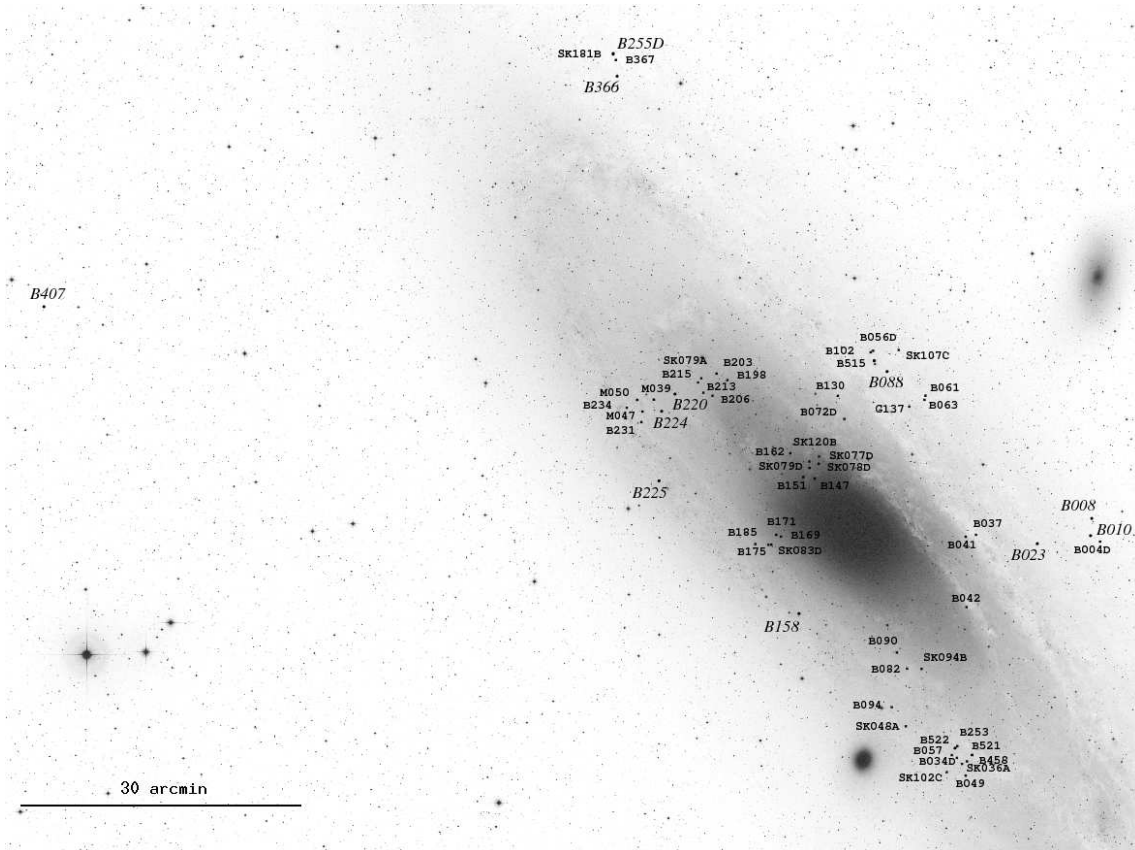
Figure 7.1: The location of the 11 primary target globular clusters, marked in italics + 52 secondary targets (see Sect.2 and 5), projected against the body of M31, with North up and East to the left.

B521=SK034A, and B522=SK038A), thus reducing the number of real objects to 67. Four confirmed clusters classified as candidate "intermediate-age GCs" by Puzia et al. (2005), and for which we have obtained good CMDs, have been excluded from the list as they will be the subject of a dedicated study (Perina et al. 2009b, in preparation).

Eighteen of the remaining 63 objects, namely B004D, B253, B034D, SK102C, G137, SK107C, B102, SK094B, B072D, SK077D, SK078D, SK079D, SK120B, SK083D, B175, SK079A, M047, and SK181B, are not *bona fide* clusters: their original RBC classification has been confirmed or revised based on the high resolution ACS images. The results of this analysis are summarised in Table 2 where we report their old and new classification flag.

Twenty of the remaining 45 objects are unequivocally confirmed as *bona fide* clusters (B037, B041, B042, B056D, B061, B063, B082, B094, SK048A, B130, B185, B198, B203, B206, B213, B215, B231, B234, B522=SK038A, and SK036A, see Fig. 7.3) and we obtained photometry of individual stars from the respective images, however we were unable to find an annulus around the cluster centre where the population of the cluster could be disentangled from the population of the surrounding field. In general this is due to the extreme compactness of the clusters, preventing to obtain good photometry for a sufficient number of stars even in the outermost coronae, but also the density of the background population plays a role. For five additional clusters, e.g. B147, B151, B162, B169, B171 (Fig. 7.3), located in the bulge of M31, at projected distances R=7.8′,7.29′, 7.17′, 6.31′ and 9.95′ from the centre, the overall crowding was so high that it resulted impossible to carry out any meaningful photometry even in the field, with the method adopted here.

The remaining 20 objects are the main subject of the present analysis and are subdivided as follows:

- Eleven *bona fide* clusters for which we could obtain a meaningful CMD, albeit of varying accuracy[4], and that were revealed by their CMD to be likely classical old globulars (i.e. having ages of several Gyr). These are the "primary targets" discussed in this paper, namely B008, B010, B023, B088, B158, B220, B224, B225, B255D, B366, and B407, according to the RBC nomenclature.

- Nine *bona fide* clusters that were listed as candidate young clusters (age ≲ 2 Gyr) by some previous study (Fig. 7.4) . Five of them, namely B049, B057, B090, B367, B458 were included in the list of the so-called "Blue Luminous Compact Clusters" (Fusi Pecci et al. 2005); three of them, namely B521=SK034A, M039=KHM31-516 (Krienke and Hodge 2008), and M050 were classified as "young" by C09 (see Table 7.6); and one, B515=KHM31-409, was included in the list of possible young/open clusters of Krienke and Hodge (2008). For six of them (B039, B049, M050, B367, B458, and B521) we were able to derive a CMD in which the cluster population can be identified and we can confirm their young age, while for the other three we obtained useful photometry only for the surrounding field.

Going back to the 11 "primary target" GCs discussed in detail in the present study, most of them lie close to the galactic plane of M31, as shown in Fig. 7.1. Three of them have been observed with the ACS/HRC and eight with the ACS/WFC. Their V images are shown in Fig. 7.2 and their HST data are listed in Table 7.1, together with their integrated magnitudes and colours taken from the RBC, when available. Similar data for all the other 52 targets considered in this paper are reported in Table 7.2.

7.3   Data reduction and the colour-magnitude diagrams

Data reduction has been performed on the prereduced images provided by STScI, using the ACS module of DOLPHOT [5] (Dolphin 2000a), a point-spread function fitting package

---

[4]depending on the cluster characteristics, the crowding conditions and the surface density of the surrounding field.

[5]See http://purcell.as.arizona.edu/dolphot/.
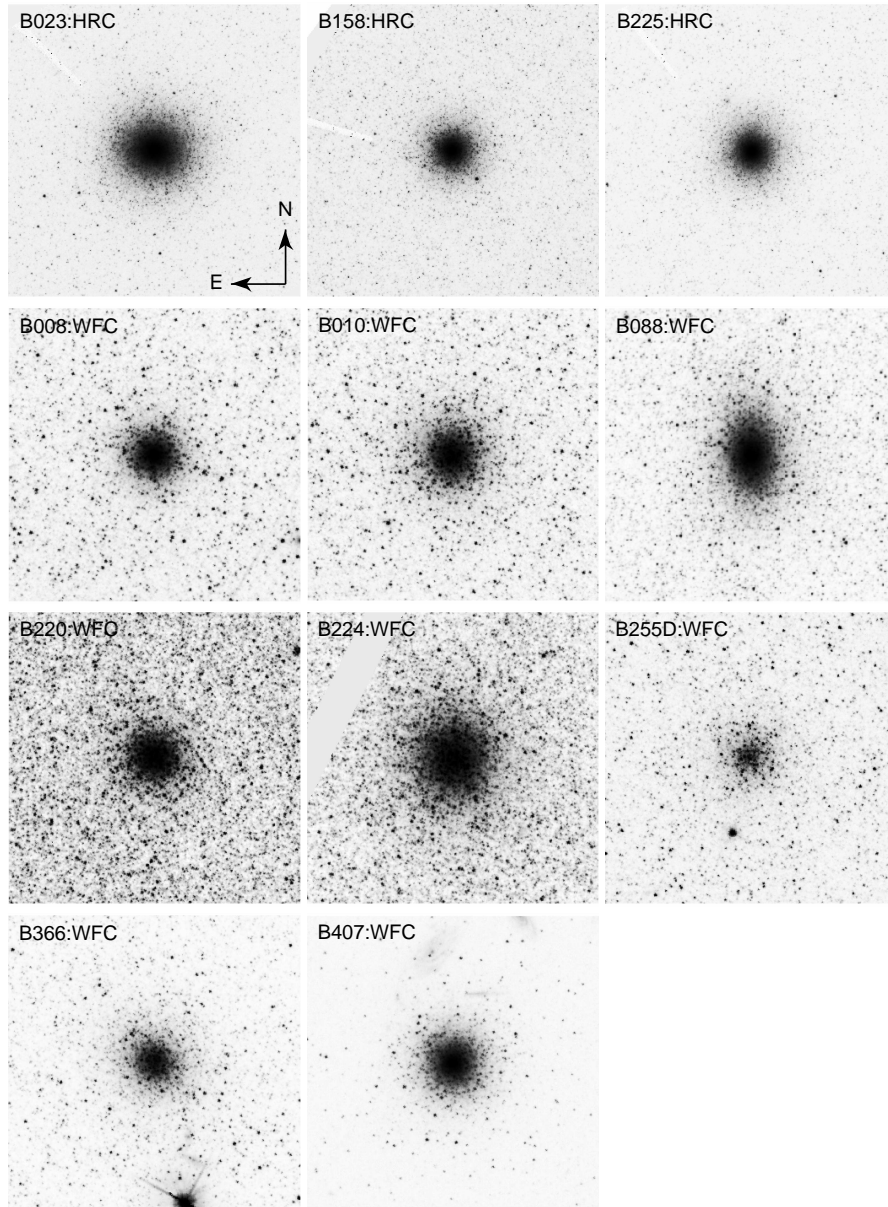
Figure 7.2: V band (F606W) images of the 11 M31 GCs analysed in the present study (the primary targets). The cluster and ACS camera identification are shown in each subraster. Each image covers $20'' \times 20''$ ($20'' = 76$ pc at the assumed M31 distance modulus of 24.47). North is up and East to the left.

specifically devoted to the photometry of HST data. The package identifies the sources above a fixed flux threshold on a stacked image and performs the photometry on individual frames, accounts for the hot-pixel and cosmic-ray masking information attached to the observational material, automatically applies the correction for the Charge Transfer Efficiency (CTE, Dolphin 2000b) and transforms instrumental magnitude to the VEGAMAG and standard BVI system using the transformations by Sirianni et al. (2005). In the following we use BVI photometry.

We fixed the threshold for the search of sources on the images at 3σ above the background. DOLPHOT provides as output the magnitudes and positions of the detected sources, as well as a number of quality parameters for a suitable sample selection, in view of the actual scientific objective one has in mind. Here we selected all the sources having valid magnitude

Figure 7.3: Same as in Fig. 7.2 for 25 additional M31 globular clusters (see Sect. 2).

Table 7.1: The primary target M31 GCs. ID, coordinates and photometry are from G04; [Fe/H] are from (^{a}): Perrett et al. (2002), and (^{b}): Huchra, Brodie & Kent(1991).

ID	RA (J2000)	Dec (J2000)	X arcm	Y arcm	V	(B-V)	(V-I)	[Fe/H]	ACS camera, bands(total t_{exp})	PID
B008-G60	00 40 30.54	+41 16 09.7	−15.41	19.86	16.56	1.10	1.05	−0.41^a	WFC,F606W(3250s),F435W(7260s)	10407
B010-G62	00 40 31.56	+41 14 22.3	−16.71	18.62	16.66	0.84	1.18	−1.87^b	WFC,F606W(3250s),F435W(7260s)	10407
B023-G78	00 41 01.26	+41 13 45.3	−13.78	13.82	14.22	1.18	1.65	−0.92^b	HRC,F606W(2020s),F814W(2860s)	9719
B088-G150	00 42 21.10	+41 32 14.3	10.00	13.32	15.42	1.12	1.47	−2.17^b	WFC,F606W(2370s),F814W(2370s)	10260
B158-G213	00 43 14.47	+41 07 20.6	−3.45	−9.90	14.70	0.86	1.15	−1.08^b	HRC,F606W(2020s),F814W(2860s)	9719
B220-G275	00 44 19.49	+41 30 35.7	22.38	−5.13	16.55	0.78	1.06	−2.07^b	WFC,F606W(1860s),F435W(2910s)	10407
B224-G279	00 44 27.21	+41 28 50.6	21.90	−7.35	15.45	0.79	1.03	−1.90^b	WFC,F606W(1860s),F435W(2910s)	10407
B225-G280	00 44 29.78	+41 21 36.6	16.52	−12.21	14.15	1.01	1.39	−0.70^b	HRC,F606W(2020s),F814W(2860s)	9719
B255D-D072	00 44 48.55	+42 06 13.3	53.70	12.71	17.92				WFC,F606W(1850s),F435W(2920s)	10407
B366-G291	00 44 46.72	+42 03 50.3	51.62	11.49	15.99	0.81	1.01	−1.39^b	WFC,F606W(1850s),F435W(2920s)	10407
B407-G352	00 50 09.98	+41 41 01.1	71.54	−49.72	16.05	0.90	1.22	−0.85^b	WFC,F606W(2400s),F814W(5100s)	9458

Table 7.2: The additional targets (see Sect. 2) grouped according to their location within the same-exposure field. All of them were observed with WFC@ACS on HST. ID, coordinates and photometry are from Galleti et al. (2004). We note the double identifications B521=SK034A and B522=SK038A.

ID	RA (J2000) Dec (J2000)	X arcm	Y arcm	V	(B-V)	(V-I)	[Fe/H]	type*	bands(exptime)	PID	Datasets
B004D-V223	00 40 26.41 +41 13 42.7	−17.82	18.98	18.81	1.18			4	F606W(3250s),F435W(7260s)	10407	J96Q07010,J96Q07020
B037-V327	00 41 35.00 +41 14 54.9	−8.98	9.51	16.82	2.05	2.63	−1.07^a	1	F606W(2370s),F814W(2370s)	10260	J8Z003010,J8Z003020
B041-G103	00 41 40.73 +41 14 45.8	−8.44	8.57	17.65	0.97	1.18	−1.22^a	1	F606W(2370s),F814W(2370s)	10260	J8Z019010,J8Z019010
B042-G104	00 41 41.69 +41 07 25.8	−14.12	3.93	16.29	1.48	1.89	−1.09^b	1	F606W(2370s),F814W(2370s)	10260	J8Z060010,J8Z022010
B057-G118†	00 41 52.84 +40 52 04.6	−24.96	−7.15	17.64	0.69	0.99	−2.12^a	1	F606W(2110s),F435W(2672s)	10407	J96Q06010,J96Q06020
B253	00 41 49.63 +40 52 59.7	−24.60	−6.11	18.01		0.55		6	F606W(2110s),F435W(2672s)	10407	J96Q06010,J96Q06020
B034D	00 41 50.13 +40 51 46.7	−25.51	−6.93	17.50				6	F606W(2110s),F435W(2672s)	10407	J96Q06010,J96Q06020
B522-SK038A	00 41 50.94 +40 52 48.3	−24.60	−6.42	17.85				1(2)	F606W(2110s),F435W(2672s)	10407	J96Q06010,J96Q06020
SK102C	00 41 55.92 +40 50 19.7	−25.98	−8.68	15.22	0.76	0.85		6(2)	F606W(2110s),F435W(2672s)	10407	J96Q06010,J96Q06020
B521-SK034A	00 41 41.67 +40 52 01.4	−26.29	−5.51					1(2)‡	F606W(2110s),F435W(2672s)	10407	J96Q06010,J96Q06020
B458-D049†	00 41 44.61 +40 51 22.3	−26.47	−6.35	17.84	0.49	0.57	−1.18^a	1	F606W(2110s),F435W(2672s)	10407	J96Q06010,J96Q06020
B049-G112†	00 41 45.60 +40 49 53.7	−27.52	−7.41	17.56	0.52	0.69	−2.14^a	1	F606W(2110s),F435W(2672s)	10407	J96Q06010,J96Q06020
SK036A	00 41 47.34 +40 51 07.5	−26.35	−6.91	19.43	1.01	1.13		1	F606W(2110s),F435W(2672s)	10407	J96Q06010,J96Q06020
B063-G124	00 42 00.80 +41 29 09.5	5.24	14.43	15.66	1.21	1.58	−0.87^b	1	F606W(2370s),F814W(2370s)	10260	J8Z008010,J8Z024010
B061-G122	00 42 00.20 +41 29 35.5	5.51	14.79	16.61	1.12	1.49	−0.79^b	1	F606W(2370s),F814W(2370s)	10260	J8Z008010,J8Z024010
G137	00 42 09.43 +41 28 30.4	5.71	12.76	17.81	−0.02			5	F606W(2370s),F814W(2370s)	10260	J8Z008010,J8Z024010
SK107C	00 42 14.18 +41 34 26.3	10.94	15.70	19.65	0.80	0.89		6(2)	F606W(2370s),F814W(2370s)	10260	J8Z007010,J8Z023010
B515^1	00 42 28.05 +41 33 24.5	11.72	13.02	18.67^2				1	F606W(2370s),F814W(2370s)	10260	J8Z007010,J8Z023010
B056D	00 42 28.45 +41 34 27.2	12.59	13.60	18.70				1	F606W(2370s),F814W(2370s)	10260	J8Z007010,J8Z023010
B102	00 42 29.85 +41 34 18.2	12.64	13.30	16.58	0.62	0.95		7	F606W(2370s),F814W(2370s)	10260	J8Z007010,J8Z023010
B082-G144	00 42 15.79 +41 01 14.3	−15.06	−4.94	15.54	1.56	1.91	−0.86^b	1	F606W(2370s),F814W(2370s)	10260	J8Z004010,J8Z020010
SK094B	00 42 07.81 +41 01 10.0	−16.05	−3.80	18.13	1.11	1.24	−0.86^b	4(2)	F606W(2370s),F814W(2370s)	10260	J8Z004010,J8Z020010
B090†	00 42 21.12 +41 02 57.3	−13.09	−4.68	18.80		1.64	−1.39^d	1	F606W(2370s),F814W(2370s)	10260	J8Z004010,J8Z020010
B094-G156	00 42 25.01 +40 57 17.2	−17.11	−8.74	15.55	0.97	1.26	−0.41^b	1	F555W(413s),F814W(502s)	10273	J92GB9BRQ,J92GB9BPQ
SK048A	00 42 17.59 +40 55 15.3	−19.58	−8.89	18.49	0.65	0.74		1	F555W(413s),F814W(502s)	10273	J92GB9BRQ,J92GB9BPQ
B130-G188	00 42 48.91 +41 29 52.9	11.35	7.77	16.93	1.15	1.41	−1.28^a	1	F555W(413s),F814W(502s)	10273	J92GB6ZLQ,J92GB6ZNQ
B072D	00 42 45.78 +41 27 26.9	9.07	6.74	18.50			−1.28^a	3(4)^3	F555W(413s),F814W(502s)	10273	J92GB6ZLQ,J92GB6ZNQ
B151-G205	00 43 09.64 +41 21 32.6	7.17	−0.43	14.83	1.23	1.45	−0.75^b	1	F606W(2370s),F814W(2370s)	10260	J8Z005010,J8Z021010
B147-G199	00 43 03.31 +41 21 21.5	6.30	0.39	15.80	0.84	1.27	−0.24^b	1	F606W(2370s),F814W(2370s)	10260	J8Z005010,J8Z021010
SK077D	00 43 00.52 +41 23 37.6	7.76	2.20	17.66	0.41	0.48		6	F606W(2370s),F814W(2370s)	10260	J8Z005010,J8Z021010
SK078D	00 43 00.86 +41 22 52.3	7.20	1.69	18.13	0.69	0.78		6	F606W(2370s),F814W(2370s)	10260	J8Z005010,J8Z021010
SK079D	00 43 06.04 +41 22 28.7	7.49	0.68	18.67	1.43	1.62		6	F606W(2370s),F814W(2370s)	10260	J8Z005010,J8Z021010
SK120B	00 43 05.97 +41 23 08.1	8.00	1.10	19.33	0.82	0.92		6(2)	F606W(2370s),F814W(2370s)	10260	J8Z005010,J8Z021010
B162-G216	00 43 16.42 +41 24 04.2	9.95	0.13	17.48	1.05	1.34		1	F606W(2370s),F814W(2370s)	10260	J8Z005010,J8Z021010
B171-G222	00 43 25.67 +41 15 37.4	4.37	−6.45	15.28	0.99	1.58	−0.48^b	1	F606W(3396s),F435W(4476s)	10407	J96Q03010,J96Q03020
B169	00 43 23.06 +41 15 25.5	3.91	−6.19	17.08	1.23	1.31		1	F606W(3396s),F435W(4476s)	10407	J96Q03010,J96Q03020
SK083D	00 43 28.60 +41 14 36.7	3.92	−7.51	14.64	1.05	1.17		6	F606W(3396s),F435W(4476s)	10407	J96Q03010,J96Q03020
B175	00 43 30.18 +41 14 36.4	4.09	−7.74	16.80	0.80			6	F606W(3396s),F435W(4476s)	10407	J96Q03010,J96Q03020
B185-G235	00 43 37.41 +41 14 43.3	5.02	−8.74	15.54	0.94	1.18	−1.03^b	1	F606W(3396s),F435W(4476s)	10407	J96Q03010,J96Q03020
B206-G257	00 43 58.70 +41 30 18.0	19.74	−2.25	15.06	0.80	1.03	−1.45^b	1	F606W(2110s),F435W(2672s)	10407	J96Q05010,J96Q05020
B198-G249	00 43 50.07 +41 31 53.1	19.99	−0.00	17.55	0.60	1.11	−1.13^a	1	F606W(2110s),F435W(2672s)	10407	J96Q05010,J96Q05020
B203-G252	00 43 56.00 +41 32 36.0	21.23	−0.43	16.68	0.93	1.20	−0.90^a	1	F606W(2110s),F435W(2672s)	10407	J96Q05010,J96Q05020
B213-G264	00 44 03.62 +41 30 38.9	20.58	−2.76	16.78	1.05	1.29	−0.99^b	1	F606W(2110s),F435W(2672s)	10407	J96Q05010,J96Q05020
SK079A	00 44 04.58 +41 32 09.3	21.88	−1.97	18.63	1.11	1.23		6(1)	F606W(2110s),F435W(2672s)	10407	J96Q05010,J96Q05020
B215-G266	00 44 06.44 +41 31 43.9	21.76	−2.51	17.13	1.02	1.20		1	F606W(2110s),F435W(2672s)	10407	J96Q05010,J96Q05020
M039^4	00 44 31.30 +41 30 04.6	23.34	−7.18	18.94	1.11	−0.53		1(2)‡	F606W(1860s),F435W(2910s)	10407	J96Q02010,J96Q02020
B234-G290	00 44 46.50 +41 29 18.3	24.50	−9.90	16.78	1.00	1.18	−0.95^a	1	F606W(3315s),F435W(4560s)	10407	J96Q04010,J96Q04020
M047	00 44 37.85 +41 28 52.1	23.16	−8.90	18.84		1.2		2^5	F435W(4560s),F606W(3315s)	10407	J96Q04010,J96Q04020
B231-G285	00 44 38.61 +41 27 46.8	22.39	−9.68	17.27	0.84	1.14	−1.49^a	1	F435W(4560s),F606W(3315s)	10407	J96Q04010,J96Q04020
M050	00 44 40.59 +41 30 06.0	24.44	−8.53	18.71		0.40		1(2)‡	F606W(3315s),F435W(4560s)	10407	J96Q04010,J96Q04020
B367-G292†	00 44 47.18 +42 05 31.9	53.00	12.48	18.45	0.32	1.30	−2.32^a	1	F606W(1850s),F435W(2920s)	10407	J96Q01010,J96Q01020
SK181B	00 44 48.64 +42 06 08.1	53.64	12.64	19.18	1.28	1.46		6(2)	F606W(1850s),F435W(2920s)	10407	J96Q01010,J96Q01020

(^{a}): Perrett et al. (2002); (^{b}): Huchra, Brodie & Kent(1991); †: BLCC, Fusi Pecci et al. (2005)

(*): classification, coded as follows: 1- confirmed cluster; 2- gc candidate; 3- controversial object 4- galaxy; 5- HII region; 6- star; 7- asterism; ‡: young cluster (from this paper and/or Caldwell et al.(2009)). In parentheses is enclosed the previous RBCv3.5 value.

(^{1}): identified as KHM31-409 in Krienke&Hodge (2008), tab.4; (^{2}): V mag from Krienke&Hodge (2008), tab.4; (^{3}): B072D, that was originally classified as a galaxy by Huxor et al. (2008), looks like a cluster, as noted also by Caldwell et al. (2009). Radial velocity is necessary in our view to yield its firm confirmation; (^{4}): identified as KHM31-516 in Krienke & Hodge (2008), tab.4; (^{5}): classified as globular cluster by Caldwell et al. (2009).
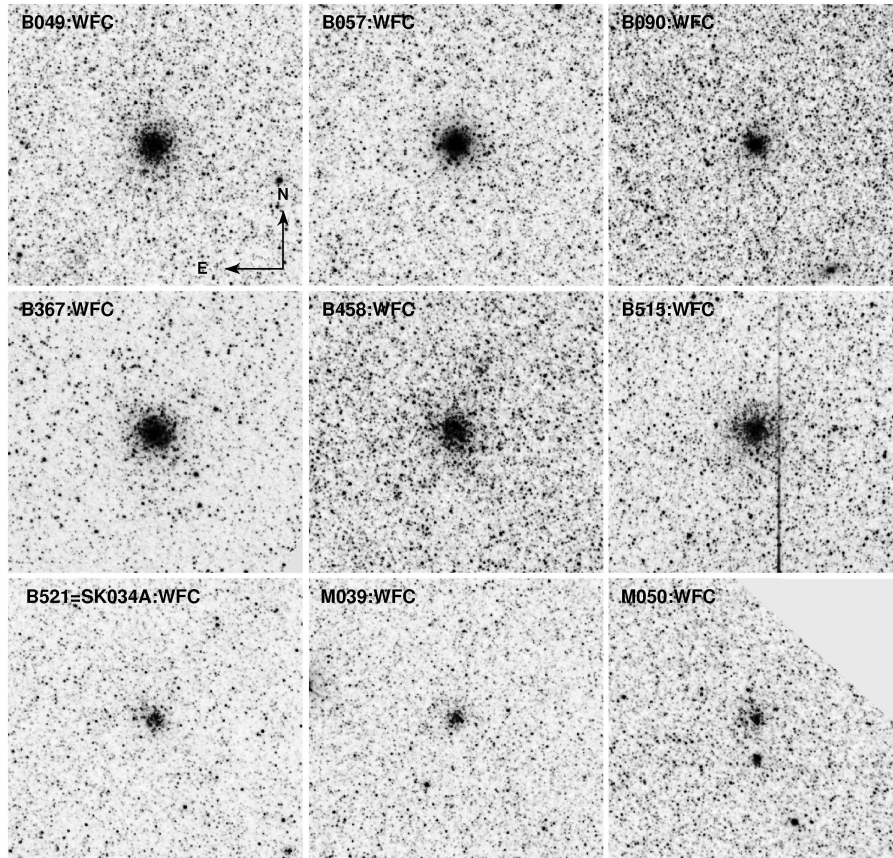
Figure 7.4: V band (F606W) images of the 9 candidate young clusters (see Sect. 5.12). The cluster and ACS camera identification are shown in each subraster. Each image covers $20'' \times 20''$.

measurements in both passbands, global quality flag = 1 (i.e., best measured stars), *crowding* parameter ≤ 0.3, $\chi^2 < 1.5$ if V< 22.5, $\chi^2 < 2.5$ for brighter stars, and *sharpness* parameter between -0.3 and 0.3 (see Dolphin 2000b for details on the parameters). This selection cleans the sample from the vast majority of spurious and/or bad measured sources without significant loss of information, and it has been found to be appropriate for the whole data set.

The limiting magnitudes of our photometry range from V~26 for the fields observed with relatively short exposure times, to V~27.5 for the deepest ones. The internal photometric errors of individual measures are in general within the range 0.01 - 0.08 mag for stars brighter than V=26 (see Fig. 7.5), depending quite strongly on the degree of crowding. However, errors increase rapidly for fainter stars, along with the impact of blending. Since we are mainly interested in the position and morphology of the main CMD branches we have not performed artificial stars experiments to study in detail the completeness of the samples as a function of magnitude. However, based on simple tests and on our previous experience, we are confident that in all of the considered cases the completeness is more than sufficient ($\gtrsim 70\%$) to achieve our scientific goals for V$\lesssim 26$.

To have an idea of the characteristic sizes of the clusters we estimated half-light radii – R_h (see Table 7.4) by aperture photometry over concentric annuli centered on the cluster and extended out to sufficiently large distances to properly sample the background. This approach is quite rough, nevertheless the values obtained here for the 5 clusters (B023, B088, B158, B225, B407) in common with Barmby et al. (2007) agree within 0.05 arcseconds (i.e. to better than 0.2 pc at the M31 distance) in all cases.

The individual CMDs are shown in Figs. 7.6 and 7.7, where the cluster and field stellar populations are indicated with different symbols (filled black and open grey circles,
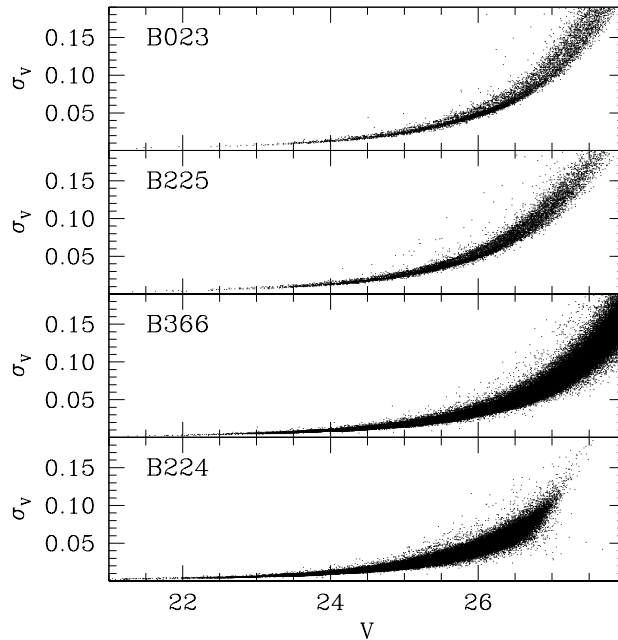
Figure 7.5: Internal photometric errors as a function of V magnitude for 4 representative clusters, two observed with ACS/HRC (B225 and B023), and two observed with ACS/WFC (B224 and B366).

respectively). The cluster CMDs shown in these figures sample the stellar population within an annulus around the cluster centre where the cluster members are more readily distinguishable with respect to the surrounding field. The inner limit of the annulus is set by the crowding level that prevents from performing useful photometry in the most central region of the cluster, the outer limit is set by the limiting radius of the cluster and by the need to avoid contamination by the surrounding field population. The inner and outer radii of the adopted annuli are indicated for each cluster. The field population is measured on an outer concentric annulus having the same area as the cluster annulus. In all the CMDs shown in Figs. 7.6 and 7.7 the cluster population can be distinguished from the field. In most cases the clusters show a thinner and much steeper RGB with respect to the field, and in many cases a Blue HB is visible, that has no (or much weaker) counterpart in the field population.

Before proceeding with the analysis of the cluster properties (discussed in Sect. 3), we have applied the field decontamination procedure described in Bellazzini et al. (1999). This method is based on a clipping routine which, making use of the local density on the CMDs of the field and of the cluster, computes the probability that a given star is a member of the cluster and retains or rejects stars from the cluster CMD according to that. To verify the reliability of this procedure we carried out several decontamination tests using different areas of the field and different techniques. In particular we applied to the most contaminated clusters a statistical subtraction procedure based on a Monte Carlo approach, where up to 5000 field-subtraction trials were used, thus obtaining globular cluster measured samples weighted by a statistical membership likelihood. Figs. 7.9 and 7.10 show that the decontamination of our primary targets was quite successful, providing "clean" CMDs in which the main cluster branches are more clearly identified (the individual cases are briefly discussed in Sect. 5). Therefore, the following analysis is based on the decontaminated CMDs.

7.3.1 Comparison with Fuentes-Carrera et al. (2008) photometry

While carrying out the present analysis, independent photometry of three objects included in our primary sample (B023=G078, B158=G213, B225=G280) was produced by Fuentes-Carrera et al. (2008) based on the same data set. Both CMDs for each of these three clusters

are shown side by side in Fig. 7.8, showing an excellent degree of consistency in magnitude and colour extension and in the quality of individual star photometry. The close coincidence of the main branches and even of most of the detected stars testifies the strict similarity and agreement of these two independent photometries.

Fuentes-Carrera et al. have focussed their analysis on the claimed existence of metallicity spreads in these very bright and populous GCs, based on the intrinsic width of the main branches. Although the quality of their data reduction is comparable to ours, we have not dealt with this aspect which is beyond the scope of the present study. We refer the interested reader to their work for a detailed discussion of this topic.

7.4 M31 vs. Galactic GCs: direct comparisons of the CMDs

We estimate the distance, metallicity, and reddening of our primary clusters by comparison with a set of CMD templates of well studied Galactic GCs, similarly to Rich et al. (2005), and Mackey et al. (2006, 2007). Relying on the hypothesis that the considered clusters are of similar nature as their Galactic counterparts we searched for the set of parameters ($(m-M)_0$, E($B-V$) and [Fe/H]) producing the best match between the observed RGBs and HBs and the ridge lines of the template clusters in the absolute plane, given the direction of the reddening vector $A_V = 3.1$E($B-V$), $A_I = 1.94$E($B-V$) and E($V-I$) = 1.375E($B-V$) (Schlegel et al. 1998).

The best match was judged by eye guided by (extensive) experience, as this approach is much more robust than most automated algorithms in presence of significant residuals from the decontamination procedure. The steepness of the RGB is of great help in judging if the branch is red because of high metallicity or because of high reddening; the fact that the HB match is mostly sensitive to vertical (magnitude) shifts, while the RGB is mostly sensitive to horizontal (colour) shifts also provides a useful guide to the solution. Colour and magnitude shifts are applied iteratively until a satisfactory match with any RGB and HB template is found: from these shifts we obtain estimates of the reddening and distance, while the metallicity is estimated by interpolation between the two RGB ridge lines bracketing the observed RGB locus.

As starting values for the iterative procedure we have used E($B-V$) = 0.08 for the foreground reddening (Barmby et al. 2007; Burstein and Heiles 1984), and the distance modulus $\mu_0 = 24.47$ mag for all the M31 clusters (McConnachie et al. 2005). The ridge lines of the reference GGCs were assembled from the observed CMDs (Piotto et al. 2002 for BV photometric data, and Rosenberg et al. 2000a,b for VI) that were shifted to the absolute reference frame by correcting for reddening and distance using the values listed in Table 7.3. These reference GGCs have been chosen to provide a sufficiently fine and regular sampling over a wide enough range of metallicities for a correct characterization of the target GCs.

In Figs. 7.9 and 7.10 we show the field decontaminated CMDs and, overplotted, the reference grid of GGC ridge lines, where the bracketing RGB reference clusters are highlighted. The values of metallicity, reddening and distance corresponding to the best match are also reported in each individual panel, as well as in Table 7.4; the typical uncertainty on the distance modulus is ±0.2 mag, ±0.04 mag in E($B-V$), and ±0.25 dex in metallicity. We think that the solutions presented in Fig. 7.9 and Fig. 7.10 are satisfactory and reliable. We have explored also alternative solutions, some of which are discussed in Sect. 5. In all cases the final adopted solution was the one which provided the best fit for both RGB and HB simultaneously.

As a matter of fact, due to the intrinsic and well-known age-metallicity degeneracy, also age could be considered as an additional free parameter, which would further complicate the analysis, having a (minor) effect on the colour of the RGB. Since the data are not deep enough (i.e. to the main sequence turn-off) to allow us to estimate the cluster ages (for ages larger than ~ 2 Gyr), we have assumed that all of the 11 primary target are classical old globulars

Table 7.3: Reference grid of template Galactic globular clusters.

ID	[Fe/H] dex	E($B-V$) mag	μ_V mag	Phot.
NGC7078 (M15)	−2.16	0.10	15.37	BV
NGC6397	−1.91	0.18	12.36	VI
NGC5824	−1.87	0.13	17.93	BV
NGC5272 (M3)	−1.66	0.01	15.12	VI
NGC6205 (M13)	−1.65	0.02	14.48	BV
NGC5904 (M5)	−1.40	0.03	14.46	VI,BV
NGC6723	−1.12	0.05	14.85	BV
47 Tuc	−0.71	0.04	13.37	VI,BV
NGC6624	−0.35	0.28	15.36	BV
NGC6553	−0.29	0.63	15.83	VI

NOTES: Metallicities are from Zinn (1985); all other parameters are from Harris (1996) (online update 2003). V,I photometry is from Rosenberg et al.(2000a,b); B,V photometry is from Piotto et al. (2002).

(i.e. age > 10 Gyrs). This assumption is supported by the overall morphology of the CMDs, in particular for those clusters displaying a Blue HB.

The best fitting procedure allowed us to estimate also the mean apparent V magnitude of the HB, V(HB), by reading the value of the HB apparent magnitude level directly on the *adopted HB ridge line* at (B–V)$_0$=0.3 or (V–I)$_0$=0.5 for the metal-poor clusters. This colour has been chosen to represent the middle of the instability strip. For the metal-rich clusters we have estimated V(HB) at the blue end of the red HB clump, with an additional correction of 0.08 mag to recover the mean level of the HB at the colour of the corresponding instability strip (see Fusi Pecci et al. 1996). The uncertainties affecting the V(HB) estimates are often quite large, due to the intrinsic quality of the available data and the possible residual field contamination. We have conservatively adopted ± 0.15 mag for all the considered clusters. V(HB) and M$_V$(HB) are reported in Table 7.4, together with the other parameters derived from the above procedure.

In the following section we briefly discuss the cases of each individual cluster.

7.5 Comments on the individual clusters

7.5.1 B008 = G060

In spite of the strong field contamination the typical cluster morphology can be identified in the decontaminated CMD of B008. The cluster displays a red HB and an RGB falling about halfway between the ridge lines of 47 Tuc and M5, with no need of adjustment with respect to the initial assumptions on distance and reddening. This leads to estimate a metallicity [Fe/H] = −1.0 ± 0.25 (the error is the typical uncertainty in the interpolation between the bracketing ridge lines). This result is in marginal disagreement (at < 2σ level) with the estimates by Perrett et al. (2002, hereafter P02; [Fe/H] = −0.41 ± 0.38), and by Galleti et al. (2009, hereafter G09; [Fe/H] = −0.47 ± 0.35), both obtained from integrated ground-based spectroscopy. We collect in Table 7.5 all the available metallicity determinations for all the target clusters, for convenience of comparison with the present estimates. On the other hand, adopting the reddening E($B-V$) =0.21 (as estimated by Barmby et al. 2000, and private communication,
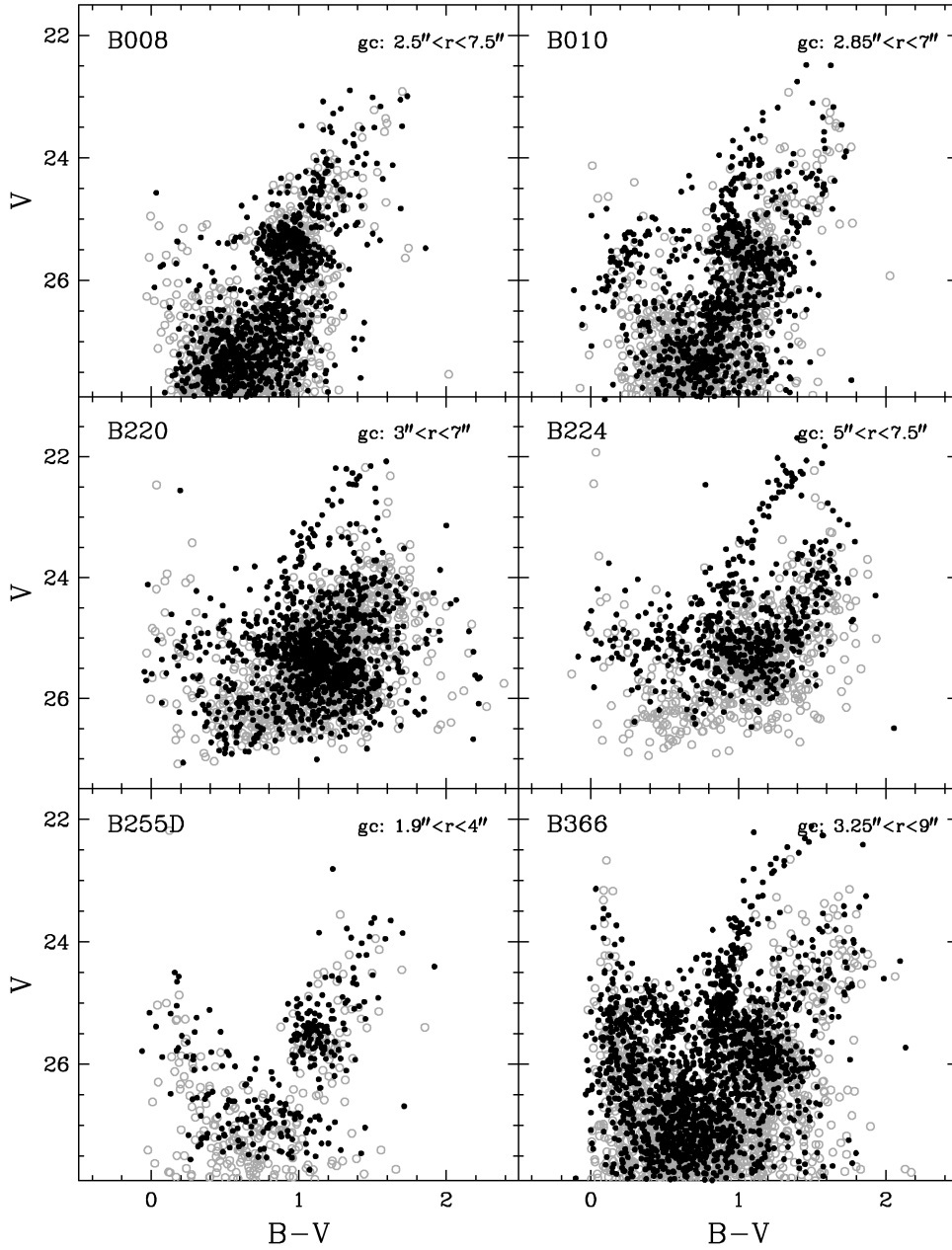
Figure 7.6: The CMDs of the target GCs B008, B010, B220, B224, B255D, and B366. *Filled black circles* are stars measured within the annulus with radii *r* in arcsec from the cluster centre (as reported in each panel). They are taken to represent the cluster population; *open grey circles* are stars measured within an outer area, of the same size, around the cluster, and represent the surrounding field population.

hereafter B00) an acceptable fit to the CMD morphology could only be obtained for $\mu_0 = 24.20$ and [Fe/H] = -1.8, with even larger disagreement with the spectroscopic metallicity estimates. Although this solution cannot be excluded in principle, we consider it as highly unlikely, as our adopted best values provide a much better fit to the observed CMD.
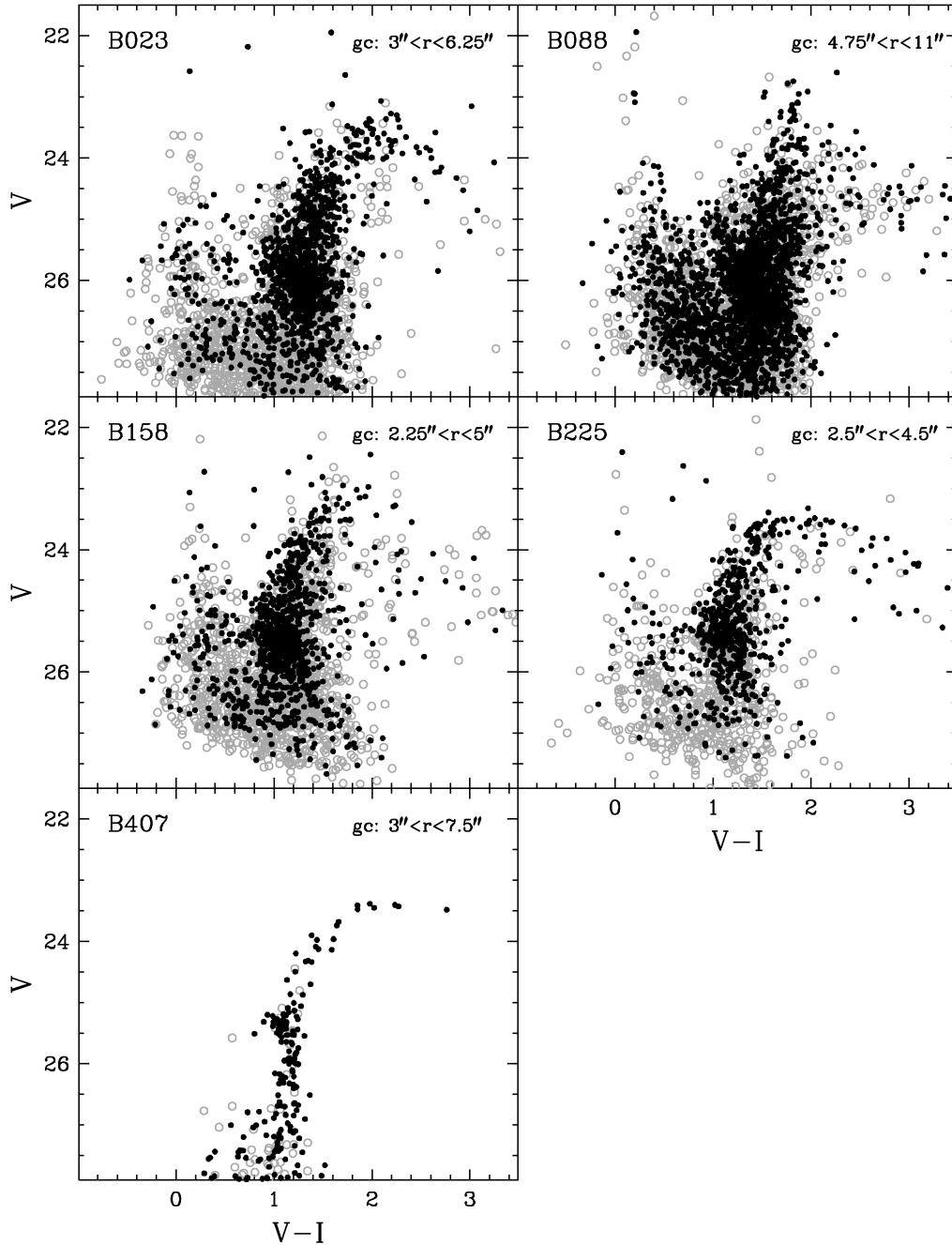
Figure 7.7: Same as in Fig. 7.6 for the GCs B023, B088, B158, B225, and B407.

7.5.2   B010 = G062

In this case, the decontaminated CMD is quite clean, showing a well defined and populated Blue HB and a steep RGB, indicating old age and low metal content. The best match of these features with the corresponding ridge lines is obtained by assuming a value of reddening $E(B-V) = 0.18$ mag and a distance modulus $\mu_0 = 24.25$. The solution relies on the best match to the blue part of the HB, considering the handful of (supposed) HB stars around $0.3 \lesssim (B-V)_0 \lesssim 0.5$ as *evolved* BHBs, i.e. post–ZAHB stars in their way to the Asymptotic

Giant Branch (and hence brighter than the genuine unevolved HB stars that we are using as standard candles).

With these assumptions, the CMD shown in Fig. 7.9 indicates that the metallicity of B010 is very similar to NGC5824, namely [Fe/H] = 1.8 ± 0.25. This value is in good agreement with the spectroscopic ground-based estimates, [Fe/H] = −1.87 ± 0.61 (Huchra et al. 1991, hereafter HBK), [Fe/H] = −1.77 ± 0.14 (P02), and [Fe/H] = −1.64 ± 0.68 (G09). Also the adopted reddening $E(B-V) = 0.18$ is fully consistent with the values reported in the literature, i.e. 0.19 (B00) and 0.22 (Fan et al. 2008, hereafter F08).

7.5.3 B220 = G275

The CMD of B220 shows the presence of a well defined BHB and a rather steep RGB, indicating old age and a low metallicity content. The best match of these features of the CMD with the corresponding reference ridge lines is obtained by assuming a value of reddening $E(B-V) = 0.07$ mag (in agreement with $E(B-V) = 0.05$ by F08, and $E(B-V) = 0.08$ by B00) and a distance modulus $\mu_0 = 24.40$. With these assumptions the CMD shown in Fig. 7.9 indicates that the metallicity of B220 is intermediate between M13 and NGC5824, [Fe/H] = −1.75 ± 0.25. This value compares fairly well with the spectroscopic estimate of HBK, [Fe/H] = −2.07 ± 0.82, whereas the values found by P02, [Fe/H] = −1.21 ± 0.09 and G09 [Fe/H] = −1.09 ± 0.42 seem too high for this cluster.

7.5.4 B224 = G279

The best match of the steep RGB and extended HB of B224 with the corresponding reference ridge lines is obtained by assuming a value of reddening $E(B-V) = 0.07$ mag and the standard distance modulus of 24.47 mag. With these values, the CMD shown in Fig. 7.9 indicates that the metallicity of B224 is intermediate between M13 and NGC5824, [Fe/H] = −1.80 ± 0.25. This value compares well with previous estimates from integrated spectroscopy: [Fe/H] = −1.90 ± 0.24 (HBK), [Fe/H] = −1.80 ± 0.05 (P02), and [Fe/H] = −1.68 ± 0.28 (G09).

Both F08 and B00 have estimated slightly higher reddening values: 0.13 and 0.12 mag, respectively. We have searched for solutions with $E(B-V) = 0.13$, and we found that the best fit would yield a similar metallicity but a much shorter distance, $\mu_0 = 24.25$. However, the overall quality of the fit is significantly worse when using this higher value of reddening, so we have adopted our primary solution.

7.5.5 B255D

The cluster is rather small and the statistical decontamination procedure becomes less effective when the number of stars is low. As a result, one can still see the presence of some residual field population on the blue side of the CMD (blue plume). Nevertheless, a sparse and metal-rich RGB as well as a red clump can be seen clearly. The best match with the ridge lines in this case is not much more than an intelligent guess, and indicates a metallicity [Fe/H] = −0.40 ± 0.25 and a distance modulus $\mu_0 = 24.40$ mag for the assumed value of reddening $E(B-V) = 0.10$ mag. There are no ground-based spectroscopic estimates for this cluster.

7.5.6 B366 = G291

B366 is a rather populous cluster lying in a high density field, as shown in Fig. 7.2. The decontamination procedure was not able to eliminate completely the field component (a blue plume as well as a red clump to the red of the cluster RGB), but the cluster population shows up quite clearly as a well defined HB with a possible blue extension, and a rather steep RGB, suggesting old age and metal deficiency. The cluster is classified as old also by C09, based on its integrated spectrum.
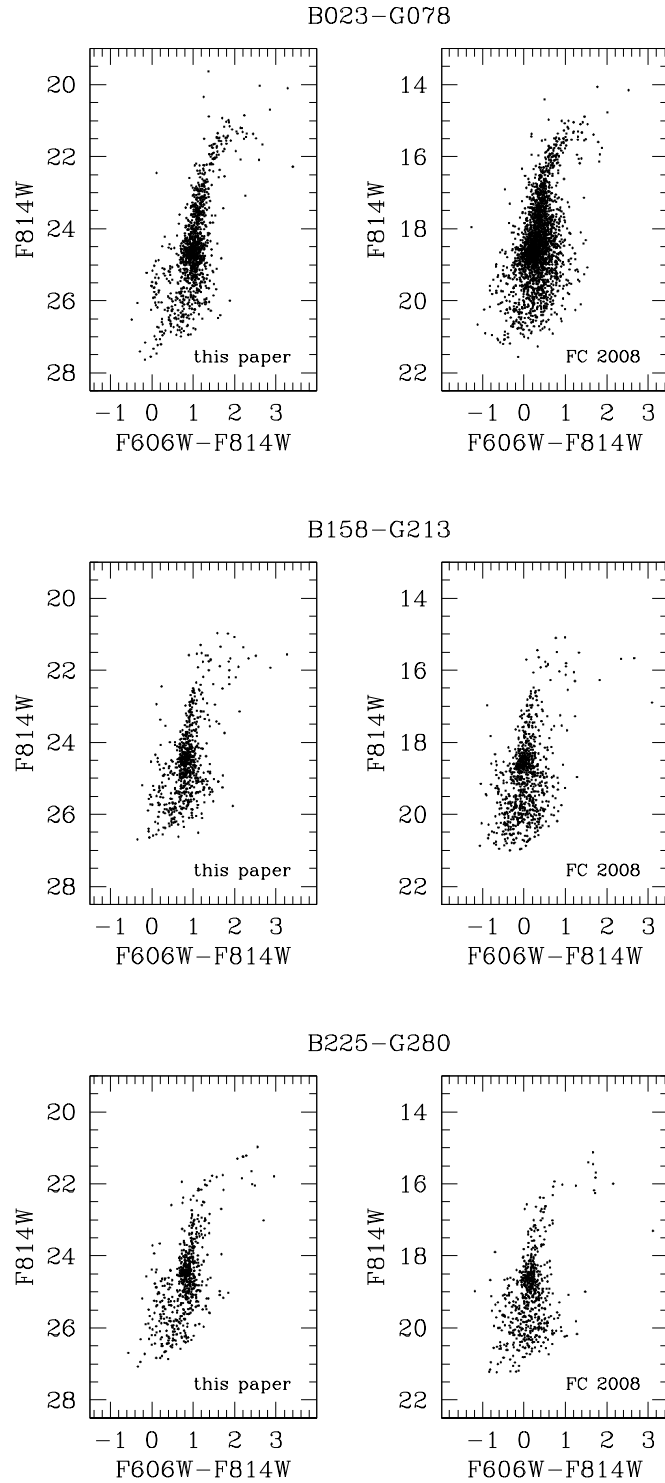
Figure 7.8: Comparison of the CMDs obtained from the present study (left) and by Fuentes-Carrera et al. (2008), their Fig. 6) (right, uncalibrated VEGAMAG magnitudes), for the clusters B023 (top), B158 (middle) and B225 (bottom).
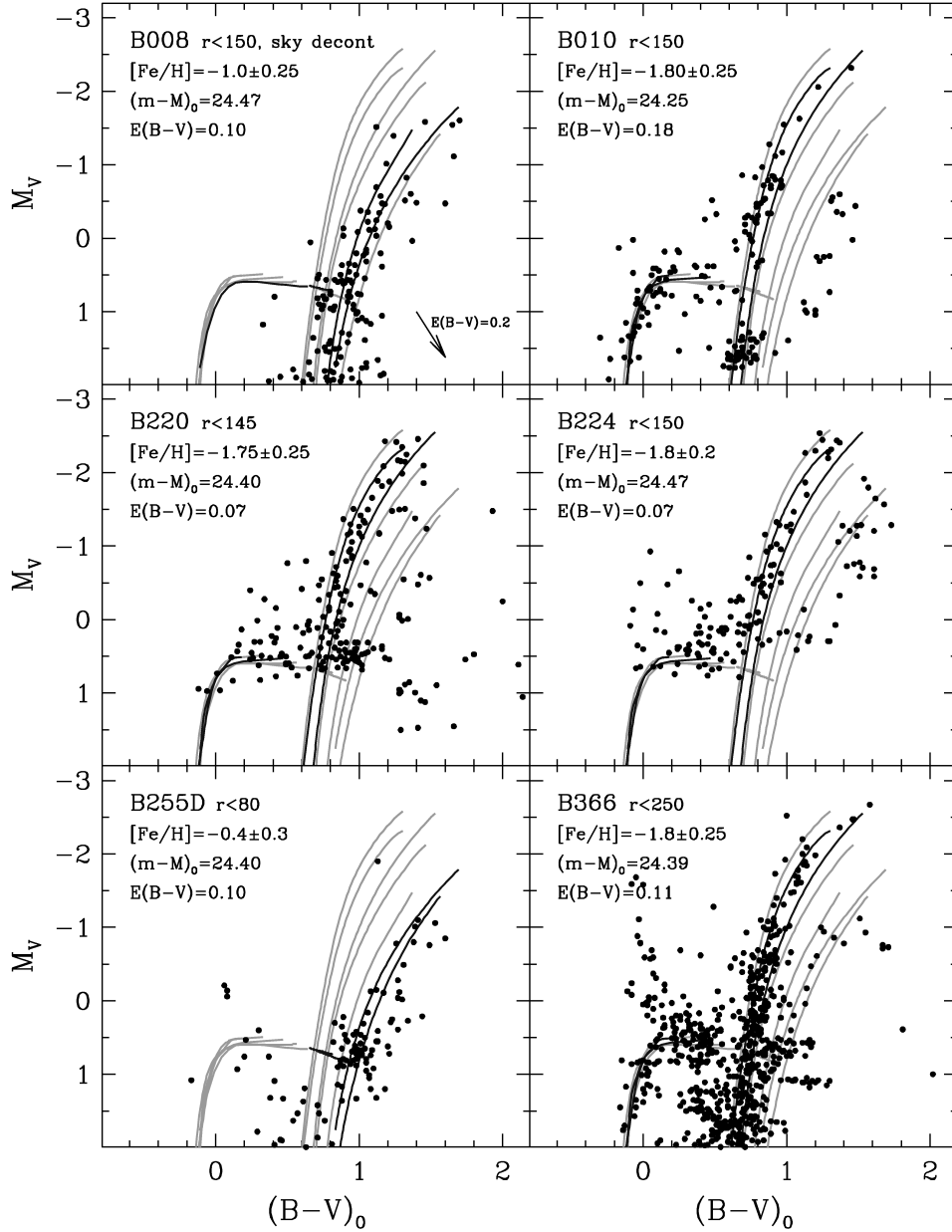
Figure 7.9: The CMDs of the primary target GCs B008, B010, B220, B224, B255D and B366. The data have been decontaminated by the field contribution. The arrow in the left top panel indicates the reddening vector corresponding to $e(B-V) = 0.2$. The *bracketing ridge lines* of reference Galactic GCs are also shown, as described in Sect. 4 and Table 7.3.
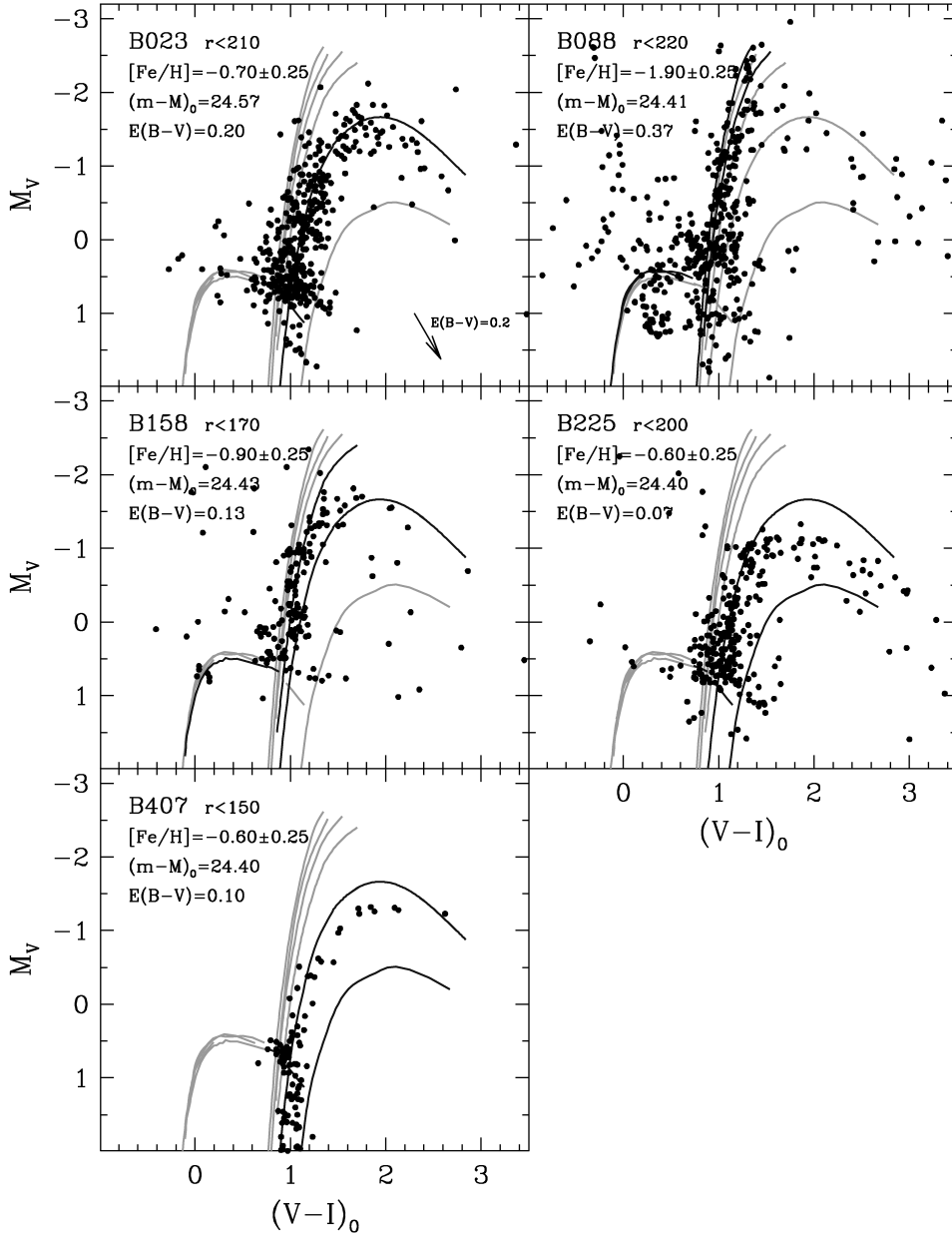
Figure 7.10: Same as in Fig. 7.9 for the GCs B023, B088, B158, B225 and B407.

The best match between the observed CMD and the template ridge lines is achieved with $E(B-V) = 0.11$ mag and $\mu_0 = 24.39$ mag. With these values, $[Fe/H] = -1.80 \pm 0.25$ is found. This value is consistent, within the uncertainties, with the spectroscopic estimates by HBK, $[Fe/H] = -1.39 \pm 0.28$, and G09, $[Fe/H] = -2.14 \pm 0.39$, while it is in excellent agreement with the results of P02, $[Fe/H] = -1.79 \pm 0.05$.

7.5.7   B023 = G078

The field decontamination has left some marginal field contribution on the bluest part of the CMD, but the main branches stand out quite clearly. The cluster has a red HB, and its RGB falls almost exactly on the ridge line of 47 Tuc.

The best match of the main branches is obtained for $E(B-V) = 0.20$ mag and $\mu_0 = 24.57$. This leads to estimate a metallicity $[Fe/H] = -0.70 \pm 0.25$, in good agreement with existing spectroscopic estimates, $[Fe/H] = -0.92 \pm 0.10$ by HBK, and $[Fe/H] = -0.91 \pm 0.15$ by G09.

We note that the reddening estimated by Barmby et al. (2007, hereafter B07), and F08 is significantly larger, $E(B-V) = 0.36$ and 0.32 mag, respectively. With these values no match can be achieved with any of the ridge lines, therefore we exclude the possibility of such a high reddening for this cluster.

7.5.8   B088 = G150

As one can see in Fig. 7.2, this cluster is very populous, has a strongly elliptical shape and lies in a rather dense field. Two other clusters in our sample, B023 and B366, show some evidence of elliptical shape, but the ellipticity of B088 is clearly larger. The values reported in the literature are $\epsilon = 0.28$ (Barmby et al. 2007), $\epsilon = 0.18$ (Staneva et al. 1996) and $\epsilon = 0.23 - 0.27$ (Lupton 1989), making this object particularly noteworthy.

In this case, where the stellar field is very crowded and variable, we have performed several statistical field subtraction experiments. In spite of the presence of some residual contamination from the field, the steep cluster RGB is clearly identified in all cases, indicating a low metal content. On the other hand the HB morphology is more confused, and the vertical match is rather tentative. A possible adopted set of parameters is $[Fe/H] = -1.90 \pm 0.25$, $E(B-V) = 0.37$ and $\mu_0 = 24.41$. The metallicity agrees very well with spectroscopic estimates, $[Fe/H] = -2.17 \pm 0.48$ (HBK), $[Fe/H] = -1.81 \pm 0.06$ (P02), and $[Fe/H] = -1.94 \pm 0.52$ (G09). A high value of reddening for this cluster was found independently by F08 (0.46 mag) and B07 (0.48 mag). Our result indicates that the cluster is located in the nearest side of the M31 disc, and lies behind some dust layer as clearly visible in the Spitzer images of this region (Gordon et al. 2006).

7.5.9   B158 = G213

Even if sparsely populated, the steep RGB of B158 stands out quite clearly in the decontaminated CMD, while the fit to a (supposed) extended HB is just tentative. Our best solution gives an estimate of the reddening $E(B-V) = 0.13$ mag, in excellent agreement with the results by F08, $E(B-V) = 0.14$, and B00, $E(B-V) = 0.12$. The adopted distance modulus is $\mu_0 = 24.43$, and the metallicity $[Fe/H] = -0.90 \pm 0.25$, which compares very well with all the ground-based estimates: $[Fe/H] = -1.08 \pm 0.05$ (HBK), $[Fe/H] = -1.02 \pm 0.02$ (P02), and $[Fe/H] = -0.74 \pm 0.15$ (G09).

7.5.10   B225 = G280

The RGB and red HB of the cluster stand out very clearly and are well consistent with the ridge lines of the metal-richest templates, on the assumption of a reddening value $E(B-V) = 0.07$ and a distance $\mu_0 = 24.40$. This leads to estimate a metallicity $[Fe/H] = -0.60 \pm 0.25$, in agreement with the spectroscopic estimates: $[Fe/H] = -0.70 \pm 0.12$ (HBK), $[Fe/H] = -0.67 \pm 0.12$ (P02), and $[Fe/H] = -0.35 \pm 0.15$ (G09).

The CMD of this cluster was previously obtained by Fusi Pecci et al. (1996), with HST/FOC and, subsequently, by Rich et al. (2005), with HST/WFPC2. Both studies obtained results in good agreement with those presented here.

Table 7.4: Parameters derived for the 11 primary target clusters from the procedure described in Sect.s 4 and 5.

ID	R_h	V_{HB}	E(B-V)	μ_0	[Fe/H]	M_V^{HB}
	arcs				dex	mag
B008-G60	0.95	25.29	0.10	24.47	-1.00 ± 0.25	0.51
B010-G62	1.40	25.30	0.18	24.25	-1.80 ± 0.25	0.49
B023-G78	0.95	25.91	0.20	24.57	-0.70 ± 0.25	0.72
B088-G150	1.11	25.99	0.37	24.41	-1.90 ± 0.25	0.43
B158-G213	0.65	25.44	0.13	24.43	-0.90 ± 0.25	0.61
B220-G275	2.15	25.08	0.07	24.40	-1.75 ± 0.25	0.46
B224-G279	1.35	25.22	0.07	24.47	-1.80 ± 0.25	0.53
B225-G280	0.61	25.35	0.07	24.40	-0.60 ± 0.25	0.73
B255D-D072	1.60	25.53	0.10	24.40	-0.40 ± 0.25	0.82
B366-G291	2.00	25.25	0.11	24.39	-1.80 ± 0.25	0.52
B407-G352	0.80	25.41	0.10	24.40	-0.60 ± 0.25	0.70

Table 7.5: Comparison of the estimates of metallicity here obtained for the target clusters (see Sect.s 4 and 5) and previous recent determinations.

ID	[Fe/H]$_{CMD}$	[Fe/H]$_{G09}$	[Fe/H]$_{P02}$	[Fe/H]$_{HBK}$
	dex	dex	dex	dex
B008-G60	-1.00 ± 0.25	-0.47 ± 0.35	-0.41 ± 0.38	
B010-G62	-1.80 ± 0.25	-1.64 ± 0.68	-1.77 ± 0.14	-1.87 ± 0.61
B023-G78	-0.70 ± 0.25	-0.91 ± 0.15		-0.92 ± 0.10
B088-G150	-1.90 ± 0.25	-1.94 ± 0.52	-1.81 ± 0.06	-2.17 ± 0.48
B158-G213	-0.90 ± 0.25	-0.74 ± 0.15	-1.02 ± 0.02	-1.08 ± 0.05
B220-G275	-1.75 ± 0.25	-1.09 ± 0.42	-1.21 ± 0.09	-2.07 ± 0.82
B224-G279	-1.80 ± 0.25	-1.68 ± 0.28	-1.80 ± 0.05	-1.90 ± 0.24
B225-G280	-0.60 ± 0.25	-0.35 ± 0.15	-0.67 ± 0.12	-0.70 ± 0.12
B255D-D072	-0.40 ± 0.25			
B366-G291	-1.80 ± 0.25	-2.14 ± 0.39	-1.79 ± 0.05	-1.39 ± 0.28
B407-G352	-0.60 ± 0.25	-0.65 ± 0.15		-0.85 ± 0.33

CMD: this paper; G09: (Galleti et al. 2009); P02: Perrett et al. (2002); HBK: Huchra et al. (1991).
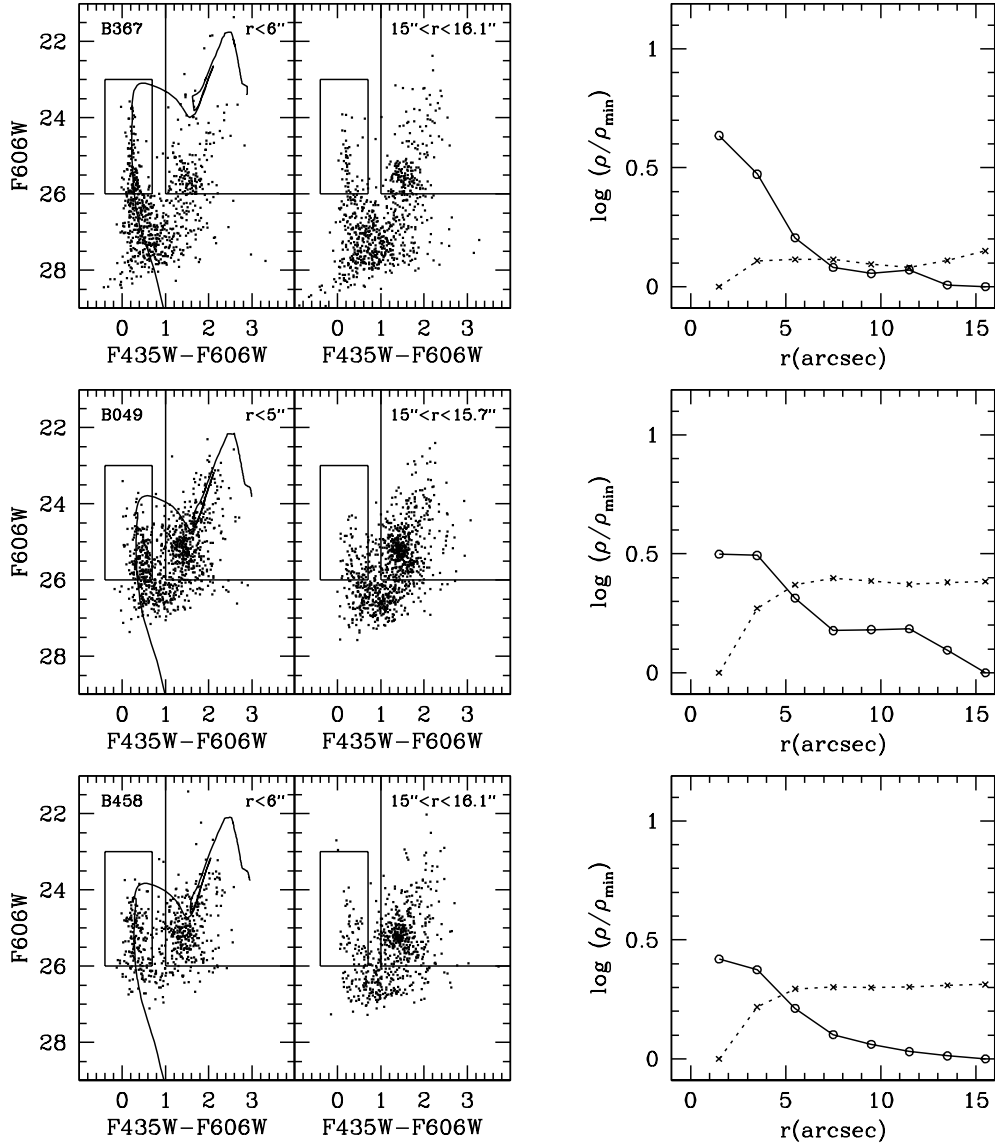
Figure 7.11: *left*: CMDs of annuli dominated by the cluster population; *right*: CMDs of the surrounding fields, measured over annuli of similar area. Right panels report the radial profiles obtained by counting stars in the two boxes reported in the CMD plots. The *solid* lines show the radial behaviour of the "blue plume" in the smaller box, presumably including most of the cluster MS, while the *dotted* lines show the corresponding trend as obtained from the bigger boxes, presumably dominated by the field. Best-fitting isochrones with solar metallicity (Girardi et al. 2002) are overimposed.

7.5.11   B407 = G352

The cluster B407 lies at a rather large projected distance from the centre of M31, in a low density region where the contamination by field stars is very low. As a consequence, the RGB and red HB of the cluster are very well defined. Their position in the CMD indicates a metallicity slightly higher than the reference cluster 47 Tuc.

The best solution is obtained for $E(B-V) = 0.10$ mag and $\mu_0 = 24.40$ mag. With these values, the metallicity of B407 is $[Fe/H] = -0.60 \pm 0.25$, fully consistent with the spectroscopic estimates by HBK, $[Fe/H] = -0.85 \pm 0.33$ and, in particular, G09, $[Fe/H] = -0.65 \pm 0.15$.

The case of B407 as a metal rich cluster in the outer halo of M31 is discussed in more detail in Section 6.
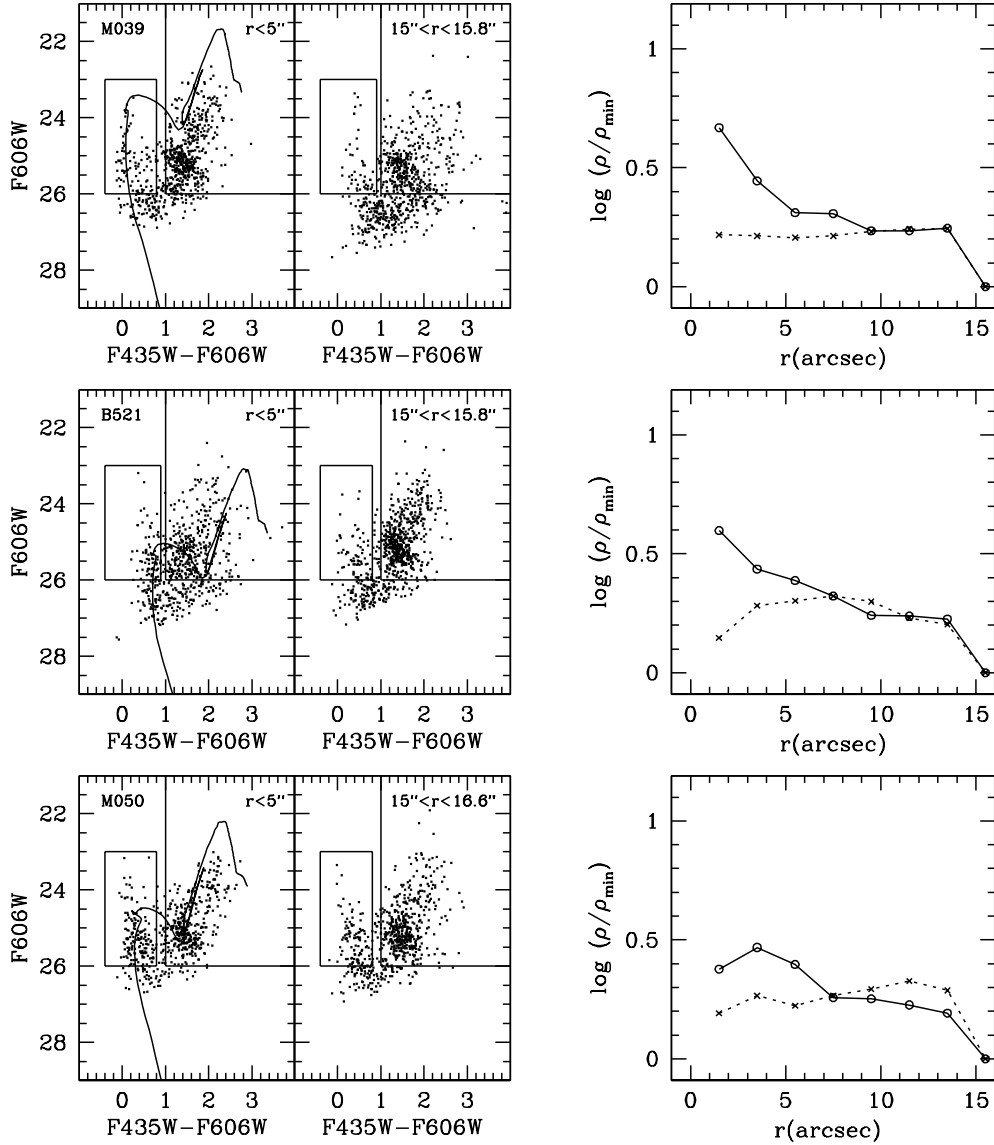
Figure 7.12: Same as Fig. 7.11 for the clusters B521, M050 and M039.

7.5.12 The candidate young clusters

As noted in Sect.2, there are 9 clusters that we consider separately as they have been classified as young by previous studies. Five of them, namely B049, B057, B090, B367, B458, were included in the list of the so-called "Blue Luminous Compact Clusters" (BLCC, Fusi Pecci et al. 2005, F05 hereafter). They are quite faint, V~ 17.5 − 18.5, but are undoubtedly clusters and some of them have the compact appearance that is typical of GCs (see Fig. 7.4; F05, Williams & Hodge 2001). B057 was included by F05 among the candidate "young" clusters due to the quite high H_β-value, 5.56, but C09 (see Table 7.6) classify it as "old" as well as B090, with a lower H_β-value, 3.38, that was included in the list of possible young candidates by Jiang et al. (2003).

Three other objects, B521, M050, M039 have been classified as "young" clusters by C09 (see Table 7.6). B521 is actually coincident with another object, SK034A, having measured radial velocity ($v_r = -531.8$ kms^{-1}, Kim et al. 2007; $v_r = -515.8$ kms^{-1}, C09). M050 is classified as a "young" cluster by C09 who found $v_r = -156.6$ kms^{-1}. It looks like a small

155

Table 7.6: Parameters derived for the candidate young clusters. Photometry is from G04 except when otherwise stated. R_h indicates the half-light radius.

ID	R_h (arcs)	V	(B-V)	$E(B-V)$ (this paper)	Age (Myr) (this paper)	$E(B-V)$ (C09)	Age (Myr) (C09)
B049-G112	1.20	17.56	0.52	0.30	280	0.25	400
B090	0.47	18.80					old
B367-G292	0.94	18.45	0.32	0.25	200	0.25	200
B458-D049	1.60	17.84	0.49	0.25	320	0.25	500
B515	1.25	18.60[1]					
B521-SK034A	0.75	19.08[1]		0.55	400	0.38	250
M039	0.62	18.94		0.10	320	0.18	320
M050	0.80	18.71		0.15	560	0.25	300
B057-G118	0.70	17.64	0.69				old

([1]): V magnitude from C09.

asymmetric aggregate of stars, but its CMD confirms that it is indeed a young cluster (see below). M039=KHM31-516 (Krienke and Hodge 2008) is faint and partially resolved, C09 list $v_r = -82.4$ kms^{-1}. B515=KHM31-409 was listed by Krienke and Hodge (2008) as an open cluster[6].

For 6 of the 9 clusters quoted above (B367, B049, B458, B521=SK034A, M039 and M050) we were able to obtain CMDs representative of the cluster populations, that are shown in Figs. 7.11 and 7.12. On the rightmost panels of these figures we report the cluster density profiles obtained by counting stars on CMD boxes selecting the young main sequence (MS) population (open circles) and the red evolved population (RGB and Red Clump; crosses). Even if in most cases the CMD of the cluster is quite similar to that of the surrounding field (sampling the star-forming thin disc of M31), the density profiles show that in all cases a significant overdensity of MS stars is found at the cluster position. Guided by the density profiles we selected the radial annuli where the CMD is expected to be dominated by cluster stars (leftmost panels), to be compared with an external annulus of the same area sampling the surrounding field (central panels).

To have a rough estimate of the age and reddening, the CMDs of the clusters were fitted (by eye) with solar abundance isochrones (from Girardi et al. 2002), as done in Williams & Hodge (2001) and Perina et al. (2009a). The results, reported in Table 7.6, are in good agreement with similar estimates by C09 who adopted however super-solar abundance isochrones. All the six clusters for which the CMD could be derived (see Figs. 7.11 and 7.12) appear indeed younger than 1 Gyr, thus confirming their previous classification.

For the remaining three clusters B057, B090 and B515, it resulted impossible to single out the cluster population from the background, thus we cannot provide any improved age estimate.

---

[6]We note that another cluster of our sample, B041 (not considered in this section), that was classified as old by C09, was instead suggested to be young by Barmby et al. (2007). According to the latter study its red integrated colour is probably due to a red, bright, non-member star which masks the true intrinsic colour of the cluster. Unfortunately our data do not provide any further insight on the age of this cluster.
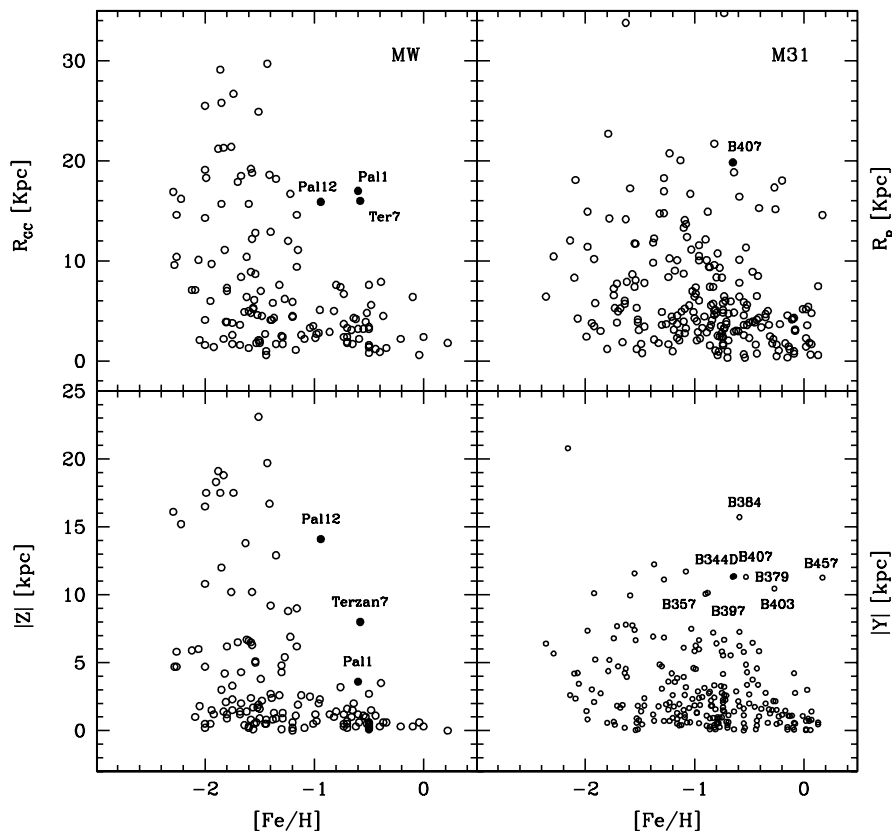
Figure 7.13: Left panels: distribution of Galactocentric distance (upper-left) and absolute height above the Galactic plane (lower-left) as a function of metallicity for Galactic GCs (from Harris 1996). The clusters having [Fe/H]≥ −1.0 and R$_{GC}$ > 10 kpc are plotted as filled circles and labelled with their names. Right panels: projected M31 galactocentric distance (upper-right) and projected distance from the major-axis (lower-right) as a function of metallicity for M31 CGs (from G09). B407, as well as other clusters having [Fe/H]≥ −1.0 and unusually high Y, are labelled with their names, B407 is highlighted as a filled circle.

It is worth noticing, that four of the clusters considered here (B367, B049, B458, and B057) have a spectroscopic metallicity estimate from P02 (see Tab. 2, above) that was obtained using a calibration that is based on (and valid only for) old clusters. Their high degree of metal deficiency reported by P02 $−1.18 < [Fe/H] < −2.32$ is very likely spurious, due to the known fact that a young age mimics the lack of metals in integrated colours and spectra (see Fusi Pecci et al. (2005) for a detailed discussion of this effect in the context of the study of the GC system of M31). Moreover, in a search for groups of M31 GCs having common origin (from the disruption of the same parent dwarf galaxy, for instance) based on the similarity in position, velocity, and metallicity, Perrett et al. (2003) identified eleven remarkable groups. Their group 9 contains B049 and B458, confirmed here as having age < 1 Gyr from their CMD, B057 and DAO408, classified as young from their H$_\beta$ and/or colour in the RBC, and B034. Thus, four of the five members of the group are young clusters having velocities in full agreement with the overall rotation pattern of M31 disc. As they likely belong to the disc, their proximity in space naturally implies similar velocities, while the similarity in metallicity is due to their young age being mis-interpreted as low metal content, as described above. We conclude that this proposed group does not trace a real overdensity in the phase-space of the M31 halo, but simply a bunch of bright young disc clusters lying in the same spot of the disc.

A thorough discussion of "young" and bright clusters in M31 with HST-based CMDs, based on a wide homogeneous sample of other 18 candidates (P.I. J. Cohen GO 10818) and also including the six clusters studied here and the four clusters by Williams and Hodge (2001), will be presented in a forthcoming paper (see Perina et al. 2009a, for a presentation of the overall project). For a discussion about faint young clusters in M31 we refer the reader to Krienke and Hodge (2007, 2008).

7.6 Clusters in Streams

Among all the clusters of our sample, B407 is the most distant from the centre of M31, lying at a projected distance of about 20 kpc. It is also one of the most metal rich, and this combination makes it worth a more detailed investigation.

In Fig. 7.13 we show the distribution of Galactocentric distance and absolute height above the Galactic plane as a function of metallicity for GCs in the Milky Way (from Harris 1996). It is quite clear that, while metal-poor clusters ([Fe/H]$\lesssim$ −1) are found at any R_{GC} and/or $|Z|$, the metal-rich ([Fe/H]$\gtrsim$ −1) clusters are confined within $R_{GC} < 8$ kpc and $|Z| < 3$ kpc[7]. The only exceptions are three metal-rich clusters that do not satisfy these conditions and stand out as obvious outliers in Fig. 7.13, namely Terzan 7, Palomar 12 and Palomar 1. Ter 7 is a member of the Sagittarius dwarf spheroidal galaxy (Ibata et al. 1994, 1995), a satellite of the MW that is currently disrupting under the strain of the Galactic tidal field. In this process it has developed two huge tidal tails (Sgr Stream) containing its former stars (Ibata et al. 2001a; Majewski et al. 2003; Belokurov et al. 2006) and clusters (Bellazzini et al. 2003a) escaped during various perigalactic passages. Pal 12 is indeed associated with the Sgr Stream (Dinescu et al. 2000; Martinez-Delgado et al. 2002; Bellazzini et al. 2003a,b; Cohen 2004). An extra-galactic origin has been invoked also for Pal 1, to explain its anomalously young age (Rosenberg et al. 1998) and its unusual abundance pattern (Venn et al. 2007; Correnti, Saviane & Monaco, private communication). These characteristics are shared also by Ter 7 (Buonanno et al. 1995; Tautvaisiené et al. 2004; Sbordone et al. 2005) and Pal 12 (Stetson et al. 1989; Brown et al. 1997; Cohen 2004). The recent extensive and homogeneous analysis of relative ages of Galactic GCs by Marin-Franch et al. (2009) identifies Pal 1, Pal 12 and Ter 7 as the three youngest clusters of their whole sample. In conclusion, the diagrams in the left panels of Fig. 7.13 are very effective in identifying as outliers three clusters that are (most likely) of extra-galactic origin.

In the right panels of Fig. 7.13 we show the similar kind of plots for the M31 GCs (metallicities from G09). Unfortunately, in the case of M31 we have at disposal only projected quantities (the projected galactocentric distance R_p, and the projected distance from the major axis, a proxy for the height above the disc), unavoidably blurring the information contained in their de-projected counterparts. Nevertheless, the overall morphology of the distributions is quite similar to the MW case. In particular there is just a bunch of metal-rich clusters having large R_p and Y, including B407.

To see if the anomaly in the position of these clusters can be traced also in their kinematics, in Fig. 7.14 we plot the projected position of metal-rich ([Fe/H]$\geq$ −1.0) clusters in the plane of the sky (upper panel), and their M31-centric radial velocity as a function of their distance along the major axis (assuming $V_{r,0} = -301$ km/s as the systemic velocity of M31, Van den Bergh 2000). It is well known that, at odds with the MW case, the bulk of M31 GCs participate to the rotation pattern of the galaxy disc, as traced by the HI rotation curve, and the correlation is tighter for metal-rich clusters (P02; Lee et al. 2008; G09, and references therein). Among the clusters labelled in Fig. 7.13 as having an anomalous position for their metallicity, three have velocities in stark contrast with the rotation pattern shared by the bulk of the metal-rich GCs: B357, B403 and B407. In particular, the latter two clusters lie within a projected distance of 3 kpc from each other, and have velocities differing by $\simeq 20$

---

[7]Incidentally, we note that the transition between the clusters confined to low R_{GC} and $|Z|$ and those distributed over the whole range spanned by these parameters seems to be *very sharp*, occurring nearly exactly at [Fe/H]= −1.2.
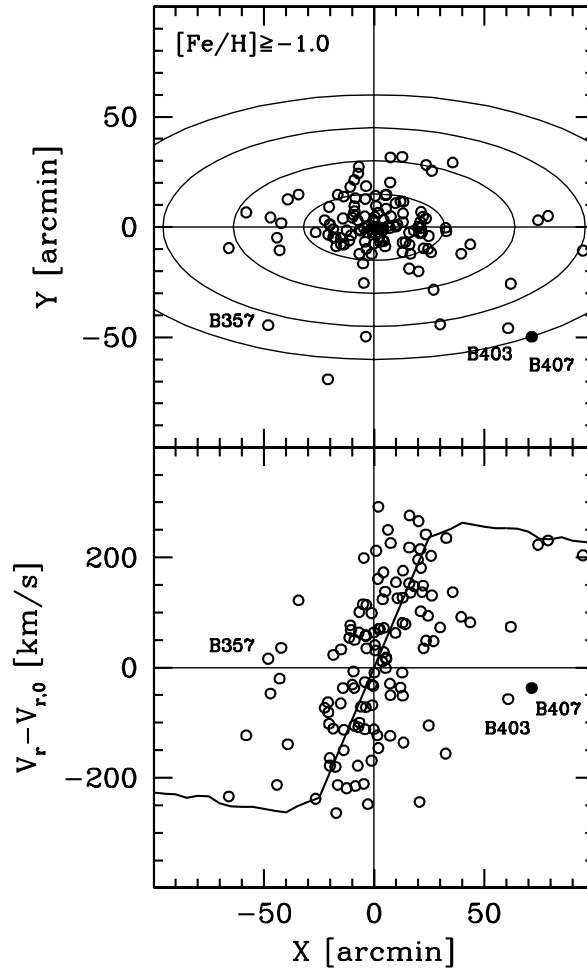
Figure 7.14: Upper panel: X,Y distribution of M31 GCs having [Fe/H]≥ -1.0. The ellipses overplotted have major axes of $30'$, $60'$, $90'$ and $120'$, respectively, and have the same axis-ratio and orientation as the disc of M31. Lower panel: Radial velocity as a function of major-axis distance for the same M31 GCs as above. The line is the HI rotation curve of the galaxy from Carignan et al. (2006). We have labelled only the clusters, among those labelled in Fig. 7.13, that do not follow the general rotation pattern.

km/s. It is tempting to suggest that the two clusters are (were) physically associated to a common structure, having a different origin from the bulk of the other clusters. Recent extensive surveys have revealed that the halo and the outer disc of M31 host a wealth of sub-structures, generally believed to be the relics of past accretion events that contributed to the build-up of the galaxy (Ibata et al. 2001b, 2005, 2007; Ferguson et al. 2005).

Indeed, the CMD of B407 presented here has been obtained from an image of the set used by Richardson et al. (2008) to study the field stellar population within the main sub-structures identified in Ferguson et al. (2005) and Ibata et al. (2007). In particular, the cluster is at the edge of an ACS image sampling the so called NE Shelf, a thin stream of stars looping over the North-Eastern edge of the M31 disc. Richardson et al. find that the structure is mainly composed by stars with metallicity similar to what we find for B407, also very similar to the population found in the largest structure identified by Ferguson et al. (2005) and Ibata et al. (2007), i.e. the "Giant Stream". Ibata et al. (2005) studied the kinematics of stars in a field of the NE Shelf not far from B407/B403. They find a bimodal V_r distribution with a major peak at the characteristic velocity of the M31 disc at this position ($V_r \sim -200$km/s), and a secondary peak at $V_r \sim -350$km/s. We note that the velocities of the considered clusters match pretty well the secondary peak ($V_r = -338, -358$km/s for B407, B403

159

respectively), supporting the hypothesis of physical association with the component of field stars that do not follows the kinematics of the disc. [8].

The case described here opens a new window for the research of substructures in M31, as it shows that it may be possible to use GCs to trace (and easily study the kinematics) of at least some of the relics of past accretion events (see also Lee et al. 2008). It also supports the idea that the ingestion of GCs from accreting dwarf galaxies may provide a significant contribution to the assembly of the globular cluster systems of giant galaxies, as already shown in the case of the Milky Way (Bellazzini et al. 2003b)

7.7 Summary and conclusions

We have analysed 63 objects listed in the RBC for which HST/ACS images were publicly available in the HST Archive. We have confirmed or revised their classification based on the inspection of these images and we were able to obtain meaningful CMD for 11 likely old GCs and 6 young bright clusters.

We estimated distance, reddening, and metallicity for the eleven old GCs, by comparing the field-decontaminated CMD of the clusters with a grid of ridge lines of well-studied template clusters of the Milky Way. Our reddening and metallicity estimates are, in general, in satisfactory agreement with previous independent measures. As reported in Table 7.4, we have also determined for each cluster an estimate of the magnitude level of the HB measured on the HB ridge line of the reference GGC that best fits the observed CMD, with a typical error of ±0.15 mag.

One of the clusters of our sample (B407) is identified as a possible member of a large substructure recently found in the halo of M31, and interpreted as a relic of past (minor) merging episodes (NE Shelf; Ibata et al. 2001b, 2005, 2007; Richardson et al. 2008). The cluster has a metallicity that is much higher than the bulk of M31 clusters residing at the same (large) distance from the M31 centre/major axis, and its kinematics is very different from the large majority of M31 GCs having similar metallicity. The GC B403 (not included in our sample) is found to share the same properties and is also indicated as a possible member of the NE Shelf.

We estimated the age also for six candidate young clusters, by comparing their observed CMD with theoretical isochrones. We confirm that all of them are younger than 1 Gyr, in good agreement with previous studies.

With the present analysis the total number of M31 confirmed GCs with published reliable optical CMDs increases from 35 to 44 for the old globulars, and from 7 to 11 for the young bright ones (BLCCs). The photometric catalogues of the clusters studied here will be made publicly available through a dedicated web page[9].

---

[8]Another cluster, B401, having very similar position and velocity ($X = 56.99, Y = -32.30, V_r = -333$km/s), was not plotted in Fig. 7.14 because of its very low metallicity ([Fe/H]$=-2.03$).

[9]http://www.bo.astro.it/M31/hstcatalog

8

The young stellar population at the center of NGC 205

L. Monaco, I.Saviane, S.Perina, M.Bellazzini, A.Buzzoni, L.Federici, F.Fusi Pecci,
& S. Galleti

Abstract

NGC 205 is a peculiar dwarf elliptical galaxy hosting in its center a population of young blue stars. Their origin is still matter of debate, the central fresh star formation activity possibly being related to dynamical interactions between NGC 205 and M31.

The star formation history in the central $30''(\sim120$ pc) around the NGC 205 central nucleus is investigated in order to obtain clues to the origin of the young stellar population.

Deep HST/ACS CCD photometry is compared with theoretical isochrones and luminosity functions to characterize the stellar content of the region under study and compute the recent SF rate. Our photometry reveals a previously undetected blue plume of young stars clearly distinguishable down to I≃26. Our analysis suggests that 1.9×10^5 M$_\odot$ were produced between approximately 62 Myr and 335 Myr ago in the NGC 205 inner regions, with a latest minor episode occurring ~25 Myr ago. This implies a star formation rate of ~7×10^{-4} M$_\odot$/yr over this period. The excellent fit of the observed luminosity function of young main sequence stars obtained with a model having a constant star formation rate argues against a tidally triggered star formation activity over the last ~300 Myr. Rather, a constant SF may be consistent with NGC 205 being on its first interaction with M 31.

8.1   Introduction

NGG 205 is one of the brightest (M$_V$=-16.6 Mateo, 1998) M 31 satellites and is a peculiar nucleated dwarf elliptical galaxy. It hosts a fairly complex stellar content. Color-magnitude

diagrams and time series revealed the presence in NGC 205 of RR Lyrae and carbon stars, i.e. both old and intermediate age stars as well as sequences of asymptotic and red giant branch stars (AGB/RGB, Sharina et al., 2006; Richer et al., 1984; Davidge, 2003, 2005). Lee (1996) broadly summarized the NGC 205 star formation (SF) history.

The presence of a population of bright blue stars in the most central region of NGC 205 has been known since the early studies (Hodge, 1973, and references therein) on this galaxy and is an unusual characteristic for a dwarf elliptical [1]. Cappellari et al. (1999, hereafter C99) revealed that many of the brightest blue sources classified as very young stars (Peletier, 1993) were in fact multiple systems, clusters or star associations. Davidge (2003, hereafter D03), studying the population of Asymptotic Giant Branch (AGB) stars, noted that multiple episodes of SF may have occurred in the most central regions (see also Bica et al., 1990; Lee, 1996) with a time spacing compatible with the putative NGC 205 orbital period (Cepa & Beckman, 1988). Therefore, tidal interactions with M 31 could have triggered the latest episodes of SF. Indeed, evidence of past dynamical interactions of NGC 205 with its bright companion has been accumulating over the years (McConnachie et al., 2004; Geha et al., 2006; De Rijcke et al., 2006) and residual gas (Welch et al., 1998) and dust (Marleau et al., 2006) have also been detected in NGC 205 (see also Davidge, 2005).

However, in spite of the great interest in the recent star formation history in the innermost region of this galaxy, previous attempts to directly analyze the young Main Sequence population have been unsuccessful, likely due to the extreme degree of crowding affecting the region of interest (Butler & Martínez-Delgado, 2005). Here we use the exceptional spatial resolution of the Advanced Camera for Survey (ACS) on board the Hubble Space Telescope (HST) to derive accurate stellar photometry in the circum-nuclear region of NGC 205, resolving for the first time the young Main Sequence (MS) population down to I$\simeq$ 26.

8.2 Data reduction

The inner 29″×26″ around the central nucleus of NGC 205 were imaged using the ACS high resolution channel (HRC) and retrieved from the archive through the MAST web interface[2]. At the distance of NGC 205 (824 kpc, see McConnachie et al. 2005), the observed field of view corresponds to about 120 pc. The data were obtained during Cycle 11 (program 9448, PI L. Ferrarese). F555W and F814W frames were taken for a total integration time of 2560s and 2440s, respectively. Images were acquired at four different pointings to improve the resolution and a pixel scale of 0.″022 px^{-1} was eventually obtained (see Valluri et al., 2005, for further details). Photometry was performed using the ACS module of Dolphot[3], with the same approach described in Galleti et al. (2006b) and Perina et al. (2009a). A final photometric catalog of about 26000 stars was built, retaining only objects classified as *bona-fide* stars (i.e., quality flag =1) and having a χ^2 <2.5. This selection allows us to exclude several spurious and/or poorly measured sources without a significant loss of information (Galleti et al., 2006b). Dolphot automatically transforms instrumental magnitudes into the VEGAMAG and the Johnson-Kron-Cousins BVRI systems adopting the calibrations by Sirianni et al. (2005). In the following we will always adopt Johnson-Kron-Cousins V,I magnitudes.

The majority of the central nucleus is unresolved and stars begin to be measured at radial distances $\geq$ 0.″9 (about 40 px) from the cluster center. At a radius of ~5″, the nucleus surface brightness profile joins the profile of the underlying galaxy (see Valluri et al., 2005; Butler & Martínez-Delgado, 2005; Jones et al., 1996). There is no particular difference in the stellar population in the annulus 1″ $\lesssim r \lesssim$ 5″, where the resolved outskirts of the nuclear cluster are mixed with the underlying population, and the surrounding field. Therefore, in the

---

[1]On the other hand, young nuclear clusters seem relatively frequent in nucleated dwarfs (Rossa et al., 2006).

[2]http://archive.stsci.edu/

[3]http://purcell.as.arizona.edu/dolphot/

following, we will consider the whole sample as representative of the circum-nuclear region of the galaxy.

8.2.1   Comparison with previous photometries

Fig. 8.1 shows the obtained I *vs* V-I color-magnitude diagram (CMD). WFPC2 photometry of the central region of NGC 205 was presented by Butler & Martínez-Delgado (2005, hereafter BM05, their fields F3 and F4). An inspection of Fig. 8.1 and their Fig. 4 reveals that the ACS photometry presented here is significantly deeper than any other obtained so far for the same field. Also, evolutionary marks like the clump of stars at V-I≈0.9; I≈21.8 (hereafter YC, young clump, see Sect. 3) have never been detected before.

While the quality of the WFPC2 and ACS photometries are comparable along the RGB (V-I≥1), the populated young MS (blue plume, BP) visible in Fig. 8.1 at V-I≈-0.2 down to the detection limit is practically absent in WFPC2 CMDs. Quite likely, such blue stars do not exist at all in the more external regions of NGC 205. However, they could have been detected in the F3 and F4 fields, which encircle the ACS area.

Blending of red stars may appear in the photometry as sequences of spurious blue stars. Extensive artificial star tests have been performed following the procedure described in Perina et al. (2009a) to assess the completeness and the impact of blending on our photometry as a function of the star color and magnitude. The bin-migration effect is quite limited for stars having V-I<0.5. In the magnitude range 22<I<24.5, only a fraction between 2% and 4.5% of the injected stars change their magnitude by $\Delta I \geq$-0.5 when recovered. This means that about 64 in the ~1764 stars under consideration (~3.6%) may be seriously affected by blending of star pairs. We are thus fully confident about the genuine nature of the detected young MS and that blending effects do not jeopardize the results presented. The lack of such BP in the BM05 photometry is likely to be due to the details of the photometry process and to the selection criteria adopted to filter the detected sources.

It has long been known that the brightest blue stars in NGC 205 are concentrated in a region of ~300 pc (100″) around the nucleus (Hodge, 1973). Several authors have presented integrated photometry surface brightness profiles over extended areas in NGC 205 (see Lee, 1996, and references therein). The galaxy colors become bluer inward within ~50″ from the center with the exception of the inner ~2″ where the colors become redder. Most of the bright blue stars were found to be concentrated within a region of ~20″ diameter around the central nucleus (Peletier, 1993). However, as already mentioned, many of these stars were in fact clusters or star associations, as pointed out by C99 using WFPC2 data.

The spatial distribution of BP stars detected in our ACS photometry, on the other hand, does not present any obvious clustering, i.e. they do not belong to associations similar to the ones discovered by C99 (which are located just outside the limits of our ACS field). The same applies also to stars belonging to the YC.

8.3   Star formation history

An overall idea of the star formation history in the observed NGC 205 regions can be readily obtained with the aid of theoretical isochrones. On top of the ACS photometry, we plotted in Fig. 8.1 a selection of isochrones (in the post MS phase) from the Girardi et al. (2002) library and the mean ridge line of the galactic globular cluster 47 Tucanae (open squares) from Saviane et al. (2000). Reddening and distances for this cluster were taken from the most recent version of the Harris (1996) catalogue.

We adopted for NGC 205 the following parameters: $(m-M)_0$=24.58, E(B-V)=0.08 from McConnachie et al. (2005) and Schlegel et al. (1998), respectively. However, this reddening value does not account for the internal extinction nor for the contribution from M31's dust clouds in front of NGC 205. While it has been suggested that NGC 205 might even lie in front of M31 (Howley et al., 2008), some degree of differential reddening is certainly present
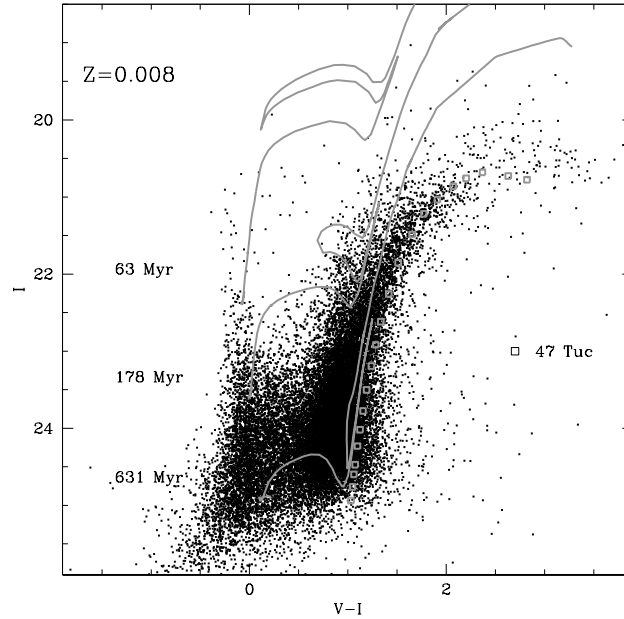
Figure 8.1: Theoretical post MS isochrones (Z=0.008) from the Girardi et al. (2002) library superimposed on the ACS photometry. The mean ridge line of the galactic globular cluster 47 Tucanae is also plotted as open squares.

in the galaxy region under consideration. Nevertheless, its overall effect on the photometry presented here is negligible (see BM05 for a discussion).

Fig. 8.1 shows that the blue plume (V-I≃-0.2) is dominated by MS stars likely older than ~50-60 Myr and reaching ~650 Myr at the detection limit. A sparse population of younger stars is also visible at I≤22. They might correspond to a ~25 Myr old simple stellar population (see below). The YC may mark instead a star formation episode occurring some ~200 Myr ago and is made up of blue-loop helium burning stars. The bulk of the RGB population is matched at its red edge by the ridge line of the old and relatively metal rich globular cluster 47 Tuc (Fe/H=-0.70, Saviane et al., 2000), and is broadly compatible with Z=0.008 isochrones a few Gyr old. Sharina et al. (2006), using the Lick indexes, derived a mean metallicity of [Z/H]≃-0.5, age of 1.9 Gyr and no alpha-enhancement for their most central field outside the nucleus (see also Mould et al., 1984, BM05). This is also consistent with the presence of a well populated red-clump along the RGB at I>24 (see also BM05) which, at odds with the BP population, is a dominant feature also in the CMDs of external regions of NGC 205 (see BM05).

8.3.1 Recent star formation history

The luminosity function (LF) of the MS can be used to derive the mass in young stars and the star formation rate (SFR) at late epochs in the central region of NGC 205 (see Saviane et al., 2004, hereafter SHR04). We assume for the moment that the SF has been continuous and constant (but see next section) for the last few hundred Myr. Thus, the overall SF activity can be approximated by the sum of a discrete number of simple stellar populations (SSPs). Each generation of stars will produce a power law LF which is added to that of the previous generations. The observed LF will result, then, from the convolution of the LFs of the SSPs (see SHR04).

We select BP stars in the color region at V-I<0.2. Besides MS stars, a negligible fraction of blue loop stars may also be present in the selected sample. In the color range under consideration, the completeness factor is ~0.66 at I=24.5 and a comparison of the surface
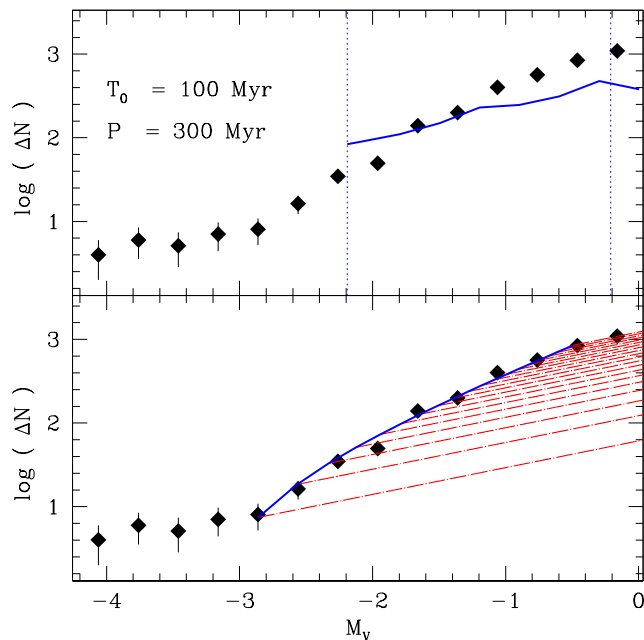
Figure 8.2: Lower panel: logarithmic integrated LF of young MS stars (filled diamonds). The LF is reproduced by the sum (thick continuous line) of 20 LFs (dot-dashed lines) of simple stellar populations. It is assumed here that the slope of the single LFs is equal to that of NGC 2004 (a young populous cluster of the Large Magellanic Cloud; α=0.32±0.04, see Fig. 13 in SHR04) and that the simple stellar population contains 0.5 times the number of stars in NGC 2004. The populations were generated at a constant rate during ~273 Myr (see §8.3.1), and all stars now evolved off the main sequence were removed from the LFs. Upper panel: the observed LF (filled diamonds) compared with a synthetic one (thick continuous line) generated with a bursting star formation. The epoch of the last episode (T_0) and the time lapse between the star formation episodes (P) are indicated. Dotted vertical lines mark the termination of the MS for the single bursts. See SHR04 and text for details.

brightness profile presented by Valluri et al. (2005) with a star-count based one reveals that no radial variations of the completeness factor are present for I≤24.5, as long as radial distances greater then r> 5″1 from the central nucleus are considered. Therefore, in the following, only stars having I≤24.5 (i.e M_V ≤-0.5) and r> 5″1 will be included in the analysis. Fig. 8.2 shows the logarithmic cumulated LF of the selected stars (diamonds), corrected for the appropriate completeness factors.

In order to estimate the mass in young stars, we followed the same approach as SHR04 (see lower panel in Fig. 8.2). For stars fainter than M_V ≃-3.0 (i.e. I≈22), the observed LF is well reproduced (heavy solid line) by the sum of 20 LFs of simple stellar populations (dot-dashed lines). The slope of the single LFs is assumed equal to that of the young Large Magellanic Cloud cluster NGC 2004 (see SHR04 for details). Each SSP contains half of the stars in NGC 2004. The populations were generated at a constant rate, and all stars now evolved off the main sequence were removed from the LFs. This way we obtain that ~1.9×10^5 M$_\odot$ were produced between ~62 Myr and ~335 Myr ago. Therefore, the star formation rate over this ~273 Myr lapse has been ~7×10^{-4} M$_\odot$/yr. Note, however, that the star formation should have been active since at least ~650 Myr ago (see Fig. 8.1).

The sparse population of stars brighter than I≈22 (M_V <-3) presents instead a flatter LF which may be compatible with an isolated SF episode. The age of this population can be estimated by assuming that the brightest stars are near the termination of the MS. Using formula B1 of SHR04, their absolute luminosity (M_V ≃-4.2) yields an age of ~25 Myr. Hence, this population would be slightly younger than the clusters studied by C99 (50 Myr and 100 Myr, respectively).

Relying on the Burstein et al. (1988, hereafter B88) IUE data, the UV flux at 1550 leads to a galaxy luminosity of $\log L_{1550} = 23.63$ ergs s^{-1} Hz^{-1} across the IUE field of view. Such a luminosity corresponds to a current SFR $\lesssim 10^{-5}$ M$_\odot$ yr^{-1}, according to the Buzzoni (2002) calibration. The IUE data indicate, therefore, a drastic reduction of galaxy SF at the current epoch.

Based on a further set of IUE observation, that sampled the nucleus of NGC 205 (region "N"), and the region 1′ north of it (region "B"), Wilcots et al. (1990) estimated a mass of young stars (M≥1 M$_\odot$) of 2 and 1×10^5 M$_\odot$ for the two galaxy regions, respectively. Region B corresponds to a part of NGC 205 where some bright blue stars were observed but does not overlap with our field. Their region N value and ours are similar. However, their value includes the contribution from the central nucleus which, instead, is excluded in our LF-based estimate. Furthermore, they estimate the mass of all stars having M≥1 M$_\odot$, while we neglect the contribution by star formation episodes older than 335 Myr, as they do not show up in the LF in the selected magnitude range (see Fig. 8.2). On the other hand, the IUE field of view is equivalent to a circular aperture with a diameter of 14″(see B88), and, as such, it corresponds to about a fifth of the observed ACS field.

8.4 Summary and discussion

We presented new, deep ACS photometry of the inner 30″(~120 pc) around the NGC 205 nucleus. The most notable feature presented here is the well populated blue plume of young MS stars visible at V-I<0.2 down to the detection limit (I≃26, see Fig. 8.1). Previous photometries were unable to probe this population, which is confined to the central galaxy regions. The LF of blue plume stars has been used to investigate the recent star formation in the central region of NGC 205. We found that ~1.9×10^5 M$_\odot$ were produced between ~62 Myr and ~335 Myr ago, corresponding to a star formation rate of ~7×10^{-4} M$_\odot$/yr. However, star formation has been active since at least ~650 Myr ago, which corresponds to our detection limit (see Fig. 8.1). A small number of ~25 Myr old stars are also present, in agreement with previous findings by C99 and Lee (1996).

BM05 and D03 concluded that the latest star formation episodes occurred a few 10^8 yr ago in NGC 205. This led them both to speculate that the recent star formation in NGC 205 might have been triggered by past interactions with M 31. This is certainly an intriguing possibility. In fact, Cepa & Beckman (1988, hereafter CB88) estimated the orbital period of NGC 205 in ~300 Myr, with the last passage through the M31 disk occurring ~100 Myr ago. However, the LF of the young MS is compatible with a constant SF rate, at least over the last ~300 Myr (see Fig. 8.2, lower panel).

In Fig. 8.2 (upper panel), we compare the young NGC 205 MS LF (filled diamonds) to the LF expected in the presence of a bursting star formation activity (thick continuous line). The BP mean ridge line and its broadening were adopted to generate a synthetic MS. For each SF episode, the termination of the MS was determined using formula B1 in SHR04. Each burst is assumed to produce the same number of stars and an NGC 2004-like LF. The resultant - synthetic - LF is the sum of the stars generated in the single bursts, normalized to the total number of observed stars.

We assumed bursts to occur with a time spacing equal to the orbital period (P=300 Myr), the last SF episode having occurred at the epoch of the last passage, T$_0$=100 Myr ago. The vertical lines mark the termination of the MS of the various SF episodes. Given the above parameters, most of the magnitude range under consideration is covered by just one episode of SF (see Fig. 8.1) and the synthetic LF is clearly not compatible with the observed one. More in general, a bursting SF with a period longer than ~100 Myr would imply an LF flatter than observed. On the other hand, a series of closely spaced star formation episodes would approximate a continuous star formation (lower panel) and, as expected, we find that the observed LF is well reproduced by a series of episodes spaced by only 10-20 Myr, the last one occurring ~63 Myr ago (see also Fig. 8.1). This kind of activity is reminiscent of the stochastic self-propagating star formation theory proposed by Gerola & Seiden (1978) and

later discussed, e.g., by Shore (1983) and Valle et al. (2005).

Furthermore, the star formation has certainly been active since more than ~650 Myr ago (see Fig. 8.1) and no indication of a significantly enhanced SF activity at any particular epoch is detected. The only feature that may be connected to an enhancement of the SF rate over a timescale comparable with the expected orbital period is the YC, that is presumably associated with a short episode that occurred ~200 Myr ago. Therefore, our photometry does not lend support the hypothesis of a tidally triggered SF at late epochs in NGC 205. Rather, a continuous SF may be consistent with NGC 205 being in its first interaction with M 31, as recently proposed by Howley et al. (2008).

The presence of a young population in a dwarf elliptical (over spatial scales much larger than the nucleus) remains puzzling, as is the significant amount of gas observed in this galaxy. The detected amount of gas, however, seems to be compatible with being returned to the interstellar medium by evolved stars during a burst of star formation starting $\sim 5 \times 10^8$ yr ago (Marleau et al., 2006). The present letter shows that the SF was indeed active on a similar time scale.

Lisker et al. (2006) discovered a number of dE with disk-like features in the Virgo cluster and introduced the term "dEdi" for those galaxies. Their analysis supports the idea that dEdis is a population of genuine disk galaxies and not just spheroids hosting a disk, perhaps only of tidal origin. These authors also flag NGC 205 as dEbc type, a subclass of the dEdis having blue centers (see Lisker et al., 2007). In fact, the large scale dynamics reveals that NGC 205 is at least partly supported by rotation (De Rijcke et al., 2006; Geha et al., 2006), with rotation being detected only along the major axis and De Rijcke et al. (2006) inferred an oblate geometry for the galaxy mass distribution. Also, recently obtained ground-based images provide compelling evidence that NGC 205 indeed hosts an embedded stellar disk (Saviane et al., in preparation). A revised classification from dE to a disk galaxy would provide a natural explanation for many of the NGC 205 peculiarities, including the presence of gas and the continuous star formation occurring in its central regions during (at least) the last ~ 650 Myr, as revealed by the present study.

List of Figures

List of Tables

Bibliography

Adelman-McCarthy, J.K. et al. 2008, ApJS, 175, 297

Ajhar, E. A., Grillmair, C. J., Lauer, T. R., Baum, W. A., et al.: 1996, AJ, 111, 1110

Armandroff, T.E. 1989, AJ, 97, 375

Ashman, K. M., & Zepf, S. E. 1992, ApJ, 384, 50

Ashman, Keith M.; Bird, Christina M.; Zepf, Stephen E. 1994, AJ, 108, 2348

Baade, W. 1935, Rep. Director Mt. Wilson Obs., 1934-35, 184

Baiesi Pillastrini, G.C., 2009, MNRAS, in press (arXiv:0905.1897)

Barmby, P., Huchra, J.P. 2001, AJ, 122, 2458

Barmby, P., Huchra, J.P., Brodie, J.P., Forbes, D.A., Schroder, L.L., Grillmair, C.J. 2000, AJ, 119, 727

Barmby, P., McLaughlin, D.E., Harris, W.E., Harris, G.L.H., Forbes, D.F. 2007, ApJ, 133, 2764

Barmby, P. et al. 2009, ApJ, 138, 1667

Barmby, P. 2003, in Extragalactic Globular Cluster Systems, ed. M. Kissler-Patig (Berlin: Springer), 143

Barmby, P., Ashby, M.L.N., Bianchi, L., et al., 2006, ApJ, 650, L45

Barmby, P., Huchra, J.P., & Brodie, J.P. 2001, AJ, 121, 1482

] Barmby, P., Holland, S., & Huchra, J. P. 2002, AJ, 123, 1937

Bastian, N., & Goodwin, 2006, MNRAS, 369, L9

Bastian, N., Gieles, M., Goodwin, S.P., Trancho, G., Smith, L.J., Konstantopoulos, I., Efremov, Y., 2008, MNRAS, 389, 223

Bastian, N., Saglia, R. P., Goudfrooij, P., Kissler-Patig, M., Maraston, C., Schweizer, F., & Zoccali, M. 2006, A&A, 448, 881

Battinelli, P., Brandimarti, A., & Capuzzo-Dolcetta, R. 1994, A&AS, 104, 379

Battistini, P.L., Bonoli, F., Casavecchia, M., Ciotti, L., Federici, L., & Fusi-Pecci, F. 1993, , 272, 77

Battistini, P.L., Bonoli, F., Braccesi, A. 1987, A&AS, 47, 847

Baumgardt, H. & Makino, J. 2003, MNRAS, 340, 227

Beasley, M.A., Brodie, J.P., Strader, J., et al. 2004, AJ, 128, 1623

Bellazzini, M., Ferraro, F. R., & Buonanno, R. 1999, MNRAS, 304, 633

Bellazzini, M., Ibata, R., Ferraro, F. R., & Testa, V. 2003a, A&A, 405, 577

Bellazzini, M., Ferraro, F. R., & Ibata, R. 2003b, AJ, 125, 188

Bellazzini, M., Perina, S., Galleti, S., Federici, L., Buzzoni, A., & Fusi Pecci, A., 2008, Mem. S.A.It., 79, 663 (B08)

Bellazzini, M., 2007, A&A, 473, 171

Bellazzini, M., Cacciari, C., Federici, L., Fusi Pecci, F., & Rich, M., 2003, A&A, 405, 867

Bellazzini, M., Fusi Pecci, F., Messineo, M., Monaco, L., & Rood, R.T., 2002a, AJ, 123, 1509

Bellazzini, M., Fusi Pecci, F., Montegriffo, P., Messineo, M., Monaco, L., & Rood, R.T., 2002b, AJ, 123, 2541

Belokurov, V., Zucker, D. B., Evans, N. W., Gilmore, G., Vidrih, S., et al. 2006, ApJ, 642, L137

Bendinelli, O., Cacciari, C., Djorgovski, S., Federici, L., Ferraro, F. R., Fusi Pecci, F., Parmeggiani, G., Weir, N., & Zavatti, F. 1993, ApJ, 409, L17

Benjamin, R. A., et al. 2003, PASP, 115, 953

Bica, E., Alloin, D., & Schmidt, A. A. 1990, A&A, 228, 23

Bica, E., Bonatto, C., Dutra, C. M., & Santos, J. F. C. 2008, MNRAS, 389, 678

Bohlin, R.C., Cornett, R.H., Hill, J.K., Hill, R.S., Stecher, T.P. 1988, ApJ, 334, 657

Bohlin, R.C., Deutsch, E.W., McQuade, K.A., et al. 1993, ApJ, 417, 127

Bonatto, C. & Bica, E. 2005, A&A, 437, 483

Bonatto, C. & Bica, E. 2008, A&A, 477, 829

Borissova, J., Kurtev, R., Hanson, M.M., Georgiev, L., Ivanov, V., Ortolani, S. 2010, Star clusters: basic galactic building blocks throughout time and space, IAUS, 266, 366-366

Boutloukos, S.G., & Lamers, H.J.G.L.M. 2003, MNRAS, 338, 717

Bragaglia, A., & Tosi, M. 2006, AJ, 131, 1544

Bragaglia, A., & Tosi, M., 2003, MNRAS, 343, 306

Brocato, E., Di Carlo, E., & Menna, G., 2001, A&A, 374, 523

Brodie, J. P., & Huchra, J. P. 1990, ApJ, 362, 503

Brodie, J.P., Strader, J., 2006, ARA&A, 44, 193

Brodie, J. P., Schroder, L. L., Huchra, J. P., Phillips, A. C., Kissler-Patig, M., & Forbes, D. A. 1998, AJ, 116, 691

Brown, T.M., Ferguson, H.C., Smith, E., Kimble, R.A., Sweigart, A.V., Renzini, A., Rich, R.M. & VandenBerg, D.A. 2003, ApJ, 592, L17

Brown, T.M., Ferguson, H.C., Smith, E., Kimble, R.A., Sweigart, A.V., Renzini, A., Rich, R.M. & VandenBerg, D.A. 2004a, AJ, 127, 2738

Brown, T.M., Ferguson, H.C., Smith, E., Kimble, R.A., Sweigart, A.V., Renzini, A., Rich, R.M. & VandenBerg, D.A. 2004b, ApJ, 613, L125

Brown, J. A., Wallerstein, G., & Zucker, D. 1997, AJ, 114, 180

Bruzual, G. & Charlot, S. 2003, MNRAS, 344, 1000

Buonanno, R., Corsi, C.E., Pulone, L., Fusi Pecci, F., Richer, H.B., Fahlman, G.C. 1995, AJ, 109, 663

Burstein D., Heiles C. 1984, ApJS, 54, 33

Burstein, D., Bertola, F., Buson, et al., 1988, ApJ, 328, 440 (B88)

Burstein, D., Li, Y., Freeman, K.C., et al. 2004, ApJ, 614, 158

Butler, D. J., & Martínez-Delgado, D. 2005, AJ, 129, 2217 (BM05)

Buzzoni, A. 1995a, ApJS, 98, 69

Buzzoni, A. 1989, ApJS, 71, 817

Buzzoni, A. 2002, AJ, 123, 1188

Côté, P., Piatek, S., Ferrarese, L., et al., 2006, ApJS, 165, 57

Caldwell, N., Harding, P., Morrison, H., Rose, J., Schiavon, R., & Kriessler, J., 2009, AJ, 137, 94 (C09)

Cappellari, M., et al. 1999, ApJ, 515, L17 (C99)

Carignan, C., Chemin, L., Hutchmeier, W.K., & Lockman, F.J., 2006, ApJ, 641, L109

Carpenter, J.M., Heyer, M.H., Snell, R.L., 2000, ApJS, 130, 381

Cepa, J., & Beckman, J. E. 1988, A&A, 200, 21 (CP88)

Cervino, M. & Luridiana, V. 2004, A&A, 413, 145

Chabrier, G. 2003, PASP, 115, 763

Chandar, R., Bianchi, L., & Ford, H. C. 1999, ApJS, 122, 431

Chandar, R., Fall, M., & Whitmore, B. 2006, ApJ, 650, L111

Chernoff, D. F. & Weinberg, M. D. 1990, ApJ, 351, 121

Clark, J. S., Negueruela, I., Crowther, P. A., & Goodwin, S. P. 2005, A&A, 434, 949

Cohen J.G., Hsieh, S., Metchev, S., Djorgovski, S.G., Malkan, M., 2007, AJ, 133, 99

Cohen J.G., Matthews K., Cameron P.B., 2006, ApJ, 634, L45

Cohen, J.G. 2004, AJ, 127, 1545

Cohen, J.G., Matthews, K., Cameron, P.B 2005, ApJ, 634, 45

Cohen, J. G. & Freeman, K. C. 1991, AJ, 101, 483

Cordier, D., Pietrinferni, A., Cassisi, S. Salaris, M., 2007, AJ, 133, 468

Cowley, A.P., Burstein, D. 1988, AJ, 95, 1071

Crampton, D., Cowley, A.P., Shade, D., Chayer, P. 1985, ApJ, 288, 494

Davidge, T. J. 2003, ApJ, 597, 289 (D03)

Davidge, T. J. 2005, AJ, 130, 2087

Davies, B., Figer, D.F., Law, C.J., Kudritzki, R.-P., Najarro, F., Herrero, A., & MacKenty, J.W., 2008, ApJ, 676, 1016

de Grijs R., Parmentier G., Lamers H.J.G.L.M., 2005, MNRAS, 364, 1054

de Grijs, R., 2009, in Basic Galactic Building Blocks throughout time and Space, R. De Grijs and J. Lepine Eds., IAU Symp. 266, in press (arXiv:0909.2322)

deGrijs, R., Goodwin, S.P., Kouwenhoven, M.B.N., & Kroupa, P., 2008, MNRAS, in press (arXiv:0803.1991)

De Marchi, G., Leibundgut, B., Paresce, F., & Pulone, L. 1999, , 343, L9

De Propris, R., Phillips, S., Drinkwater, M.J., et al., 2005, ApJ, 623, L105

De Rijcke, S., et al., 2006, MNRAS, 369, 1321

Dean, J.F., Warren, P.R., & Cousins, A.W.J., 1978, MNRAS, 183, 569

Dinescu, D.I., Majewski, S.R., Girard, T.M., & Cudworth, K.M. 2000, AJ, 120, 1892

Djorgovski, S. & Meylan, G. 1994, AJ, 108, 1292

Djorgovski, S. & King, I. R. 1986, ApJ, 305, L61

Djorgovski, S. G., Gal, R. R., McCarthy, J. K., Cohen, J. G., deCarvalho, R. R., Meylan, G., Bendinelli, O., & Parmeggiani, G. 1997, ApJ, 474, L19

Djorgovski, S. 1995, ApJ, 438, L29

Dolphin, A.E. 2000a, PASP, 112, 1383

Dolphin, A.E. 2000b, PASP, 112, 1397

Elson, R.A.W., Fall, S.M. 1985, PASP, 97,692

Elson, R.A.W., Walterbos, R. A. M. 1988, ApJ, 333, 594

Elson, R. A. W., Fall, S. M., & Freeman, K. C. 1987, ApJ, 323, 54

Epchtein N. et al. 1997, The Messenger No. 87, p. 27

. Hammer, M. Puech, L. Chemin, H. Flores, & M. D. Lehnert, 2007, ApJ, 662, 322

Fall, S. M., & Rees, M. J. 1985, ApJ, 298, 18

Fan, Z., Ma, J., de Grijs, R., & Zhou, X., 2008, MNRAS, 385, 1973

Federici, L., Bellazzini, M., Galleti, S., Fusi Pecci, F., Buzzoni, A., & Parmeggiani, G. 2007, A&A, 473, 429

Ferguson, A.M.N., Johnson, R.A., Faria, D.C., Irwin, M.J., Ibata, R.A., Johnston, K.V., Lewis, G.F., & Tanvir, N.R. 2005, ApJ, 622, L109

Figer, D.F., 2008, in Massive Stars as Cosmic Engines, IAU Symp. 250, F. Bresolin, P. A. Crowther, and J. Puls Eds., Cambridge, Cambridge Univ. Press, 247

Friel, E. D. 1995 The old open clusters of the Milky Way. ARA&A, **33**, 381–414.

Friel, E. D., Janes, K. A., Tavarez, M., Scott, J., Katsanis, R., Lotz, J., Hong, L. & Miller, N. 2002 Metallicities of old open clusters. AJ, **124**, 2693–2720.

Frogel, J. A., Cohen, J. G., & Persson, S. E. 1983, ApJ, 275, 773

Fuentes-Carrera, I.; Jablonka, P.; Sarajedini, A.; Bridges, T.; Djorgovski, G.; Meylan, G. 2008, A&A, 483, 769 [FC08]

Fusi Pecci, F., et al. 1996, AJ, 112, 1461

Fusi Pecci, F., Bellazzini, M., Buzzoni, A., De Simone, E., Federici, L., Galleti, S., 2005, AJ, 130, 554 (F05)

Fusi Pecci, F., et al. 1994, A&A, 284, 349

Gallart, C., Zoccali, M., Aparicio, A., 2005, ARA&A, 43, 387

Galleti, S., Federici, L.,Bellazzini, M., Buzzoni, A. & Fusi Pecci, F. 2006a, A&A, 456, 985

Galleti, S., Bellazzini, M., Federici, L., Buzzoni, A. & Fusi Pecci, F. 2007, A&A, 471, 127

Galleti, S., Federici, L., Bellazzini, M., et al., 2004, A&A, 416, 917

Galleti, S.; Federici, L.; Bellazzini, M.; Buzzoni, A.; Pecci, F. Fusi 2006, ApJ, 650, 107

Galleti, S.; Bellazzini, M.; Buzzoni, A.; Federici, L.; Fusi Pecci, F. 2009, , 508, 1285

Geha, M., Guhathakurta, P., Rich, R. M., & Cooper, M. C. 2006, AJ, 131, 332

Gerola, H., & Seiden, P. E. 1978, ApJ, 223, 129

Gieles, M. et al. 2006, MNRAS, 371, 793

Gieles, M., Lamers, H.J.G.L.M., Portegies-Zwart, S.F., 2007, ApJ, 668, 268

Gieles, M., Lamers, H.J.G.L.M., & Baumgardt, H., 2008, in Dynamical Evolution of Dense Stellar Systems, IAU Symp. 246, 171

Gieles , M. 2009, MNRAS, 394, 2113

Gilmozzi, R., Kinney, E.K., Ewald, S.P., Panagia, N., & Romaniello, M., 1994, ApJ, 435, L43

Girardi, L., Bertelli, G., Bressan, A., et al. 2002, A&A, 391, 195

Girardi, L. 2006, http://pleiadi.pd.astro.it

Gnedin, O. Y. & Ostriker, J. P. 1997, ApJ, 474, 223

Goodwin, S. P. & Bastian, N. 2006, MNRAS, 373, 752

Gordon, K.D., Bailin, J., Engelbracht, C.W., Rieke, G.H., Misselt, K.A. and 14 coauthors 2006, ApJ, 638, L92

Gouliermis, D., Keller, S.C., Kontizas, M., Kontizas, E., & Bellas-Velidis, I., 2004, A&A, 416, 137

Gratton, R.G., Fusi Pecci, F., Carretta, E., Clementini, G., Corsi, C.E., & Lattanzi, M. 1997, ApJ, 491, 749

Grillmair C.J., Freeman K.C., Irwin M., Quinn P.J., 1995, AJ 109, 2553

Grillmair, C. J., Ajhar, E. A., Faber, S. M., Baum, W. A., Holtzman, J. A., Lauer, T. R., Lynds, C. R., & O'Neil, Jr., E. J. 1996, AJ, 111, 2293

Hammer F., Puech M., Chemin L., Flores H., & Lehnert M.D. 2007, ApJ, 662, 322

179

Harris W.E. 2001, in *Star clusters*, Saas-Fee Advanced Course 28, Lecture Notes 1998, eds. L. Labhardt and B. Binggeli (Springer, Berlin), p.223

Harris, W.E. 2003, Catalog of parameters for Milky Way Globular Clusters, Feb. 2003 update at `http://physwww.mcmaster.ca/~harris/mwgc.dat`

Harris, W.E. 1991, ARA&A, 29, 543

Harris, W.E. 1996, AJ, 112, 1487 (see also: `http://physwww.physics.mcmaster.ca/~harris/mwgc.dat` for catalog update)

Harris, W. E. 2009 Globular cluster systems in giant ellipticals: the mass/metallicity relation. ApJ, **699**, 254–280.

Hartigan, J.A., & Hartigan, P.M., 1985, The Annals of Statistics, 13, 70

Haşegan, M. et al. 2005, ApJ, 627, 203

Herschel, W. 1814 Astronomical observations relating to the sidereal part of the heavens, and its connection with the nebulous part. *Phil. Trans. R. Soc. London*, **104**, 248–284.

Hodge, P., Mateo, M., Lee, M. G., & Geisler, D. 1987, PASP, 99, 173

Hodge, P., Krienke, O.K., Bellazzini, M., Perina, S., Barmby, P., Cohen, J.G., Puzia, T.H., & J. Strader, 2009, AJ, 138, 770 (Pap-II)

Hodge, P. W. 1973, ApJ, 182, 671

Hodge, P.W. 1979, AJ, 84, 744

Hodge, P., 1992, The Andromeda Galaxy, Dordrecht, Kluwer

Hodge, P., 1981, Atlas of the Andromeda Galaxy, Seattle and London, University of Washington Press

Hodge, P., Krienke, O.K., Bellazzini, M., Perina, S., Barmby, P., Cohen, J.G., Puzia, T.H., & J. Strader, 2009, AJ, 138, 770 (Pap-II)

Hodge, P. W. 1961, ApJ, 133, 413

Holland, S., Fahlman, G. G., & Richer, R. B. 1997, AJ, 114, 1488 (HFR)

Holmberg, J., Flynn, C., & Portinari, L., 2006, MNRAS, 367, 449

Holtzman, J. A., et al. 1992, AJ, 103, 691

Holtzman, J., Burrows, C., Casertano, S., Hester, J., Trauger, J., Watson, A., & Worthey, G. 1995, PASP, 107, 1065

Howley, K. M., et al. 2008, ApJ, 683, 722

Hubble, E., 1929, ApJ, 69, 103

Hubble, E. 1932, AJ, 76, 44.

Hubble, E. 1936, Realm of the Nebulae (New Haven, CT: Yale Univ. Press), frontespiece

Huchra, J. P., Brodie, J. P., & Kent, S. M. 1991, ApJ, 370, 495

Hunter, D. A., Elmegreen, B. G., Dupuy, T., & Mortonson, M. 2003, AJ, 126, 1836

Huxor, A.; Tanvir, N. R.; Irwin, M.; Ferguson, A.; Ibata, R.; Lewis, G.; Bridges, T. 2004, ASPC, 327, 118

Huxor, A. P.; Tanvir, N. R.; Irwin, M. J.; Ibata, R.; Collett, J. L.; Ferguson, A. M. N.; Bridges, T.; Lewis, G. F. 2005, MNRAS, 360, 1007

Huxor, A. P.; Tanvir, N. R.; Ferguson, A. M. N.; Irwin, M. J.; Ibata, R.; Bridges, T.; Lewis, G. F. 2008, MNRAS, 385, 1989

Ibata, R.A., Gilmore, G., Irwin, M.J. 1995, MNRAS, 277, 781

Ibata, R., Irwin, M., Lewis, G., Ferguson, A.M.N., Tanvir, N. 2001b, Nature, 412, 49

Ibata, R., Chapman, S., Ferguson, A.M.N., Lewis, G., Irwin, M., Tanvir, N. 2005, ApJ, 634, 287

Ibata, R., Martin, N.F., Irwin, M., Chapman, S., Ferguson, A.M.N., Lewis, G.F.,& McConnachie, A. W. 2007, ApJ, 671, 1591

Ivanov, V.D., Messineo, M., Zhu, Q., Figer, D., Borissova, J., Kurtev, R., Ivanov, G.R. 2010, Star clusters: basic galactic building blocks throughout time and space, IAUS, 266, 203-210

Jablonka, P., Courbin, F., Meylan, G., Sarajedini, A., Bridges, T.J. & Magain, P. 2000, A&A, 359, 131

Jiang, L., Ma, J., Zhou, X., Chen, J., Wu, H., et al. 2003, AJ, 125, 727

Johnson, R.A., Beaulieu, S.F., Gilmore, G.F., Hurley, J., Santiago, B.X., Tanvir, M.R., & Elson, R.A.W., 2001, MNRAS, 324, 367

Jones, D. H., et al. 1996, ApJ, 466, 742

Jordán, A. 2004, ApJ, 613, L117

Kharchenko, N. V., Piskunov, A. E., Röser, S., Schilbach, E., & Scholz, R.-D. 2005, A&A, 438, 1163

Kim, S.C., Lee, M.G., Geisler, D., Sarajedini, A., Park, H.S. et al. 2007, AJ, 134, 706

King, I.R., 1966, AJ, 71, 64 (K66)

King, J.R., Lupton, R.H. 1991, in *The formation and evolution of star clusters*, p. 575

King, I. 1962, AJ, 67, 471

Kinman, T., 1959, MNRAS, 119, 538

Kissler-Patig, M., Jordán, A., & Bastian, N. 2006, A&A, 448, 1031

Koposov, S., de Jong, J.T.A., Belokurov, V., Rix, H.-W., Zucker, D.B. Evans, N.W., Gilmore, G., Irwin, M.J. & Bell, E.F. 2007, AJ, 669, 337

Krienke, O.K., & Hodge, P.W., 2007, PASP, 119, 7

Krienke, O.K., & Hodge, P.W., 2008, PASP, 120, 1

Kroupa, P. 2001, MNRAS, 322, 231

Kruijssen, J. & Lamers, H. 2008, Formation and Evolution of Galaxy Disks (ASP Conf. Ser. 396), ed. J. G. Funes & E. M. Corsini (San Francisco, CA: ASP), 149

Kruijssen, J. M. D. & Lamers, H. J. G. L. M. 2008, A&A, 490, 151

Kruijssen, J. M. D. 2008, A&A, 486, L21

Kubiak, M., Kaluzny, J., Krzeminski, W., Mateo, M., 1992, AcA, 42, 155

Kundu, A. 2008, AJ, 136, 1013

Kurtev, R., Borissova, J., Georgiev, L., Ortolani, S., Ivanov, V. D. 2007,, 475, 209

Kurtev R., Ivanov V.D., Borissova J. & Ortolani S. 2008, , 489, 583

Lada, C. J., & Lada, E. A. 2003, ARA&A, 41, 57

Lada, E. A., Depoy, D. L., Evans, N. J., II, & Gatley, I. 1991, ApJ, 371, 171

Lamers, H.J.G.L.M., & Gieles, M., 2006, A&A, 455, L17 (LG06)

Lamers, H. J. G. L. M., Gieles, M., & Portegies Zwart, S. F. 2005, , 429, 173

Larsen, S. S. & Richtler, T. 2000 Young massive star clusters in nearby galaxies. III. Correlations between cluster populations and host galaxy properties. A&A, **354**, 836–846.

Larsen, S. S. & Richtler, T. 2004 Dynamical mass estimates for two luminous young stellar clusters in Messier 83. A&A, **427**, 495–504.

Larsen, S. S. 2003, Extragalactic Globular Cluster Systems, 54

Larsen, S. S. & Richtler, T. 1999, A&A, 345, 59

Larsen, S. S. 2004, A&A, 416, 537

Lata, S., Pandey, A.K., Sagar, R., & Mohan, V. 2002, A&A, 388, 158

Lauer, T.R., 1985, ApJS, 57, 473

Lee, M.-G., Ho, Hwang, H.-S., Kim, S.-C., Park, H.-S., Geisler, D., Sarajedini, A., & Harris, W.E., 2008, ApJ, 674, 886

Lee, M. G. 1996, AJ, 112, 1438

Lee, M.-G., Ho, Hwang, H.-S., Kim, S.-C., Park, H.-S., Geisler, D., Sarajedini, A., & Harris, W.E., 2008, ApJ, 674, 886

Lisker, T., Grebel, E. K., & Binggeli, B. 2006, AJ, 132, 497

Lisker, T., Grebel, E. K., Binggeli, B., & Glatt, K. 2007, ApJ, 660, 1186

Lupton, R.H. 1989, AJ, 97, 1350

Lupton, R., 2005, www.sdss.org/dr4/algorithms/sdssUBVRITransform.html#Lupton2005

Mackey, A. D.; Huxor, A.; Ferguson, A. M. N.; Tanvir, N. R.; Irwin, M.; Ibata, R.; Bridges, T.; Johnson, R. A.; Lewis, G. 2006, ApJ, 653, 105

Mackey, A. D.; Huxor, A.; Ferguson, A. M. N.; Tanvir, N. R.; Irwin, M.; Ibata, R.; Bridges, T.; Johnson, R. A.; Lewis, G. 2007, ApJ, 655, 85

Mackey, A.D., & van den Bergh, S., 2005, MNRAS, 360, 631

Mackey, A. D., & Gilmore, G. F. 2003, MNRAS, 338, 85

Majewski, S.R., Skrutskie, M.F., Weinberg, M.D., & Ostheimer, J.C. 2003, ApJ, 599, 1082

Marín-Franch, A. et al. 2009, ApJ, 694, 1498-1516

Maraston, C. 1998, MNRAS, 300, 872

Maraston, C. 2005, MNRAS, 362, 799

Marigo, P., Girardi, L., Bressan, A., Groenewegen, M.A.T., Silva, L., Granato, G.L., 2008, A&A, 482, 883 (M08)

Marleau, F. R., et al. 2006, ApJ, 646, 929

Martin, N. F., Ibata, R. A., Irwin, M. J., Chapman, S., Lewis, G. F., Ferguson, A. M. N., Tanvir, N., & McConnachie, A. W. 2006, MNRAS, 371, 1983

Martin, N., de Jong, J.T.A., & Rix. H.-W., 2008, ApJ, 684, 1075

Martìnez-Delgado, D., Zinn, R., Carrera, R., & Gallart, C. 2002, ApJ, 537, L19

Massey, P., 2003, ARA&A, 41, 15

Massey, P., Olsen, K.A.G., Hodge, P.W., Strong, S.B., Jacoby, G.H., Schlingman, W., Smith. R.C., 2006, AJ, 131, 2478 (M06)

Mateo, M. L. 1998, ARA&A, 36, 435

McConnachie, A.W., Irwin, M.J. & Ferguson, A.M.N. 2005, MNRAS, 356, 979

McConnachie, A. W., et al. 2004, MNRAS, 351, L94

McCrady, N. & Graham, J. R. 2007 Super star cluster velocity dispersions and virial masses in the M82 nuclear starburst. ApJ, **663**, 844–856.

McLaughlin, D.E., & van der Marel, R.P., 2006, `2006yCat..21610304M`

McLaughlin, D. E. & van der Marel, R. P. 2005, ApJS, 161, 304

McLaughlin, D. E., Barmby, P., Harris, W. E., Forbes, D. A., & Harris, G. L. H. 2008, MNRAS, 384, 563

McLaughlin, D. E. 2000, ApJ, 539, 618

McLaughlin , D. E. 2003, in Astronomical Society of the Pacific Conference Series, Vol. 296, New Horizons in Globular Cluster Astronomy, ed. G. Piotto, G. Meylan, S. G. Djorgovski, & M. Riello, 101

Messineo, M., et al., 2009, ApJ, 697, 701 (M09)

Meylan, G., Sarajedini, A., Jablonka, P., Djorgovski, S. G., Bridges, T., & Rich, R. M. 2001, AJ, 122, 830

Meylan, G. & Djorgovski, S. 1987, ApJ, 322, L91

Morrison, H., Harding, P., Perrett, K.M., Hurley-Keller, D. 2004, ApJ, 603, 87

Mould, J., Kristian, J., & Da Costa, G. S. 1984, ApJ, 278, 575

Noyola, E. & Gebhardt, K. 2006, AJ, 132, 447

Nantais, J.B., Huchra, J.P., Barmby, P., Olsen, K.A.G., Jarrett, T.H., 2006, AJ, 131, 1416

Odenkirchen, M., et al. 2003, AJ, 126, 2385

Oort, J. H. 1958, Ricerche Astronomiche, 5, 507

Pandey, A.K., Bhatt, B.C., Mahra, H.S., & Sagar, R. 1989, MNRAS, 236, 263

Park, W., Park, H., Lee, M., 2009, ApJ, 700, 103

Peebles, P. J. E., & Dicke, R. H. 1968, ApJ, 154, 891

Peletier, R.F., 1993, A&A, 271, 51

Pels, G., Oort, J. H., Pels-Kluyver, H. A., 1975, A&A, 43, 423

Perina, S., Federici L., Bellazzini M., Cacciari C., Fusi Pecci F., Galleti S. 2009, , 507, 137

Perina, S., Barmby, P., Beasley, M., et al. 2009a, A&A, 494, 933 (Pap-I)

Perina, S.; Barmby, P.; Beasley, M. A.; Bellazzini M., et al. 2010, 511, A23

Perrett, K.M., Stiff, D.A., Hanes, D.A., & Bridges, T.J. 2003, ApJ, 589, 790

Perrett, K. M., Bridges, T. J., Hanes, D. A., Irwin, M. J., Brodie, J. P., Carter, D., Huchra, J. P., & Watson, F. G. 2002, AJ, 123, 2490

Pfalzner, S. 2009, A&A, 498, L37

Phelps, R. L., & Schick, M. 2003, ApJ, 126, 265

Pietrinferni, A., Cassisi, S., Salaris, M., & Castelli F., 2004, ApJ, 612, 168

Piotto, G., King, I.R., Djorgovski, S.G., Sosin, C., Zoccali, M. et al. 2002, A&A, 391, 945

Piotto, G., Cool, A.M., King, I.R., AJ, 113, 1345

Piskunov, A. E., Kharchenko, N. V., Schilbach, E., Röser, S., Scholz, R.-D. & Zinnecker, H. 2008 The initial luminosity and mass functions of the Galactic open clusters. A&A, **487**, 557–566.

Piskunov, A. E., Schilbach, E., Kharchenko, N. V., Röser, S., & Scholz, R.-D. 2007, A&A, 468, 151

et al. 2008, A&A, 477, 165

Portegies Zwart, S.F., McMillan, S.L.W., Gieles M. 2010 arXiv:1002.1961v1

Pritchet, C.J., & van den Bergh, S., 1994, AJ, 107, 1730

Puzia, T. H., Saglia, R. P., Kissler-Patig, M., Maraston, C., Greggio, L., Renzini, A., & Ortolani, S. 2002, , 395, 45

Puzia, T. H., Perrett, K. M., & Bridges, T. J. 2005, , 434, 909

Racine, R. & Harris, W. E. 1992, AJ, 104, 1068

Racine, R. 1991, AJ, 101, 865

Rafelski, M. & Zaritsky, D. 2005, AJ, 129, 2701

Renzini, A., & Fusi Pecci, F. 1988, ARA&A, 26, 199

Reyle C. & Robin A.C. 2002, Ap&SS, 281, 115-118

Rich, R.M., Mighell, K.J., Freedman, W., & Neill, J.D. 1996, AJ, 111, 768

Rich, R.M, Corsi, C.E., Cacciari, C., federici, L., Fusi Pecci, Djorgovski, S.G., & Freedman, W., 2005, AJ, 129, 2670

Rich, R. M. 2003, in ASP Conf. Ser. 296, New Horizons in Globular Cluster Astronomy, ed. G. Piotto et al. (San Francisco: ASP), 533

Richardson, J.C., Ferguson, A.M.N., Johnson, R.A., Irwin, M.J., Tanvir, N.R., Faria, D.C., Ibata, R.A., et al. 2008, AJ, 135, 1998

Richer, H. B., Crabtree, D. R., & Pritchet, C. J. 1984, ApJ, 287, 138

Rieke, G. H., & Lebofsky, M. J., 1985, ApJ, 288, 618

Rosenberg, A., Saviane, I., Piotto, G., Aparicio, A., & Zaggia, S.R. 1998, AJ, 115, 648

Rosenberg, A., Piotto, G., Saviane, I., & Aparicio, A. 2000a, A&AS, 144, 5

Rosenberg, A., Aparicio, A., Saviane, I., & Piotto, G. 2000b, A&AS, 145, 451

Rosenberg, H. 1910, Astronomische Nachrichten, 186, 71

Rossa, J., van der Marel, R.P., Böker, T.,et al., 2006, PASP, 109, 907

Sérsic, J.-L. 1968, Atlas de Galaxias Australes (Cordoba: Observatoria Astronomico)

Sagar, R., Joshi, U.C., & Sinvhal, S.D. 1983, Bull. Astron. Soc. India 11, 44

Sagar et al., 1991, A&AS, 90, 387

Salasnich, B., et al., 2000, A&A, 361, 1023

Salpeter, E.E., 1955, ApJ, 121, 161

San Roman, I., Sarajedini, A., Garnett, D.R., Holtzman, J.A., 2009, ApJ, 699, 839

Sarajedini, A., Mancone, C.L., 2007, AJ, 134, 447

Sarajedini, A., et al. 2007, AJ, 133, 1658

Saviane, I., Rosenberg, A., Piotto, G., & Aparicio, A. 2000, A&A, 355, 966

Saviane, I., Hibbard, J. E., Rich, R. M. 2004, AJ, 127, 660 (SHR04)

Sbordone, L., Bonifacio, P., Marconi, G., Buonanno, R., & Zaggia, S. 2005, A&A, 437, 905

Schilbach, E., Kharchenko, N. V., Piskunov, A. E., Röser, S., & Scholz, R.-D. 2006, A&A, 456, 523

Schlegel, D.J., Finkbeiner, D.P., & Davis, M. 1998, ApJ, 500, 525

Searle, L. 1978, NATO Advanced Study Institute on *Globular Clusters*, Cambridge University

Shapley, H. 1915 Contrib. Mt. Wilson Sol. Obs., No. 116

Shapley, H. 1916 Studies based on the colors and magnitudes in stellar clusters. I. The general problem of clusters. *Contrib. Mt Wilson Solar Obs.*, **115**, 1–21.

Sharina, M. E., Afanasiev, V. L., & Puzia, T. H. 2006, MNRAS, 372, 1259

Sharov, A.S., Lyutyi, V.M., & Esipov, V.F., 1995, Astr. Lett, 21, 275

Shore, S. N. 1983, ApJ, 265, 202

Simien, F., Athanassoula, E., Pellet, A., et al., 1978, A&A, 67, 73

Sirianni, M., Jee, M.J., Bemitez, N., et al., 2005, PASP, 117, 1049

Skrutskie, M. F., et al. 1997, The Impact of Large-Scale Near-IR Sky Surveys, ed. F. Garzon et al. (Dordrecht: Kluwer), 25

Skrutskie, M.F., Cutri, R.M., Stirning, R., et al., 2006, AJ, 131, 1163

Smith L.J. et al. 2007, ApJ, 667, 145

Spassova, N.M., & Beav, P.V. 1985, Ap&SS, 112, 111

Spinrad, H., Schweizer, F. 1972, ApJ, 171, 403

Spitzer, L. J., & Harm, R. 1958, ApJ, 127, 544

Spitzer, L. J. 1958, ApJ, 127, 17

Spitzer, L. J. 1987, *Dynamical Evolution of Globular Clusters* (Princeton Univ. Press). 127, 17

Stanek, K. Z. & Garnavich, P. M. 1998, ApJ, 503, L131

Staneva, A., Spassova, N., Golev, V. 1996, A&AS, 116, 447

Stephens, A.W., Frogel, J.A., Freedman, W., Gallart, C., Jablonka, P., Ortolani, S., Renzini, A., Rich, R.M., Davies, R. 2001, AJ, 121, 2597

Sternberg, A., 1998, ApJ, 506, 721

Stetson, P.B., Hesser, J.E., Smith, G.H., Vandenberg, D.A., % Bolte, M. 1989, AJ, 97, 1360

Stetson, P. 1987, PASP, 99, 191

Strader, J., Smith, G. H., Larsen, S., Brodie, J. P., & Huchra, J. P. 2009, AJ, 138, 547

Tautvaisiené, G., Wallerstein, G., Geisler, D., Gonzales, G., & Charbonnel, C. 2004, AJ, 127, 373

Tinsley, B.M., Gunn, J.E. 1976, ApJ, 203, 52

Tosi, M., Sabbi, E., Bellazzini, M., Aloisi, A., Greggio, L., Leitherer, C., Montegriffo, P., 2001, AJ, 122, 1271

Valle, G., Cignoni, M., & Shore, S. N. 2005, A&A, 440, 473

Vallenari, A., Aparicio, A., Fagotto, F., Chiosi, C., Ortolani, S., & Meylan, G., 1994, A&A, 284, 447

Valluri, M., Ferrarese, L., Merritt, D., & Joseph, C. L. 2005, ApJ, 628, 137

Van den Bergh, S. 2000, The galaxies of the Local Group (Cambridge: Cambridge University Press)

van den Bergh, S., & Lafontaine, A. 1984, AJ, 89, 1822

van den Bergh, S. 1967, AJ, 72, 70

van den Bergh, S. 1969, ApJS, 19, 145

van den Bergh, S. 1981, , 46, 79

van den Bergh, S. 1991, ApJ, 369, 1

van den Bergh, S. 2000, The Galaxies of the Local Group (Cambridge: Cambridge Univ. Press)

van den Bergh, S., 1964, ApJS, 9, 65

van den Bergh, S., 1969, ApJS, 171, 19

van den Bergh, S. 1994, AJ, 108, 2145

Vansevicius, V., Kodaira, K., Narbutis, D., Stonkute, R., Bridzius, A., Deveikis, V., & Semionov, D, 2009, ApJ, in press (arXiv:0909.1912)

Venn, K., Chutter, A., Irwin, M., Arimoto, N., Aoki, W., & Sadakane, K. 2007, American Astronomical Society Meeting 210, # 123.14

Vesperini, E. 1998, MNRAS, 299, 1019

Vetesnik, M. 1962, Bull. Astron. Inst. Czechoslovakia, 13, 180

Weidner, C., Kroupa, P., & Larsen, S. S. 2004, MNRAS, 350, 1503

Welch, G. A., Sage, L. J., & Mitchell, G. F. 1998, ApJ, 499, 209

Whitmore, B. C. & Schweizer, F. 1995, AJ, 109, 960

Whitmore, B. C., & Schweizer, F. 1995, AJ, 109, 960

Whitmore, B. C., Zhang, Q., Leitherer, C., Fall, S. M., Schweizer, F., & Miller, B. W. 1999, AJ, 118, 1551

Whitmore, B.C., Chandar, R., & Fall, S.M., 2007, AJ, 133, 1067

Wielen, R. 1971, A&A, 13, 309

Wielen, R. 1985, in IAU Symp. 113: Dynamics of Star Clusters, ed. J. Goodman & P. Hut, 449–460

Wilcots, E. M., Hodge, P., Eskridge, et al, 1990, ApJ, 364, 87

Williams, B.F., Hodge, P.W. 2001a, ApJ, 548, 190

Williams, B.F., Hodge, P.W. 2001b, ApJ, 559, 851

Wilson, C. P. 1975, AJ, 80, 175

Whitmore, B.C., Chandar, R., & Fall, S.M., 2007, AJ, 133, 1067

Wolff, S. C., Strom, S. E., Dror, D., & Venn, K. 2007, AJ, 133, 1092

Yin, J., Hou, J. L., Prantzos, N., Boissier, S., Chang, R. X., Shen, S. Y., & Zhangh, B., 2009, A&A, in press (arXiv:0906.4821)

Zhang, Q. & Fall, S. M. 1999 The mass function of young star clusters in the 'Antennae' galaxies. ApJ, **527**, L81–L84.

Zinn, R.J. 1985, ApJ, 293, 424

Zinn, R. 1985, ApJ, 293, 424

Zloczewski, K., Kaluzny, J., Hartman, J., 2008, AcA, 58, 23

Zloczewski, K., Kaluzny, J., Hartman, J., 2008, AcA, 58, 23

Acnowledgements